The initiation and evolution of ignimbrite faults, Gran Canaria, Spain

Aisling Mary Soden
B.A. (Hons.), Trinity College Dublin

Thesis presented for the degree of Doctor of Philosophy (Ph.D.)

University of Glasgow

Department of Geographical & Earth Sciences

January 2008

Abstract

Understanding how faults initiate and fault architecture evolves is central to predicting bulk fault zone properties such as fault zone permeability and mechanical strength. The study of faults at the Earth's surface and at near-surface levels is significant for the development of high level nuclear waste repositories, and CO_2 sequestration facilities. Additionally, with growing concern over water resources, understanding the impact faults have on contaminant transport between the unsaturated and saturated zone has become increasingly important. The proposal of a high-level nuclear waste repository in the tuffs of Yucca Mountain, Nevada has stimulated interest into research on the characterisation of brittle deformation in non-welded to densely welded tuffs and the nature of fluid flow in these faults and fractures.

The majority of research on the initiation and development of faults has focussed on shear faults in overall compressional stress regimes. Dilational structures have been examined in compressional settings e.g. overlapping faults generating extensional oversteps, or in normal faults cutting mechanical layered stratigraphy. Previous work has shown the affect mechanical stratigraphy has on fault dip angle; competent layers have steeply dipping segments and less competent layers have shallowly dipping segments. Displacement is accommodated by shear failure of the shallow segments and hybrid failure of the steeply dipping segments. As the fault walls of the shear failure segment slip past each other the walls of the hybrid failure segment are displaced horizontally as well as vertically thus forming dilation structures such as pull-aparts or extensional bends. Work on truly extensional faults has been at the kilometre scale of fissure swarms in rift systems where the focus is on fault geometry and direction of fault propagation.

This study examines dilational faults with offsets of centimetres to 10's of meters within moderately and densely welded ignimbrite units on the caldera island of Gran Canaria, Spain. Through the investigation of fault populations within different ignimbrite units I have examined how the fault architecture changes with accumulated displacement, identified the factors controlling fault core evolution and using these observations developed a new model for the initiation and growth of dilational faults in ignimbrites.

The faults in this study do not have a linear correlation of increasing fault core thickness with displacement. Fault core width varies along fault dip and the largest offset faults have the narrowest

fault cores. Furthermore, the damage zone joint frequency shows a limited increase with increasing displacement and faults and joints are sub-parallel. From these observations I have developed a new model for fault initiation and evolution in which the petrophysical properties of the host rock are the primary control on fault architecture. Faults initiate on existing sub-parallel joints and grow by the incorporation of material from joint surfaces and joint bound slabs. The growth of the fault depends on the joint spacing and the competency of the host rock. In densely welded ignimbrites, joint spacing is controlled by sub-layers within the ignimbrite unit which are formed by flattening and stretching of fiamme. In moderately welded ignimbrites, fiamme and lithic inclusions in the ash matrix act as sites of joint initiation; the greater the abundance of such flaws the higher the joint frequency. Whether fault growth is promoted or inhibited depends to some extent on the competency of the material. Faults cutting ash-rich friable units have narrow fault cores regardless of displacement. This suggests that the material is easily abraded in the fault core inhibiting fracturing of the host rock and incorporation of new material. Hence host rock fabric and composition have an important influence on fault architecture in these ignimbrite units. The other influence on fault evolution is the tensile stress regime in which faulting occurs. The faults in this study form by hybrid failure and so have both vertical and horizontal displacements. The dilation of existing joints causes slip on the joints and allows material to fall into the joint forming a fault core. This work identifies distinct differences between the mechanism of dilational fault initiation and resultant fault architecture compared to that of shear faults.

The observations made in this study indicate that the host rock petrophysical properties, stress regime at time of faulting (tensile or compressive) and confining pressure are primary influences on fault architecture and not displacement; contradicting the widely accepted fault thickness-displacement scaling relationship. I suggest that the architecture of dilational faults can be predicted by examining the host rock properties and using the data from this study have developed a framework that illustrates how ignimbrite host rock properties may affect deformation structures. Such frameworks for individual lithologies may be more useful in predicting fault zone properties as opposed to global scaling relationships. The results of this study have implications for conceptual models of fluid flow based on fault architectures predicted using the thickness-displacement relationship.

Table of Contents

Abstract ..... **i**

Table of Contents ..... **iii**

List of figures ..... **vi**

List of tables ..... **x**

Acknowledgments ..... **xii**

Declaration ..... **xiii**

Introduction **1**

1.1 Fault zone architecture 1

1.2 Fault initiation 2

1.2.1 Shear failure 4

1.2.2 Hybrid-Tensile failure 6

1.3 Evolution of fault zone architecture 8

1.3.1 Fault core and damage zone growth 9

1.3.2 Fault zone deformation structures 11

1.4 Aim of this study 13

1.5 Thesis outline 13

Geological setting & Ignimbrite descriptions **15**

2.1 Geology of Gran Canaria 15

2.1.1 Overview 15

2.1.2 Mogan Group 20

2.1.3 Caldera collapse structures 22

2.2 Ignimbrite characteristics & depositional processes 27

2.3 Host rock descriptions & methodology 34

2.3.1 Methodology 34

2.3.2 Ignimbrite A 42

2.3.3 Ignimbrite B 50

2.3.4 Ignimbrite X 61

2.4 Summary 65

Ignimbrite A: analysis of fault zone architecture **68**

3.1 Aim 68
3.2 Ignimbrite A 68
3.2.1 Protolith 68
3.2.2 Fault architecture 68
3.3 Comparison of fault zone architecture 84
3.3.1 Damage zone 84
3.3.2 Fault core width 87
3.3.3 Fault core elements – Clast morphology 88
3.4 Summary 90

Ignimbrite B: analysis of fault zone architecture 91
4.1 Aim 91
4.2 Ignimbrite B 91
4.2.1 Protolith 91
4.2.2 Fault architecture 91
4.3 Comparison of fault zone architecture 102
4.3.1 Damage zone 102
4.3.2 Fault core width 105
4.3.3 Fault core elements – Clast morphology 106
4.4 Summary 109

Mechanism of fault initiation and evolution 111
5.1 Fault growth model 113
5.1.1 Ignimbrite A 113
5.1.2 Ignimbrite B 116
5.2 Discussion 118
5.2.1 Fault initiation 118
5.2.1.1 Joint orientation 118
5.2.1.2 Failure angle 124
5.2.1.3 Joint frequency and spacing 127
Fault core evolution 132
5.2.1.4 Fault core growth 132
5.3 Summary 138

Influence of ignimbrite petrophysical properties 140
6.1 Introduction 140
6.2 Controls on joint density 140
6.2.1 Mechanical layer thickness 140
6.2.2 Flaws 143
6.3 Influence of ignimbrite petrophysical properties 145
6.3.1 Mechanical layer thickness 145
6.3.2 Influence of flaws 155

6.3.3 Joint morphology 160
6.3.4 Clast morphology 162
6.4 Summary 167

Discussion 169

7.1 Comparison of fault growth models and architecture 169
7.2 Effect of host rock on fault growth and architecture 172
7.3 Effect of stress state on fault growth and architecture 176
7.4 Implications for fluid flow 178
7.5 Predicting fault architecture and hydraulics 185
7.6 Summary 195

Conclusions and future work 196

8.1 Conclusions 196
8.2 Future work 201

Appendix A: Figure and sample locations 203

Barranco de Tauro 203
Montana Cedro 204
Los Frailes 204
Thin section and SEM samples 205

Appendix B 206

References 214

List of figures

Figure 1: Mohr circles illustrating three failure modes 4
Figure 2: Shear fault initiation 5
Figure 3: Normal fault initiation in an tectonically extending setting 7
Figure 4: Processes that contribute to fault core growth 10
Figure 5: Geological map of Gran Canaria 16
Figure 6: Simplified geological map of Gran Canaria 17
Figure 7: Stratigraphic column and enlarged sections of geological map showing the geology of the three study sites and the orientation of the major faults examined at the locations. 18
Figure 8: Simplified stratigraphic column Gran Canaria showing units as they were erupted 19
Figure 9: Upper Mogan formation ignimbrite A, B and C 22
Figure 10: Gran Canaria caldera collapse structures and schematic development 23
Figure 11: Map showing ignimbrite flow directions 24
Figure 12: Emplacement of units across the concentric growth fault at Montana Cedro 26
Figure 13: Fabrics in densely welded ignimbrites 28
Figure 14: Flow fold in ignimbrite E of the Mogan group 31
Figure 15: Textures in thin section used to identify devitrification/VPA and VPC 33
Figure 16: Location image Los Frailes and Barranco de Tauro 35
Figure 17: Satellite image of Los Frailes location 35
Figure 18: Satellite image and photo of Barranco de Tauro 36
Figure 19: Satellite image of the western side of Montana Cedro. 37
Figure 20:Montana Cedro faults 37
Figure 21: Box and whisker plot. 41
Figure 22: Logs of ignimbrite A Tauro, Los Frailes and Cedro 42
Figure 23: 25cm^2 section of ignimbrite A flow unit A1. 44
Figure 24: A1 host rock in thin section 44
Figure 25: Sub-units in ignimbrite A 45
Figure 26: ignimbrite A host rock in thin section 46
Figure 27: Plane polarised light image of A2 material. 46
Figure 28: Stereonet of joints in ignimbrite A 47

Figure 29: Ignimbrite A host rock section 48
Figure 30: Minor faults in the upper surface of ignimbrite A 49
Figure 31: Log of ignimbrite B at Cedro, Tauro and Los Frailes 50
Figure 32: Ignimbrite B overlying ignimbrite A at Barranco Tauro 52
Figure 33: Foliation fabric in the base of ignimbrite B 53
Figure 34: Ignimbrite B host rock at Cedro in plane polarised light 55
Figure 35: Ignimbrite B from the unit base at Los Frailes in plane polarised light 55
Figure 36: Ignimbrite B from the unit base at Tauro in plane polarised light. 56
Figure 37: Ignimbrite B host rock 57
Figure 38: Orthogonal joints in unfaulted ignimbrite B at Los Frailes. 58
Figure 39: Stereonet of joints ignimbrite B protolith 58
Figure 40: Stepped joint in the base of ignimbrite B at Los Frailes. 59
Figure 41: Ignimbrite B host rock section 60
Figure 42: Ignimbrite X ~10 m from the fault core at Cedro 61
Figure 43: Ignimbrite X host rock in plane polarised light 62
Figure 44: Fault core log of ignimbrite X 63
Figure 45: Ignimbrite X fault core 64
Figure 46: Minor offset faults at Barranco Tauro 70
Figure 47: Barranco Tauro ignimbrite A fault and stereonet 71
Figure 48: Photograph and sketch of the TA2 footwall damage zone. 72
Figure 49: Joint in ignimbrite A TA2 damage zone 73
Figure 50: Ta2.5 fault core. 74
Figure 51: TA2.5 damage zone 75
Figure 52: C5 fault core log, stereonets and line transects 76
Figure 53: Ca5 fault 77
Figure 54: Ca5 fault core 78
Figure 55: Sub-unit A2 in thin section 78
Figure 56: C15 fault core log, stereonet and line transects 79
Figure 57: Ca15 fault core 80
Figure 58: Gouge and clasts in Ca15 fault core 81
Figure 59: Ca30 fault core log, stereonet and line transect 82
Figure 60: Ca30 fault core 83
Figure 61: CA30 damage zone 83
Figure 62: Joint spacing in ignimbrite A damage zone 84
Figure 63: Joint frequency in ignimbrite A damage zone 84
Figure 64: Stereonets for ignimbrite A host rock and damage zone joints 87
Figure 65: Log-normal plot of ignimbrite A fault core width vs. displacement. 87
Figure 66: Ignimbrite A clast size vs. displacement 88

Figure 67: Ignimbrite A fault core clast axial ratio 89
Figure 68: Tb2.5 fault core and stereonet 92
Figure 69: Tb2.5 damage zone 94
Figure 70: Cb5 fault core log, stereonet and line transect 95
Figure 71: C5 fault core 96
Figure 72: Cb15 fault core log, stereonet and line transect 97
Figure 73: C15 fault core 98
Figure 74: Cb22 fault core log, stereonet and line transect 99
Figure 75: Cb22 fault core 100
Figure 76: Cb22 fault wall 101
Figure 77: Joint frequency in ignimbrite B damage zone 102
Figure 78: Joint spacing in ignimbrite B damage zones 103
Figure 79: Stereonets for joints in ignimbrite B damage zones 104
Figure 80: Stereonet of joints in unfaulted ignimbrite B protolith at Tauro and Los Frailes 105
Figure 81: Ignimbrite B fault core width vs. displacement 106
Figure 82: Ignimbrite B fault core clast size vs. displacement 107
Figure 83: Ignimbrite B fault core clast axial ratios 109
Figure 84: Model of fault initiation and growth in Ignimbrite A, see text for discussion 115
Figure 85: Close up of TA0.17 116
Figure 86: Model of fault initiation and growth in ignimbrite B, see text for discussion. 117
Figure 87: Location map of stereonets showing host rock joints and damage zone joints 119
Figure 88: Fischer statistic method 121
Figure 89: Shear, tensile and hybrid failure modes 125
Figure 90: Line graphs of damage zone joint frequency 128
Figure 91: Damage zone joint spacing against displacement for a) ignimbrite A and b) ignimbrite B 130
Figure 92: Evolution and growth of faults. 131
Figure 93: Ignimbrite A fault core width against joint spacing and displacement. 133
Figure 94: Ignimbrite B fault core width against joint spacing and displacement. 136
Figure 95:Influence of joint orientation on fault wall morphology. 137
Figure 96: Fiamme at the top and bottom of Ignimbrite B Los Frailes 147
Figure 97: Graph of fiamme minimum axis and aspect ratio using the regression equation for Los Frailes. 149
Figure 98: SEM images of ignimbrite B Los Frailes 150
Figure 99:Influence of sub-mechanical layers on joint spacing 152
Figure 100: Los Frailes fiamme aspect ratio v joint spacing 152

Figure 101: Fiamme in ignimbrite B Cedro.....154
Figure 102: Fractures cutting fiamme, ...155
Figure 103: Joints in the A3 sub-unit of ignimbrite A at Cedro.....156
Figure 104: Thin section image of ignimbrite A subunit A1 157
Figure 105: SEM images of ignimbrite A 158
Figure 106:SEM images of ignimbrite X, Cedro 159
Figure 107: Joint morphology, ignimbrite B 160
Figure 108: Fiamme-joint interactions 161
Figure 109: Ignimbrite B fault core clast size vs. median joint spacing 162
Figure 110: Ignimbrite B fault core clast axis vs. mean joint spacing 164
Figure 111: Fracturing of ignimbrite B fault core clasts, in Cb22 fault 165
Figure 112: Ignimbrite A fault core clast size vs. median joint spacing 166
Figure 113: Effect of fracture geometry on fracture connectivity.....179
Figure 114: Dilatant and shear fault architecture 181
Figure 115: Log-log plot of a compilation of FC thickness-Displacement datasets 187
Figure 116: Controls on ignimbrite fault architecture 188
Figure 117: Stratigraphic log of proposed host repository horizons at Yucca Mtn 191
Figure 118: Stratigraphic log and host rock properties of Borrowdale Volcanic Group, Sellafield from the Nirex Report no 525.....194

List of tables

Table 1: Size grades of ignimbrite material and sedimentary equivalent 27
Table 2: Mechanical properties of ignimbrite A 43
Table 3: Mean dimensions and mean aspect ratios of Ignimbrite B fiamme, Los frailes 51
Table 4: Mean dimensions and mean aspect ratios of Ignimbrite B fiamme, Cedro 51
Table 5: Mechanical properties of Ignimbrite B 54
Table 6: Values of joint spacing in the ignimbrite A damage zone of each fault.... 85
Table 7: Values for ignimbrite A clast size populations in each of the Cedro fault cores 88
Table 8: Mean and median values of clast axial ratio for each of the three fault cores in ignimbrite A 89
Table 9: Fault core clast size in each of the Ig nimbrite B fault cores 107
Table 10: Clast axial ratios for clasts in each of the Ignimbrite B fault cores 108
Table 11: Ignimbrite A damage zone joint statistics, Cedro 121
Table 12: Ignimbrite B damage zone joint statistics, Cedro 122
Table 13: Ignimbrite A fault and damage zone joint statistics 123
Table 14: Ignimbrite B fault and damage zone joint statistics 123
Table 15: Predicted and actual failure angle for each fault in ignimbrite A and B 126
Table 16: Composition of ignimbrite A A1 flow unit 134
Table 17: Values for Ignimbrite A fault core widths and damage zone joint spacing 135
Table 18: S/Tf ratios from the literature divided into ranges, presented by (Bai and Pollard, 2000) 143
Table 19: S/T_f and FSR values for damage zone joints in ignimbrite A 145
Table 20: S/T_f and FSR values for damage zone joints in ignimbrite B 146
Table 21: S/T_f and FSR values for damage zone joints in ignimbrite X 146
Table 22: S/Tf for the basal portion of B 147
Table 23: Mean values of fiamme size, shape and abundance from 148
Table 24: Ignimbrite B fiamme regression analysis 148
Table 25: Layers are undersaturated, joints are more widely spaced then expected 151
Table 26: Fiamme dimensions, ignimbrite B Cedro 153
Table 27: Results of the regression analysis of fiamme in ignimbrite B at Cedro.

.....153
Table 28: Fiamme dimensions for two sample squares in A1 and one sample square in A3. 155
Table 29:Percentage porosity, pumice, phenocrysts and lithic content was 157
Table 30: Ignimbrite B joint spacing and fault core clast size 163
Table 31: Ignimbrite B fault core clast aspect ratio 165
Table 32: Ignimbrite A fault core clast size and joint spacing 166

Acknowledgments

Firstly I would like to thank my supervisor Zoë Shipton for giving me the opportunity to carry out this research at the University of Glasgow. I would like to thank her for her support, guidance, encouragement and the endless enthusiasm and energy she has for her students, research and science in general – inspiring and occasionally exhausting (!). I would also like to thank Dr. Val Troll for his advice and guidance during this project and showing me the wonderful geology (and restaurants) of Gran Canaria. Thanks also to the staff and postdocs in the Gregory building for all discussions, suggestions, technical help and general banter which was much appreciated. Thanks to all the postgrads who I have shared an office with for three years – their sage advice on good watering holes and eateries has played a pivotal role in the completion of this research. Jamie, Duncan, Paul and Dan, who have increased my knowledge of football, and other sundry sporting activities such as mountaineering, cricket and skiing tenfold, thank you it's been fun. Thanks to Kate and Davie for their friendship from the outset, there have been many good times from Burns night to the Clockwork orange, long may they continue!

A very special thank you must go to my two trusty field assistants. Dad and Errol thanks for climbing Cedro so many times and carrying rocks back down, driving me round, looking after me and putting up with my mood swings and more stressful moments. Without you this work would not have been possible.

Thanks to both my parents who have supported, encouraged and believed in me always; without them I would not have done so much. I would also like to thank my brother and sister-in-law for always welcoming me into their home, where the laughs, get-togethers (and whiskey) were a welcome relief from writing-up. Last but by no means least, Errol thank you. You have put up with my field stress to my writing-up stress and everything between. Your endless love and support has got me through it all.

Thank you all.

Declaration

The material presented in this thesis is the result of the independent research undertaken by myself between September 2004 and January 2008. This work was supervised by Dr. Zoë Shipton. All work by other researchers that is quoted in this thesis is given full acknowledgement in the text.

Aisling M. Soden

January 2008

1

Introduction

1.1 Fault zone architecture

Generally a fault zone is composed of a fault core surrounded by a damage zone (Caine et al., 1996). The fault core may contain one or more principal slip surfaces which accommodates most of the displacement. In the absence of a slip surface displacement is distributed across the fault core. The fault core material usually contains varying proportions of fine grained gouge and larger clasts produced by comminution and fracturing of the host rock respectively. The damage zone is the surrounding network of joints, veins, small faults and pressure solution seams that are mechanically related to the growth of the fault (Caine et al., 1996; Faulkner et al., 2003). The deformation structures formed depends on the lithification state of the material. In poorly lithified sediments the dominant deformation structure is the deformation band (Heynekamp et al., 1999; Rawling et al., 2001). Lithified sedimentary and crystalline rocks deform by brittle fracturing (Caine et al., 1996; Chester et al., 1993).

Characterization of these fault zone components is important in predicting bulk fault zone properties such as fault zone permeability and mechanical strength. The percentage of fault core and damage zone in a fault zone determines whether the fault will act as a conduit or barrier to fluid flow (Caine et al., 1996). The density and connectivity of deformation structures in the damage zone greatly affects the pattern and rate of fluid flow (Caine and Forster, 1999). The permeability structure of faults is vital to the production of hydrocarbons compartmentalised by fault zones, identification of ore deposits, CO_2 sequestration and the viability of proposed nuclear waste repositories. The latter is of particular interest to this study as proposed repositories at Yucca Mountain, Nevada and Sellafield, Cumbria are located in densely welded ignimbrites.

Elements of fault zone architecture such as slip surface width and the intensity of deformation around slip surfaces are important in models of earthquake rupture mechanics. In the thermal-pressurisation model (Wibberley and Shimamoto, 2005), frictional heating of the pore fluid in the slip zone generates excess fluid pressures and lowers the effective strength of the fault. The effectiveness of this slip-weakening mechanism depends upon the width of the slip zone, which

affects the rate of frictional heating and the slip-weakening distances (i.e. the critical distance over which the fault weakens). A planar fault segment with a narrow (<50 mm) low permeability slip zone is the most likely site for an earthquake rupture. The process of thermal pressurisation is less effective in wider slip zones and areas of diffuse deformation. The acoustic fluidisation model (Melosh, 1996) requires the fluidisation of a zone 1 to 20 cm thick. High levels of fracturing and comminution of fault rocks around fault surfaces reduces the rocks elastic moduli and increases the probability of fault slip (Bruhn et al., 1994). In the damage zone the creation of new fractures and/or slip on existing faults act as energy sinks, thus the width of the damage zone constrains the size of the energy sink.

As knowledge of fault zone architecture is vital to models of fluid flow and earthquake nucleation much work has been carried out to establish relationships from which these parameters can be predicted. Such as the scaling relationship between fault zone width and displacement or the affect of increasing confining pressure on fault architecture, these relationships will be discussed further in section 1.3.

In order to establish such relationships it is necessary to understand the deformation processes active during fault initiation and growth, the controls on these processes and how deformation can change through out the history of the fault. Some factors that affect deformation processes are the petrophysical properties of the host rock, confining pressure during faulting and the presence or absence of fluids. Examination of fault zones with a range of displacements and in various geological settings allows us to identify the deformation processes, and the lithological and environmental conditions influencing them. In the following sections I present current models of fault initiation and growth and the scaling relationships that have been based upon them.

1.2 Fault initiation

It is widely recognised that faults in the brittle upper crust initiate on opening-mode structures such as joints, veins or microcracks (Crider and Peacock, 2004; Myers and Aydin, 2004; Wilkins et al., 2001). Crider and Peacock (2004) identified structures as being either pre-existing or pre-cursory. Pre-existing structures formed during an earlier deformation event in a stress field unrelated to faulting; pre-cursory structures were formed in the same stress field as the fault. (Angelier, 1994) describes two types of isolated faults i.e. faults without linked segments at the mesoscale. “Neoformed faults” form and slip within the same stress field (e.g. faulted joints) and “inherited faults” are pre-existing planes of weakness that slip within a stress field different from the stress field in which they formed.

The stress field at the time of faulting controls the failure mode by which slip occurs (shear, tensile or hybrid failure). The failure mode in turn controls the fault formation mechanism and subsequent

fault evolution, thereby controlling the resultant fault architecture. The mode of failure is identified by the failure angle, which is the angle between the failure plane and the maximum compressive stress (S_1). For shear failure in competent rocks the failure angle is between 10°-20° and 15°-45° in less competent rocks (Figure 1a). The failure angle for tensile failure is zero (Figure 1b) and displacement is perpendicular to the joint surface. Dilatant faults where there is both vertical and horizontal movement are the result of hybrid failure. Hybrid failure angles are low (Figure 1c), and lie between 0° and the angle predicted by Equation 1, where f is the angle of internal friction (Ferrill and Morris, 2003).

$$? = +/- (45^{o} – f/2)$$

Equation 1: Prediction of shear failure angle from the angle of internal friction, where ? is the angle of she ar failure and f is the angle of friction.

(Ramsey and Chester, 2004) carried out a series of triaxial extension experiments at different confining pressures. They observed an increase in failure angle with confining pressure and a failure mode transition from tensile through hybrid to shear failure; hybrid failure formed fractures inclined 3^0 to 13^0 from S_1. They suggested that hybrid failure was a mixed mode of tensile and compressive stress states (Figure 1c). Hybrid failure forming dilatant faults is evident in true tensional settings such as mid-ocean ridges and continental rifts. Dilatant faulting also occurs in multilayer sequences composed of mechanically contrasting layers that alter the dip of the fault. Both of these situations are discussed further in section 1.2.2.

In the following sections I examine the mechanism of fault formation in contractional (shear failure) and extensional settings (tensile failure), and the fault architecture that forms as a result.

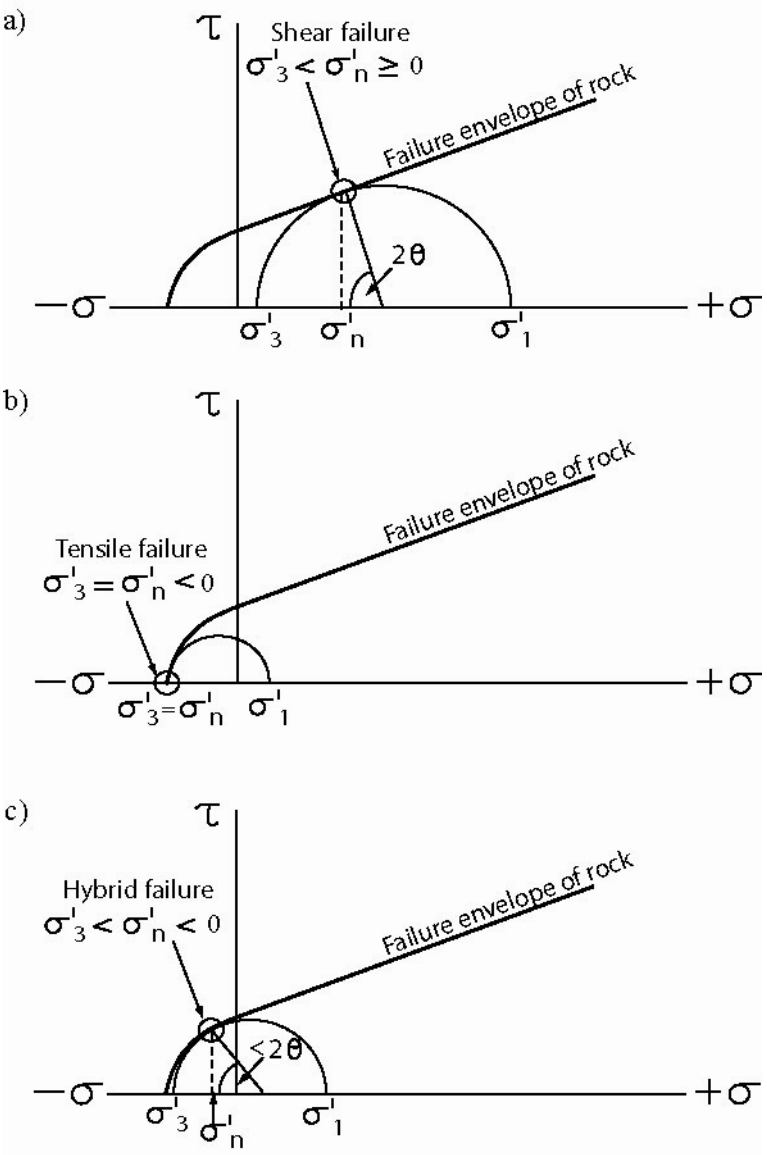

Figure 1: Mohr circles illustrating three failure modes

a) shear failure , b) tensile failure where s'3 = tensile strength of the rock c) hybrid failure, where s'3 < tensile strength of the rock. Diagram is adapted from Ferril and Morris (2003).

1.2.1 Shear failure

The initiation and development of faults failing in shear can be summarised as follows. A set of en echelon joints develop parallel to the greatest compressive stress (Figure 2a). Shear occurs on these joints resulting in the formation of splay-fractures at the joint terminations or cross-joints between closely spaced joints (Figure 2b & c). The secondary structures link the joints, which results in an increase of fault length and displacement. With increasing displacement pull-aparts and rock bridges are formed along the wing-cracks and cross-joints. The material is rotated, broken down and zones of brecciation are formed (Figure 2d). Shear is localised along this weakened zone and a through going slip zone is formed. The formation of splay-fractures at the joint tips requires a rotation of the regional compressive stress. The cross-joints form as a result of local perturbations of the regional stress field in the shear zone (Bai et al., 2002; Crider and Peacock, 2004).

This model describes fault nucleation in granites (Martel, 1990; Segall and Pollard, 1983), dolomites (Mollema and Antonellini, 1999) and sandstones with porosities from 18% to 24% (Myers and Aydin, 2004). A similar model is described for the nucleation of faults in limestone (Willemse et al., 1997), in this case however slip-planes initiate as pressure solution seams or veins. The development of the fault follows the same steps as above, but shear localization and development of a through-going slip plane is accommodated by pressure-solution seams as opposed to opening-mode cracks.

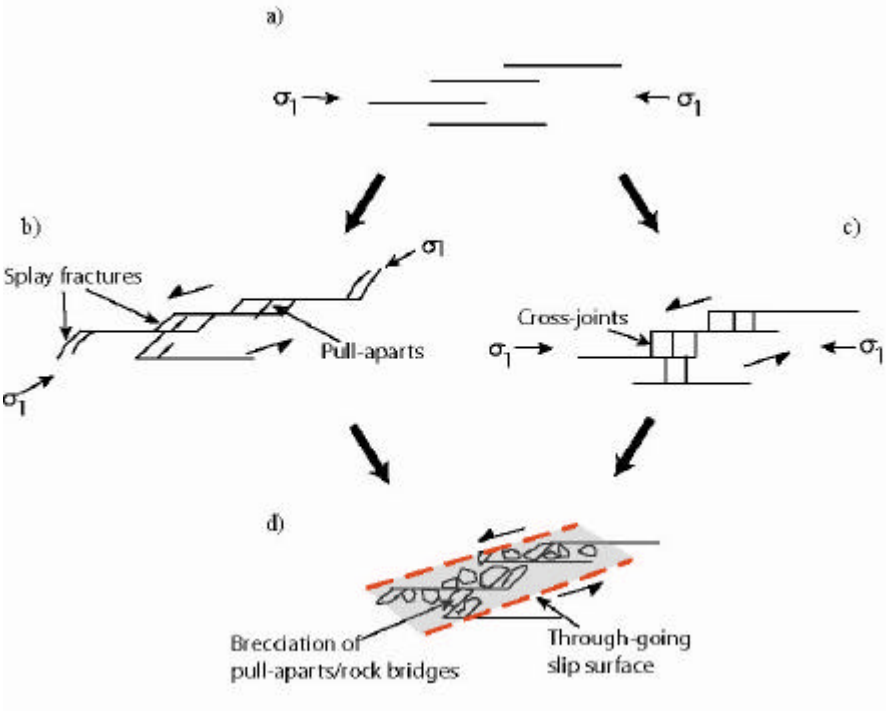

Figure 2: Shear fault initiation

a) Shear faults initiate as a set of en echelon or sub-parallel joints parallel to the maximum compressive stress (Myers and Aydin, 2004) b) rotation of stress causes shear on the primary joints producing splay fractures linking the primary joints and creating pull-aparts c) when there is no rotation of stress the rock bridges between the primary joints bend and fracture producing cross-joints (Mollema and Antonellini, 1999) d) subsequent deformation is accommodated by the fragmentation of the pull-aparts and rock bridges producing a through-going shear zone. Note the primary joints are at a high angle to the shear zone.

Although host rock composition can affect the deformation elements formed, ultimately the formation mechanism is the same and in general faults formed by this mechanism consist of the same fundamental structural components: joints, sheared joints, zones of fragmentation and slip surfaces (Myers and Aydin, 2004). The initial sheared joints are at a high angle to the shear zone due to the stress rotation. During subsequent faulting joints open oblique to the fault and indicate the orientation of the regional compressive stress at the time of faulting (d'Alessio and Martel, 2005).

1.2.2 Hybrid-Tensile failure

The previous model of fault initiation has been based on contractional stress systems. Investigations of fault formation in tectonically extending regions has been limited and mainly focused on kilometre scale fault systems such as the Ethopian rift system (Acocella et al., 2003) and Iceland (Grant and Kattenhorn, 2004; Gudmundsson, 1992). There are two theories regarding the nucleation and propagation direction of normal faults in tensional settings. The development of normal faults from tension fractures propagating downwards has been examined by Gudmundsson (1992) and Acocella et al. (2003). They suggest that a tensile joint opens at the surface and propagates along its strike and dip (Figure 3 A1). At a critical depth of ~0.5 km the vertical component at the tip of the propagating joint equals the tensile strength of the rock, inhibiting pure tensile behaviour and thus further opening of the join t (Figure 3 A2). The stress conditions at the tip switch from extensional to shear failure and a normal fault is formed. At this point the dip of the fault changes from vertical to a more typical normal fault dip (Figure 3 A3). The converse of this model is that normal faults nucleate in the subsurface and propagate upwards (Figure 3 B1) (Grant and Kattenhorn, 2004). As the fault propagates upwards a vertical tension fracture forms at the faults' upper tip (Figure 3 B2). The fracture propagates to the surface (Figure 3 B3) and subsequent displacement causes dilation of the fracture (Figure 3 B4).

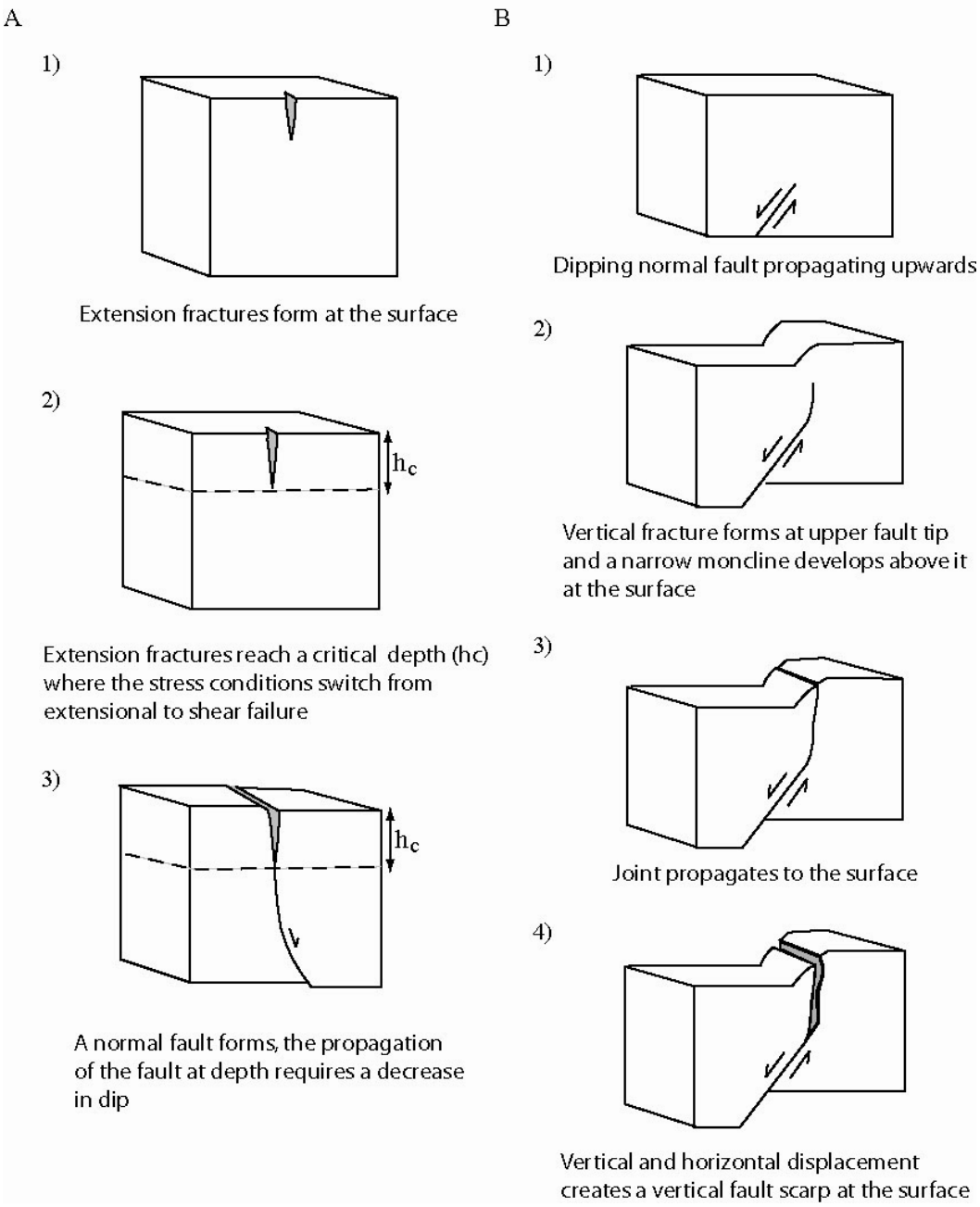

Figure 3: Normal fault initiation in an tectonically extending setting

A) Downward fault propagation (figure from Acocella et al. 2003) 1) Extension fractures form at the surface, propagating downwards and along strike 2) the fracture reaches a critical depth below which tensile stresses cannot be sustained 3)the failure mechanism switches from tensile to shear failure and the fracture becomes a normal fault. B) Upward fault propagation (figure adapted from Grant and Kattenhorn, 2004) 1) a dipping normal fault initiates and propagates upwards 2) a fracture forms at the tip of the fault and a monocline forms at the surface above the fault tip 3) the joint propagates to the surface and breaches the monocline at the upper hinge 4) the vertical and horizontal displacements dilate the fault and create a vertical fault scarp.

Regardless of the direction of fault propagation, dilatant faults share similar characteristics. Both the faults and surrounding extension fractures are vertical or near vertical at the surface and the faults have dialtional as well as vertical displacements (Grant and Kattenhorn, 2004). Acocella et al. (2003) reported extension fractures with 4 m of dilation and normal faults with a minimum

opening of 2 m. They also noted that parts of the normal faults were pure extension fractures. Holland et al. (2006) carried out analogue modelling of dilatant normal fault evolution; their results corresponded with field observations of volcanic growth faults in the basalts of Hawaii. At the onset of extension dilatant fractures propagated from the surface downwards, some of these fractures become inactive and others developed into dilatant normal faults. They observed that during faulting unstable fragments of the fault wall fell into the open fault and was reworked during subsequent displacement. The dominant deformation processes active during faulting were "brecciation, block rotation and gravitational transport of fragments along the fault" (Holland et al., 2006).

Dilational faulting can also occur in compressional settings, related to the interaction of two sub-parallel fault tips forming extensional oversteps or faulting in layers with contrasting competencies. Extensional oversteps are associated with block rotation and pull-aparts that may be filled with breccia or mineral precipitates. Faults that initiate in brittle layers as extension fractures are refracted in the adjacent ductile layers thereby forming pull-aparts in the brittle layer (Ferrill and Morris, 2003; Peacock and Zhang, 1994). Schopfer et al. (2006) examined fault formation in multilayer sequences of alternating strong and weak layers. They found that faults localise in the strong, brittle layers and are later linked via the weak, ductile layers. The vertical faults formed in the strong layers are linked by ~50^0 dipping faults in the weak layers, resulting in an average fault dip of ~60^0. The refraction is due to extensional failure in the strong layer and shear failure in the weak layers. The influence of lithology on fault architecture is discussed further in section 1.3.2.

1.3 Evolution of fault zone architecture

As I discussed in section 1.1 understanding the deformation elements the fault zone is composed of, such as fault core width or connectivity and intensity of damage zone joints is central to making predictions about the behaviour of the fault zone. In an attempt to predict fault architecture, scaling relationships have been proposed that correlate the development of the fault zone with displacement. However fault zone architecture is not solely a product of displacement accumulation. Other factors influence the deformation processes active within the fault and the development of the fault deformation elements, these factors can be of greater importance to the evolution of the fault architecture than displacement. In the following sections I review some of the scaling relationships for fault zone evolution, followed by an examination of the factors other than displacement that influence fault architecture.

1.3.1 Fault core and damage zone growth

The simplest deformation mechanism for fault core growth is the attrition and abrasion of the opposing fault surfaces during frictional sliding producing wear material (gouge and breccia). This is the wear model proposed by Scholz (1987) and predicts that the thickness of the gouge zone for brittle faults will increase linearly with displacement. Hull (1988) also presented displacement-thickness data in quartzofeldspathic rocks that showed an increase in fault thickness with displacement. However some authors have found problems with this relationship. (Blenkinsop, 1989) and (Evans, 1990) argued that the data from many fault populations in a wide range of lithologies on which the relationship was based, covered too broad a range of lithologies and structural settings as to be reliable. They suggested that data from individual faults or from faults with a common evolution should be used for the purpose of establishing a scaling relationship. (Shipton et al., 2006)observed that the data used by Scholz (1987) and Hull (1988) often did not state how net displacement was calculated or in what direction fault thickness was measured relative to the slip vector. Furthermore fault thickness values vary by three orders of magnitude for a single displacement value.

Power et al. (1988) suggested that fault core expansion occurred through a process of asperity grinding. Displacement of two opposing rough surfaces causes a mismatch between them, isolating and breaking down asperities to form breccia and gouge (Figure 4b). The amount of mismatch between the two surfaces increases with slip isolating increasingly larger asperities thus producing greater volumes of wear material. Power et al. (1988) proposed that due to the self-similar roughness of the fault surfaces the volume of mismatched asperities would increase in proportion to the amount of displacement. However, where the largest asperities are juxtaposed contact points will occur and the thickness of wear material will be much less than predicted by the linear relationship.

Childs et al. (1996) suggested that tip-line and asperity bifurcation leads to complex fault cores with several slip planes. The propagation of an irregular fault tip-line results in the bifurcation of the tip-line and formation of two sub-parallel slip surfaces. With continued propagation, the two slip surfaces re-join enclosing a lensoid body of rock. Segmentation of the tip-line can occur at a variety of scales and isolate rock lenses of varying sizes. Childs et al. (1996) also invoke a larger scale expression of Power et al. (1988) asperity grinding as a mechanism of fault growth, which they refer to as asperity bifurcation. Irregularities on a slip surface are sheared of by the propagation of a new slip surface causing widening of the fault core. Both these processes cause intermittent thickening of the fault core and localised thinning of the core may occur (Figure 4c).

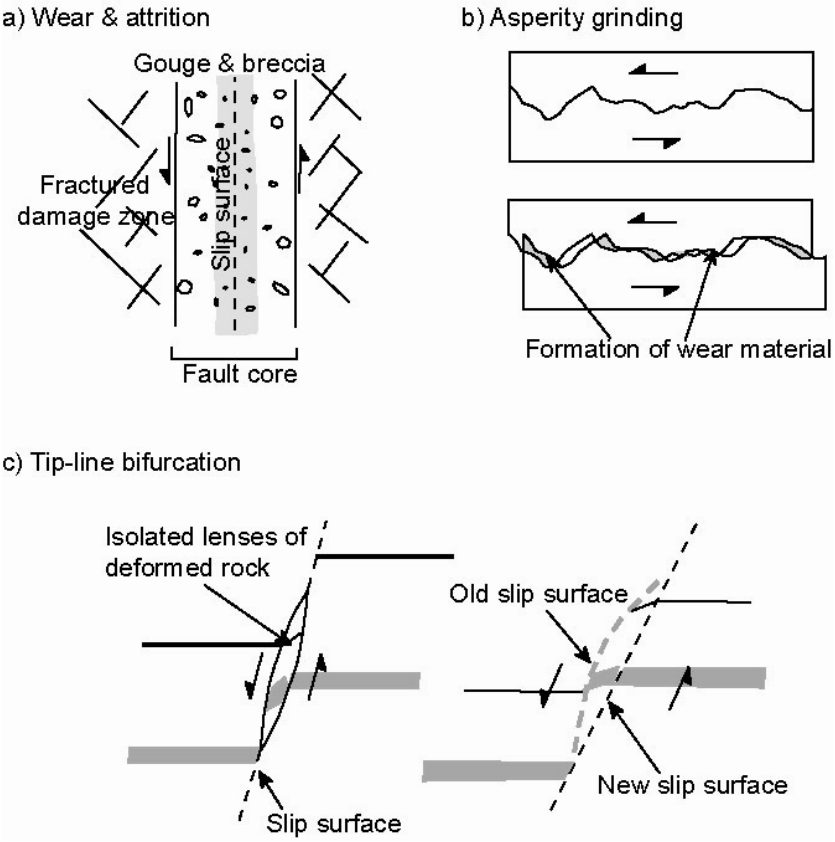

Figure 4: Processes that contribute to fault core growth

a) Wear and attrition of the walls in the fault core will result in widening of the core (Scholz, 1987) at the expense of the surrounding damage zone. Wear and attrition of clasts in the fault core will result in a decrease in grain size and sorting of the fault gouge b) Grinding of geometrical irregularities will result in smoothing of the fault walls and incorporation of material into the fault gouge (Power et al., 1988). c) Multiple fault strands could be gene rated when a propagating tip bifurcates around an asperity (Childs et al., 1996).

The fault growth models of Power et al. (1988) and Childs et al. (1996) indicate how geometric irregularities of the fault walls and slip surface can lead to variations in fault core thickness. Other factors can also alter fault architecture and are discussed further in the following section.

The development of the fault damage zone is also linked to increasing displacement. As displacement accumulates there is an increase in the frequency and connectivity of joints in the damage zone (Caine and Forster, 1999). The intensity of damage increases towards the major slip plane as fracturing is mechanically related to fault movement (Antonellini and Aydin, 1994; Micarelli et al., 2006; Sagy et al., 2001). Wide damage zones are considered to represent multiple episodes of slip and overprinting of deformation structures from successive slip events (Caine et al. 1996).

There are fault zones in which neither fault core width nor damage zone width relate to displacement. Shipton and Cowie (2001) identified deformation band faults in which fault core thickness was independent of displacement and varied significantly along strike. The width of the

damage zone did increase with displacement therefore deformation was being accommodated in the damage zone despite the formation of a through-going fault. Micarelli et al. (2006) showed that growth of the damage zone in high porosity carbonates is retarded once the fault core reaches a certain width. He suggested this was due to strain–softening in the fault core accommodating most of the strain. Therefore factors other than displacement play a role in the evolution of the fault zone.

The wear material within the fault core, the gouge and breccia is affected by increasing displacement. In general as displacement increases i.e. as the number of fracturing events increase, the grains in the fault core decrease in size and change shape (Billi and Storti, 2004; Blenkinsop, 1991; Engelder, 1974). A study of fault gouge particles made by Sammis et al. (1987) revealed a great degree of self-similarity between the particles. They proposed that this self-similarity was a result of repeated tensile splitting of the grains and the grains most likely to split where those that had nearest neighbour particles of the same size. This process of "constrained comminution" they suggested maintains the self-similarity of the fault gouge. Billi and Storti (2004) investigated the particle size distributions of fault gouge from faults cutting carbonate rocks. They found that the particle size distribution varied within the fault core and suggested this was due to the evolution of the cataclastic process through time and space. In the initial stages of displacement the dominant deformation process was particle fracturing. With increasing displacement and cataclasis the particle size was reduced and the particle size distribution was similar to that observed in the constrained comminution model (Sammis et al., 1987). Finally shear localization at the fault boundaries formed extremely fine-grained gouge through rolling-induced particle abrasion.

Mechanisms of fault zone evolution and models used to predict fault zone architecture have displacement as the controlling factor. But as I mentioned in section 1.1 the deformation processes active during faulting are influenced by other factors such as lithology and confining pressure. As the deformation processes are responsible for fault growth the influence of these factors should also be taken into account when considering fault evolution and architecture. In the following section I discuss the influence lithology and confining pressure has on fault architecture.

1.3.2 Fault zone deformation structures

The deformation structures that form in a fault zone are highly dependent on the host rock lithology. High porosity sandstones deform by cataclasis and form deformation bands. At lower porosities brittle fracturing, fragmentation and brecciation are dominant and form joints and shear joints (Antonellini and Aydin, 1995; Davatzes et al., 2005). Similar processes of deformation were found in ignimbrites (Wilson et al., 2003). Welded, low-porosity ignimbrites formed joints and non-welded high-porosity units formed deformation bands. Ignimbrites that were non-welded but

had undergone porosity reduction, due to vapour phase alteration (secondary mineral precipitation), formed either deformation bands or joints depending on the degree and type of secondary alteration.

Changes in confining pressure also influence the fault zone architecture. In laboratory experiments Patton et al. (1998) investigated the affects of confining pressure on single layer and multi-layer limestone specimens. At 100MPa (3.7 km depth) the single layer specimen behaved in a brittle manner, fewer faults were formed and these had more irregular profiles compared to the equivalent displacement at 200 MPa (7.3 km depth). At 100 MPa through-going faults formed at very small displacements and were composed of an array of several smaller linked faults. For the same amount of displacement but at 200MPa confining pressure, arcuate faults were generated in the hanging wall that steepened upwards and died out. Several arcuate faults formed prior to establishment of a through-going fault and resulted in an upward widening fan of nested faults (Patton et al., 1998). The mechanical strength of the layer is altered with increasing confining pressure, at high confining pressures (>100 MPa) strong layers will fail in shear rather than in tension (Schopfer et al., 2006).

When Patton et al. (1998) incorporated multiple layers into their model at 100 MPa confining pressure the bulk ductility of the specimen increased. The faults propagated by the linkage of isolated fractures in each of the layers and the resultant fault architecture was composed of slightly nested arcuate faults that fanned out moving upwards, reminiscent of the fault geometry produced at 200 MPa. Schopfer et al. (2006) examined normal faults cutting dipping multi-layers using numerical and analogue modelling. They found that when bedding is dipping and has a different strike to the fault zone the fault will exhibit along strike refraction.

As mentioned in section 1.2.2 the strength contrast between mechanical layers controls fault dip; faults in the strong layers dip steeply but the dip becomes much shallower in the weaker layer (Ferril and morris, 2003). The result of changes in dip between strong and weak layers forms pull aparts, fault bends and complex fault cores (Schopfer et al., 2006; Watterson et al., 1998).

It is clear that mechanisms of fault initiation and evolution are not controlled solely by displacement. The deformation processes active during faulting are controlled by a number of physical factors such as lithology, regional and local stress state, confining pressure, cementation and host rock properties such as porosity, heterogeneity, mechanical strength, unit thickness and fabric. The interaction between petrophysical and environmental factors produces complex fault zone architectures. Overtime these factors may change and different combinations may dominate thereby altering the deformation processes active in the fault and thus fault zone evolution and architecture.

Generalised scaling laws and models that isolate one factor e.g. displacement, as the primary

control on deformation process and fault evolution are oversimplified and will not make accurate predictions about the permeability or strength of a fault. In order to make accurate predictions of fault zone properties it is necessary to know not only how each physical factor influences deformation processes, but how factors influence and interact with each other to change the fault deformation processes. Different models of fault initiation may be invoked depending on the lithology and conditions under which the rocks are faulted, the development of the fault over time will reflect changes in the physical environment.

1.4 Aim of this study

This study examines fault initiation and evolution in ignimbrite units with different petrophysical properties on the island of Gran Canaria, Spain. The aims of the investigation were:

- Identify the deformation processes active and deformation elements present as these faults accumulate displacement. This is made possible by the occurrence of fault populations that have displacement from centimetres to tens of metres. This is the classic "space-for-time" substitution.
- Identify the controls on deformation processes and consequently the controlling factors on fault growth. The juxtaposition of petrophysically different ignimbrite units, having undergone the same amount of displacement means that displacement can be excluded as being responsible for different fault architectures. Variations in fault elements between ignimbrite units are therefore a result of host rock characteristics.
- Construct a model for the initiation and evolution of faults in moderately and densely welded ignimbrites based on faults observed in two ignimbrite units on Gran Canaria.
- Compare the fault growth models and scaling relationships developed in this study with previously established models and relationships e.g. displacement scaling relationship.

The field data shows how the tectonic regime, pre-cursory structures and host rock properties influence the mechanism of fault formation, fault core evolution, fault morphology and breccia clast size.

1.5 Thesis outline

Chapter 2 provides an account of the geological history of the island of Gran Canaria and the formation of the ignimbrite units investigated in the study. An overview of ignimbrite depositional processes are presented and the methodology used in the recording and analysis of the field data. This is followed by a detailed description of each of the ignimbrite units examined, their field

characteristics, petrology and deformation structures.

Chapter 3 and **Chapter 4** present an analysis of the fault zone architecture (fault core width, morphology, fault core material and damage zone) in two different ignimbrite units (Chapter 3, ignimbrite A; Chapter 4, ignimbrite B). The components of each fault are then discussed in relation to fault displacement.

Chapter 5 presents the fault initiation and evolution models for each of the studied ignimbrite units. Followed by a discussion of the evidence upon which these models are based and the factors that influence fault core growth.

Chapter 6 examines in detail the influence the petrophysical properties of the ignimbrite units have on fault zone architecture. The affect mechanical layer thickness and flaw density has on joint formation, the control material strength has on fault core growth and the nature of the fault core material is discussed.

Chapter 7 compares the ignimbrite fault model to established models of fault initiation and growth and the implications my results have for established scaling relationships and the conceptual models based upon these. The likely effect that these fault architectures will have on fluid flow through ignimbrites is also discussed.

Chapter 8 lists the conclusions of the study and presents recommendations for future work.

Results from ignimbrite B and the model of fault formation in ignimbrite B (Chapters 4 and 5) have been submitted for publication to Geology (The evolution of fault zone architecture in dilational faults: Gran Canaria, Spain). The ignimbrite B model of fault formation and the influence of pre-exiting joints and host rock fabric on fault architecture have been presented at EGU 2007. The discussion on fault core thickness scaling has been presented at TSG 2006 and has partly been published in: Shipton, Z. K., Soden, A. M., Kirkpatrick, J. D., Bright, A. M., and Lunn, R. J., 2006, *How thick is a fault? Fault displacement-thickness scaling revisited*: Geophysical Monograph Series. The paper is included as an appendix in this thesis.

2

Geological setting & Ignimbrite descriptions

2.1 Geology of Gran Canaria

In order to understand the processes of fault growth it is necessary to understand the stress system in which the faults formed and also the petrophysical properties of the rocks being faulted. The stress state at the time of faulting is relevant to the mechanisms of fault initiation and growth, and requires an understanding of the regional tectonic setting. The host rock properties affect the style of deformation and the deformation mechanisms. In Gran Canaria the host rock properties are a result of ignimbrite emplacement processes and the composition of the ignimbrite material. In the following sections I give a brief overview of the structural and stratigraphical evolution of Gran Canaria and the processes of ignimbrite emplacement; followed by a more detailed account of the ignimbrite units pertinent to this study.

2.1.1 Overview

The island of Gran Canaria (Figure 5 and Figure 7) is a multicyclic caldera and has been volcanically active intermittently throughout the past 15 my (Schmincke, 1998). The geology of the island can be subdivided into three volcanic phases or cycles of activity that correspond to the evolution and differentiation of the magmatic source from which the island was erupted (Figure 6).

The first cycle was the Miocene volcanic phase (15 Ma to 9 Ma) which itself consists of three stages of activity (Figure 8). The initial shield volcano building stage from 16 to 14 Ma erupted alkalic to tholeiitic basalts that comprise more than 90% of the volume of the island. The basaltic shield volcano is thought to have become subaerial at 14.5 Ma. At 14 Ma caldera collapse triggered the explosive eruption of more evolved magmas. This eruption generated in excess of 150 km^3 of trachytic and rhyolitic rock known as the Mogan Group, over a 0.6 m.y. period and formed a caldera 20 km in diameter. Over the next 4 m.y. more than 500 km^3 of silica-undersaturated trachyphonolitic volcanic material was erupted, accompanied by the intrusion of a large cone sheet swarm in the centre of the caldera; this material forms the Fataga group.

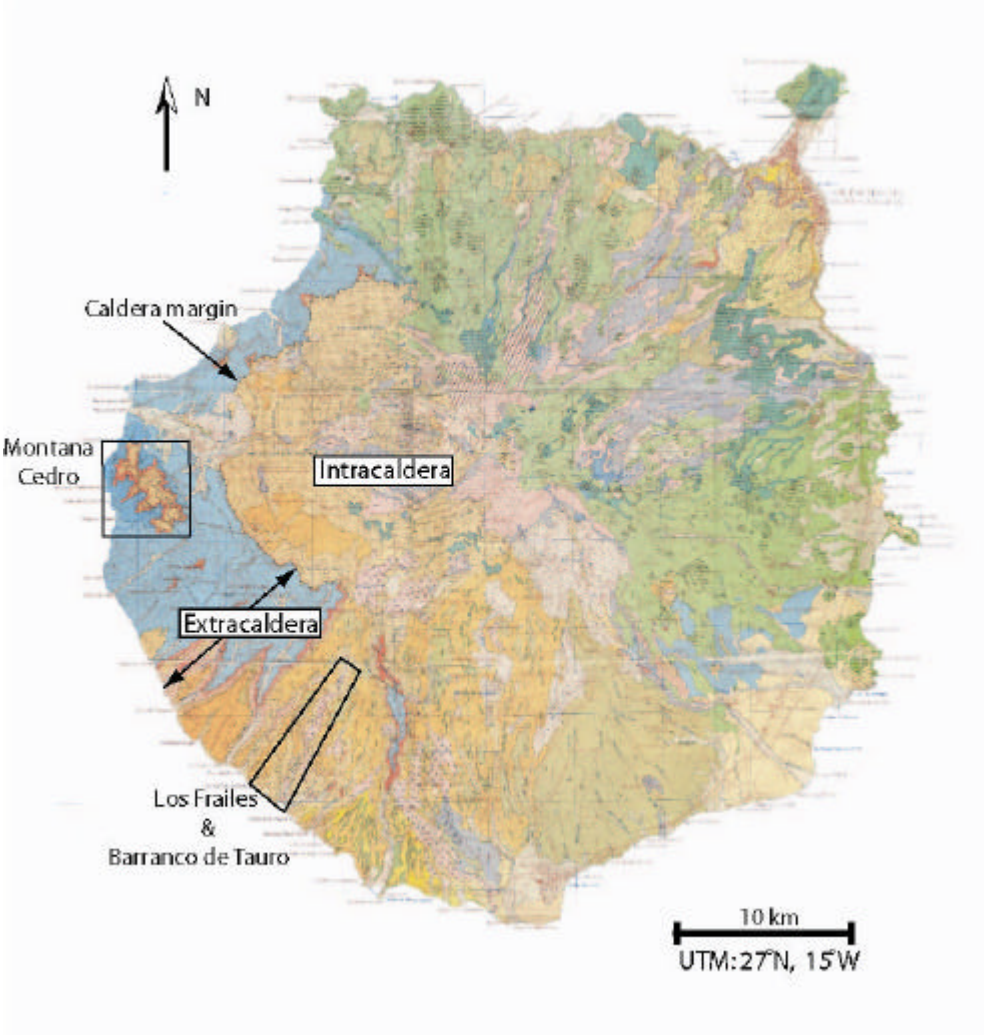

Figure 5: Geological map of Gran Canaria

The lithologies of the island are divided into intracaldera and extracaldera. Extracaldera are dominantly ignimbrite units interbedded with lavas. Intracaldera units comprise ignimbrites but also intrusive units such as cone sheets. The field sites investigated in this study are located in extracaldera lithologies at Montana Cedro, Los Frailes and Barranco De Tauro. Enlarged views of these sites and a simplified stratigraphic column and colour key are shown in Figure 7. Satellite image of the study areas are found in section 2.3 (Map from Mapa Geologico De Espana, Instituto Tecnologico GeoMinero de Espana, Isla De Gran Canaria)

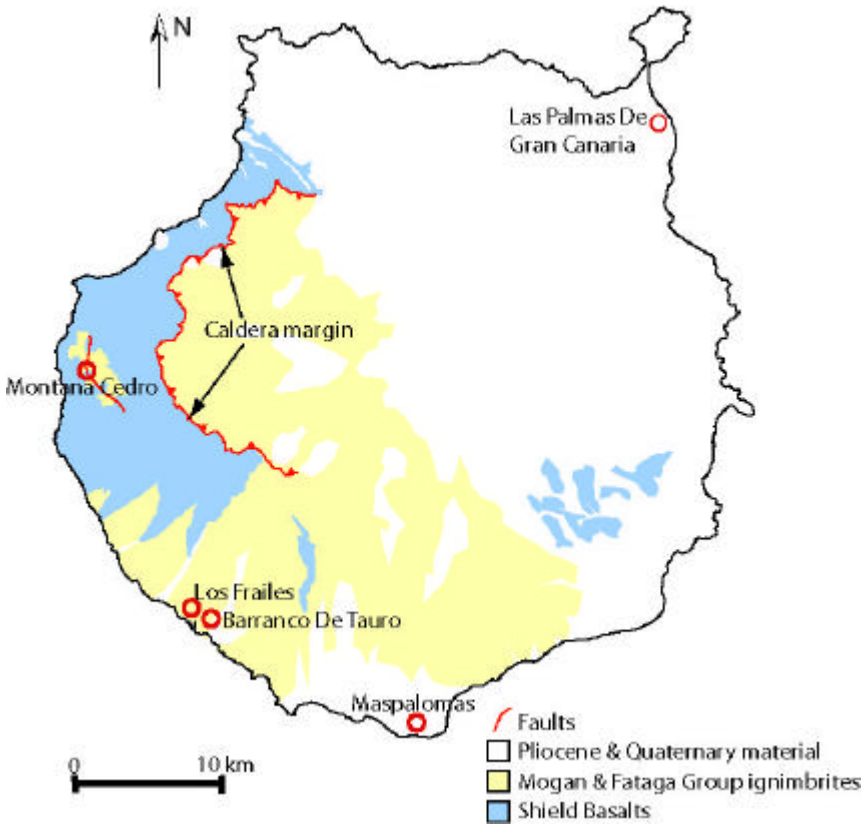

Figure 6: Simplified geological map of Gran Canaria

The map shows the aerial extent of the shield volcano basalts and the Miocence Mogan and Fataga pyroclastic flows. The north-east part of the island is covered with Pliocene volcanics and debris flows of the Roque Nublo group and younger Quaternary scoria cones and lapilli beds. The caldera perimeter and the extracaldera concentric fault at Montana Cedro are also shown. (Map modified from Mapa Geologico De Espana, Instituto Tecnologico GeoMinero de Espana, Isla De Gran Canaria)

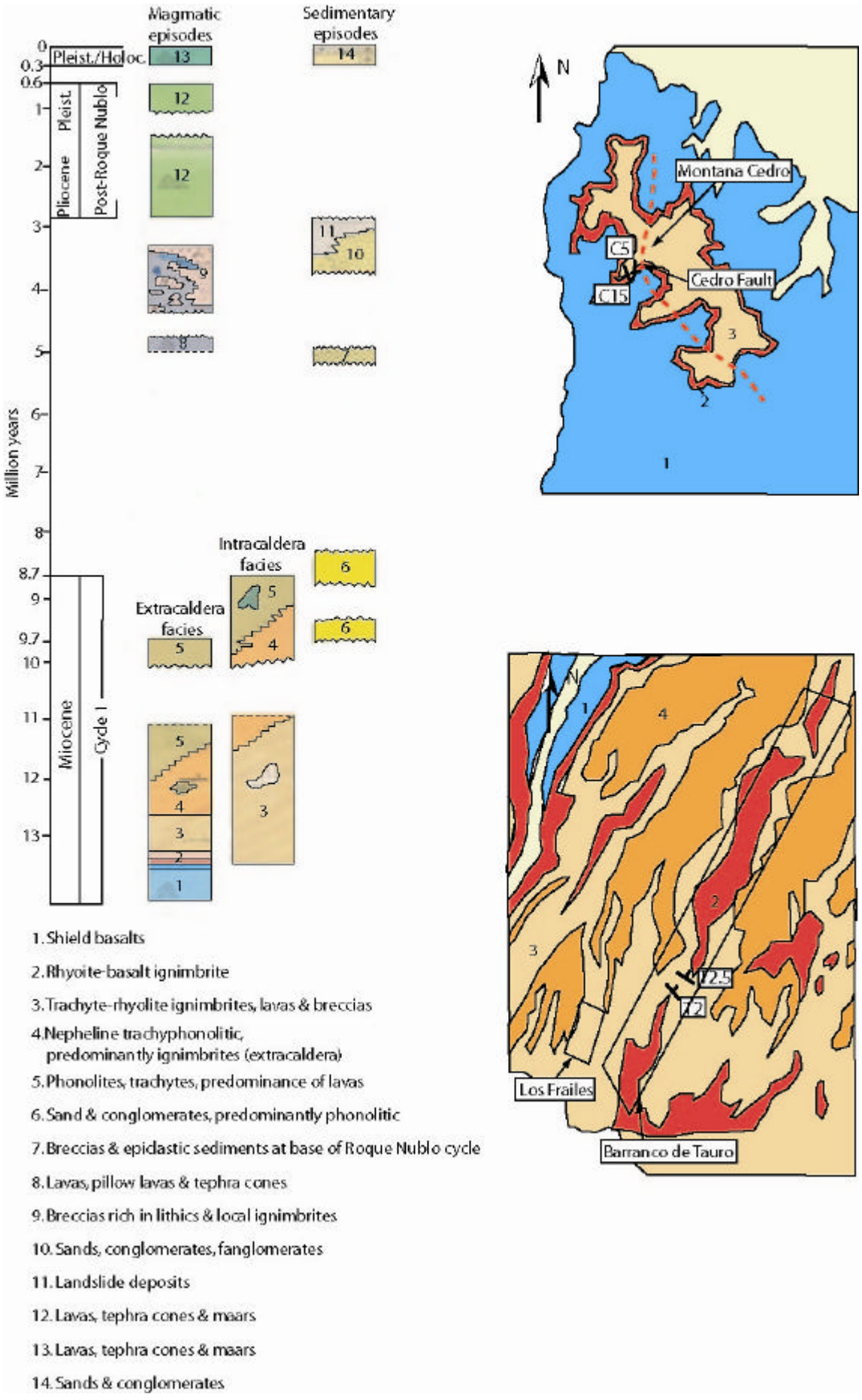

Figure 7: Stratigraphic column and enlarged sections of geological map showing the geology of the three study sites and the orientation of the major faults examined at the locations.

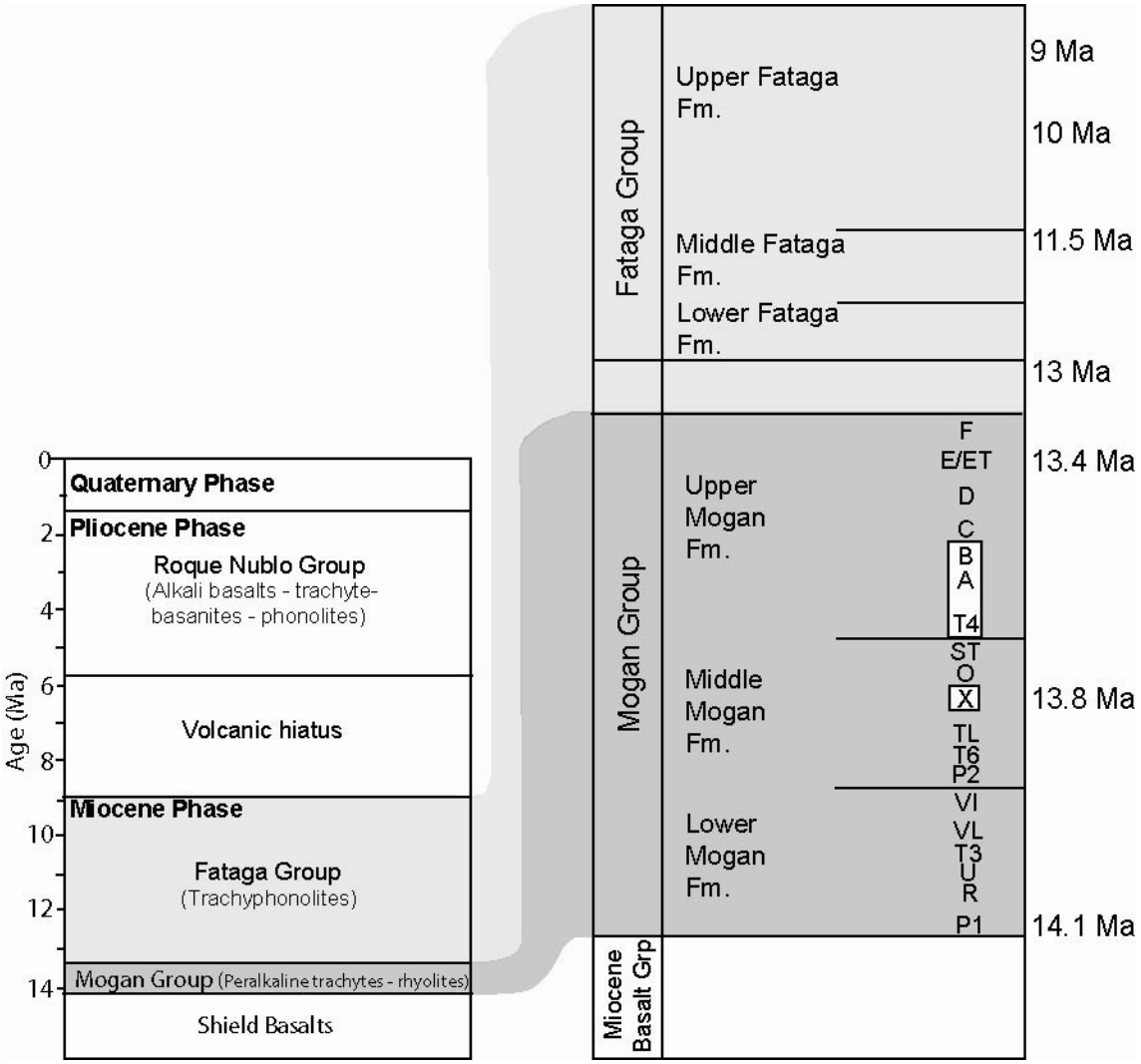

Figure 8: Simplified stratigraphic column Gran Canaria showing units as they were erupted Volcanic activity is divided into three cycles: Miocene phase, Pliocene phase and the Quaternary phase. The Miocene phase is subdivided into Mogan and Fataga groups. The ignimbrite units investigated in this study are part of the Mogan group ignimbrites and are highlighted in white (adapted from Schmincke, 1998)

After a hiatus in magmatic activity of 3 m.y. the second cycle, the Pliocene volcanic phase, began at 5 Ma with the eruption of ultrabasic and basic lavas (nephelinites, basanites and tholeittes) that became increasingly silica saturated, ranging from alkali basalts, phonolites to trachytes. The lavas are interbedded with pyroclastic flows and lithic-rich pumice flows, which in turn are intruded by trachytic and phonolite domes. The construction and destruction of a high stratocone took place between ca. 4.5 and 3.5 Ma. Collectively these volcanic facies are called the Roque Nublo group.

The final phase of volcanic activity, the Quaternary volcanic phase, was confined to the northern half of the island. From 3.2 Ma several hundred meters of highly undersaturated nephelinitic and basaltic lava flows and scoria cones were erupted in the northern and north-eastern half of the island. The youngest of these cones and lava flows were erupted ~0.01 Ma and one cinder cone has

been dated at 3500 BP

The evolution of the source magma during the eruption of the material has resulted in distinct compositional and physical differences between different eruptive packages upon which the stratigraphy of the area has been defined. The most useful distinguishing features in the field are colour of the ignimbrite material, degree of welding (flattening of fiamme), type and abundance of lithic and/or phenocryst. In many cases a vitrophyre marks the base of each individual ignimbrite package although some flow packages may be composed of a number of smaller flow units that also have a basal vitrophyre. In cases such as these the colour of the material, lithic and phenocryst type are the critical features used to identify the unit. The units are also distinguishable through their chemical composition. The eruptive material evolves from a mafic to more felsic composition moving up through the Mogan group. Chemically the Fataga group differs from the Mogan by lower silica and higher Al_2O_3,K_2O, CaO, MgO and Nb concentrations (Schmincke, 1998). The criteria used to distinguish the units involved in this studied are presented in the following section.

2.1.2 Mogan Group

The ignimbrite units focussed on in this research are part of the Mogan group (Figure 8). Here I give a more detailed account of the formation of the group so as to place the studied ignimbrite units in context and the general physical attributes used to distinguish the ignimbrite units in the field. This is followed by a detailed description of the petrophysical characteristics of the particular units in this study. The stratigraphy used here is from Schmincke (1998)

The Mogan group contains more than 20 trachytic to rhyolitic extra-caldera ignimbrites (Troll et al., 2002) and is subdivided into three formations (Figure 8). The Lower Mogan formation contains the pyroclastic flows P1, R, U, VL, VI and a basalt, T3, that was erupted between flows U and VL. The eruption of P1 at 14.1 +/-0.1 Ma (Bogaard et al., 1988) occurred synchronously with caldera collapse and was the first large volume eruption of silicic magma, covering an area of more than 400 km^2 (Schmincke, 1998). Ignimbrite P1 is zoned from rhyolitic tuff containing trachytic fiamme and quenched basalt inclusions in its lower part, to basalt tuff, columnar and clastic basalt at the top of the cooling unit. The rhyolitic part of the unit has a fine-grained and crystal poor basal portion, changing to inclusion rich with large anorthoclase crystals moving upwards. The large anorthoclase phenocrysts in a fine-grained dark grey matrix are the most distinguishing feature of the P1 unit. P1 marks the change in magmatic evolution from mafic basaltic shield magmas to more silica-saturated peralkaline magmas and heralds the onset of explosive silicic ignimbrite and lava eruptions.

Units after P1 are compositionally peralkaline, trachytic to low-silica rhyloitic ignimbrites. The degree of magma differentiation increases moving up through the Mogan sequence, the volcanic

material becoming more potassium rich until the end of the middle Mogan. The middle Mogan formation contains ignimbrite units P2, TL, O and X, basalt T6 occurs between P2 and TL. The P2 unit is red-brown, highly indurated and contains thick columns and red lava lithic inclusions. The fiamme are dark with large partially resorbed plagioclase phenocrysts within them. Ignimbrite TL is strongly welded, dark grey-brown and locally has an irregular lava-like surface due to surface brecciation. Fiamme are either dark with plagioclase phenocrysts or pumiceous. Ignimbrite X is a light cream to light green colour, extremely rich in large millimetre size crystals and poor in number of fiamme. Ignimbrite O is light green, contains less crystals than ignimbrite X but more than the overlying ignimbrites. Again the unit is fiamme poor but those that are present are dark and contain large partially resorbed plagioclase phenocrysts.

The eruption of the highly evolved peralkaline ignimbrites O and X was followed by eruption of the T4 basalt across most of the southern half of the island. The eruption of the T4 basalt marks the end of the middle Mogan formation and the start of a new cycle of magma differentiation that formed the upper Mogan. The T4 lava flows are interspersed with scoria and lapilli fallout beds. The basalt portions of the unit are grey -blue and fine-grained, in some localities the basalt is surrounded by purple-red fine grained material rich in pumice fragments. Locally yellow-orange lapilli beds occur.

The upper Mogan formation began with the eruption of the less evolved trachytic ignimbrites A and B and continued to higher levels of differentiation with ignimbrites C and D. Each of the four units are compositionally zoned becoming more mafic and crystal-rich upwards. Ignimbrite E and F are more mafic and are transitional in composition to the overlying Fataga group.

In the field ignimbrite A is red-brown and ranges in composition from fine-grained ash rich material to moderately indurated coarse grained material rich in fiamme, lithics and phenocrysts. The fiamme are dark brown and round to slightly oblate in shape. Ignimbrite B is dark green, densely welded with very occasional plagioclase phenocrysts. The fiamme are a yellow brown colour and range in shape from extremely flattened and stretched to oblate, fiamme. Ignimbrite C is also green but contains abundant lithic fragments in its lower third, mainly from the top of ignimbrite B. Pressure shadows can be observed around the lithics.

The faults examined in this study are exposed in the Middle Mogan ignimbrite X and the Upper Mogan T4 lava and ignimbrites A and B. Figure 9 shows a typical section of the upper Mogan ignimbrites A, B and C; the base of each ignimbrite unit is marked by a fully devitrified yellow vitrophyre.

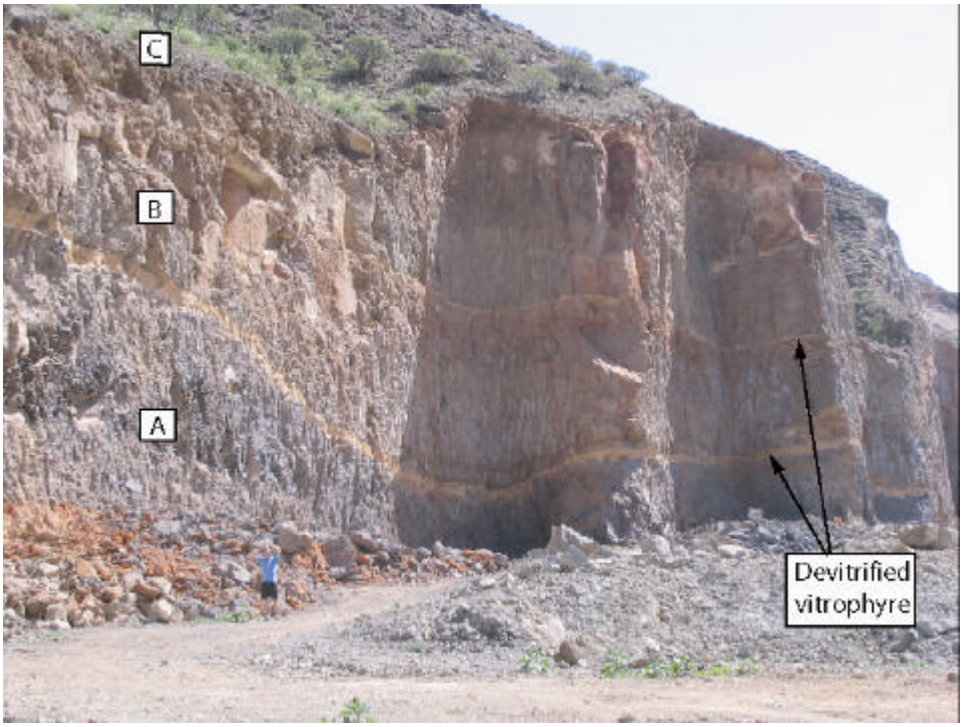

Figure 9: Upper Mogan formation ignimbrite A, B and C

The lower part of the Upper Mogan formation at Barranco de Taurito (looking south) showing ignimbrite A, B and C. Here ignimbrite B is ~6 m thick (person for scale is 1.65 m in height). Note the thick yellow band separating each of the units (fully devitrified vitrophyres) and the undulating contact between A and B to the left of the photograph.

2.1.3 Caldera collapse structures

Caldera collapse generated a complex system of intra and extracaldera faults (Figure 10). The collapse of the magma chamber roof into the underlying magma chamber occurs on concentric, outward dipping bell-shaped reverse faults or ring faults (Acocella et al., 2000; Branney, 1995; Walter and Troll, 2001). The majority of subsidence is typically accommodated on one reverse ring fault connected to the margins of the magma chamber that delimits the intracaldera area (Roche et al., 2000). In Gran Canaria the ring fault has not been observed. Workers have identified the topographic caldera margin (Figure 5 and Figure 11) that dips 50° to 80° inwards to the caldera centre (Schminke, 1998; Troll et al., 2002).

a)

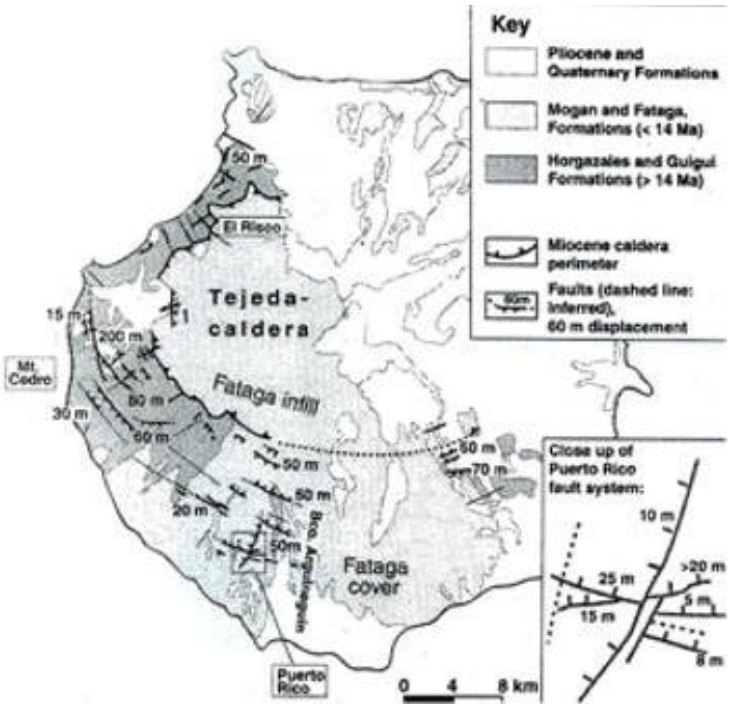

b)

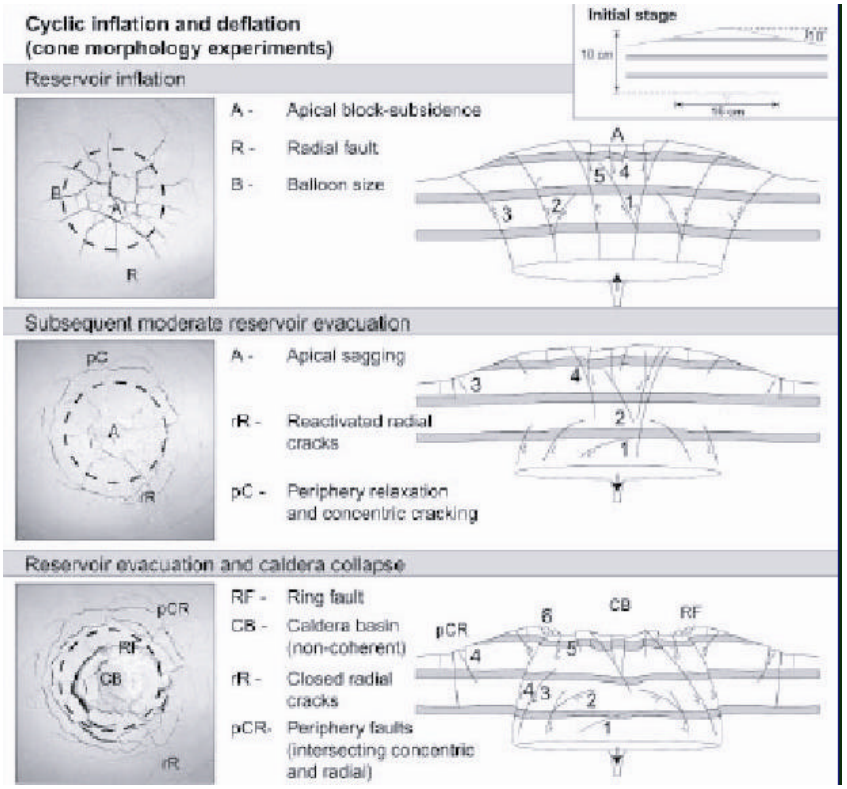

Figure 10: Gran Canaria caldera collapse structures and schematic development

a) Diagram from Troll et al. (2002) Illustrating the caldera margin and concentric faults in the extracaldera area (main picture). Inset shows the cross-cutting concentric and radial faults in the Puerto Rica area in the south of the island. The cross-cutting faults form horst and graben structures. b) The figure is from Walter and Troll (2001), the photographs (left) show the results of caldera inflation and deflation experiments they carried out using flour. The diagrams (right) are schematic profiles of the experiments showing the fault development during chamber inflation and subsequent deflation. The numbers indicate the order in which the faults formed. Inflation occurs on inward dipping faults and downsag of the chamber roof is accommodated on outward dipping bell shape faults.

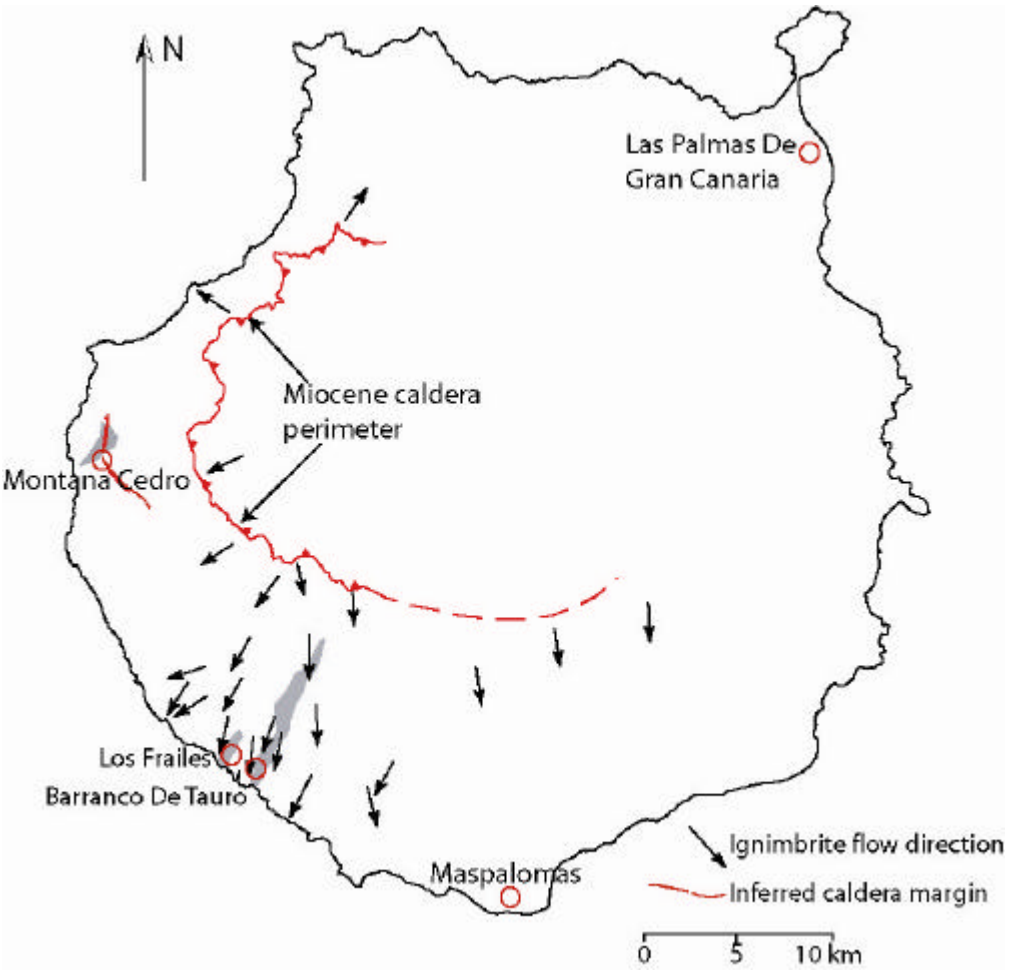

Figure 11: Map showing ignimbrite flow directions

Map shows study locations at Montana Cedro, Barranco Tauro and Los Frailes and the orientation of the large growth fault cutting Montana Cedro. The short black arrows indicate the flow directions for the Mogan group ignimbrites, modified from Schmincke (1998). UTM grid references for Montana Cedro 27°58'N 15°46'W, Los Frailes 27°47'N 15°42'W and Barranco de Tauro 27°46'N 15°42'W

The extracaldera area extends from the main reverse ring fault to the outermost concentric faults. This area is characterised by concentric normal faults that accommodate extension and 'downsag' during evacuation of the magma chamber and caldera collapse (Branney 1995, Walter & Troll, 2001). Doming of the magma chamber prior to caldera formation and later caldera resurgence forms a radial fracture pattern. Radial fractures are extensional and propagate out from the centre of the dome. Deflation of the chamber during eruption closes the fractures (Holohan et al., 2005; Troll et al., 2002). Both radial and concentric faults have been reactivated many times during later eruptive cycles.

On Gran Canaria the radial and concentric faults crosscut each other and the concentric faults form complex horst and graben structures up to 10 km outside the caldera margin (Troll et al., 2002). At Montana Cedro on the west of the island (Figure 5and Figure 7) approximately 5 km from the caldera margin there is an extensive concentric fault. The fault has a trace length of at least 2.4 km and at Montana Cedro a vertical exposure of ~90 m. The western side of the fault, or outer flank of

the island, is downthrown. The Montana Cedro fault together with the caldera margin to the east defines a large horst. Upper Mogan ignimbrites A and B increase in thickness across the fault to the west, below these middle Mogan ignimbrites O and X have greater thicknesses on the eastern side of the fault (Figure 12). The thickness changes illustrate the multiple reactivations of the fault throughout the Mogan and also the reversal in slip direction between the emplacement of the middle and upper Mogan. The switch from a steeply dipping reverse fault to a steeply dipping normal fault occurred post T4 emplacement (Figure 12d).

In the following sections I describe each of the ignimbrite units investigated - the host rock petrophysical properties, emplacement structures and regional deformation structures. However, before discussing each unit in detail I present an overview of general ignimbrite properties, processes of emplacement and influences on the physical properties of ignimbrites.

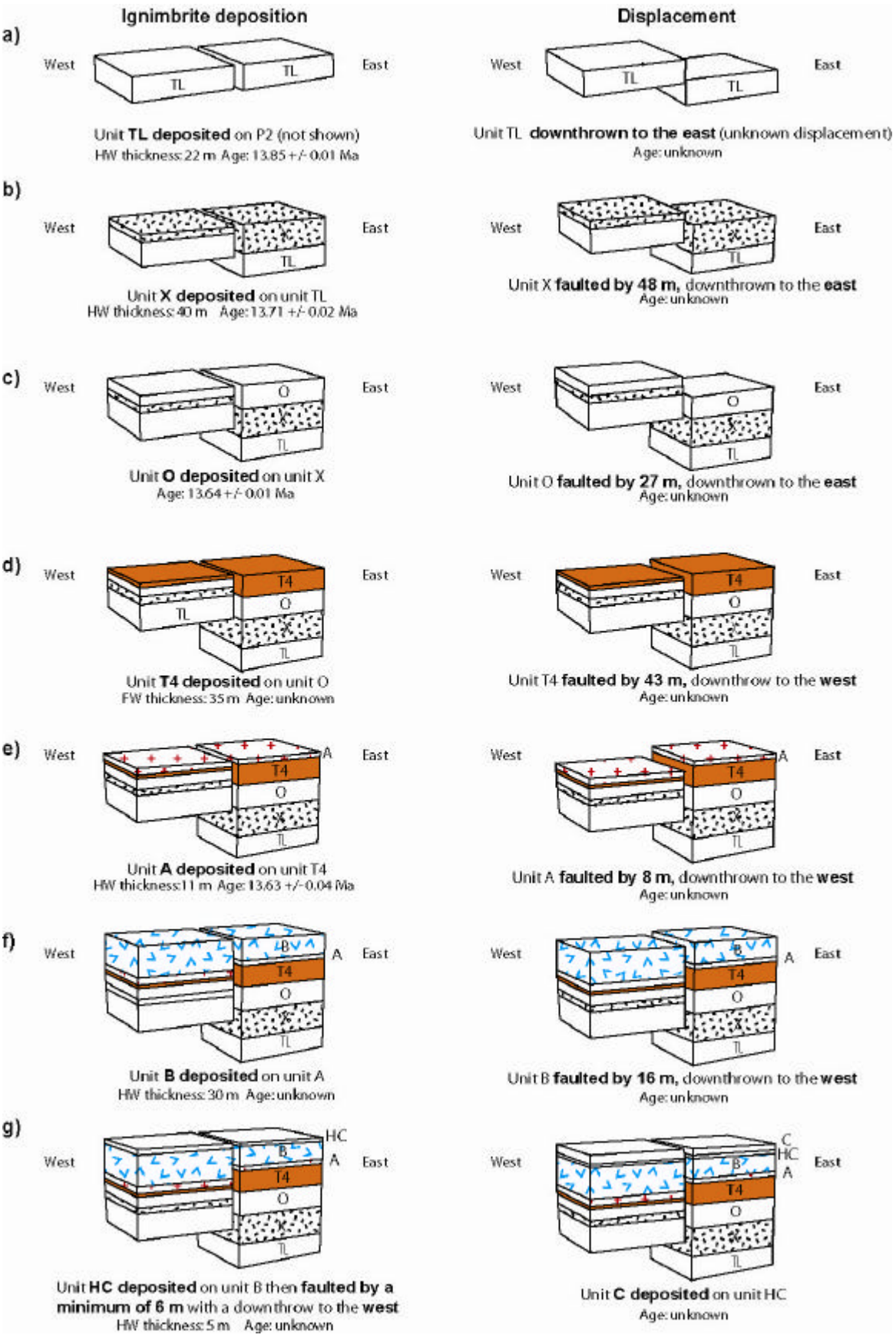

Figure 12: Emplacement of units across the concentric growth fault at Montana Cedro The diagram (Byrne pers comm.) was compiled using GPS locations of the upper and lower contacts of each unit on either side of the fault (Troll pers comm.). The ignimbrite unit thickness data was gathered in this study. The ignimbrite flow direction was east to west. Downthrow to the east switched to the west after emplacement of T4 and the start of a new eruptive cycle that formed the Upper Mogan formation.

2.2 Ignimbrite characteristics & depositional processes

Anatomy of an ignimbrite

Ignimbrites or ash-flow tuffs are high temperature pyroclastic flow deposits typically rich in ash and pumice clasts. They are usually composed of a poorly sorted mixture of pumice and lithic lapilli in a matrix of vitric shards and crystal fragments; more than 50% of particles in ash-flow tuffs are less than 4 mm in diameter (Fisher and Schmincke, 1984; Ross and Smith, 1961). Flows that contain a large proportion of juvenile vesicular lava blocks and non-pumiceous ash of similar composition are called block-and-ash flows (Branney, 1995). The size classification of volcanic fragmental material and the sedimentary equivalents (Wentworth and Williams, 1932) are shown in Table 1.

Size (mm)	Pyroclastic rocks	Clastic sediments
>32	**Block**	Boulder Cobble
32-4	**Lapilli**	Pebble gravel
4-2		Granule gravel
1-0.125	**Coarse ash**	Very coarse – fine sand
<0.125	**Fine ash**	Very fine sand Silt Clay

Table 1: Size grades of ignimbrite material and sedimentary equivalent

The basic mechanical unit of an ignimbrite is the ash-flow deposited from a single pyroclastic flow; an ignimbrite unit may be composed of one or multiple ash-flows (Ross and Smith, 1961; Smith et al., 1994; Wilson et al., 2003). Smith (1960) introduced the term cooling unit to describe the cooling history of ash-flows; a cooling unit is a body of material that has undergone continuous cooling i.e. the initial deposit was still hot when the later material was emplaced (Wilson et al., 2003). A simple cooling unit is composed of one or more ash-flows that accumulated rapidly enough so as to allow the whole body of material to cool as one. Such ignimbrite units have a poorly welded base and top and a welding maximum within the lower half of the unit. When the very base of an ignimbrite unit is marked by a vitrophyre, a massive rapidly cooled fine-grained glassy layer, this indicates complete cooling of the underlying ignimbrite and a substantial interval between pyroclastic flow deposits. Often the glassy vitrophyre is fully devitrified to a yellow brittle fine-grained powder (Figure 9).

Ash-flow tuffs are composed of varying amounts of glass shards, fiamme, abundant lithic fragments and broken phenocrysts ranging in size from millimetres up to 1 and 2 centimetres (Figure 13a). Typical characteristics of ignimbrite units are nonwelded unit tops, bottoms and sides and gradual thinning of the unit at the edges (Henry and Wolff, 1992).

a)

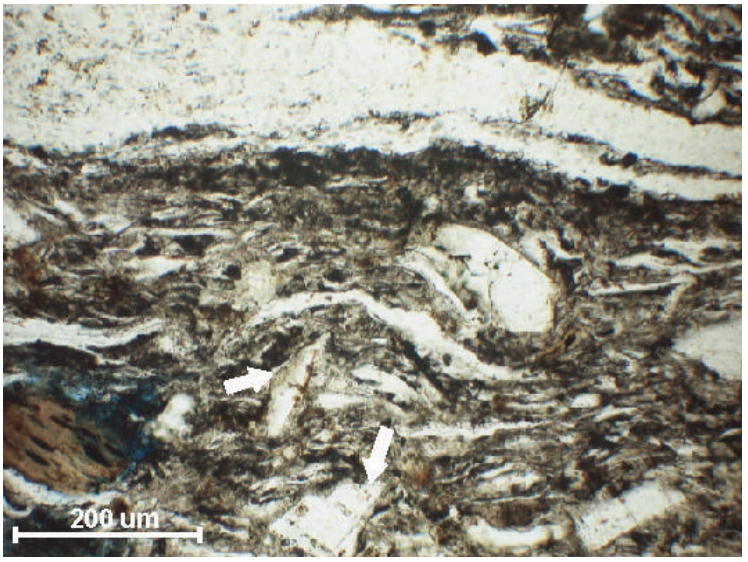

b)

Figure 13: Fabrics in densely welded ignimbrites

a) Thin section showing flattened fiamme (white) retaining some of their glass structure (wispy tails) and fractured angular phenocrysts (white arrows) in a brown matrix of extremely fine ash particles. The fiamme are slightly wrapped a round the inclusions indicating compaction of the material b) Eutaxitic texture: disk shape fiamme (dark brown) in an ash matrix (light brown), formed by extreme flattening and stretching of fiamme. The compaction bends the fiamme a round any inclusions present, note the pressure shadow on the left of the inclusion.

Ignimbrites are generally poorly sorted and massive, however some ash-flows show grading of pumice and lithic fragments. There may also be alignments of platy or elongate particles (Fischer & Schmincke, 1984) and flattening and elongation of fiamme during deposition forming a eutaxitic texture; disc shape fiamme in an ashy matrix (Figure 13b). With increasing distance from the source vent the proportion of fine-grained materials increases and some sorting of the ash-flow material takes place, in the distal parts of the flow coarser pumice concentrates at the top, bottom and sides of the flow (Ross & Smith, 1961). Therefore the character of the ignimbrite unit can change laterally as well as vertically.

Ignimbrite deposition

Two schools of thought exist on the mechanism of ignimbrite sedimentation from a pyroclastic flow. Some authors favour en masse deposition of the material, while others consider the process of progressive aggradation to fit better with the field observations. In en masse deposition the pyroclastic material is transported via plug flow (Sparks, 1976), a non-turbulent flow in which an upper non-shearing layer is carried on a laminar shearing layer (Branney, 1995). The flow stops en masse and produces a massive unit with an inverse-graded base. The velocity of the flow does not vary with height (Sparks, 1976). In progressive aggradation the pyroclastic flow is divided into an upper turbulent flow and a basal non-turbulent laminar flow. Deposition of the material occurs in the basal laminar part of the flow which is fed by material from the upper turbulent zone (Branney, 1995). Directional fabrics such as alignment of elongate particles, shear deformation in the laminar part of the flow and post-emplacement slumping or sliding suggest that progressive aggradation is the more plausible deposition mechanism (Branney, 1995).

Post-Depositional processes

The degree to which an ignimbrite unit is consolidated is a result of three processes: welding compaction, vapour-phase crystallisation (VPC) and devitrification/vapour-phase alteration (VPA) and are described in detail below. These processes can occur during and after deposition of the ignimbrite and were described by Sheridan and Wang (2005) as “events related to the progressive closing of pore space”. The intensity of each process can vary greatly both between and within ignimbrite units and result in very different petrographic (e.g. fabric) and physical (e.g. density, porosity) properties of the deposit. In any one unit the level of welding compaction varies vertically, and the extent of VPC and VPA can vary vertically and laterally often forming zones within a unit. The extent to which each process is developed and the combination of processes can have a major impact on the style of deformation. Wilson et al. (2003) found that non-welded units, unaltered by vapour-phase processes formed deformation bands, while welded vapour-phase altered units were cut by fractures. Ross & Smith (1961) observed that the most closely spaced joints are found in the most intensely welded material.

Welding: Ignimbrites may be poorly lithified and uncompacted or partly to entirely densely indurated (Branney, 1995; Sheridan and Wang, 2005; Smith et al., 1994) depending on the intensity of welding the material has undergone. Welding is the sintering together and deformation of glass shards and pumice fragments by compaction and viscous flow, at temperatures above the glass transition temperature (Quane and Russell, 2003; Ross and Smith, 1961; Smith et al., 1994). Compaction causes flattening of the pumice clasts to form fiamme (Figure 13) and overall densification of the volcanic material (Grunder and Russell, 2005). The majority of welding and compaction occurs after deposition of the ignimbrite material. However, if particles in a pyroclastic flow are sufficiently hot and molten, welding can occur prior to emplacement. This immediate welding is referred to as agglutination (Branney, 1995) and is irrespective of any post-depositional welding via compaction.

The amount of welding-compaction the material has undergone is referred to as the 'grade' of the ignimbrite. Low-grade ignimbrites can be non-welded or incipiently welded, the glass shards bond at their points of contact and pumice clasts are barely deformed retaining their vesicle structure. Low-grade ignimbrites generally have high porosities and low densities. High-grade ignimbrites are densely welded; the glass shards and pumice clasts are completely flattened and form eutaxitic texture (Figure 13). The pumice vesicles are collapsed, pore space is eliminated and the material has high densities. Extremely high grade ignimbrites are intensely welded to their upper surfaces and may exhibit lava-like zones (Branney, 1995; Smith et al., 1994).

The degree to which an ignimbrite is welded depends on a number of parameters: temperature and viscosity of the flow, accumulation rate, thickness of the deposit, composition and water content of the flow, and processes of devitrification and vapour-phase alteration during welding and compaction (Grunder & Russell, 2005). The main controlling parameter is time spent above the glass transition temperature (Tg), the temperature above which the material deforms plastically. Tg is dependent on composition and varies with water content. A range of Tg values from 700°C to 350°C have been measured experimentally (Giordano et al., 2005). The Tg value provides a lower limit for emplacement temperatures of densely welded ignimbrites.

A combination of strain measurements are used to calculate the degree of welding in a unit. The fiamme axial ratio, bulk unit porosity and density are used to quantify the level of mechanical compaction and viscous deformation of the material. Densely welded ignimbrite units have high densities, low porosities, eutaxitic texture and planar foliations defined by fiamme with high axial ratios.

Ideal ignimbrite density profiles display vertical gradations produced by welding; the base and top of the unit have low densities (poorly welded), with the maximum density (densely welded) occurring in the lower central part of the sheet as it retains its heat the longest (Sheridan and Wang, 2005). However, deviations from this profile do occur. Elevated temperatures in the ignimbrite unit that forms the substrate can cause further compaction in the lower part of the depositing unit; secondary vesiculation in high temperature tuffs increases porosity (Schmincke, 1974); and mineral precipitation from vapour-phase crystallisation will reduce porosity and increase density.

In some high temperature ignimbrites further welding of the material can occur by rheomorphic flow. This can be a syn- or post-depositional process and requires the temperature of the flow to remain above Tg thus allowing ductile deformation of the material. Syn-depositional adhesion of particles within the lower part of a high-temperature flow causes agglutination and deformation of the particles. The consequence of this increase in particle size is the establishment of a non-particulate basal laminar flow (Branney, 1995; Pioli and Rosi, 2005). The laminar flow in the base aligns and stretches the fiamme along a preferred direction (parataxitic texture) forming a pervasive foliation of stretched fiamme alternating with cm thick ash layers (Kobberger and Schmincke, 1999; Pioli and Rosi, 2005). Flow folds (Figure 14) and asymmetric pressure shadows around clasts at both macro (Figure 13b) and micro-scales are also indicative of rheomorphic flow.

Figure 14: Flow fold in ignimbrite E of the Mogan group
The material has undergone extreme shear deformation through rheomorphic flow. Lens cap for scale. The photograph was take at the northern end of Barranco de Tauro where Ignimbrite B is accessible.

Post-deposition rheomorphic flow occurs when the flow is remobilized either on dipping slopes or due to increasing overburden and shear stress during continued aggradation of the ignimbrite material. Remobilization of the material causes a shear zone at the base of the unit stretching the

fiamme and glass shards and through the localization of shear strain forming discrete dislocation gliding planes (Kobberger and Schmincke, 1999). The formation of such discontinuity planes also occurs during progressive cooling of the material from the base upwards. As basal material cools it increases in viscosity thus reducing flow speed, while the upper material continues to flow. The basal parts of units tend to display the greatest number of flow structures (Pioli and Rosi, 2005).

Devitrification/vapour phase alteration (VPA) is the in situ breakdown of glass shards and pumice clasts at temperatures much less than Tg (McArthur et al., 1998), to form intergrowths of elongate fibres (axiolitic intergrowths) of cristobalite, tridymite, sodium-rich and potassium-rich alkali feldspars (Ross and Smith, 1961; Smith et al., 1994). Devitrification takes place within the boundaries of the shard or clast with axiolitic growth initiating from the sides of the shard inwards (Figure 15a). The pumice structure is obliterated; the outline of the clast or shard may still be visible depending on the degree of alteration.

Vapour phase crystallisation (VPC) is defined as precipitation of minerals in pore space from hot gases sourced from juvenile vitric particles and heated groundwater, percolating through the ignimbrite during cooling. VPC occurs above and below the glass transition temperature of the material (McArthur et al., 1998). The products of VPC are tridymite, cristobalite, alkalic feldspar and quartz. The crystals grow as discrete crystals (Figure 15c) and aggregates of radial crystals called spherulites (Figure 15b & e) and have a coarser texture than devitrification products (Ross and Smith, 1961; Smith et al., 1994). Spherulites are thought to only crystallise at temperatures greater then the glass transition temperature (McArthur et al., 1998). At high rates of cooling the fibres that make up the spherulites are fine and compact (Figure 15b), lower cooling rates form coarser fibres and the spherulite has a more open structure (Figure 15e). The precipitates fill pumice vesicles and pore spaces, commonly lining the cavity wall (Figure 15a) or growing as a mesh of crystals within the space (Figure 15c). The processes of devitrification and growth of secondary mineral phases from VPC reduces pore space and strengthens the material by interlocking of coarse crystals, producing coherent rock. Thus induration of an ignimbrite is possible without welding compaction.

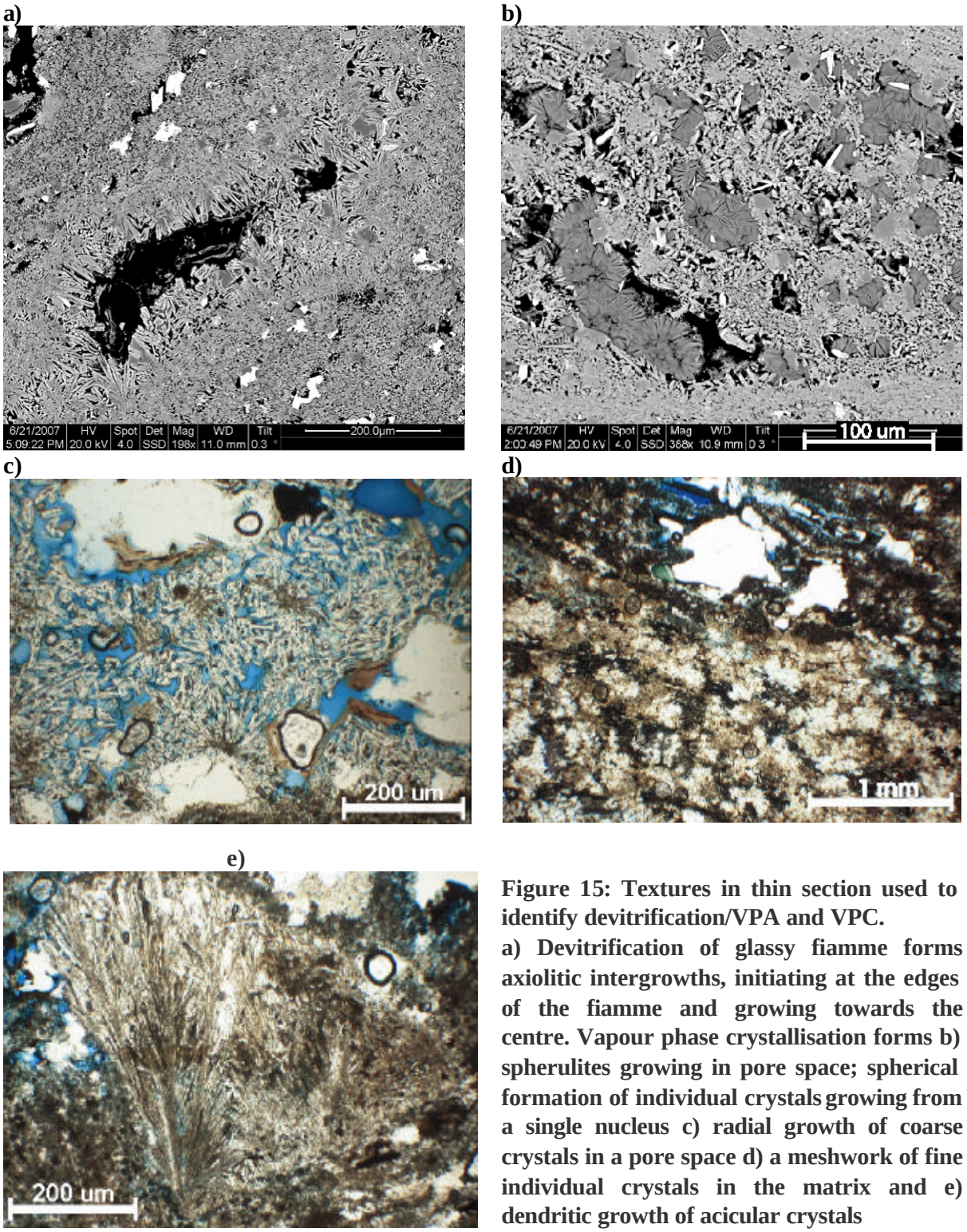

Figure 15: Textures in thin section used to identify devitrification/VPA and VPC.
a) Devitrification of glassy fiamme forms axiolitic intergrowths, initiating at the edges of the fiamme and growing towards the centre. Vapour phase crystallisation forms b) spherulites growing in pore space; spherical formation of individual crystals growing from a single nucleus c) radial growth of coarse crystals in a pore space d) a meshwork of fine individual crystals in the matrix and e) dendritic growth of acicular crystals

Jointing: Columnar joints can form at advanced stages of ignimbrite lithification and cooling (Kobberger & Schmincke, 1999). Columnar joints are a common feature in welded tuffs but normally do not occur in noncrystalline, non-welded units (Ross & Smith, 1961). Various polygonal and orthogonal joint patterns can form as a result of cooling. For example in the Bandelier Tuff New Mexico, the colonnade cooling unit contains orthogonal cooling joints but the cooling units above and below contain polygonal cooling joint patterns (Lewis pers. comm.). The joints delineate columns that are approximately rectangular or sometime square in plan view (Ross

& Smith, 1961). Observations of joint spacing by Ross & Smith (1961) in the Valles Mountains found spacing ranges from a few inches to feet and the most closely spaced joints generally occur in the most intensely welded ignimbrites. They also suggest that joint spacing is controlled by a number of factors such as cooling, thickness and degree of welding.

2.3 Host rock descriptions & methodology

2.3.1 Methodology

The three ignimbrite units investigated in this study are A, B and X. Ignimbrites A and B are examined at three separate locations and ignimbrite X at one locality. Faults are found at both Barranco Tauro and Montana Cedro; Los Frailes was used as an unfaulted type section for ignimbrites A and B (Figure 5).

Barranco Tauro and Los Frailes are located in the south of the island; the topography is cut by deep ravines (Barranco) forming steep sided ridges (Figure 16). The region is arid with little vegetation however the slopes are heavily weathered and scree covered. Clean fresh exposures are found where trails or roads have been constructed, thus the exposures are cross-sections. Occasional blast holes are seen in the sections but there is little damage surrounding these, suggesting that fractures are a result of natural processes. At Los Frailes a constructed trail slopes upwards along the side of the ridge, as a result sections are truncated at one end by the path and inaccessible at the other end due to steep topography (Figure 17). At Barranco de Tauro the road-cuts cross-cut the ridges, as a result the exposures pinch out at the ends of the outcrop (Figure 18). The top two meters of ignimbrite A is exposed at both sites, the lower four to five meters of ignimbrites B is accessible at Barranco Tauro and the entire ignimbrite B unit is accessible at Los Frailes.

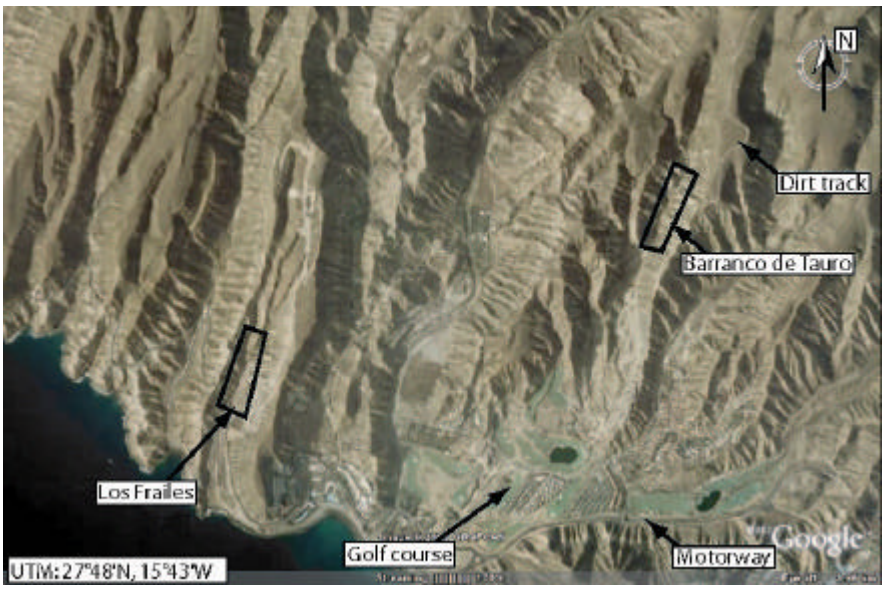

Figure 16: Location image Los Frailes and Barranco de Tauro

Google satellite image showing the locations of Los Frailes and Barranco de Tauro in the south of the island. The topography is cut by deep ravines (barrancos) forming high ridges and steep slopes. The slopes are heavily weathered and covered with scree, where trails or roadcuts are constructed fresh vertical cross-sections are exposed.

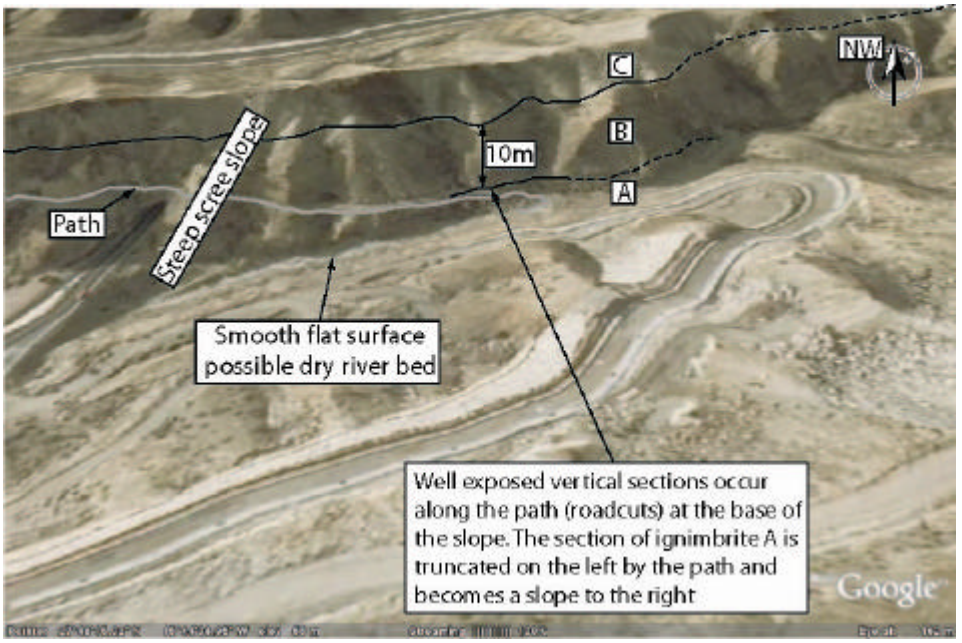

Figure 17: Satellite image of Los Frailes location

The exposure at Los Frailes is along a trail cut into the side of the ridge, the best exposure is found along the trail. Here the face is vertical, fresh and free from scree; the upper areas of the slope are heavily weathered. As a result the examined sections are truncated to the left by the trail and on the right are inaccessible due to the steepness of the slope.

a)

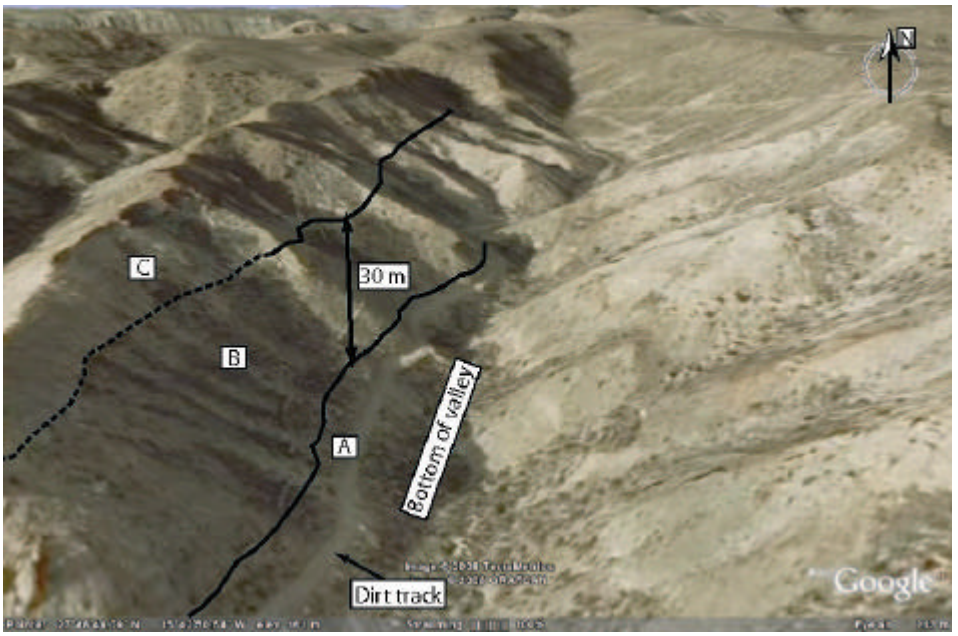

b)

Figure 18: Satellite image and photo of Barranco de Tauro

a) At Barranco de Tauro the ravine is flanked by steep scree covered slopes, the best exposure occurs along the road-cuts. b) The flanks of the valley have an undulating topography. The road-cut cross-cuts the ridges and as a result the outcrops pinch out at their ends.

The sections at Montana Cedro are natural exposures, the best exposures occur on the western side of the mountain as it is unprotected from wind, rain and sun. The eastern side is sheltered from wind and rain, and the narrowness of the ravine affords protection from the sun. As a result the eastern flank has a greater covering of moss and other vegetation. On the western flank a narrow path runs down along the mountain side through each of the units allowing access to the full thickness of ignimbrite A, B and X. The sections are truncated both where the topography becomes too steep or where the rock face has been sloped through weathering and features are not easily identifiable.

Figure 19: Satellite image of the western side of Montana Cedro.
The hangingwall (LHS) of the largest concentric fault in the area (labelled here as C22) is composed of ignimbrite A and B and cut by two smaller faults (C5 and C15). The fault trace of C22 disappears moving west as it extends out into the valley. Note the steep gradient of the flank firstly in the drop in altitude coming down the path and secondly in the adjacent valley to the west.

a)

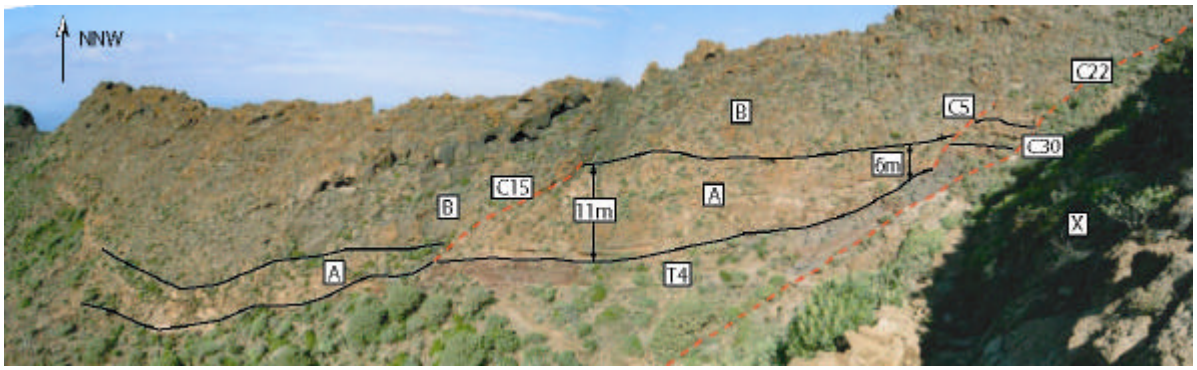

b)

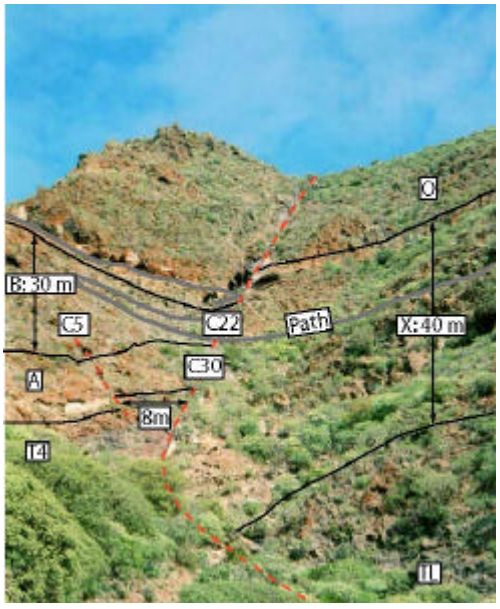

Figure 20:Montana Cedro faults
a) Photograph shows the south face of the hangingwall ridge of the main concentric fault (C30/C22). The hangingwall is composed of T4, ignimbrite A and B, and is cut by two smaller offset faults. C5 displaces ignimbrite B against A by 5 m and C15 offsets A and B by 15 m. The exposure of the faults and the adjacent rock is good, however there are sections where the material is heavily weathered and covered with scree. b) View of the large concentric fault that offsets younger ignimbrites of the upper Mogan group (A & B) against older middle Mogan ignimbrites (TL, X & O). The fault trace is curved and disappears in the TL unit as it extends out into the valley.

Unfaulted sections or sections over 10's of meters away from the faults were used to characterize

the protolith properties. The joint density of unfaulted host rock (background joint density) was measured for ignimbrite units A and B. The type section for ignimbrite B at Los Frailes facilitated the measurement of joints from the base to the top of the unit. However, only the top 2m of Ignimbrite A were exposed below ignimbrite B. Establishing the background joint density from only two locations presents some problems which are discussed in the summary section at the end of this chapter.

To quantify the degree of welding in the host rock the aspect ratio of fiamme were measured at different heights in the unit, where the entire thickness of the unit was accessible. Thin sections were used to measure percentage porosity of the host rock, mineralogical composition, aspect ratio and abundance of fiamme, as well as to identify the presence and type of secondary alteration products (either VPA or VPC).

Each fault was examined and the nature of the deformation elements in both was recorded, on the basis of this inspection the fault was divided into fault core and damage zone. The fault core is defined by a incoherent zone of fine-grained gouge and clasts ranging from 1 mm to 63 cm in length bounded on either side by fault walls. The fault wall is a smooth surface against which the gouge and breccia lie. The fault wall marks the edge of the fault core and the start of coherent jointed rock in the damage zone. The damage zone is the area of rock adjacent to the fault wall that has a joint density greater than that of the protolith background joint density; when joint density falls below the background level that is taken as the end of the damage zone. The joint spacing (perpendicular distance between adjacent joints) in the damage zone was measured along line transects perpendicular to the fault from the fault wall out; mean joint density (# joints/metre) was calculated from this. Each line section extended from the edge of the fault wall to the termination of the section, due to either truncation by the path, inaccessible topography or heavily weathered, sloped outcrop. The joints in the damage zone are approximately vertical and parallel to each other.

Fault core logs were complied for all meter-scale faults. The logs were compiled by measuring the width of the fault core perpendicular to the fault wall at one-meter intervals along the fault. As the fault cores are exposed along an oblique cross-section the logs record fault core width both along strike and up-dip. Fault core widths where two ignimbrites are juxtaposed is the distance from the fault wall to the contact with the fault core material of the opposite ignimbrite unit, or more rarely to a definite slip surface. Only the large growth fault at Cedro (Ca30 and Cb22) contains a recognizable principal slip surface in the fault core; in the remaining faults deformation is distributed across the fault core.

Faults are labeled according to their locality and the amount of displacement accumulated on the fault e.g. a fault with 2 m offset at Tauro is labeled T2. When discussing a fault in a particular ignimbrite unit the fault is labeled as locality, ignimbrite unit the damage zone/fault core or part

thereof is in and the amount of displacement that ignimbrite unit has undergone. A fault that occurs solely in ignimbrite A at Cedro and has 10 meters displacement is labeled CA10. Faults that juxtapose two different ignimbrite units e.g. ignimbrite A against ignimbrite B, by 10 m at Cedro is labeled as an entire fault C10. The part of the fault core that is composed of ignimbrite B is Cb10 and the part composed of ignimbrite A is Ca10. The damage zones are labeled as locality, ignimbrite unit and fault displacement e.g. the damage zone adjacent to a 10 meter offset fault in ignimbrite A at Cedro is labeled CA10 damage zone. Displacement values were calculated from the offset at the base of the ignimbrite unit.

The maximum and minimum axis of clasts deemed as having being generated in the fault core (i.e. identified as being from the adjacent rock as opposed to material that had fallen or washed in to the core) were measured. The reason for this distinction was that in the lower offset faults where the fault core is clast supported, there is a large amount of space and limited gouge around the clasts and therefore material from outside the fault can fall into the fault core. In the larger offset faults the fault core is packed with gouge and breccia so the issue of external material entering did not arise, however clasts were still correlated to the adjacent host rock. Forty clasts were measured in each of the fault core one-meter intervals; the lower measurable clast size limit was 0.01 cm^2. The maximum and minimum clast axes were measured to calculate clast size or surface area (maximum x minimum) and clast aspect ratio (maximum/minimum). The percentage of clasts to gouge in the core was estimated for each of the meter intervals.

In the laboratory the strength of the ignimbrites was calculated using a Portable Ultrasonic Non-destructive Digital Indicating Tester (PUNDIT) machine. The PUNDIT generates low frequency ultrasonic pulses and measures the time taken for them to pass from one transducer to the other through the material between. The blocks of ignimbrite used had dimensions ranging from 8 x 6.4 cm to 20 x 5.6. A flat surface top and bottom was cut parallel to the foliations or long axis of the fiamme (base parallel) and the transducer placed on these areas. Thus measuring the properties of the material as they would occur in situ and in the direction the joints and faults propagate, perpendicular to the unit base. Using an empirical relationship of pulse velocity to modulus of elasticity, the elastic modulus of each specimen was obtained. These values were compared with published values of elastic modulus for ignimbrites with similar petrophysical characteristics to those tested. I then assumed that ignimbrites with comparable elastic modulus and petrophysical properties would also be alike in other material properties. Where values of friction, tensile or compressive strength are stated these are for ignimbrites in the literature with the same elastic modulus and characteristics as those in this study. The results of the PUNDIT testing are presented in section 2.3.2 Table 2 and section 2.3.3 Table 5. Percentage porosity measurements were made using pixel counts of black (porosity) versus grey (grains) in 40 BSE images per thin section. The percentage of lithic, pumice and phenocrysts in the host rocks were estimated from thin section

analysis.

Much of the data presented in the following chapters is plotted on box and whisker plots (Figure 21). Box plots represent the distribution of the data and shows more detail than plotting mean values. The line across the box is the median value of the data set (Figure 21). Either ends of the box are the upper and lower quartiles; they mark the extent of data lying 25% below and 25% above the median. Therefore the box represents 50 % of the data values and the length of the box represents the spread or range of the data from the median. This range is called the inter-quartile range (IQR) and is the difference between the upper and lower quartiles. Large IQR values indicate a wide spread in data around the median i.e. values lie far away from the median and are therefore much greater or much less than the median. Low IOR values indicate that the data is clustered around the median i.e. values that are similar to the median. If one quartile is bigger then the other that indicates that the values in that quartile lie further from the median and the data is skewed e.g. a large lower quartile indicates that the difference between the lower quartile value and the median is greater than between the upper quartile value and the median . The "whiskers" at either end of the box represent data lying 1.5 x IQR away from the upper and lower quartiles, values outside this are outliers and are marked by a cross.

Box and whisker plots were used instead of more commonly employed methods of mean and standard deviation as I felt the box plots present the data in greater detail. For example the spread of values for fault core width ranges from 1 cm to 200 cm, presenting the mean of such a range would over simplify the data. To illustrate the loss of information conventional means would result in the mean for each population has been plotted on to the box and whisker graphs. Standard deviation values for each data population are useful in demonstrating the spread of the entire population around the mean. The standard deviation is similar to the range presented by the box and whiskers, however what the standard deviation does not show is whether the data is normally distributed around the mean or skewed. The upper and lower quartiles of the box plots give some indication how 50% of the data is distributed around the median, whether values lie close to the median or are much greater/less than the median. However the standard deviation does account for the spread of all data points - greatest and least value. In the box plots values greater then upper and lower limits are plotted as outliers removed from the central portion of the data population. As a result interesting features in the data tails may be overlooked. To allow a comparison between the two methods mean and standard deviations have been plotted on the box and whisker plots where possible.

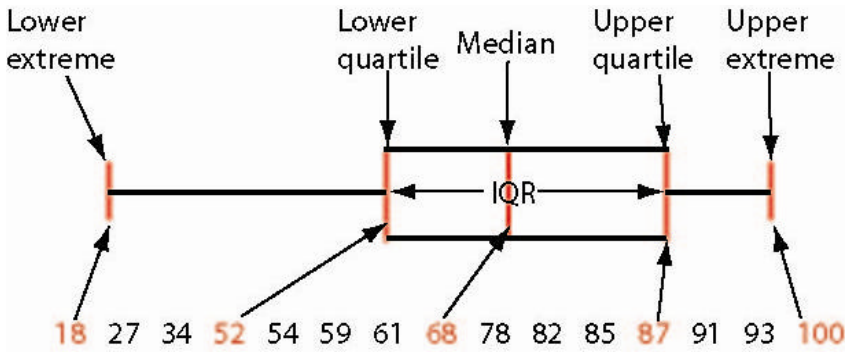

Figure 21: Box and whisker plot.

The upper quartile of the box is longer than the lower quartile as the difference between the upper quartile and the median is greater than the lower quartile and the median and so the upper quartile lies further away from the median than the lower quartile.

The following sections contain descriptions of the ignimbrite units investigated; the host rock petrophysical properties and the nature of deformation structures within the host rock.

2.3.2 Ignimbrite A

Ignimbrite A was investigated in three localities – Barranco de Tauro (T), Los Frailes (LF) and Montana Cedro (C) (Figure 11 & Figure 22). The composition of the unit is similar in all three locations although some variations do exist. Tauro and Los Frailes are located in the south of the island and are only 2 miles apart. In both localities only the top few meters of ignimbrite A are exposed. The ignimbrite A unit at Los Frailes is unfaulted and along with a location further to the west (Barranco de Taurito) was used as a type section for ignimbrite A.

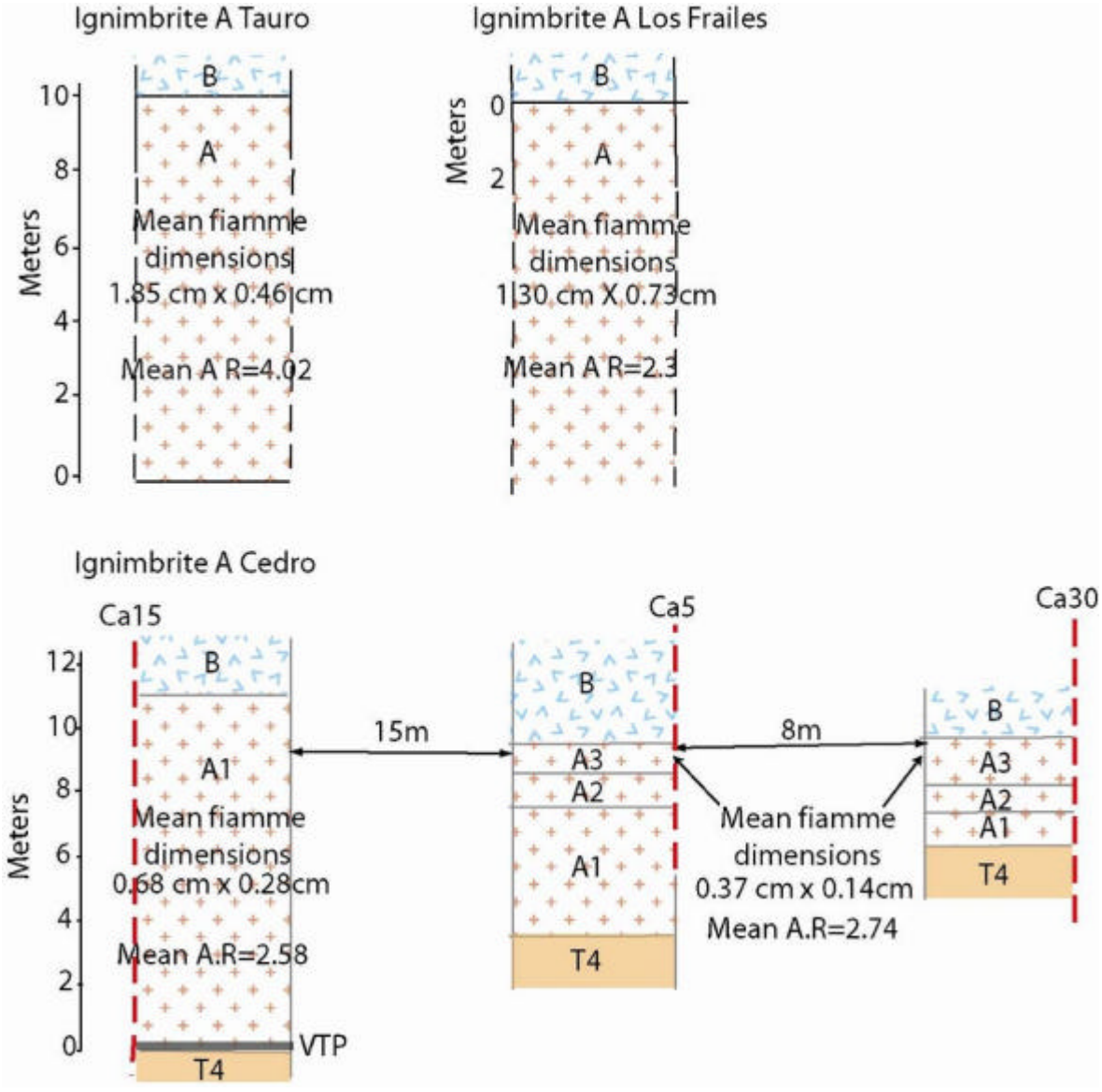

Figure 22: Logs of ignimbrite A Tauro, Los Frailes and Cedro
Ignimbrite A in unfaulted protolith at Tauro & Los Frailes, the dashed black line indicates the unexposed part of the unit. Ignimbrite A adjacent to the Ca5, Ca15 and Ca30 faults at Cedro, the horizontal arrows indicate the distance the faults lie from each other. Mean fiamme dimensions (maximum & minimum axes) and mean fiamme aspect ratio (A.R) are shown for each unit.

At Tauro ignimbrite A is 10 m thick, however the majority of this is inaccessible and the exposure that was investigated in this study comprises the top 2.5 m. The unit is red-brown and moderately to densely welded. The occurrence of fiamme varies along strike; the majority of the fiamme have been weathered out giving the surface of the unit a rough texture. Where fiamme are still present the surface is smoother. Most of the unit is a rusty brown colour however occasional fresh surfaces reveal green patches. Fiamme are black or orange with an average aspect ratio of 4.02 and maximum and minimum aspect ratios of 4.3 and 2.5. The cavities left by the weathered out fiamme show them to have been rounder than the fiamme that remain. The unit is quite crystal rich (15%) and contains fresh euhedral feldspars and small black crystals. Some joint surfaces within the protolith are stained red.

At Los Frailes the top 2m of ignimbrite A is exposed and the unit is a similar red brown colour to that at Tauro. There is a large number of small fiamme with an average fiamme aspect ratio of 2.3 and maximum and minimum aspect ratios of 7.5 and 1.06.

At Montana Cedro Ignimbrite A is composed of three layers that I have divided into A1 the base layer, A2 the middle layer and A3 the top layer (Figure 22). A2 is poorly welded while A1 and A3 are moderately welded. A1 and A3 are relatively hard and well fused but not particularly compacted, there are no foliations and the fiamme are not very flattened or streaked out. The elastic moduli of A1 and A3 are shown in Table 2

	Elastic Modulus (Gpa)	**Uniaxial compressive strength (MPa)**	**Uniaxial tensile strength (MPa)**	**Friction angle (f)**	**Cohesion**
A1	9.5	-	-	-	-
A3	10	-	-	-	-
Owharoa ignimbrite	-	45 - 54	6.8 – 7.1	33 - 34	1.3 - 1.4
Calico Hills tuff	9.8 – 10.3	38.6 - 48	-	-	-

Table 2: Mechanical properties of ignimbrite A

Elastic modulus of the A1 and A3 flow units of ignimbrite A calculated using a PUNDIT machine. The Owharoa ignimbrite, New Zealand (Moon, 1993) and Calico Hills tuff, Yucca mountain , Nevada (Schultz and Li, 1995) have similar petrophysical properties and elastic moduli to ignimbrite A; therefore the other material properties are assumed to reflect those of ignimbrite A.

The base of A1 is marked by a 10 cm thick vitrophyre that is completely devitrified to soft yellow granular material. Above the vitrophyre the unit is green for ~1m upwards, above which the unit is characteristically red-brown. A1 is eleven metres thick thinning to one metre next to the large growth fault. A1 contains numerous, dark, fine grained fiamme with mean maximum and minimum axes of 0.68 cm and 0.28 cm respectively, mean aspect ratio of 2.58 and max and min aspect ratios of 10.45 and 1.01 (Figure 23). The unit also contains abundant (~30%) millimetre size euhedral feldspar phenocrysts.

Figure 23: 25cm^2 section of ignimbrite A flow unit A1.
Fiamme (dark brown) are not completely flattened and stretched but have a oblate shape.

In thin section, ignimbrite A1 is composed of large fiamme (25-30%), feldspar and quartz phenocrysts (15-20%) and minor amounts of lithics (2-5%) in a very fine grained matrix (Figure 24). Fiamme are moderately flattened; the mean aspect ratio is 2.58 and the max and min aspect ratios are 10.45 and 1.02 respectively. The fiamme are fully devitrifed and in places wrap around phenocrysts. Unflattened inclusions that are infilled with radial growths of acicular crystals suggest these were cavities in which vapour-phase crystallisation minerals were precipitated. The phenocrysts range in size from 0.1 cm to 0.3 cm. The majority are rectangular in shape although some are fragments of larger clasts and others show signs that they have been reabsorbed. Occasional pumice clasts retain their pumice structure and in places the outline of relict glass shards are visible. Some dark fine grained lithic clasts contain euhedral phenocrysts.

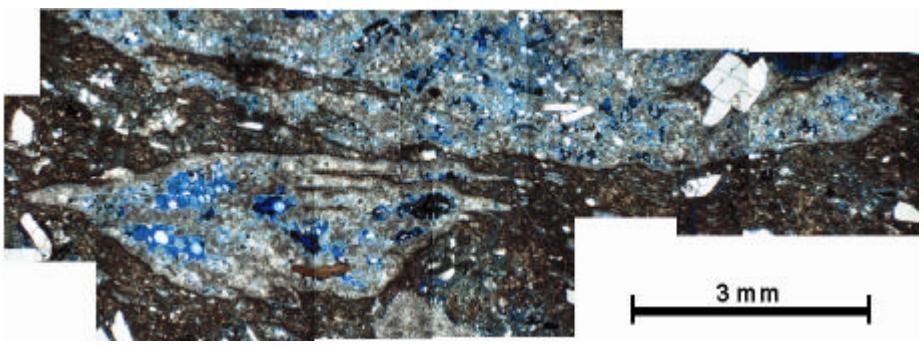

Figure 24: A1 host rock in thin section
Thin section in plane polarised light, the blue colour is a dye highlighting the pore space in the fiamme

A2 is one to two metres thick, ash-rich, extremely friable and fiamme poor (Figure 25a). It contains millimetre size euhedral feldspar and mica phenocrysts, slightly flattened fiamme (~10%) and pumice bombs (40%) (Figure 27). There are small fragments of A1 (densely welded, red brown colour) throughout the layer. A3 is a much more competent than A2 (Figure 25b). A3 is composed mostly of ash sized material with 30% pumice material and minor amounts of fragmented euhedral feldspar and quartz phenocrysts (5%) and lithics (1%) (Figure 26). Fiamme in A3 are smaller than in A1, the mean maximum and minimum axes are 0.37 cm and 0.14 cm, the mean aspect ratio is 2.73 and max and min aspect ratios are 11.02 and 1.01. The layer changes in thickness from 3 m to 1.4 m towards the large growth fault. The contact between the A2 flow unit and A3 flow unit is sharp but uneven in places.

a) **b)**

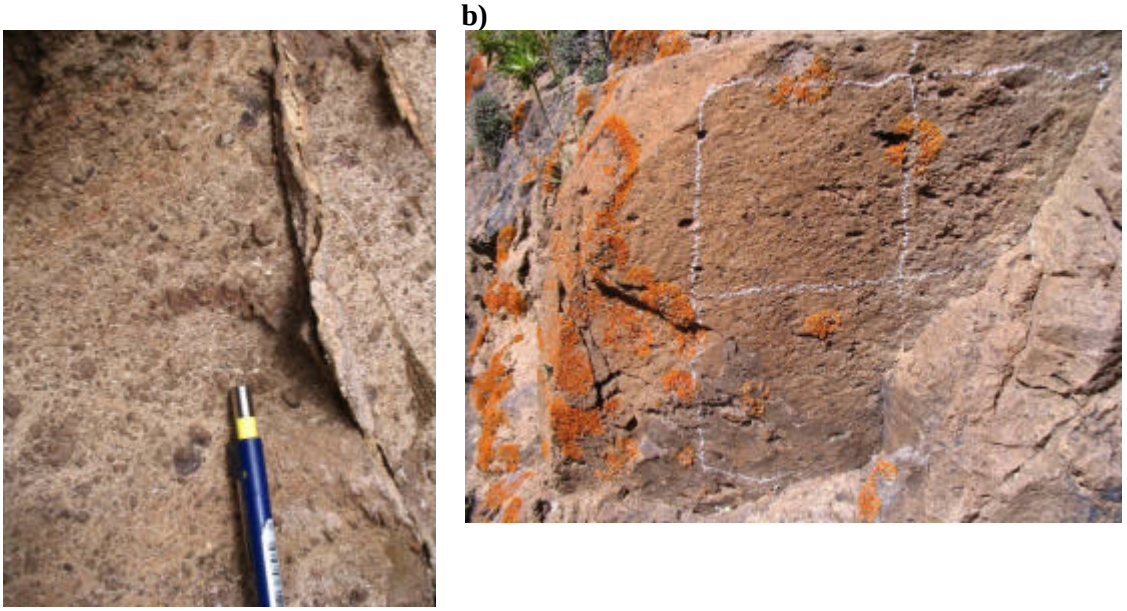

Figure 25: Sub-units in ignimbrite A

a) Flow unit A2 in ignimbrite A, ashy matrix with clasts of A1. b) A3 flow unit is more competent, contains low numbers of fiamme that are quite rounded. The chalk square measures 25 cm x 25 cm

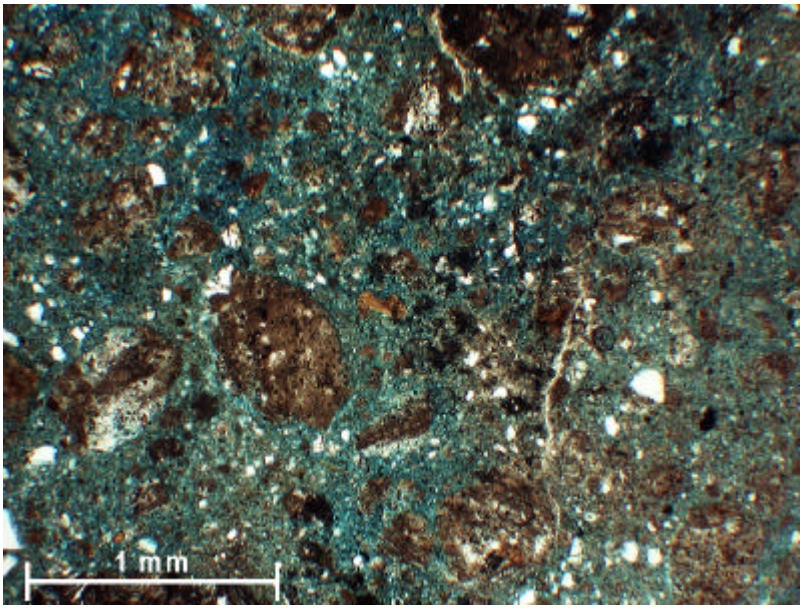

Figure 27: Plane polarised light image of A2 material.
Clasts of pumice and ignimbrite are sub-rounded and surrounded by a fine ashy matrix Green colour of the matrix is due to blue dye impregnation.

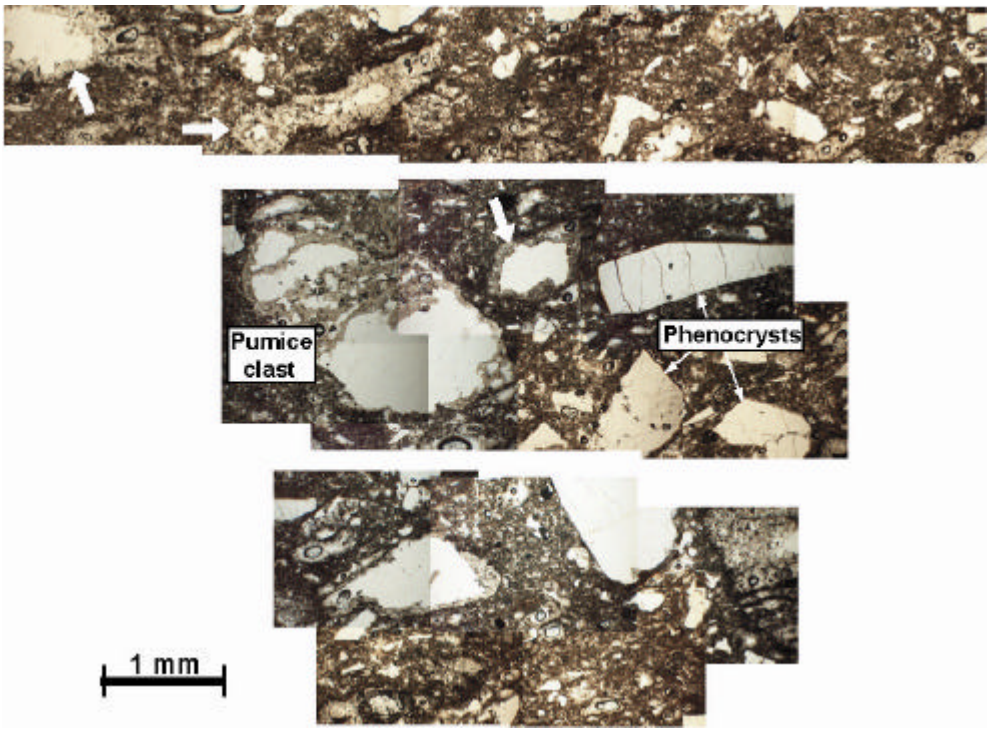

Figure 26: ignimbrite A host rock in thin section
Sample taken from the top 2 m section at Los Frailes (equivalent of A3). Arrows indicate pore spaces lined with crystals. The middle section shows a devitrifying pumice clast and broken phenocryst fragments

Deformation structures

Joints

As the section at Los Frailes is not cut by any faults, joints in the section represent pre-existing joints unrelated to faulting in the immediate area. Joints are sub-vertical, planar, 0.5 m to 2 m in height and have 0.1 cm to 0.7 cm apertures. Joint surfaces are smooth and slightly undulating. There are two joint sets oblique to each other cutting the top part of ignimbrite A, one set trends E-W and the other trends NW-SE (Figure 28). The NW-SE joint set is concentric to the caldera margin and the E-W set is oblique to the margin.

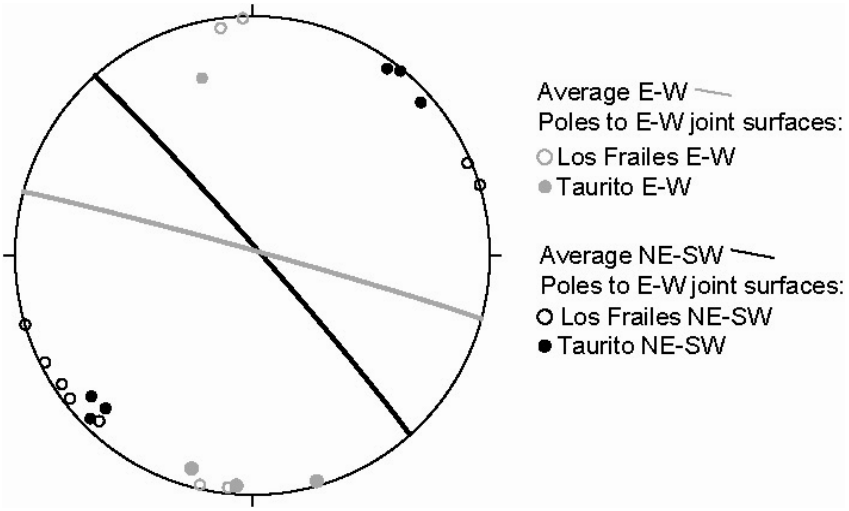

Figure 28: Stereonet of joints in ignimbrite A
Orientation of joints in ignimbrite A at los Frailes and Barranco de Taurito. There are two main joint sets striking E-W and NW-SE.

Spacing between joints at Los Frailes ranges from 0.11 m to 2.10 m with an average joint spacing of 0.66 m. The average joint density or background joint level is 1.5 joints per meter; some sections are more fractured and jointed than others (Figure 29). The joints do not continue up into the overlying unit ignimbrite B. A second section at Barranco de Taurito was used to collect additional joint orientation data (Figure 28) but was not investigated beyond that. Again this section is in the top part of ignimbrite A and joints have mostly NW-SE trends with occasional N-S orientations. It is probable that the NW-SE set formed due to regional scale inflation and deflation of the caldera magma chamber. The E-W set may be cooling joints that formed after deposition of the unit and were later cut by the regional tectonic joints.

a)

b)

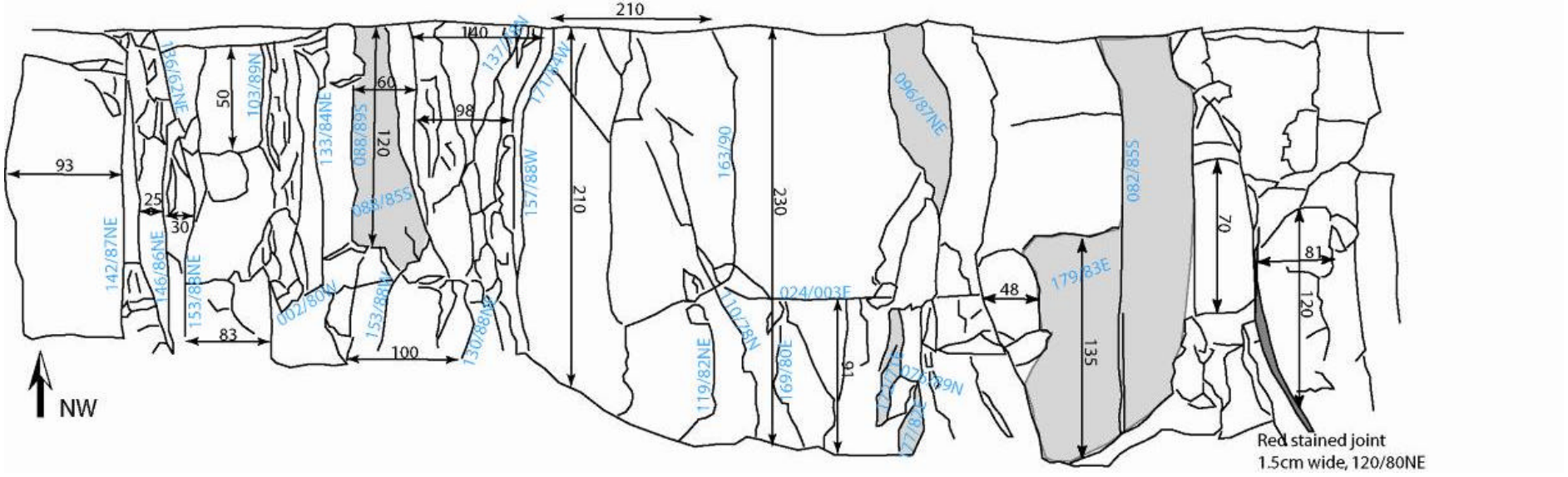

Figure 29: Ignimbrite A host rock section

a) Unfaulted section of ignimbrite A at Los Frailes, field notebook (16.5 cm long) for scale and b) sketch of the cross-section with joint spacing (black arrows, measurements are in centimetres) and joint orientations (blue), sketch is not to scale.

At Barranco Tauro there are places where the top of ignimbrite A contains a number of centimetre-scale faults (Figure 30a); these do not continue upwards into the overlying ignimbrite B. Changes in the thickness of the B vitrophyre are seen as it flows across small faults and ponds against the scarp (Figure 30b), therefore these small offset faults were present prior to ignimbrite B emplacement and were not reactivated at later stages.

a) **b)**

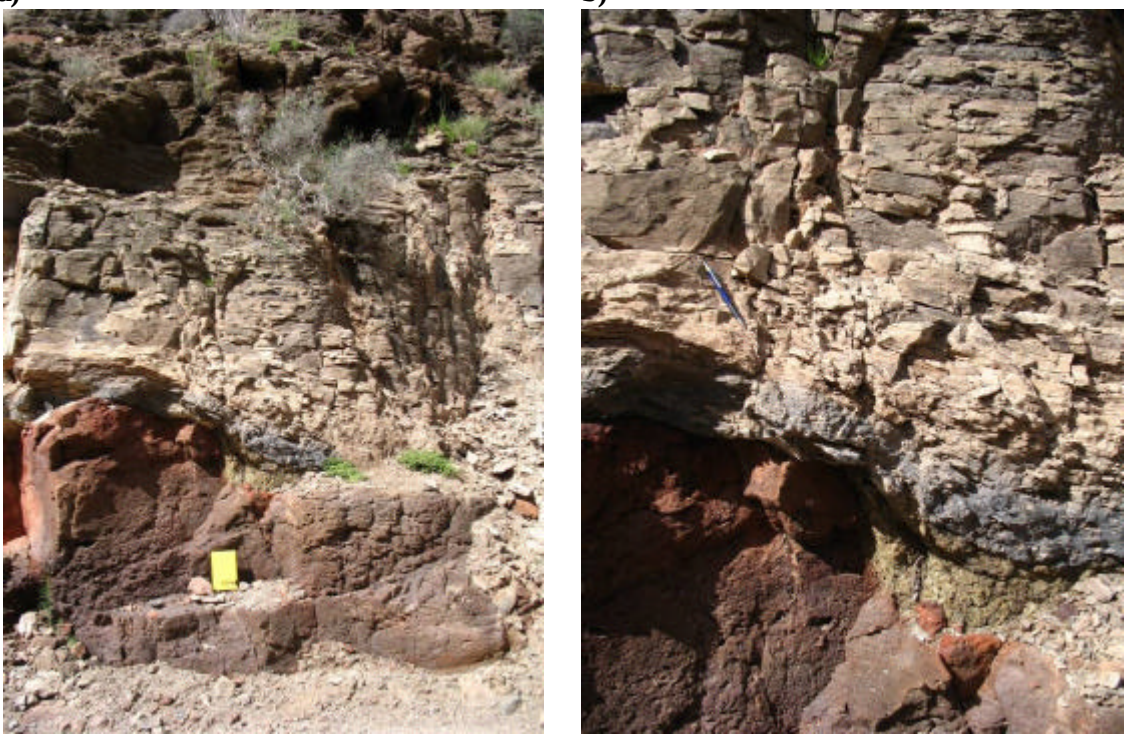

Figure 30: Minor faults in the upper surface of ignimbrite A
Top of ignimbrite A is offset, ignimbrite B flows across the offset and ponds against the scarp. a) note the bending of the black glassy vitrophyre and foliations at the base of B b) the fault in ignimbrite A does not cut the vitrophyre, although joint surfaces in ignimbrite B give the impression of a continuation into the overlying unit. Flow direction is from right to left (NE to SW)

Deformation at Montana Cedro occurs as deformation bands in the ashy section and as joints in the competent layers. In the A2 unit there are 2-3 deformation bands close to the faults, these are oblique to the fault. Joints in the competent A1 and A3 layers are planar and parallel to the fault. As all deformation structures in ignimbrite A at Cedro occur in the fault damage zone they are discussed in chapter 3.

2.3.3 Ignimbrite B

Ignimbrite B was investigated in the same locations as ignimbrite A as it is the overlying ignimbrite unit. The same procedures were followed in the examination of the fault core and damage zone. At Tauro over 30 meters of ignimbrite B are exposed although only the base portion is accessible. At Los Frailes it is possible to walk up through the entire 10 m thick unit, as is the case at Montana Cedro where the unit is 30 m thick (Figure 31).

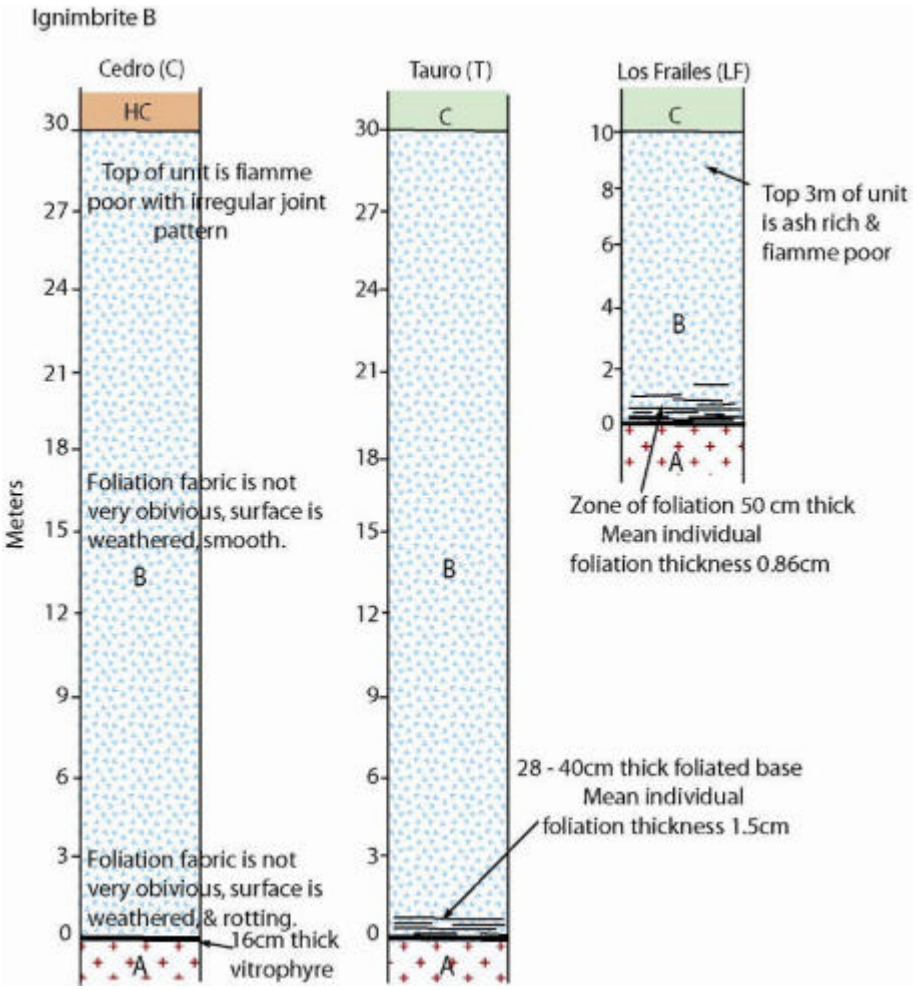

Figure 31: Log of ignimbrite B at Cedro, Tauro and Los Frailes
The dimensions and aspect ratios of the fiamme change from the base of the unit to the top, shown in Table 3 and Table 4

Ignimbrite B is ash and fiamme rich with some lithics, varies from blue-green to pale green and is densely welded throughout with a strong eutaxitic texture developed in the mid to lower portions of the unit. The base of ignimbrite B at Tauro and Los Frailes is marked by a thick devitrified yellow vitrophyre that is very friable (Figure 32a). The weathered surface is green and a fresh surface reveals a paler white-green colour. Immediately above the vitrophyre is a foliated zone composed of alternating layers of ash and highly flattened fiamme (Figure 32b). In Los Frailes this foliated zone is 50 cm thick. In Tauro it is up to 1.5 m thick and the individual foliations are 0.1 cm to 4.3 cm thick and merge into the layers above and below along strike.

Los Frailes	Mean major axis (cm)	Mean minor axis (cm)	Mean aspect ratio
Unit base	1.70	0.21	9.85
1m above base	1.29	0.23	4.95
3m above base	1.42	0.23	5.55
8m above base	1.74	0.32	5.06

Table 3: Mean dimensions and mean aspect ratios of Ignimbrite B fiamme, Los frailes Fiamme were measured at increasing heights above the base of the ignimbrite unit.

Cedro	Mean major axis (cm)	Mean minor (cm)	Aspect ratio
18 m above unit base	1.56	0.44	3.68
27 m above unit base	0.74	0.23	3.32

Table 4: Mean dimensions and mean aspect ratios of Ignimbrite B fiamme, Cedro Fiamme were measured at the mid-section and top of the ignimbrite unit.

a)

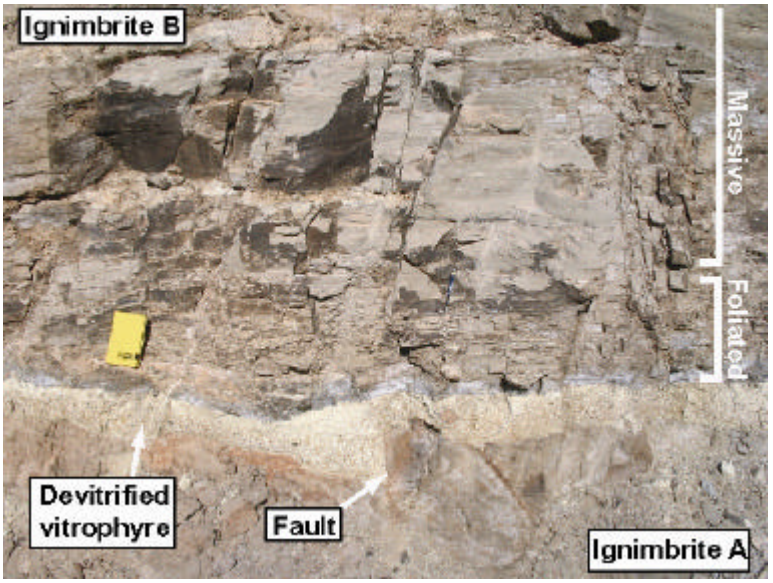

b)

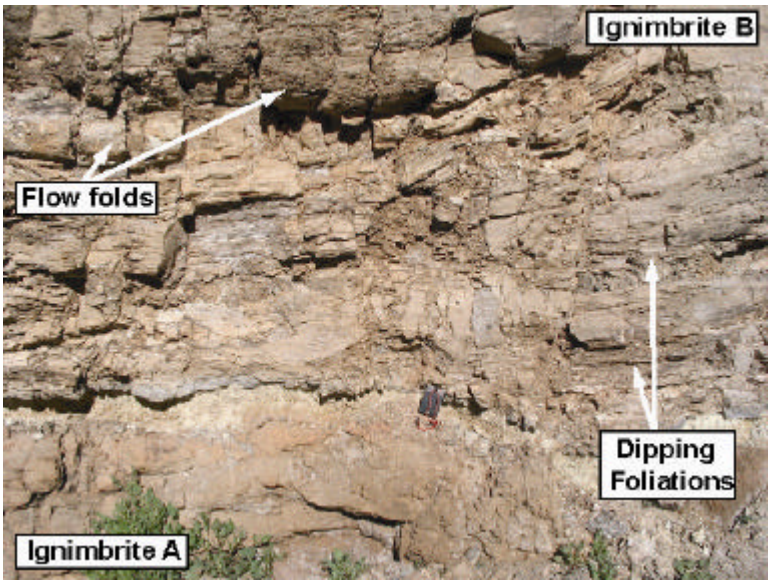

Figure 32: Ignimbrite B overlying ignimbrite A at Barranco Tauro
a) Yellow devitrified vitrophyre marks the base of ignimbrite B, vitrophyre thickens where it flows across a small fault in the top of ignimbrite A. The bottom 50 cm of ignimbrite B is foliated and above this the unit becomes massive. b) ignimbrite B is highly foliated up to 1.5 m above the base, the concave structures to the top left are the side view of flow folds. Where the unit is highly foliated and flow folds are present the rock is generally very fragmented. Photo is looking NW

The fiamme at the base of ignimbrite B both at Los Frailes and Tauro are extremely flattened and stretched (Figure 33a) the mean aspect ratio is 9.9. Moving up through ignimbrite B the degree of fiamme flattening decreases to an aspect ratio of 4.97. At Los Frailes the decrease in fiamme aspect ratio coincides with a decrease in joint density moving from the base to the top of the unit. The implications of this observation are discussed more thoroughly in Chapter 6, section 6.3. The contact between ignimbrite B and A at Los Frailes is horizontal. The foliations in Tauro are either parallel to the underlying contact with A or dipping between 10° and 25° south (Figure 32b). The

upper surface of ignimbrite A is not horizontal but slopes 6° to the west. Clasts in the lower part of ignimbrite B are surrounded by flow banding that form pressure shadows (Figure 33b). In places the unit's base contains flow folds (Figure 32b) and the contact with the underlying ignimbrite A is uneven and irregular. Where the flow folds occur the material is more broken than elsewhere and where folds occur above small faults in the underlying ignimbrite A the unit is highly jointed. These flow indicators and the extremely stretched fiamme (Figure 33a) indicate rheomorphic flow having occurred in the material. The dipping substrate on to which it was emplaced would argue for remobilization of the material while still above the glass transition temperature. A similar process has been observed in the overlying ignimbrites D and E at Barranco Tauro (Kobberger and Schmincke, 1999; Leat and Schmincke, 1993). Above the foliated zone ignimbrite B becomes smoother, the foliations are absent and the fiamme are less flattened and less abundant.

a)

b)

Figure 33: Foliation fabric in the base of ignimbrite B
a) Highly stretched and flattened fiamme (dark brown) in the base of ignimbrite B at Los Frailes. b) Pressure shadows around lithics in the base of ignimbrite B at Tauro. Both features indicate flow at the base of the unit.

At Cedro ignimbrite B is rather weathered, the foliation is not as obvious as at Tauro and Los Frailes and at the base of the unit it is difficult to identify fiamme. The unit base is composed of a

16cm thick blue-green band that is very fine-grained and quite hard. The fiamme are quite flattened, the mean aspect ratio in the mid-section of the unit is 3.65. This is the case for the majority of the unit apart from the upper 5 m, which is extremely fiamme poor. The elastic modulus values for the unit at Tauro and Los Frailes and different parts of the unit at Cedro are shown in Table 5.

	Elastic Modulus (Gpa)	Uniaxial compressive strength (MPa)	Uniaxial tensile strength (MPa	Friction angle (f)	Cohesion
Los Frailes	9.2	-	-	-	-
Tauro base	6	-	-	-	-
Tauro 3 m above base	10.5	-	-	-	-
Cedro 5m above base	9	-	-	-	-
Cedro mid unit	8	-	-	-	-
Cedro mid unit	13.8	-	-	-	-
OWH	-	26 - 54	3.8 – 7.1	27 - 34	0.8 – 1.4
Calico hills	5.4 – 10.3	26 - 48	-	-	-

Table 5: Mechanical properties of Ignimbrite B

Elastic moduli for each ignimbrite B unit and at different heights in the unit at Cedro and Tauro calculated using a PUNDIT machine. Sections of the Owharoa ignimbrite, New Zealand (Moon, 1993) and Calico Hills tuff, Yucca mountain , Nevada (Schultz & Li, 1995) have similar petrophysical properties and elastic moduli to ignimbrite B; therefore the other material properties are assumed to reflect those of ignimbrite B.

In thin section (Figure 34), ignimbrite B at Cedro is composed of a fine grained matrix that has a mottled appearance. The original glass structure of the fiamme has been completely destroyed, only the outline remains surrounding very coarse acicular crystals. Cavities also contain coarse crystals and spherulites indicating vapour-phase crystallisation has taken place. Some fiamme are flattened while others are more irregular in shape and have been folded. Flattened fiamme bend around phenocrysts indicating a high level of compression. There are minor amounts of phenocrysts (1%) present ranging in size from 0.07 cm to 0.15 cm; these are broken rectangular fragments.

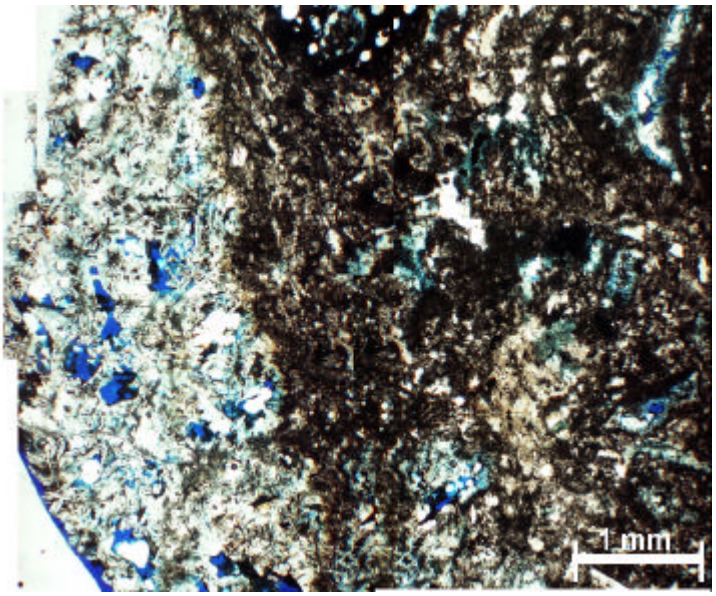

Figure 34: Ignimbrite B host rock at Cedro in plane polarised light
Cavities are filled with coarse crystals. The matrix is extremely fine grained and individual grains cannot be resolved using a light microscope. Section is stained with blue dye.

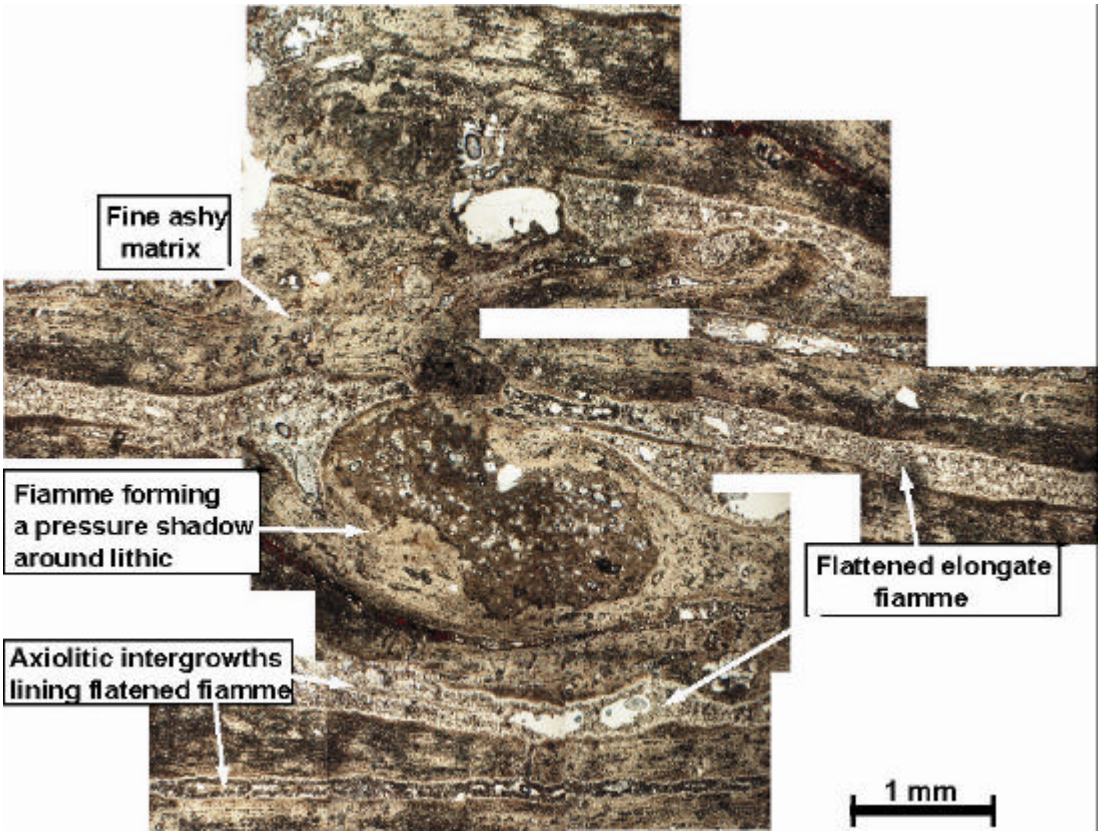

Figure 35: Ignimbrite B from the unit base at Los Frailes in plane polarised light
The fiamme are extremely flattened and elongated. Note the fiamme forming a pressure shadow on the left of the clast.

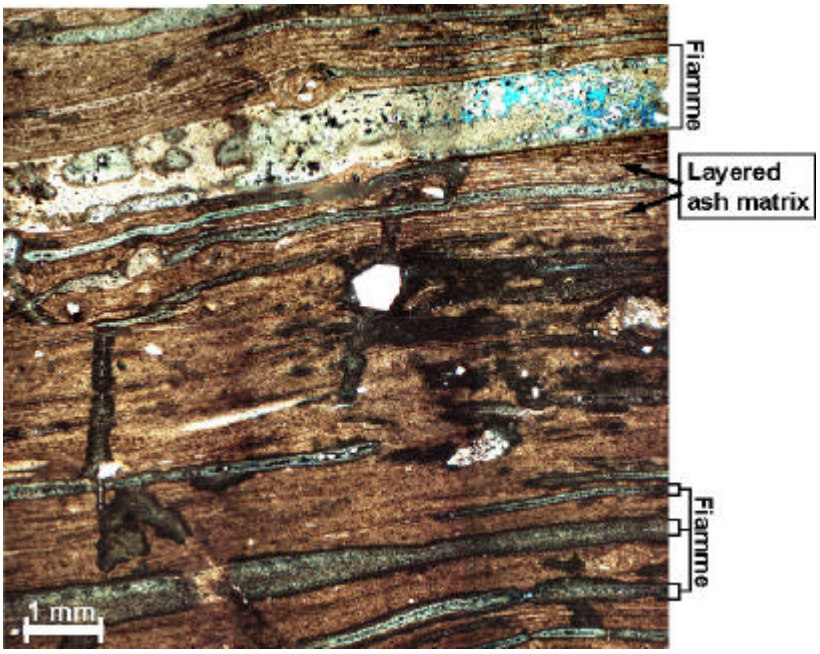

Figure 36: Ignimbrite B from the unit base at Tauro in plane polarised light. Section has been stained with blue dye to highlight the fractures and pore space. Fiamme are highly flattened and stretched, the ash matrix also has a layered appearance. Note the axiolitic crystal growth in the thin fiamme at the base of the image.

Thin sections from the base of ignimbrite B at Tauro and Los Frailes are composed of highly flattened fiamme, minor amounts of pumice clasts (2%) and phenocrysts (5%) in a very fine grained matrix (Figure 35 & Figure 36). Fiamme thickness varies from 0.001 cm to 0.08 cm and reach lengths of 2.5 cm. Both the fiamme and matrix are fully devitrified, fiamme form asymmetric pressure shadows where they are wrapped around lithic clasts (Figure 35).

Deformation structures

Joints

Unfaulted protolith sections at Los Frailes and Tauro are cut by major vertical planar joints, meters in height that are ubiquitous throughout the unit (Figure 37); such columnar structure is characteristic of many ash-flow tuffs (Ross and Smith, 1961).

Figure 37: Ignimbrite B host rock
Ignimbrite B is ubiquitously cut by metre scale smooth joints that are approximately evenly spaced. Photograph is off the east side of Barranco de Tauro, taken looking southwards.

There are two joint sets that are orthogonal to each other and radial (NE-SW) and concentric (NW-SE) to the caldera margin (Figure 38). Ross & Smith (1961) noted that many welded tuffs have joint bound columns that are approximately rectangular or square that are generally considered to be tensional cooling joints. The orientation of the joints in ignimbrite B may have been influenced by caldera movement or they may be of a tectonic origin formed during cycles of caldera doming and collapse, prior and subsequent to eruptions (Figure 39).

Figure 38: Orthogonal joints in unfaulted ignimbrite B at Los Frailes.

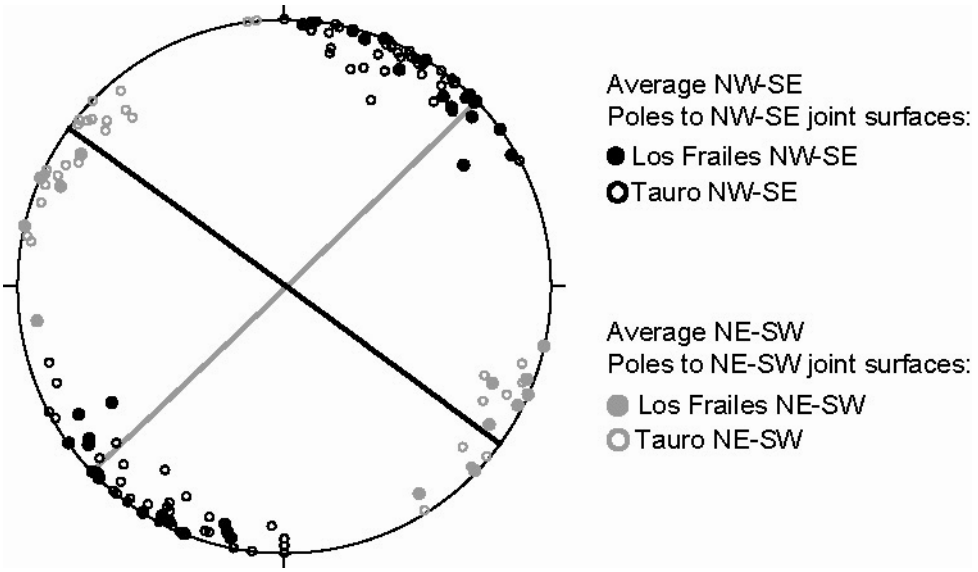

Figure 39: Stereonet of joints ignimbrite B protolith
Great circles for joints in Los Frailes and unfaulted Tauro. The orthogonal joint sets have orientations concentric (NW-SE) and radial (NE-SW) to the caldera margin.

Protolith joint spacing at Tauro ranges from 0.04 m to 1.91 m with a mean spacing of 0.46 m and a joint density of 2.1 joints per meter. At Los Frailes joint spacing and density decreases from the base of the unit, where there is a strong foliation, upwards to non-foliated areas. At the base joint spacing ranges from 0.08 m to 1.15 m and has a mean spacing of 0.31 m and a joint density of 3.2 joints per meter. The remainder of the unit has joint spacing from 0.06 m to 13.50 m (Figure 41), the mean joint spacing is 1.55 m and joint density is 0.64 joints per meter. The background joint density level therefore lies between 0.64 and 2.1 joints per meter with an average of 1.98 joints per meter. The majority of joints are planar and sub-parallel but some joints follow the foliations in the base of the Tauro and Los Frailes units creating a stepped joint morphology (Figure 40).

Figure 40: Stepped joint in the base of ignimbrite B at Los Frailes. The joint cuts across the foliation but in places follows the foliation.

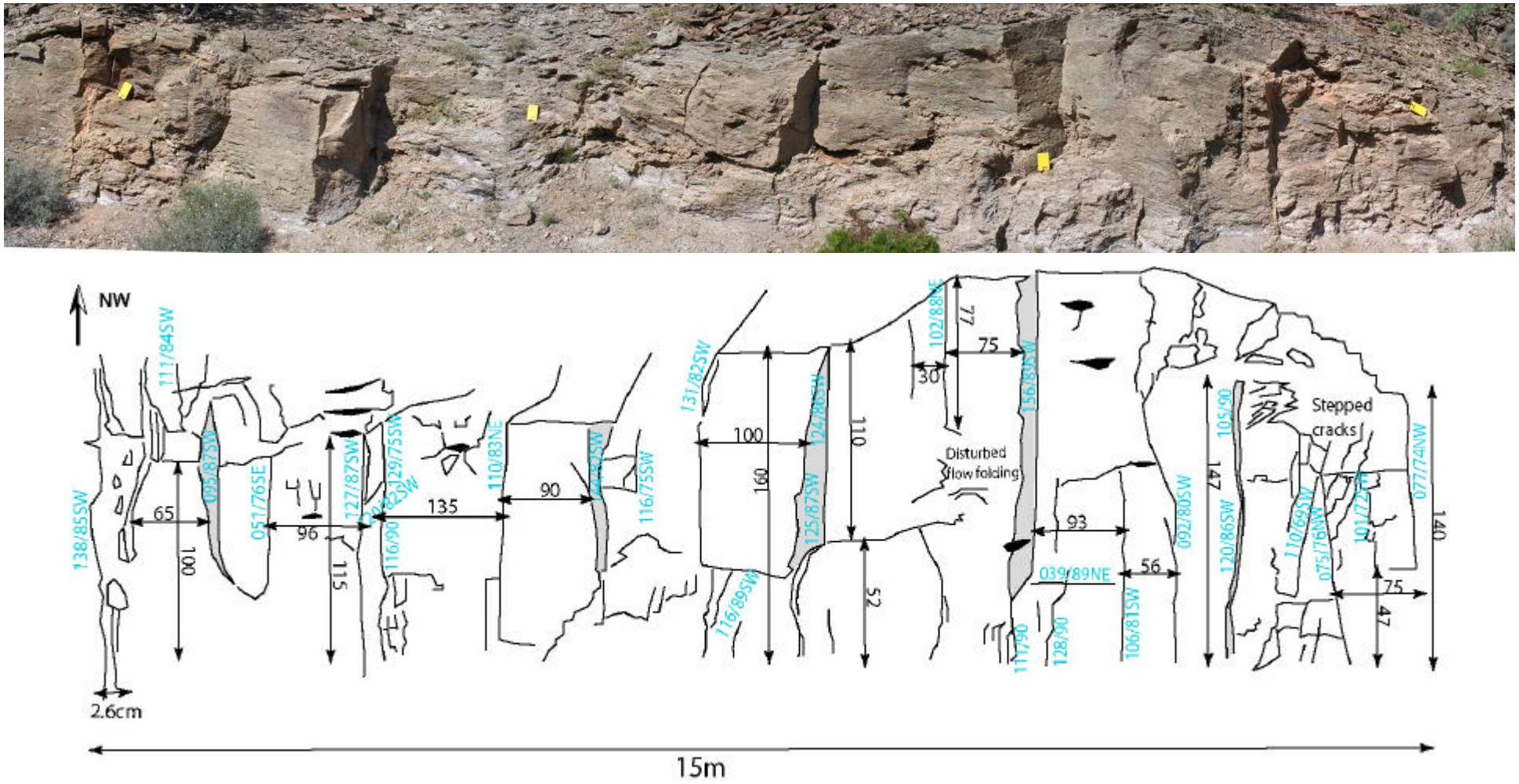

Figure 41: Ignimbrite B host rock section

Cross-section of unfaulted ignimbrite B at Los frailes, section is ~6 m above the base of the unit. The sketch shows joint spacing (black arrows, measurements in centimetres) and joint orientations (blue) , sketch is not to scale.

2.3.4 Ignimbrite X

Ignimbrite X was investigated at Montana Cedro only, as a population of faults with various displacement amounts was not observed it is not possible to examine the evolution of the fault in the same detail as ignimbrite A and B. As a result I present here the fault data related to ignimbrite X as well as the unit's petrophysical properties.

Protolith

The unit is 40 m thick and has accumulated at least 148 m of displacement as a result of the sense of slip reversal it underwent prior to the eruption of the upper Mogan group (Figure 12). Ignimbrite X is crystal-rich containing millimetre size crystals of feldspar and quartz, there are abundant lithics but minor amounts of fiamme (Figure 42a). The unit is relatively undeformed and is cut by occasional vertical planar joints and horizontal partings (Figure 42b). Above the partings, grain size is coarse and fines upwards, suggesting that these horizontal joints are related to ignimbrite deposition. The density of vertical joints increases slightly approaching the fault. The top 5 m of the unit is composed of an ash-rich, crystal-poor unit with minor amounts of lithics and fiamme.

a) **b)**

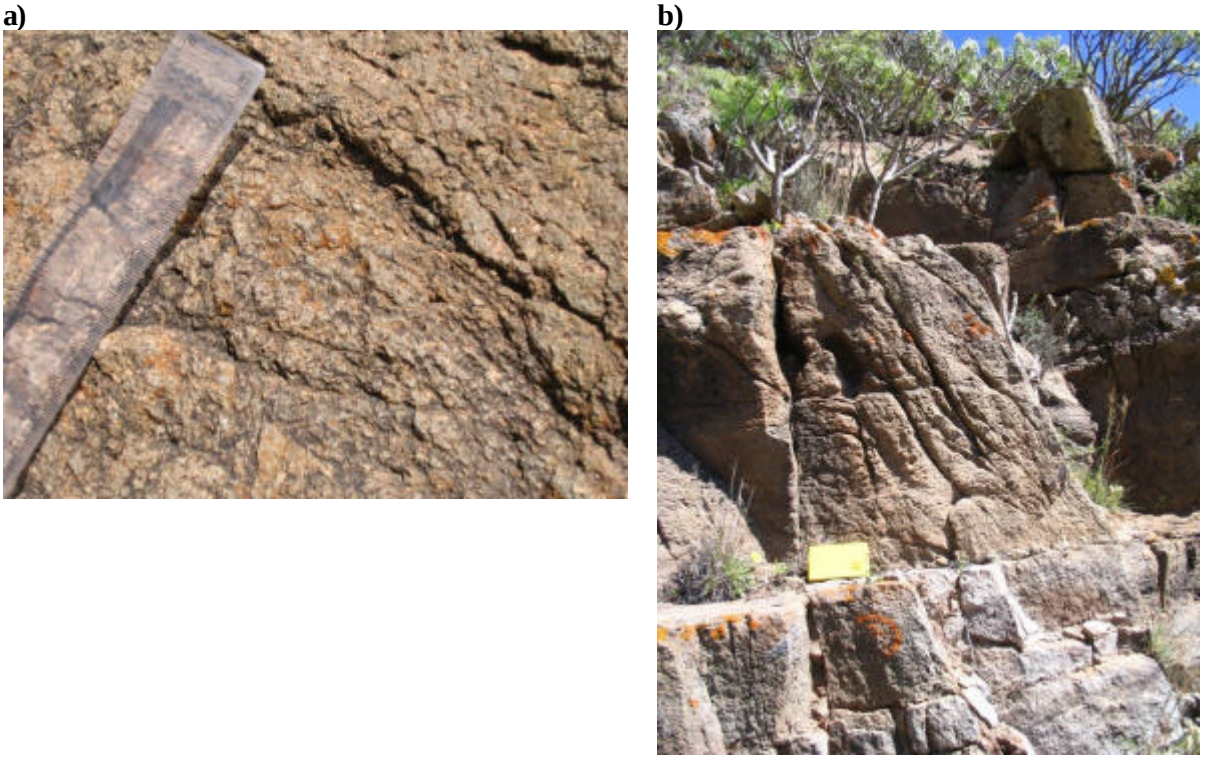

Figure 42: Ignimbrite X ~10 m from the fault core at Cedro
a) Ignimbrite X is a massive unit, crystal rich and fiamme poor (15 cm ruler for scale) b) The fieldbook (16.5 cm long) sits on a ledge created by a horizontal parting. The fractures on the surface are not true joints but grooves formed by weathering.

In thin section ignimbrite X contains abundant large angular phenocrysts of feldspar and minor amounts of hornblende (Figure 43). The feldspar phenocrysts range in size from 0.02 cm to 0.40 cm. The phenocrysts lie in a highly porous matrix, as shown by the blue staining. Denser patches show a fine grained matrix that contains flattened wispy glassy fiamme, with no evidence of devitrification. Some of the shards have retained there delicate Y-shaped structures indicating low levels of compaction and others are wrapped around the phenocrysts.

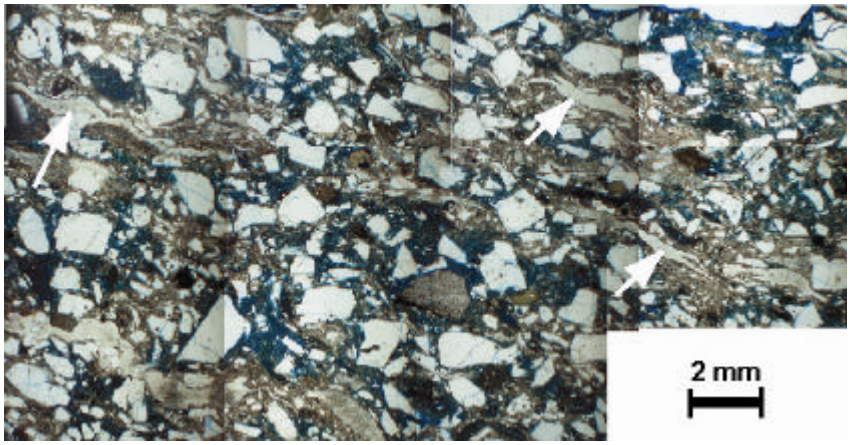

Figure 43: Ignimbrite X host rock in plane polarised light
Very small fiamme, ~2 to 4 mm long (white arrows) are interspersed with the feldspar phenocrysts, the fiamme retain some of their glassy texture.

Fault core

The fault core is only exposed where it is offset against ignimbrite B and the T4 lava, 23m above the base of ignimbrite X (Figure 44). The ignimbrite X fault core adjacent to T4 is 0.45-0.58 cm wide and is a creamy, very fine-grained powdery unit with some small clasts 0.4-3cm in size (Figure 45). Occasionally the fault core gouge has a banded appearance. Next to the slip surface there are bands of fine-grained, light green soft gouge containing clasts of ignimbrite X. Beside these are bands of coarse-grained, dark green, hard gouge that contains brown and black clasts, these lithic clasts are also seen in the host rock. At the top of ignimbrite X the fault core contains a number of deformation bands that also mark out colour changes in the gouge. At the fault plane X forms a fine-grained gouge containing centimetre size clasts 1-2 cm and 10-20 cm in size.

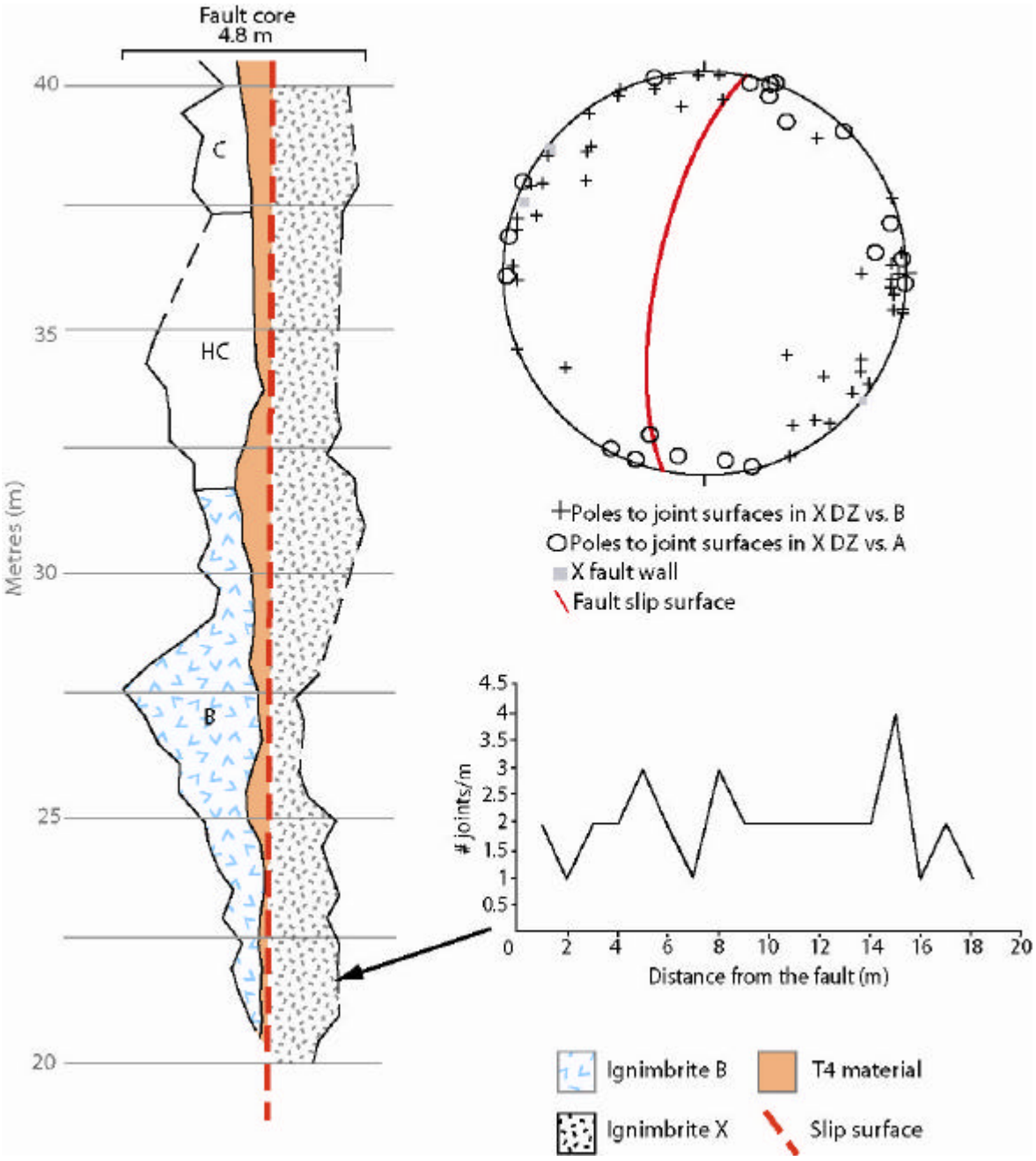

Figure 44: Fault core log of ignimbrite X
In the fault core ignimbrite X is juxtaposed with ignimbrite B, HC and C. The joint line transect starts near the base of the exposed fault core.

Where X is offset against ignimbrite B the fault core width ranges from 0.9 m to 1.8 m. The core is matrix supported; clast matrix ratio is 30:70. The gouge is a dark grey colour, clasts are rounded to subrounded, randomly orientated and are either clasts of ignimbrite X or lithics from the unit.

The contact between the red gouge that comprises the fault slip surface and ignimbrite X gouge is sharp and planar (Figure 45). The red material forms a flat surface cut by a few fractures with occasional clasts of blue lava protruding out from it. The X gouge does not mix with the red slip-surface gouge. The fault core-fault wall contact is exposed in small sections along the fault. In places there is a definite fault wall against which the X gouge lies, towards the top of the unit there

are no discernable fault walls and the fault core blends into the damage zone. At these locations an increase in grain size and joints cutting competent rock are used as indicators of the start of the damage zone.

a)

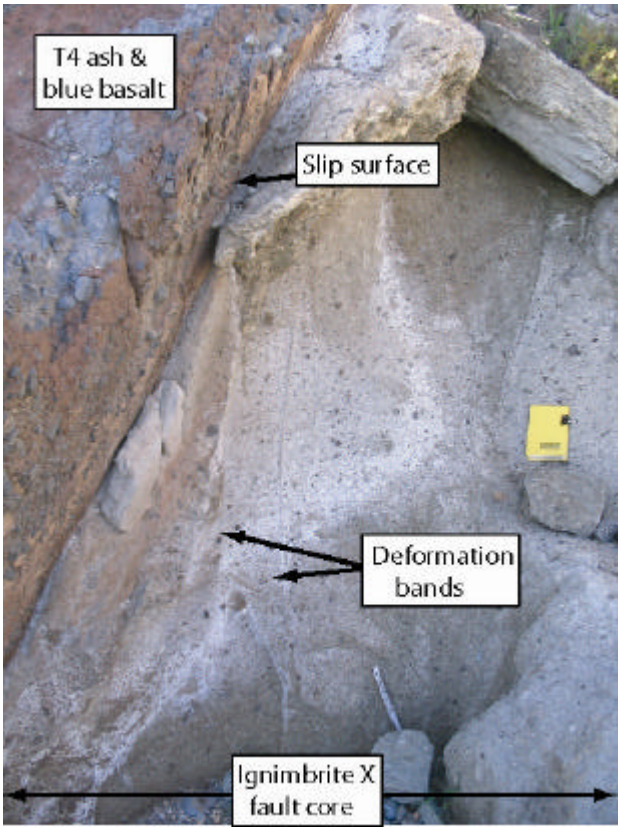

b)

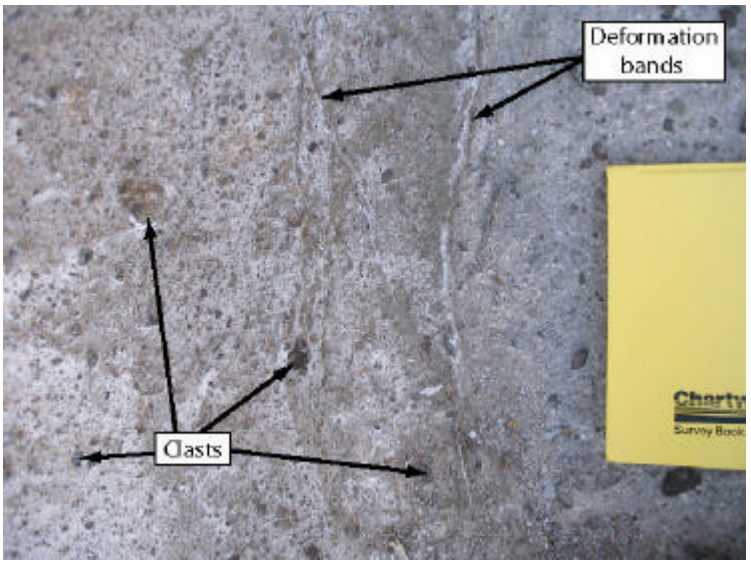

Figure 45: Ignimbrite X fault core

a) The ignimbrite X fault core is composed of fine grained gouge and clasts cut by meter long thin deformation bands. The contact between the ignimbrite X fault core material and the slip surface is sharp and planar. b) The core contains small sub-rounded clasts of ignimbrite X and some lithics that are can be identified in the host rock.

Damage zone

The damage zone is made up of highly indurated rock. Deformation in X adjacent to the fault core is limited to the first 0.5 m out from the fault wall. The remainder of the unit has a joint density of 1 joint per meter; as only this faulted section was examined it is not possible to say whether background joint levels are also 1 joint per metre or less. The joints are vertical, planar, and approximately evenly spaced. Joints in ignimbrite X adjacent to ignimbrite B have N-S and NE-SW orientations and joints in X adjacent to T4 are orientated N-S and ESE-WNW. There are two parting joints one meter apart that indicate flow unit boundaries; these are crosscut by the vertical joints. The top ashy unit of ignimbrite X is not jointed but there are a few deformation bands extending down from the overlying vitrophyre.

Both the fault core gouge and the damage zone are cut by small faults. In the gouge these faults are composed of ridges of material finer than the surrounding gouge (deformation bands), in the damage zone the faults are composed of small rotated blocks. The unit changes colour across the deformation bands.

2.4 Summary

The three ignimbrite units investigated differ significantly in their physical and compositional properties. This creates the opportunity to investigate how different aspects of the host rock properties affect fault growth. Examining petrophysically different rock types having undergone the same amount of displacement in the same structural setting allows us to exclude the affect of displacement on fault growth and focus on the influences of the host rock properties (ignimbrite A and B in T2, T2.5, C5 and C15). Examining units that have accumulated greatly different amounts of displacement allows us to consider the role of displacement in fault growth by examining a fault population within the one ignimbrite unit (Cb22 and Ca30 offset against Cx140).

In general ignimbrite A is ash and crystal-rich and moderately to densely welded, fiamme have a mean aspect ratio of 2.5. At Montana Cedro ignimbrite A is composed of three flow units. The first flow unit emplaced was A1; it is moderately welded, contains abundant millimetre size fiamme and feldspar phenocrysts. The next unit A2 is ashy, extremely friable, contains large amounts of pumice clasts but is fiamme poor. A3 is moderately welded, ash and pumice-rich with minor amounts of phenocrysts. Fiamme are much smaller in A3 compared to A1.

Unfaulted sections of ignimbrite A are cut by sub-vertical, smooth, planar joints. There are two joint sets oblique to each other trending E-W and NW-SE. The NW-SE joint set is concentric to the caldera margin and the E-W set is oblique to the margin. The average joint density in the unfaulted sections (background joint level) is 1.5 joints per metre.

Ignimbrite B is ash and fiamme rich with minor amounts of lithics and phenocrysts. The unit is densely welded and has a well developed eutaxitic texture and foliation, particularly above the base of the unit. The fiamme become less abundant and less flattened moving upwards and the foliations are absent. The base of the unit also contains occasional flow folds these, along with the foliation, indicate rheomorphic flow.

Vertical, sub-parallel, planar joints metres in height cut the unfaulted sections of ignimbrite B. There are two orthogonal joints sets orientated NW-SE and NE-SW; the first set is concentric to the caldera margin the latter is radial to the margin. The background joint level at Tauro is 2.1 joints per metre and at Los Frailes 1.98 joints per metre.

Only one section of ignimbrite X was examined, this is cut by the large growth fault at Montana Cedro, therefore a background joint level was not attainable. Ignimbrite X is moderately welded, fiamme poor and crystal-rich; phenocrysts of feldspar and quartz are millimetres in size. The top of the unit is ash rich and moderately to poorly welded. The unit is cut by vertical planar joints, joint density is 1 joint per metre increasing slightly adjacent to the fault. The top ashy part of the unit is cut by occasional deformation bands. Deformation bands are also observed in the fine grained fault core of ignimbrite X.

In this study there are some problems with the method used to establish the background joint density. Firstly a sample number of two (Los Frailes for ignimbrite A and B and Tauro for ignimbrite B) is too small to statistically establish a picture of what the background joint density is in these rocks. However this was unavoidable due to the lack of accessible exposure in the area. Secondly the full range of compositions possible within an individual ignimbrite unit, such as different degrees of welding, vapour phase alteration, lithic and fiamme content, could not be covered with such a sample size. At Los Frailes there is no evidence of faulting, which may suggest that the ignimbrite units in this area are in fact not prone to fault formation. Possibly the result of secondary vapour phase alteration reducing porosity and creating a rock composition that is stronger, less likely to form joints and therefore not typical of a section that is liable to faulting.

Another issue is the topography onto which the unit was deposited. Kobberger and Schmincke (1999) examining ignimbrite D further up in the stratigraphy observed that ignimbrite emplacement onto a sloped surface caused flow of the unit and stretching of the material (rheomorphic flow). Initially flow of the hot pyroclastic material caused shear strain; stretching fiamme, forming lineations and rotational fabrics (pressure shadows around lithics). As the material cooled towards the plastic-brittle transition new fabrics such as compressional folds and kink bands formed. Further cooling and the commencement of lithification reduced the viscosity contrast between the fiamme and matrix and resulted in subvertical, extensional cracks forming in the matrix. The rheomorphic flow and subsequent deformation structures were caused by a slope of a mere 6°, the

same as the slope ignimbrite B was deposited on at Tauro. At Los Frailes the deposition surface was horizontal. Therefore emplacement onto a sloping surface may increase the number of joints formed and thus background joint density levels.

To establish a more accurate picture of background joint density several unfaulted sections in the same ignimbrite unit should be examined. These ignimbrite sections should encompass different depositional topography, degrees of welding and secondary alteration, different porosities etc. In relation to the background sections examined in this study they encompass deposition on sloping and horizontal topography

Descriptions of the faults examined in each ignimbrite unit and a more detailed discussion of fault zone deformation elements (fault core morphology, fault core clast size & shape, damage zone joint density/orientation/morphology) and how they relate to fault processes are given in chapter 3, 4 and 5.

3

Ignimbrite A: analysis of fault zone architecture

3.1 Aim

The fault populations examined occur in two distinctly different ignimbrite unit – ignimbrite A and ignimbrite B. In the following two chapters I present descriptions of the fault zone components (fault core, damage zone, and clast size), and their architecture.

Comparing faults with varying amounts of displacement within each unit allows the investigation of the influence of displacement on fault core growth. The comparison of faults within two different units but with the same amount of displacement i.e. two juxtaposed units, highlights the influence host rock composition has on fault growth (see section 5.2.2 and chapter 6).

3.2 Ignimbrite A

3.2.1 Protolith

Faults in ignimbrite A were examined at Barranco de Tauro and Montana Cedro. At Tauro the faults are exposed in the uppermost flow unit of ignimbrite A (A3 analogue). At Montana Cedro faults are exposed in all three flow units of Ignimbrite A. For a full description of ignimbrite A see section 2.3.2.

3.2.2 Fault architecture

Seven normal faults cutting ignimbrite A were examined. At Barranco de Tauro four faults offset the top of A against the base of B by varying amounts of displacement:

TA0.17 (0.17 m displacement)

TA0.32 (0.32 m displacement)

TA0.35 (0.35 m displacement)

TA2 (2 m displacement)

Ta2.5 (2.5 m displacement)

At Montana Cedro A is offset against B by:

Ca5 (5 m displacement)

Ca15 (15 m displacement)

Ca30 (30 m displacement)

The Ca30 fault is part of the large normal growth fault that occurs at Montana Cedro. Ignimbrite A is in the hangingwall of the growth fault and has been offset across the fault by 30 m. The entire fault has a total accumulated displacement of over 140 m. Here ignimbrite A is offset against the stratigraphically lower ignimbrite X (section 2.1.3)

The structural analysis is based on the four larger faults (TA2, Ca5, Ca15 and Ca30) as they have clearly identifiable fault cores and damage zones. The centimetre offset faults are in the TA2 hangingwall damage zone (Figure 46). The Ta2.5 fault is not discussed in great detail as only the top 30 cm of ignimbrite A is exposed beneath ignimbrite B.

Barranco de Tauro: At Tauro there are two metre-scale faults with 2 m and 2.5 m of displacement and three minor centimetre-scale offset faults. The faults offset the top part of ignimbrite A against the overlying ignimbrite B. Neither fault at Tauro contains a discrete slip surface within the fault core nor are there any clasts of A in either of the Tauro faults.

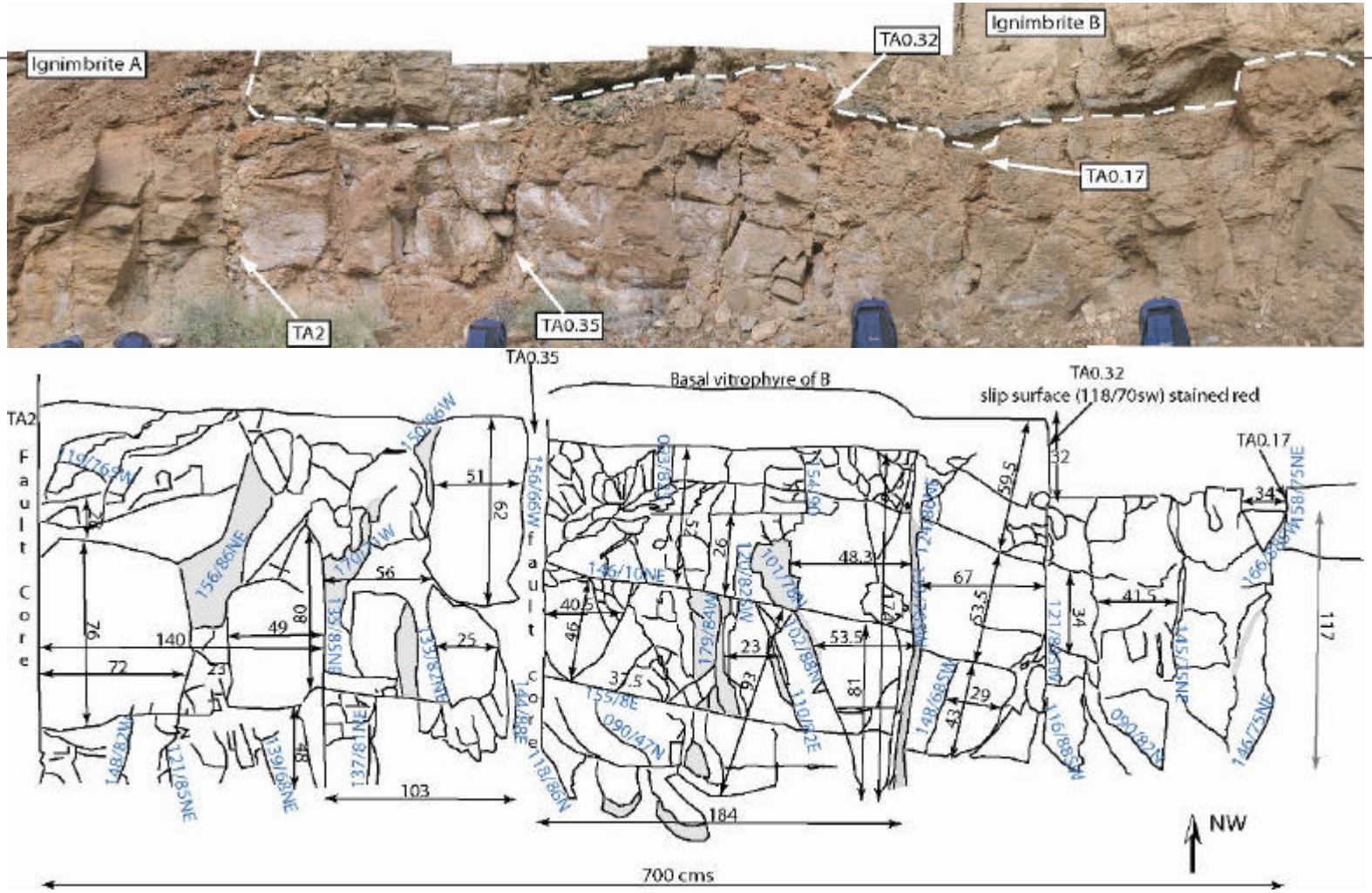

Figure 46: Minor offset faults at Barranco Tauro

Photo shows four of the five faults at Barranco Tauro; the TA2 fault (left) and the three centimetre scale faults that occur in the TA2 damage zone. The sketch of the section is not to scale, the black arrows are labelled with the actual joint spacing measurement (cm) and the joint orientations are shown in blue. Note that the TA0.17 fault and an unlabelled fault to its right (far right in photo) do not extend up into ignimbrite B.

TA2:

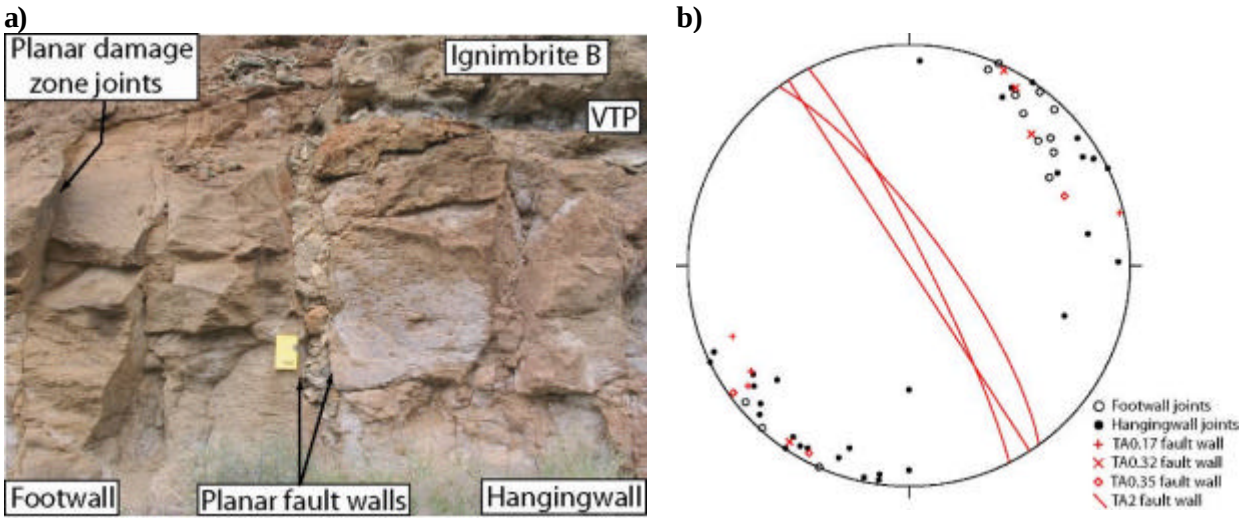

Figure 47: Barranco Tauro ignimbrite A fault and stereonet
a) TA2 fault and b) stereonet showing poles to joint surfaces in the footwall and hangingwall damage zone, great circles are for the TA2 fault walls.

Fault core: T2 is exposed in a vertical cross-section, the fault trends 147° with a dip of 84°-90° NE (Figure 47). The fault core in ignimbrite A ranges from 7 cm to 18 cm in width. The fault walls are smooth, slightly undulating and have a sharp contact with the fault core material. The TA2 fault core is composed entirely of blocks of the overlying ignimbrite B. The fault core is clast supported; the spaces between large clasts are filled by smaller centimetre-size clasts and negligible amounts of ash sized material. The presence of clasts of the overlying ignimbrite B in the fault core indicates that material has fallen into the fault from above. Therefore the ash sized material is not likely to be fault gouge as it may have washed in/fallen in from above. The ignimbrite B clasts have an angular cuboid shape and are randomly orientated. Clast size decreases towards the base of the exposed fault.

Damage zone: The joints in the TA2 footwall have smooth undulating surfaces; the orientation of an individual joint surface can change within 30 cm along dip (Figure 48). The majority of joints have apertures <1 mm wide and are unfilled. Damage zone joint spacing ranges from 0.17 cm to 0.8 cm, average joint spacing is 0.41 cm and joint density is 2.38 joints per metre.

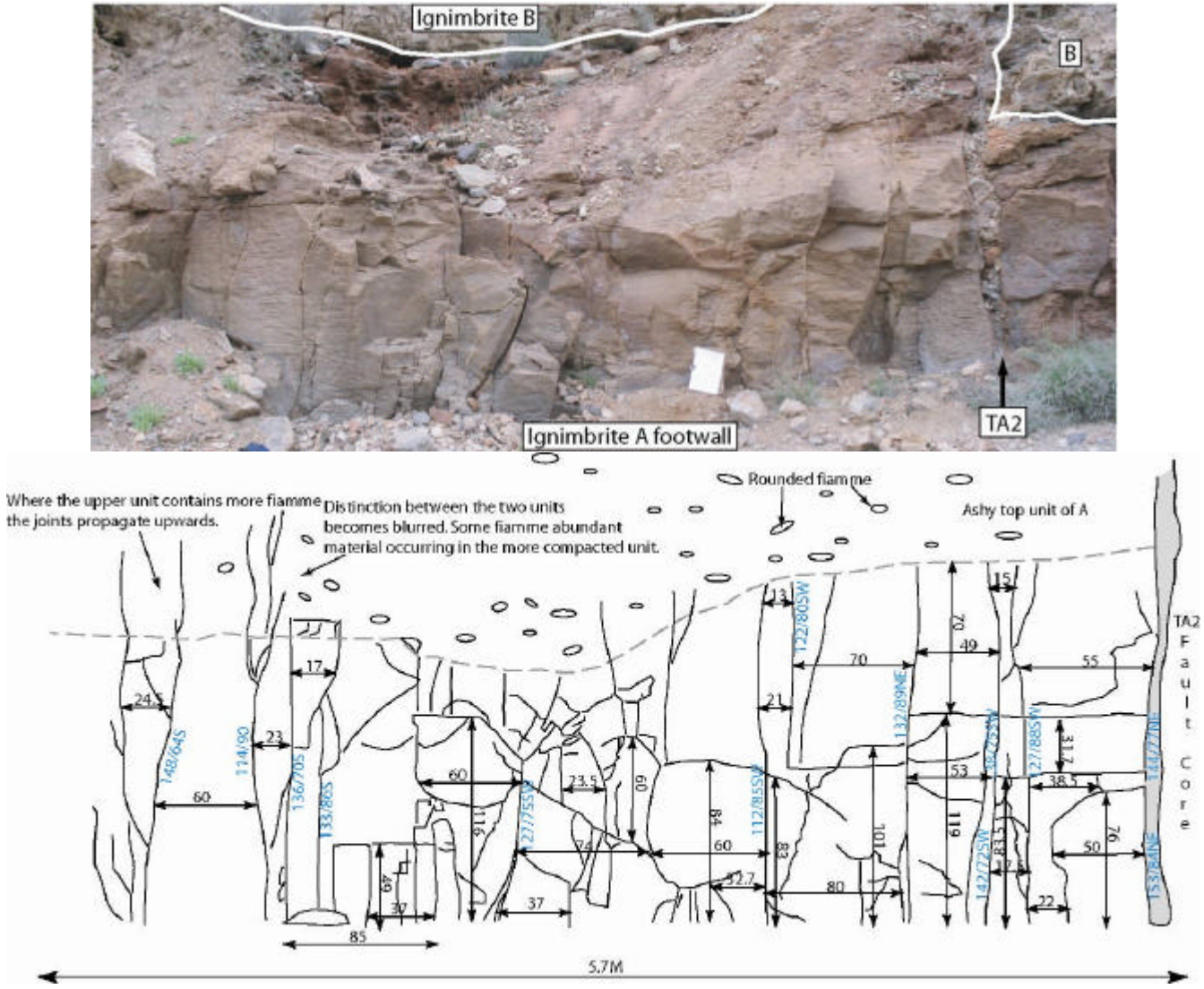

Figure 48: Photograph and sketch of the TA2 footwall damage zone.

The footwall has lower joint frequencies than the hanging wall. There is a main sub-vertical planar joint set and occasional horizontal joints. The sketch is not to scale, the black arrows are labelled with the joint spacing measurement (cm) and joint orientations are in blue.

The hangingwall joints are more irregular in orientation and not as vertically extensive (Figure 46). Three joint sets can be identified in the TA2 damage zone; horizontal joints, meter-scale vertical joints and centimetre-scale vertical joints The main vertical joint set is planar, metres in height and has a NW-SE orientation. Spacing of the main vertical joint set ranges from 0.17 m to 0.8 m and the average joint spacing is 0.42 m; the average joint density is 2.4 joints per meter. There are three sub-horizontal, metre-scale, planar joints that are cross-cut by the main vertical joint set; thus delineating meter size blocks (Figure 46). The blocks are infilled by short centimetre-scale vertical and sub-vertical joints. Joint density in the TA2 damage zones is only slightly greater than the Los Frailes background joint density despite being cut by a 2 m offset fault and a number of smaller faults. The footwall and hangingwall damage zones are 3 to 4 meters wide.

As the main vertical joints cross-cut the horizontal joints it suggests that the horizontal joints are partings between individual flow units. The main vertical joint set is orientated concentrically to the caldera margin and is on the same length scale as the TA2 fault. The vertical extent of these joints and their orientation to the caldera margin suggests they are related to regional scale caldera doming and collapse rather than small scale localised faulting. The short vertical joint set abuts against the horizontal parting joints suggesting they were formed by damage associated with the local small-scale faulting; the absence of similar small-scale joints at Los Frailes further strengthens this idea. The dip of the short vertical joints is altered when they cut across fiamme or are deflected by weathered out fiamme (Figure 49), occasionally sections of the short joints run horizontally along fiamme.

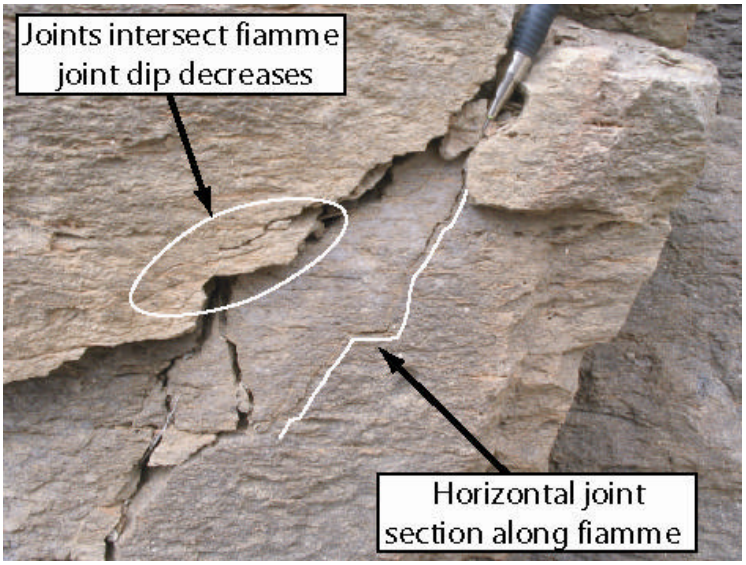

Figure 49: Joint in ignimbrite A TA2 damage zone
The dip of the joint is deflected when it intersects fiamme. Photograph is of a joint section in the footwall of TA2.

Ta2.5:

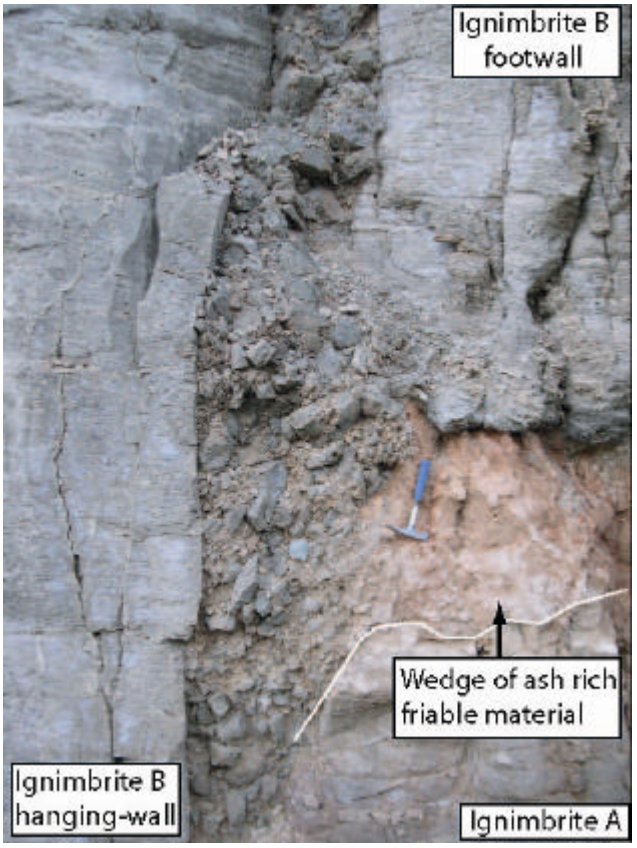

Figure 50: Ta2.5 fault core.

Ignimbrite A in the footwall is composed of two units (Figure 51). The fault core contains angular clasts of ignimbrite B, the interstices are filled by small clasts of B and very fine grained unconsolidated material.

Fault core: The T2.5 fault trends 130° with a dip of 84°-86° NE (Figure 50). Here only the top 0.5 m of ignimbrite A is exposed in a vertical cross-section. The fault core adjacent to ignimbrite A is 50 cm wide and clast supported. As in the TA2 fault core, the fault core material is large angular blocks of ignimbrite B with the interstices filled by smaller clasts of B. The blocks increase in size moving up the fault core. Fine grained red material is found between some of the clasts. This may be gouge from ignimbrite A or it may have washed down from above. The contact between the fault core material and ignimbrite A is diffuse and irregular at the top of the unit becoming sharper moving down the fault.

Damage zone: The exposure of the damage zone in ignimbrite A is limited. In A the damage zone is in two units (Figure 51). The lower unit is relatively competent material with small fiamme 2 -3 cm long, very fractured & jointed. The upper unit directly below B and immediately next to the fault wall is red orange in colour, and composed of large round clasts in a very fine-grained friable red matrix. This red orange layer wedges out away from the fault and at a distance of 5.6 meters it is only a cm thick.

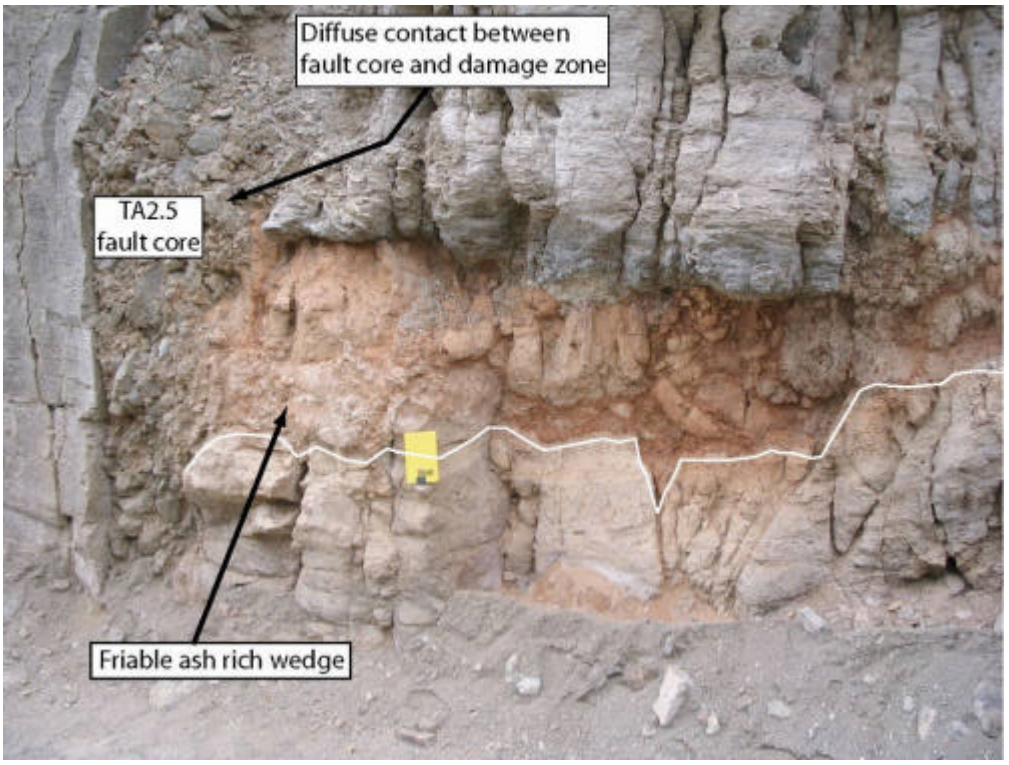

Figure 51: TA2.5 damage zone
Ignimbrite A is composed of two units, a competent fiamme rich unit overlain by a friable ashy wedge that thins moving away from the fault. Note also the foliated base of ignimbrite B.

Three minor faults offset the top of ignimbrite A against the base of ignimbrite B. They have 35 cm, 32 cm and 17 cm of displacement and orientations of 150°/82° W, 127°/78° E and 152°/77° E respectively (Figure 46). The 17 cm fault is a single planar surface in a zone of fractured ignimbrite A ~6.5 cm wide that terminates at the B vitrophyre. The 32 cm fault is a fracture 1 cm wide filled with fine grained, white, brittle clay and centimetre size fragments of ignimbrite A. The material adjacent to the slip surface is more fractured then the surrounding rock. The 35 cm fault is composed of two sharp planar surfaces defining a zone 12 cm wide. This zone contains fractured ignimbrite A in situ and a very fine-grained red gouge (30% gouge to 70% clasts). The material adjacent to the footwall slip surface is fractured and rotated towards the fault core.

Montana Cedro: There are three large faults at Montana Cedro. Two offset ignimbrite A against ignimbrite B with 5 m and 15 m of displacement. The largest fault is the growth fault previously discussed in section22. The fault has accumulated over 140 meters of displacement since the emplacement of ignimbrite X. The hangingwall is composed of T4 lava and upper Mogan ignimbrites A, B and C. The footwall contains middle Mogan ignimbrites TL, X, O and the T4 Lava. Ignimbrite A in this fault has accumulated 30 m of slip (Ca30) and is offset against ignimbrite X. All three faults are exposed along an oblique cross-section that allows examination of the fault core both up dip and along strike.

Ca5:

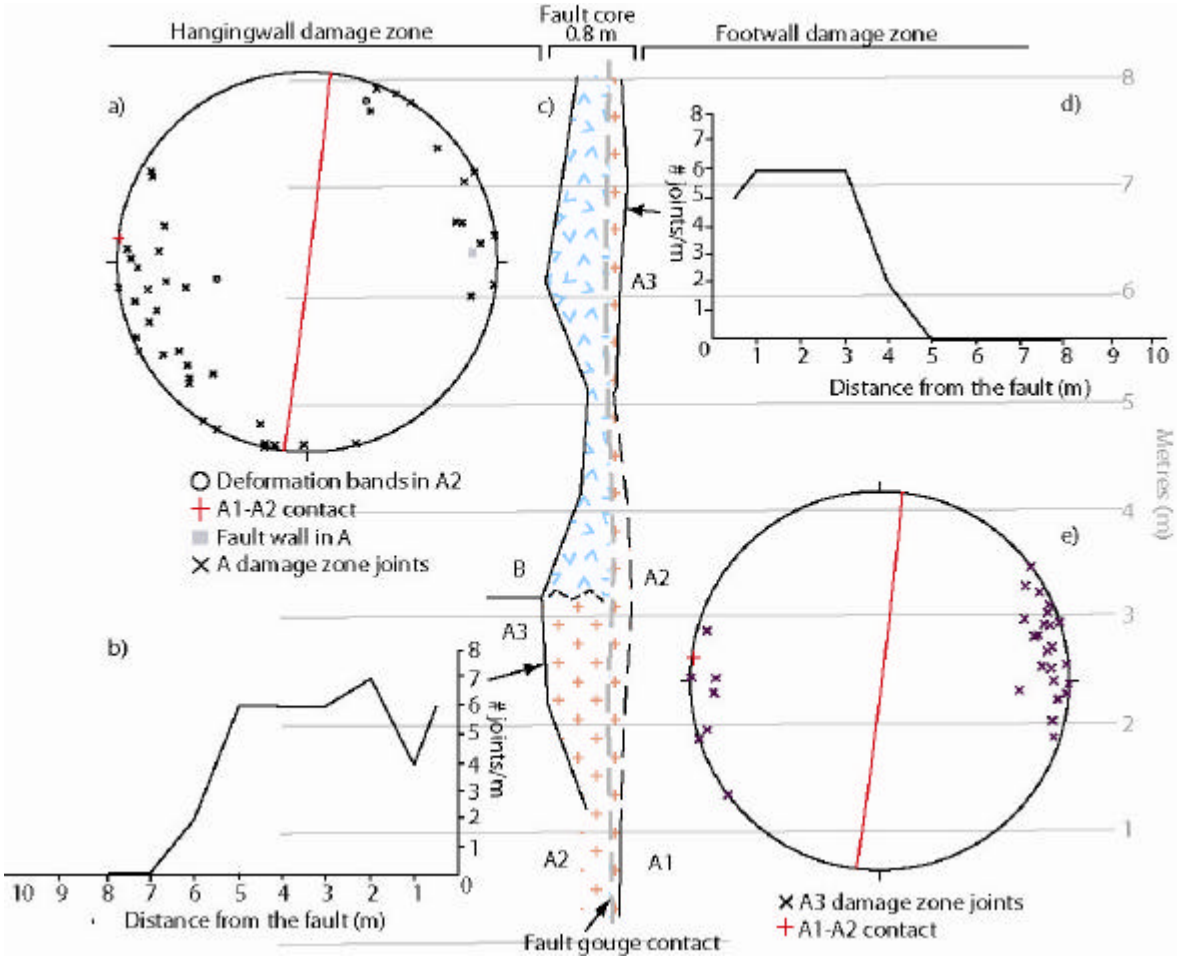

Figure 52: C5 fault core log, stereonets and line transects
a) Poles to planes of damage zone joints in flow unit A3, the great circle is the orientation of the contact between A1 and A2 b) Hangingwall damage zone joint density along line transect in A3, arrow points to start point of the transect c) Log of fault core in ignimbrite A and ignimbrite B, note the change in fault core width moving up the fault. The contact between A2 and A1 is sharp and planar (Figure 54b), the contact between the A and B gouge (grey dashed line) is sharp but irregular d) Footwall damage zone joint density in A3 e) Poles to planes of joints in the footwall damage zone and great circle of the A1-A2 contact.

Fault core: The C5 fault hangingwall is composed of A2 and A3 offset against A1 in the footwall. Moving up the fault the hangingwall is composed of ignimbrite B offset against all three layers of ignimbrite A in the footwall (Figure 52 and Figure 53). The ignimbrite A fault core width in the hangingwall ranges from 0.06 m to 0.55 m, the footwall fault core width ranges from 0.1 m to 0.26 m, the fault orientation is 007/89 SE.

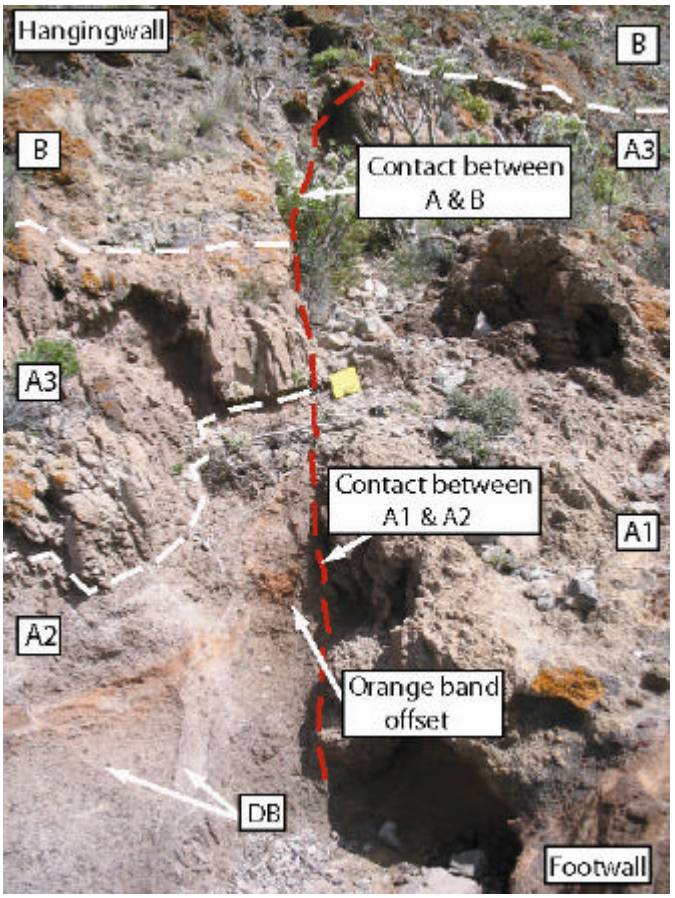

Figure 53: Ca5 fault

The exposure is inclined allowing examination of the fault along strike as well as along dip. The contact between A1 and A2 is sharp and planar and the contact between A and B is irregular, however the majority of the fault core is not exposed. Deformation bands (DB) cut the ashy A2 unit and offset a orange band in the unit. Photo is looking east.

The fault core between A2 (hangingwall) and A1 (footwall) is marked on the footwall side by a planar fault wall (177/76W) that has a sharp contact with the A2 material which comprises the fault core. The fault core-footwall contact is marked by a layer of extremely fine-grained gouge (Figure 54a). The boundary of the fault core in A2 is a deformation band that offsets an orange band in the A2 unit (Figure 54b). The A1 material in the fault wall is cut by fine fractures forming centimetre size clasts.

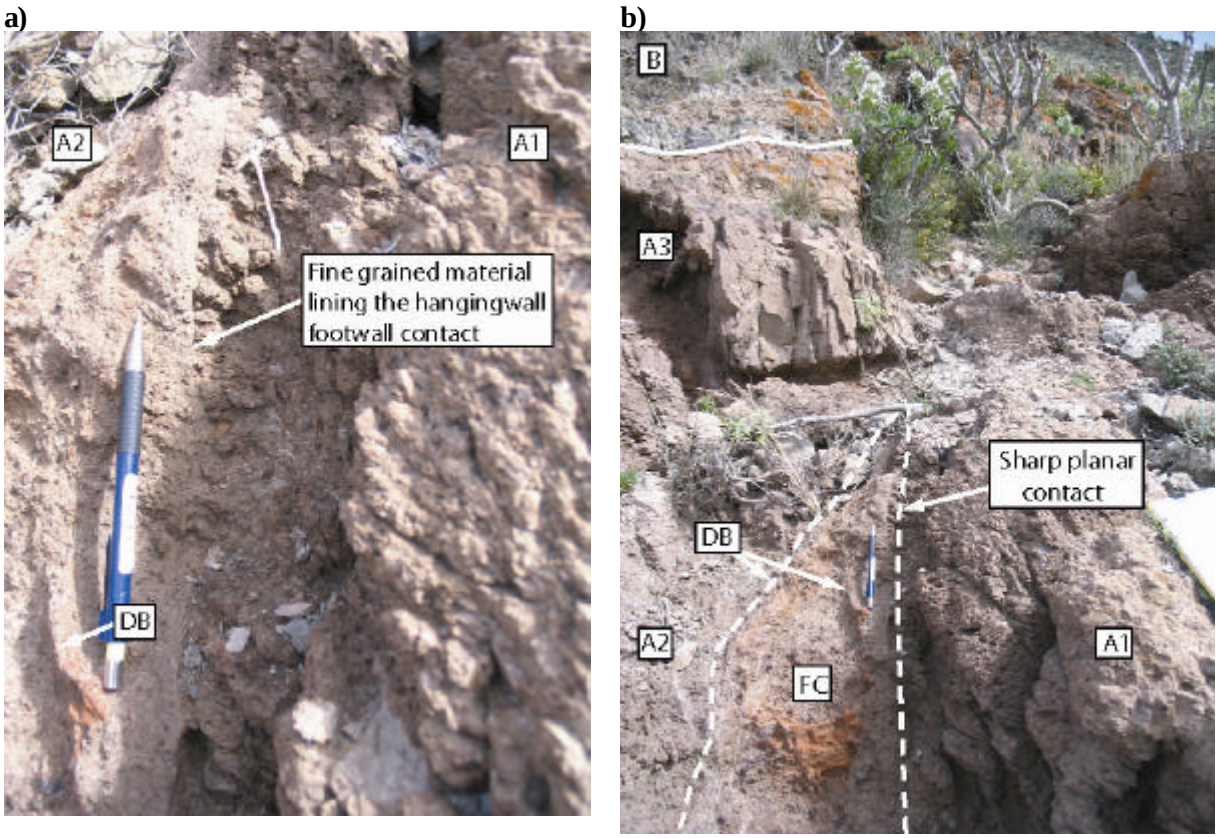

Figure 54: Ca5 fault core

a) The planar contact is lined with a very fine grained material; note the fine fractures cutting the A1 material in the fault wall. b) The lower part of the Ca5 fault core (FC) is bounded by a planar contact in the footwall and a deformation band (DB) in the hangingwall

In thin section we see that the fault core is composed of a fine grained matrix containing abundant crystal fragments and ignimbrite clasts (Figure 55). The crystal fragments are mainly feldspars with minor amounts of biotite. Crystal fragments range in size from 0.005 cm to 0.05 cm. The ignimbrite clasts range in size from 0.05 cm^2 to 0.15 cm^2. The clasts are composed of phenocrysts and occasional devitrified fiamme in a fine grained dark brown matrix and closely resemble the A1 unit.

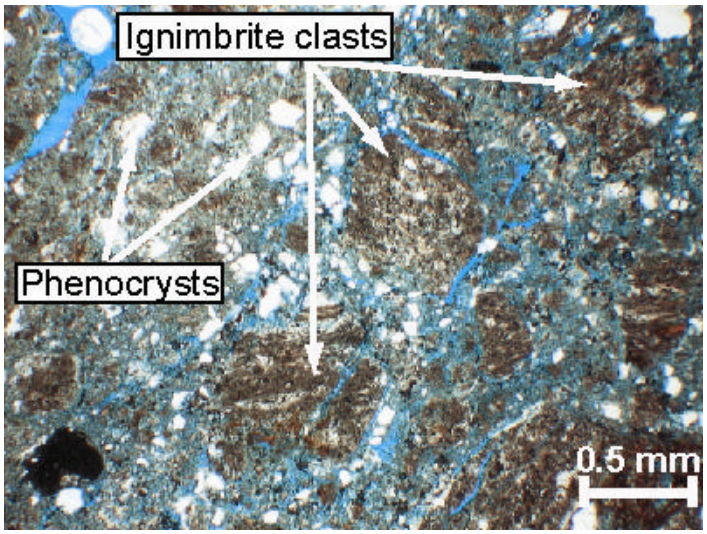

Figure 55: Sub-unit A2 in thin section

Fault core adjacent to A2 contains fractured ignimbrite clasts and broken phenocrysts

Damage zone: Measurements of the CA5 damage zone were made only in the A3 layer of ignimbrite A. The underlying ashy A2 layer has little macro-scale deformation and is cut by occasional deformation bands; the A1 layer is poorly exposed. The damage zone in A3 is intensely jointed; joints are vertical with a smooth planar morphology and a NW-SE orientation. Joint spacing ranges from 0.01 m to 0.41 m with an average joint spacing of 0.15 m. The hangingwall damage zone is 6 m wide and has a mean joint density of 6.1 joints per meter. The footwall damage zone in A3 is 4 m wide and has a mean joint density of 6.25 joints per meter.

Ca15:

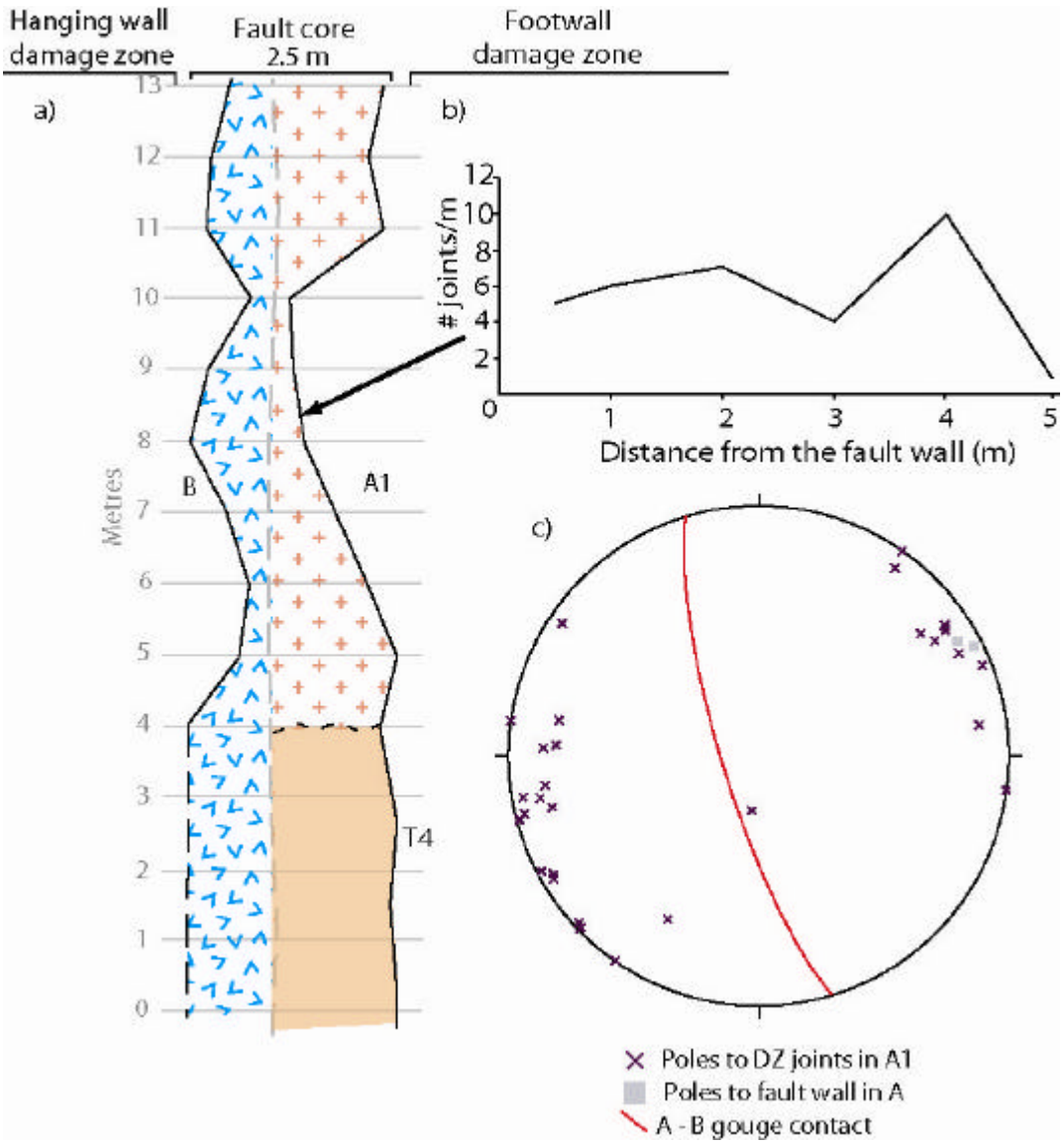

Figure 56: C15 fault core log, stereonet and line transects

a) C15 fault core log, the width of the fault core changes dramatically along dip, the contact between A and B gouge is irregular and sharp b) Number of joints per meter in the A1 damage zone (DZ). The arrow points to the start point of the line transect c) Poles to planes of damage zone joints and great circle is the trend of the contact between the A & B fault gouge in the fault core.

Fault core: The A1 layer of ignimbrite A is offset against ignimbrite B by 15 m and the fault orientation is 163/78W. The fault continues into the underlying T4 unit where the fault dip becomes increasingly shallow. The lower part of the fault where the hangingwall is composed of both ignimbrite A and B is obscured by scree and vegetation, in the footwall the A1 layer is fully exposed.

The fault core width of A1 in the footwall ranges from 0.02 m to 1.70 m (Figure 56). The fault wall in A1 is planar but intensely fractured and appears to be breaking up to form blocks of material. The fault core immediately adjacent to the fault wall contains large intensely fractured blocks of A surrounded by a coarse breccia and gouge (Figure 57). Moving away from the fault wall into the fault core the clast size decreases and finer breccias are forming.

Figure 57: Ca15 fault core
The fault wall is on the right hand side. In the fault core a block is fracturing forming smaller clasts. Clast size becomes smaller moving into the fault core (to the left)

Fault core clasts are angular to sub-angular in shape and randomly orientated (Figure 58). The centre of the fault core is marked by a band of very fine-grained red breccia and gouge; this band marks the contact between the ignimbrite A and B breccia and gouge. The contact is sharp but can be undulose or planar, there is no mixing of material across it.

Figure 58: Gouge and clasts in Ca15 fault core
The clasts are sub-rounded and surrounded by gouge. Note the clast size becomes smaller moving into the centre of the core (right to left).

Damage zone: The footwall damage zone in A1 is 4 m wide. The damage zone joints are planar, vertically extensive and are orientated NNW-SSE. Joint spacing ranges from 0.01m to 0.41 m with an average joint spacing of 0.13 m and an average joint density of 6.6 joints per meter.

Ca30:

Fault core: In Ca30 ignimbrite A is juxtaposed against ignimbrite X. The fault core is poorly exposed and the contact between A and X is not seen. The fault core is visible in A2 and A3, the A2 unit here is 0.96 m thick and A3 is 2.9 m thick (Chapter 2). As in Ca5, the ashy friable nature of the A2 layer means that there is no clear change in clast or grain size or formation of a fault wall to define the fault core and damage zone. The fault core adjacent to A2 contains deformation bands. In the A3 layer there is a discernable fault core–damage zone transition. The fault core is composed of white coloured gouge with sub-rounded clasts of ignimbrite A randomly orientated within it (Figure 60a). The core is matrix supported with a clast to matrix ratio of 30:70. The fault wall is smooth but slightly undulating, the majority of the fault wall surface is covered by a very fine-grained brown layer that varies in thickness from 0.6 cm to 7 cm (Figure 60a, b).

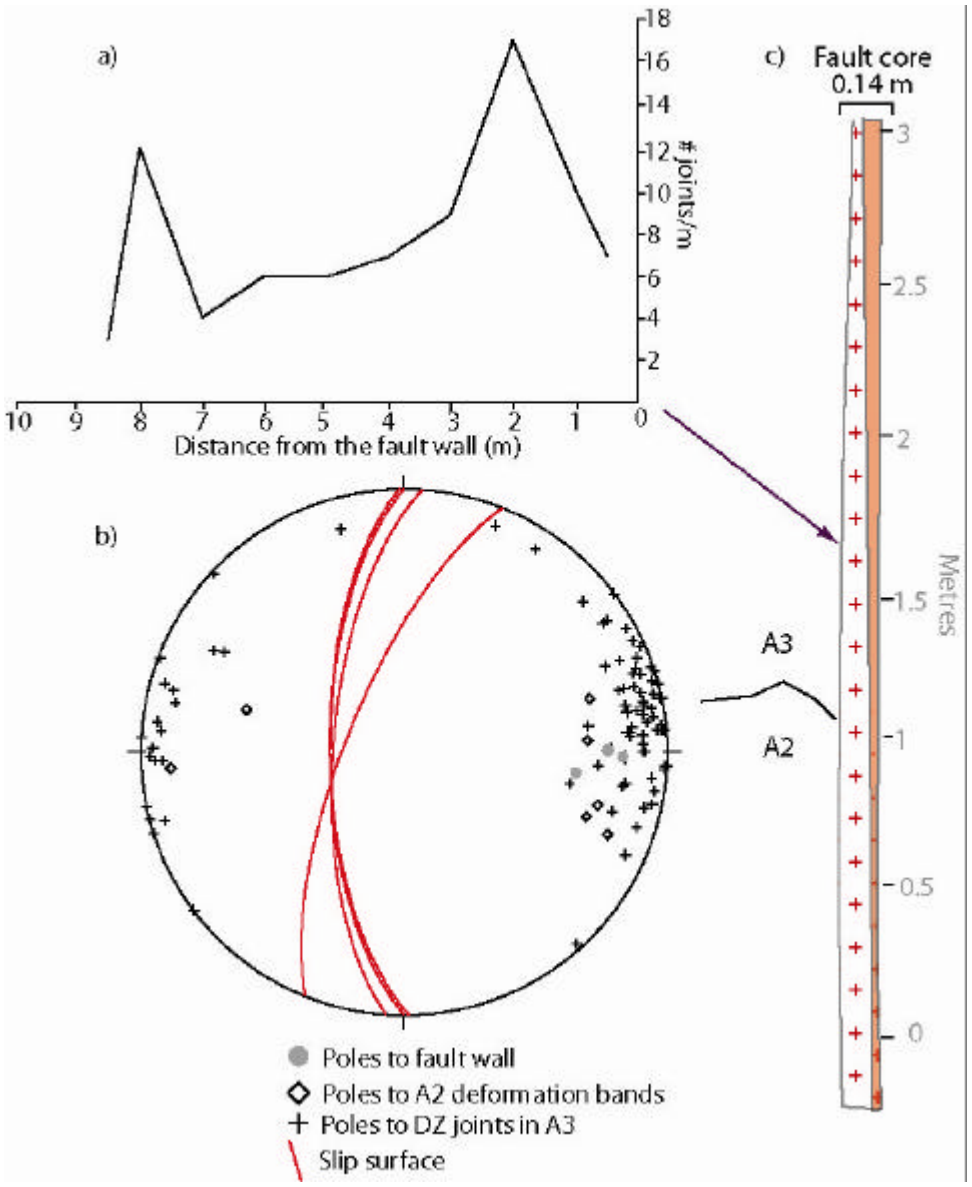

Figure 59: Ca30 fault core log, stereonet and line transect

a) Joint density in the damage zone in the A3 flow unit b) Poles to damage zone joints and great circles for the slip surface c) Fault core log, fault core width is relatively constant. The orange band represents the brown layer that covers the slip surface, the thickness of the layer increases from 0.6 cm to 7 cm moving up the fault core.

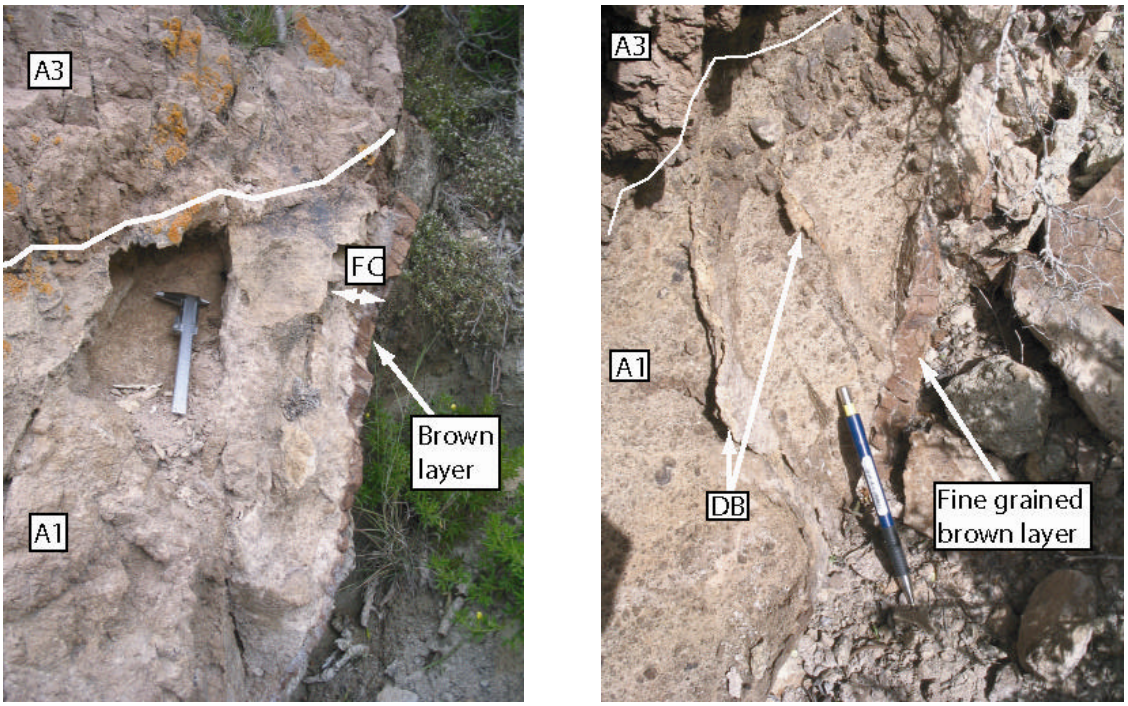

Figure 60: Ca30 fault core
a) Fault core in A2, note the deformation bands standing proud. b) The fault core in A3, the A3 damage zone is in the top left. The slip surface of the Ca30 fault is covered with a dark brown extremely fine grained material.

Damage zone: The damage zone in A3 is intensely fractured; the joints are planar and orientated N-S (Figure 59b). Joint spacing ranges from 0.02 m to 0.46 m with an average joint spacing of 0.10 m, average joint density is 9.8 joints per meter. Damage zone width is taken as 6 m because the Ca30 and Ca5 faults are 10 m apart and the increase in joint density at the end of the Ca30 line transect may be the start of the Ca5 damage zone (Figure 59a). In the damage zone the contact between the top of A3 and the base of ignimbrite B is sharp and straight but offset in places by minor faults. The contact between the base of A2 and the underlying T4 is inclined towards the fault at 173/37E for ~1.75m from the fault plane.

Figure 61: CA30 damage zone
A3 overlies A2, the contact between the two flow units is irregular. A3 is intensely jointed, A2 contains occasional deformation bands.

3.3 Comparison of fault zone architecture

3.3.1 Damage zone

Levels of damage zone joint density increase slightly with increasing displacement (Figure 62 and Figure 63). The Tauro faults have joint densities only slightly greater than background levels. Joint frequencies are similar in CA5 and CA15. CA30 has two points of high joint levels. The highest joint frequency within individual faults does not occur next to the fault wall and there is not a systematic decrease in joint number with increasing distance from the fault. Rather the CA15 and CA30 peaks in joint frequency are found at distances greater than 2 m from the fault wall; whereas joint frequency in TA2 and CA5 damage zones are relatively constant around 3 and 6 joints per meter respectively. Overall there is not a linear correlation between increasing joint intensity and displacement (Figure 62) in the damage zone or decreasing levels of jointing moving away from a fault (Figure 63).

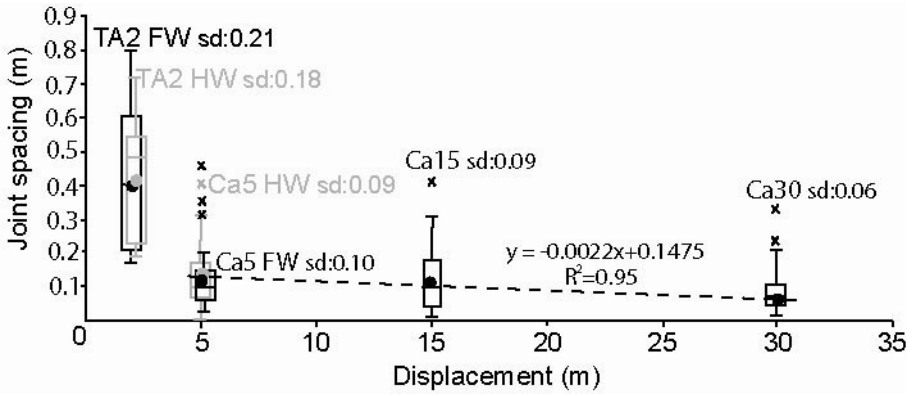

Figure 62: Joint spacing in ignimbrite A damage zone

Joint spacing (i.e. number of joints) in the fault damage zones decreases from the TA2 fault to the Cedro faults. However the damage zone joint spacing at Cedro is relatively constant regardless of displacement. The best fit trend line for the mean (black dots) of the Ca5, Ca15 and Ca30 joint spacing populations is almost horizontal (0.0022) therefore the means are almost identical.

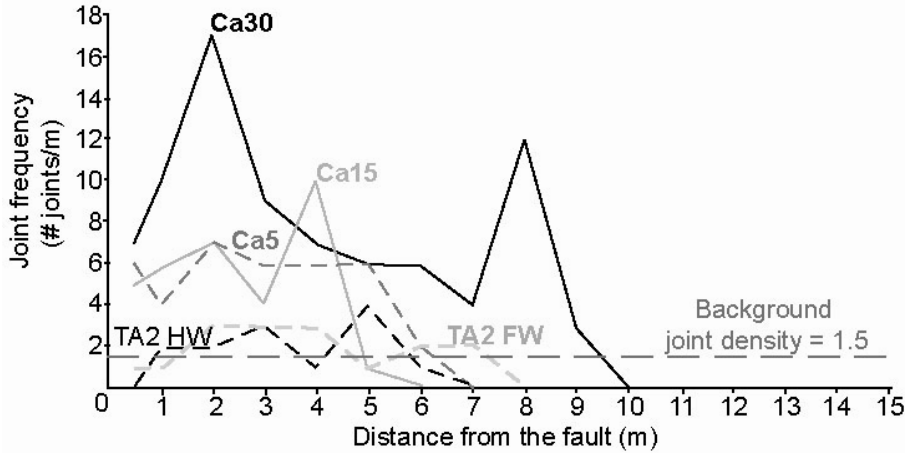

Figure 63: Joint frequency in ignimbrite A damage zone

Each plot is a single line transect perpendicular to the fault wall recording the number of joints in a meter interval. The protolith average is calculated from the Los Frailes unfaulted section. Moving away from the fault the frequency of joints increases in Ca30 and Ca15 then

decreases. Damage around the low offset fault at Tauro (T2) is only slightly greater than background levels.

In the analysis of the data in chapter 5 joint spacing rather then joint density is used as the width of slabs adjacent to the fault is of greater relevance to my fault growth model (section 5.1); slab width is controlled by joint spacing.

Figure 63 is a box plot of joint spacing in each of the fault damage zones. The TA2 fault has the largest median spacing and the greatest variation in joint spacing. With increasing displacement the median joint spacing decreases as does the range of spacing. The joint spacing median and range is relatively constant for all the Cedro faults.

Joint spacing	**Median (m)**	**IQR**	**Lower extreme (m)**	**Upper extreme (m)**
TA2 HW	0.48	0.32	0.19	0.72
TA2 FW	0.4	0.39	0.17	0.8
CA5 HW	0.11	0.1	0.01	0.33
CA5 FW	0.1	0.08	0.03	0.46
CA15	0.1	0.13	0.01	0.31
CA30	0.07	0.06	0.02	0.2

Table 6: Values of joint spacing in the ignimbrite A damage zone of each fault.

The joints in each of the damage zones are sub-parallel, smooth and planar. The orientation of the damage zone joints and fault walls for each fault are shown in the stereonets below (Figure 64). Also plotted are the unfaulted protolith joint orientations from Los Frailes and Taurito.

a)

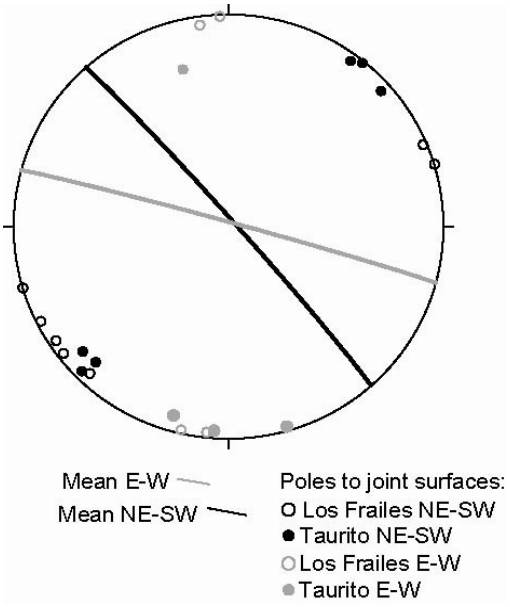
Mean E-W
Mean NE-SW
Poles to joint surfaces:
Los Frailes NE-SW
Taurito NE-SW
Los Frailes E-W
Taurito E-W

b)

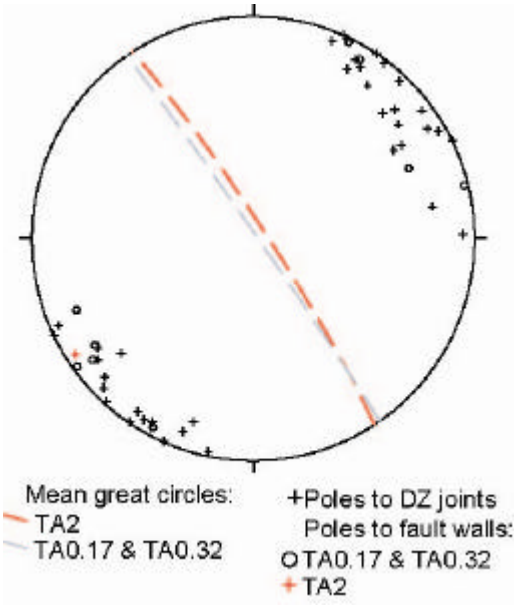
Mean great circles:
TA2
TA0.17 & TA0.32
+Poles to DZ joints
Poles to fault walls:
TA0.17 & TA0.32
TA2

c)

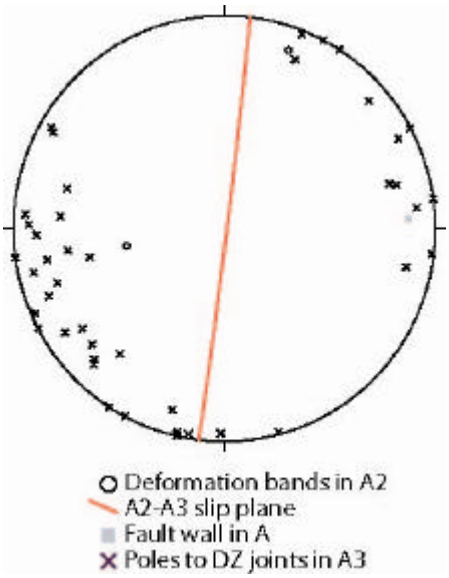
Deformation bands in A2
A2-A3 slip plane
Fault wall in A
Poles to DZ joints in A3

d)

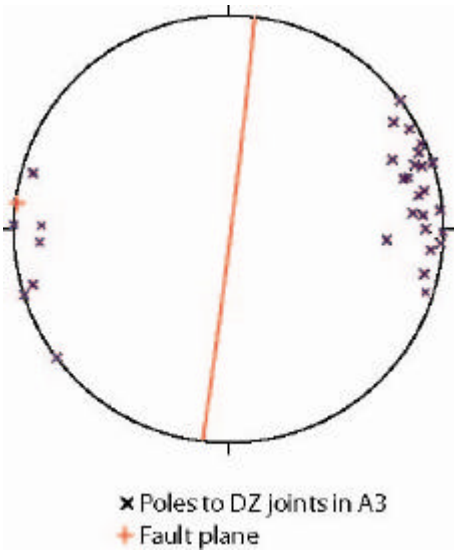
Poles to DZ joints in A3
Fault plane

e)

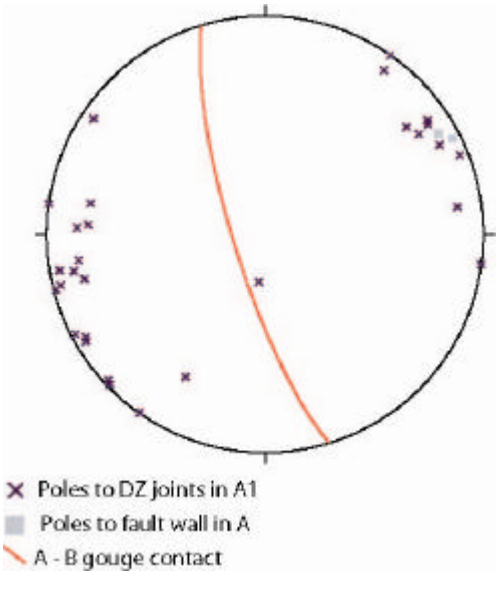
Poles to DZ joints in A1
Poles to fault wall in A
A - B gouge contact

f)

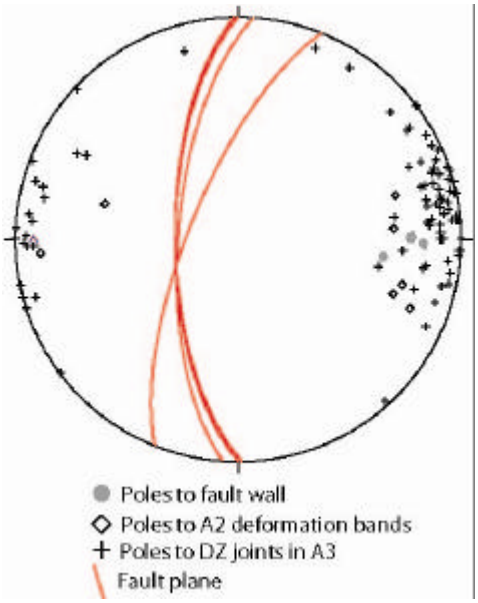
Poles to fault wall
Poles to A2 deformation bands
Poles to DZ joints in A3
Fault plane

Figure 64: Stereonets for ignimbrite A host rock and damage zone joints a) Protolith joint orientation at Los Frailes and Barranco Taurito. b) Poles to joints in TA2 damage zone c) Ca5 poles to damage zone joints in the hangingwall and d) footwall e) Damage zone joint orientation in Ca15 and f) Ca30 damage zones. The fault plane orientation is shown by the great circle and poles to fault walls are shown by grey boxes.

All faults examined are concentric to the caldera margin (Figure 64). At Cedro on the west coast the faults have a concentric orientation approximately north-south, at Tauro in the south-west of the island the concentric faults trend NW-SE. The plots show that TA2 damage zone joints and fault walls have the same orientation as each other and the same orientation as the nearby Los Frailes protolith joints. Similarly the damage zone joints in Ca5, Ca15 and Ca30 all share a similar orientation and have the same orientation as the faults and the fault walls.

Neither the joints at Tauro or Cedro have the expected fault related joint angle of 30^0 (Chapter 1). Joints in Tauro are parallel to the unfaulted host rock joints and concentric to the caldera margin as are the joints at Cedro, which would suggest the joints share a common origin.

3.3.2 Fault core width

There is an increase in fault core width with displacement from TA2 to Ca15 however there is a wide range of fault core widths within any one fault (Figure 65). The TA2 and Ca5 fault cores have widths that range from 0.07 m to 0.55 m. The Ca15 fault core has the greatest variation in fault core width along dip from 0.2 m to 1.7 m. The fault core in Ca30 has a more constant width between 0.1 m and 0.14 m, similar to that of the much lower offset TA2 fault.

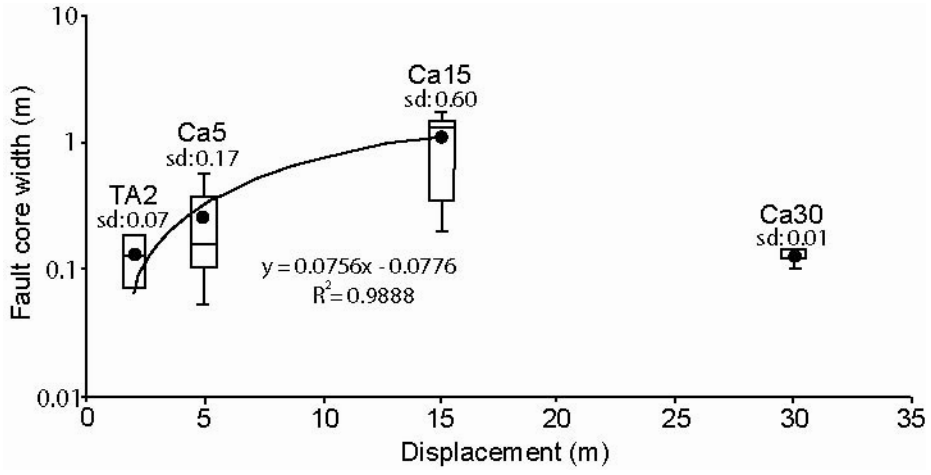

Figure 65: Log-normal plot of ignimbrite A fault core width vs. displacement. Fault core width does not increase greatly with displacement between TA2, Ca5 and Ca30. The highest offset fault Ca30 has one of the narrower fault core widths. The Ca5 and Ca15 show some variation in fault core width along dip, TA2 has a relatively consistent fault core width.

3.3.3 Fault core elements – Clast morphology

The size and shape of clasts in the fault core of Ca5, Ca15 and Ca30 were analysed in terms of displacement under the assumption that increasing displacement decreases clast size, via processes of attrition and abrasion that make the clasts more rounded. No clasts of ignimbrite A are found in the T2 and T2.5 fault core, it is composed entirely of angular clasts of the overlying ignimbrite B unit.

There is a wide range of clast sizes between the three faults at Cedro (Figure 66). The Ca30 fault having accumulated the greatest amount of displacement has the smallest median clast size and the lowest inter-quartile range therefore the least amount of variation in clast size population. However the opposite is not true, the lowest offset fault does not have the largest clast sizes or range of clast size. Instead the Ca15 fault has the largest median and upper extreme and the greatest inter-quartile range. Clast size does not decrease linearly with increasing displacement but instead decreases from 15 m slip to 5 m slip to 30 m slip.

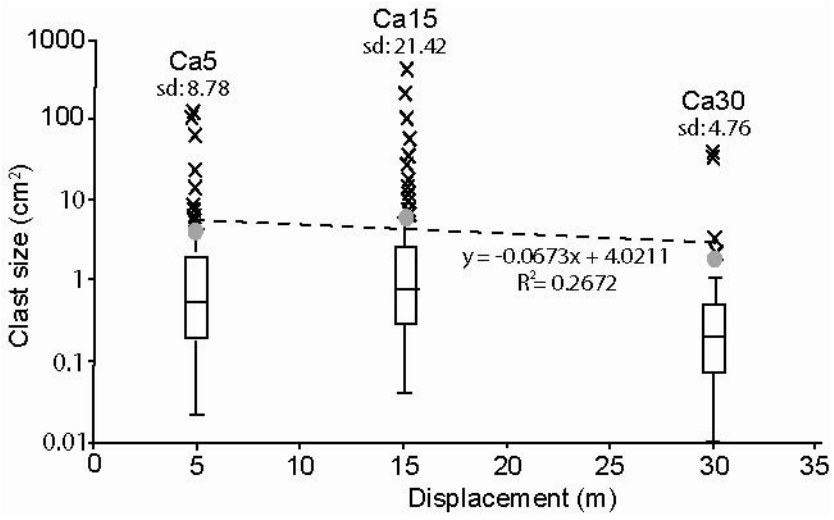

Figure 66: Ignimbrite A clast size vs. displacement

The smallest clast sizes and range of clast size occurs in the Ca30 fault. The largest clasts are in the Ca15 fault. Mean clast size (grey dots) increases slightly with increasing slip from Ca5 to Ca15. Note clast size is on a log scale.

Clast size	**Median (cm^2)**	**IQR**	**Lower extreme (cm^2)**	**Upper extreme (cm^2)**
CA5	0.35	0.56	0.0225	1.5275
CA15	0.63	1.79	0.04	4.63
CA30	0.16	0.33	0.01	0.9

Table 7: Values for ignimbrite A clast size populations in each of the Cedro fault cores

The shape of the clasts in the fault core was examined using the ratio of long to short axis. With increasing slip the median clast axial ratio moves towards one, so the clasts are becoming more equant possibly due to attrition and abrasion in the fault core (Figure 67). The axial ratio does not indicate the level of roundness of the clasts, only that they are becoming more symmetrical. But field observations shows the clasts are mostly rounded to sub-rounded

Ca5 has the largest median clast axial ratio and the greatest range of clast aspect ratios (Table 8); Ca15 has the narrowest range of clast axial ratios. Overall the shape of clasts is similar in each of the fault cores despite having undergone different amounts of displacement.

Clast axial ratio	Median	IQR	Mean	Lower extreme	Upper extreme
Ca5	1.38	0.89	1.56	1	3.33
Ca15	1.29	0.44	1.4	1	2.21
Ca30	1.25	0.63	1.56	1	2.5

Table 8: Mean and median values of clast axial ratio for each of the three fault cores in ignimbrite A

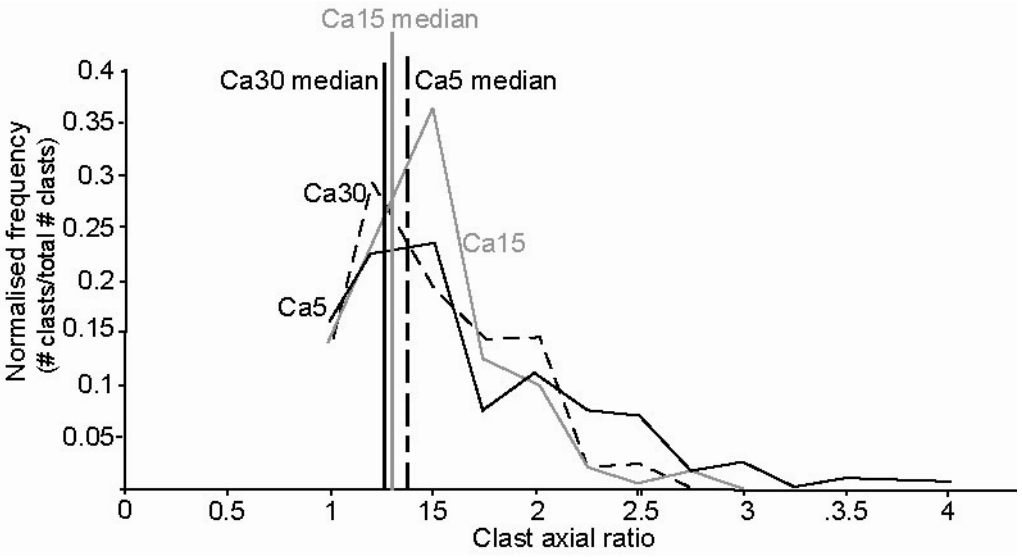

Figure 67: Ignimbrite A fault core clast axial ratio

As the amount of displacement increases clasts become more symmetrical. Ca5 and Ca30 have a greater variety of clast shapes in their fault cores, but also have a greater proportion of clasts in the more symmetrical range (closer to 1). Normalised frequency is the number of clasts in each bin size (0.5 cm^2 0.75 cm^2, 0.1 cm^2……4 cm^2, 4.5 cm^2, 5cm^2) divided by the total number of clasts measured in that fault core.

3.4 Summary

The field data presented tests the hypothesis that displacement is the controlling factor on development of fault architecture (section 1.3). The expected correlations between increasing displacement and increasing damage zone joint density, fault core width and decreasing clast size are not found, suggesting that displacement is not the main controlling factor on fault initiation and growth. The similarities in fault core width and clast size in faults occurring in the same unit A3 or unit type (TA2, Ca5 and Ca30) and the contrast with Ca15 in A1 suggests that there is a lithological control on fault growth.

In chapter 4 I present observations of these faults in the overlying unit ignimbrite B and examine the relationship with displacement of the faults as they occur in ignimbrite B. In chapter 5 I present a new mechanism for fault initiation and growth for both ignimbrite A and B, compare the fault architectures found in each ignimbrite and discuss the possible host rock properties influencing fault initiation and growth.

4

Ignimbrite B: analysis of fault zone architecture

4.1 Aim

This chapter presents structural data from faults in Ignimbrite B. the investigative and comparative procedures are the same as those used for ignimbrite A (Chapter 3)

4.2 Ignimbrite B

4.2.1 Protolith

Four of the faults are the continuation of the faults in ignimbrite A – T2.5, C5, C15 and Cb22 which is the growth fault at Montana Cedro. TA2 was not examined in ignimbrite B as the fault core and damage zone exposure was not accessible. All of the faults examined in ignimbrite B are exposed in the base of the ignimbrite B unit. The Cb22 fault extends from the base to the top of the unit and the entirety of the fault is accessible.

4.2.2 Fault architecture

Six normal faults were examined in ignimbrite B:

Barranco de Tauro:

Tb0.20 (0.20 m slip)

Tb0.35 (0.35 m slip)

Tb2.5 (2.5 m slip)

Montana Cedro

Cb5 (5 m slip)

Cb15 (15 m slip)

Cb22 (22 m slip)

The CB22 is part of the large normal growth fault at Cedro of which CA30 is a part. Ignimbrite B has been offset across the fault by 22 m against ignimbrite X.

Barranco de Tauro

Tb2.5:

a)

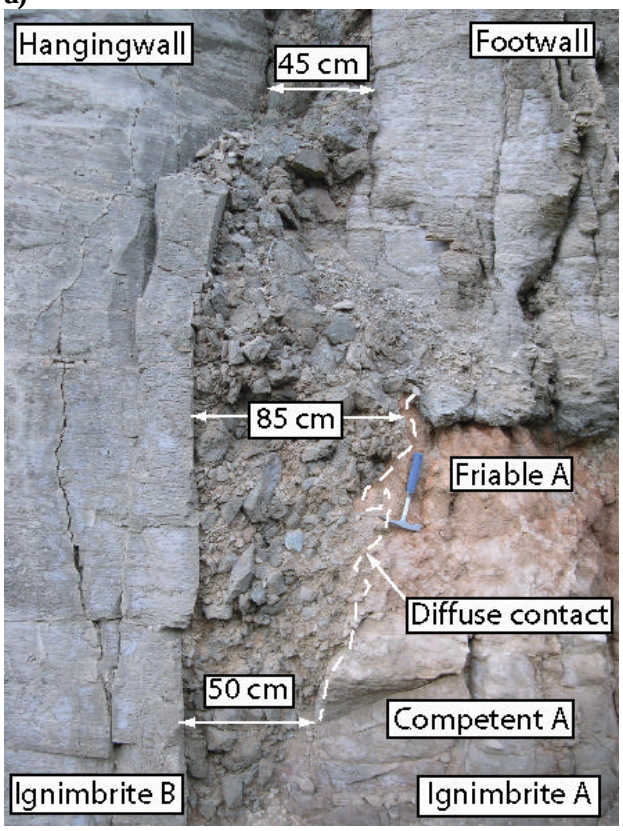

b)

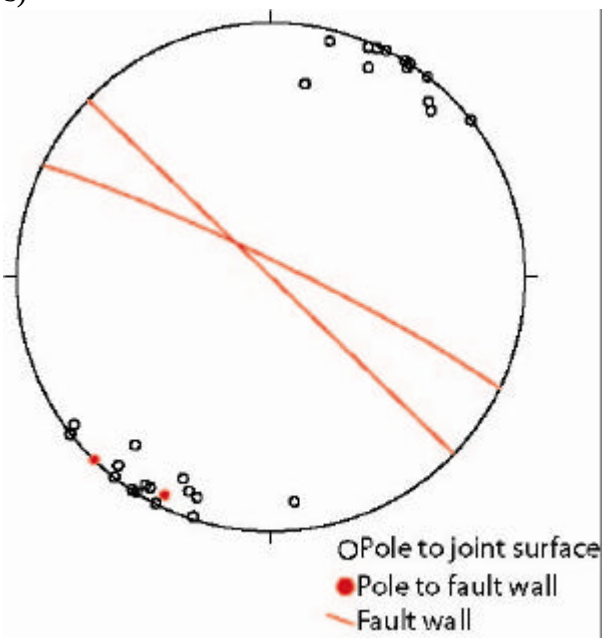

Figure 68: Tb2.5 fault core and stereonet

a) Tb2.5 fault core is composed of randomly orientated blocks of B. The ignimbrite B footwall-fault core and hangingwall-fault core contact is sharp, the contact becomes diffuse where the fault cuts ignimbrite A b) Poles to damage zone joints in ignimbrite B, great circles for fault walls in ignimbrite B.

Fault core: The fault core in B ranges from 0.45 m to 0.85 m thick (Figure 68). The fault core contains large angular clasts of B that are randomly orientated and increase in size moving up the fault core. The core is clast supported and the minimal gouge that is present is a red, friable fine-grained powder. The ignimbrite B fault walls are smooth and slightly undulating, the contact with the fault core material is sharp.

Damage zone: Deformation in the hanging-wall damage zone is limited; the average joint density is 2.18 joints per meter, joint spacing ranges from 0.04 m to 1.25 m and average joint spacing is 44 cm. Joint morphology in the footwall varies, joints are planar with smooth walls for the first 3 m out from the fault wall and are stepped from 4.8 to 6.4 m from the fault wall. The footwall damage zone in ignimbrite B is intensely jointed; joints are planar and parallel to each other. Joint spacing ranges from 0.02 m to 0.45 m with an average spacing of 0.14 m and average joint density of 6.2 joints per meter, the damage zone is 5 to 6 m wide.

The Tb0.20 fault in the Tb2.5 hangingwall, 3 m from the Tb2.5 fault wall offsets ignimbrite B against ignimbrite A by 0.20 m (Figure 69a). The fault core in B is 0.08 m to 0.15 m wide and matrix supported. The fault core contains very fine-grained yellow brown clayey gouge and clasts of centimetre-sized foliated blocks of B (Figure 69b). The clasts closest to the base of B have been rotated while those further up dip have foliations that remain parallel to the unit base.

a)

b)

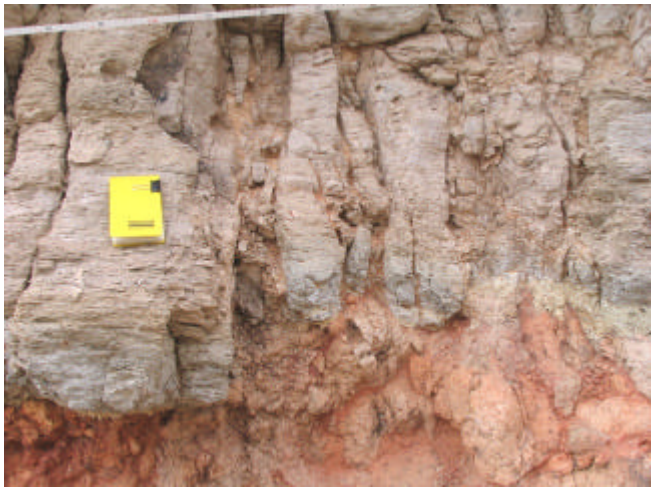

c)

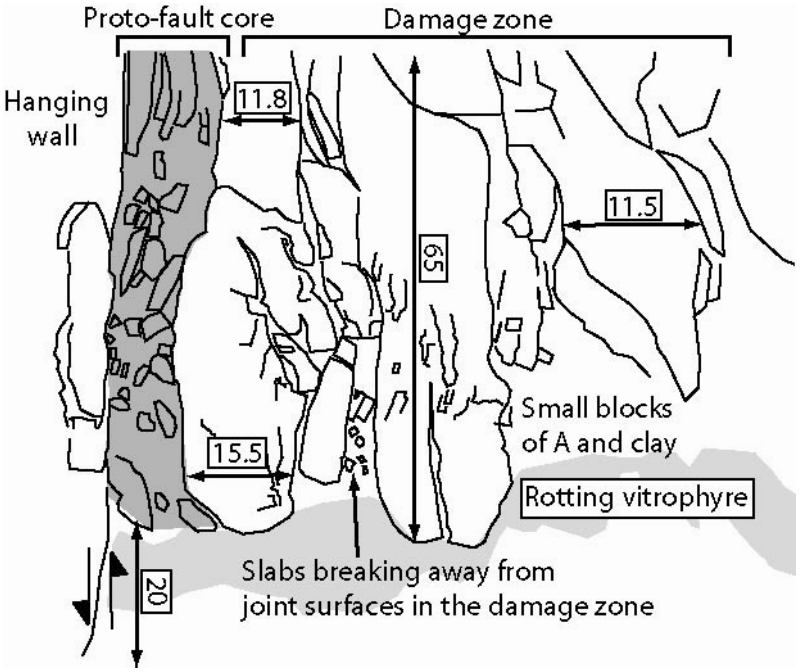

Figure 69: Tb2.5 damage zone

a) The Tb0.20 fault (left of the field notebook) 3 metres from the Tb2.5 fault wall, the Tb2.5 footwall damage zone is intensely jointed b) close up of the Tb0.20 fault (right of field notebook) and c) sketch of the Tb0.20 fault (not to scale). Slabs of rock are breaking away from the joint & fault wall surfaces, blocks at the base of the Tb0.20 fault are being rotated. Measurements on the black arrows are in centimetres.

Cb5:

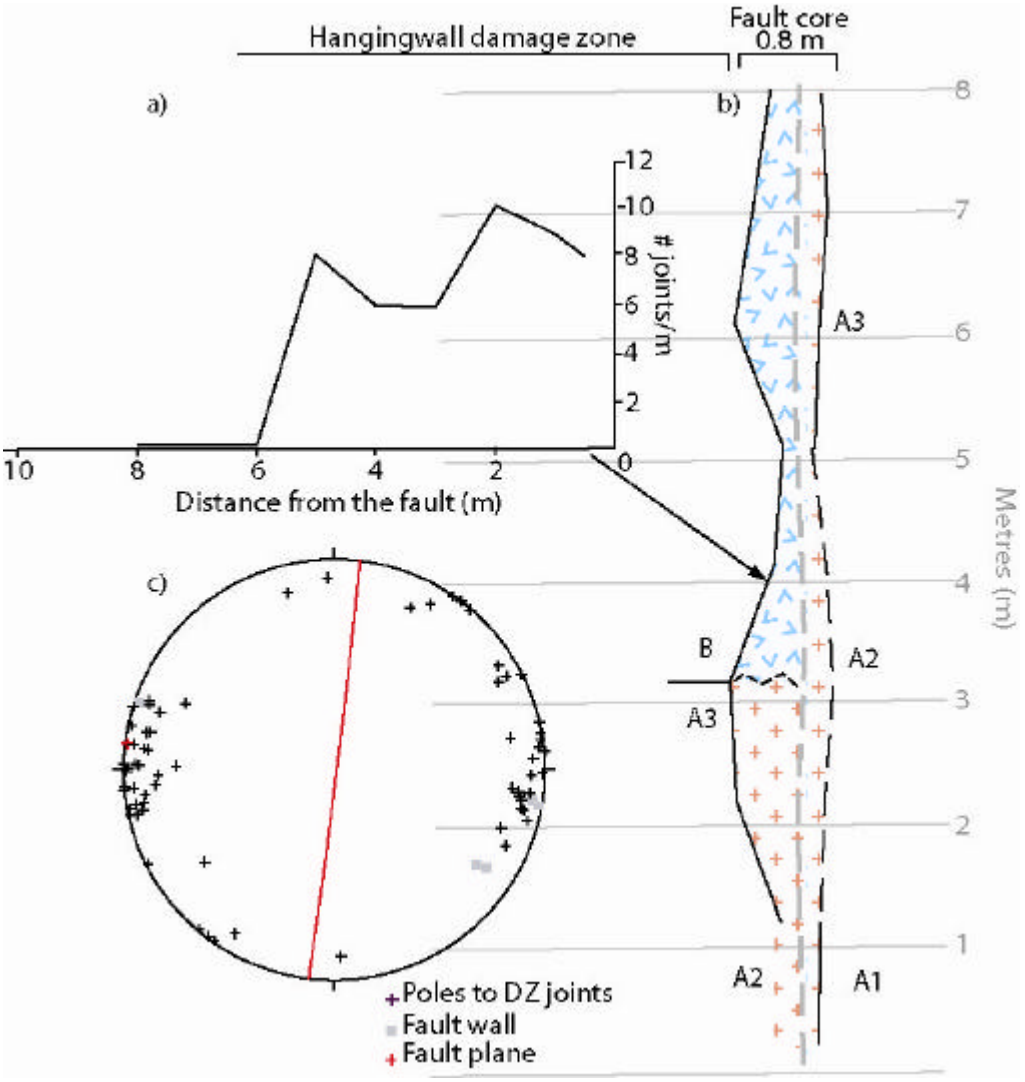

Figure 70: Cb5 fault core log, stereonet and line transect
a) Cb5 damage zone joint density line transect perpendicular to fault wall (arrow indicates start point of line transect) b) Cb5 log showing changes in fault core width moving up dip, the contact between the gouges is sharp and irregular (Figure 71) c) Poles to damage zone joint surfaces and Cb5 fault wall, great circle for the contact between the B and A gouges.

Fault core: Ignimbrite B is in the hangingwall of the C5 fault. The fault core width in ignimbrite B ranges from 0.06 m to 0.61 m (Figure 70b). The fault wall-fault core contact is sharp. The fault core material has a clast to matrix ratio of 45:55. Moving upwards the B gouge becomes coarser and the fault core becomes clast dominated (65:25). Clast size ranges from 0.04 cm^2 to 50 cm^2

At the top of the fault the contact between the B and A gouge is clearly visible. The contact is not a discrete smooth planar slip surface but an irregular boundary between the two gouges (Figure 71a & b), there is no mixing of material across the contact.

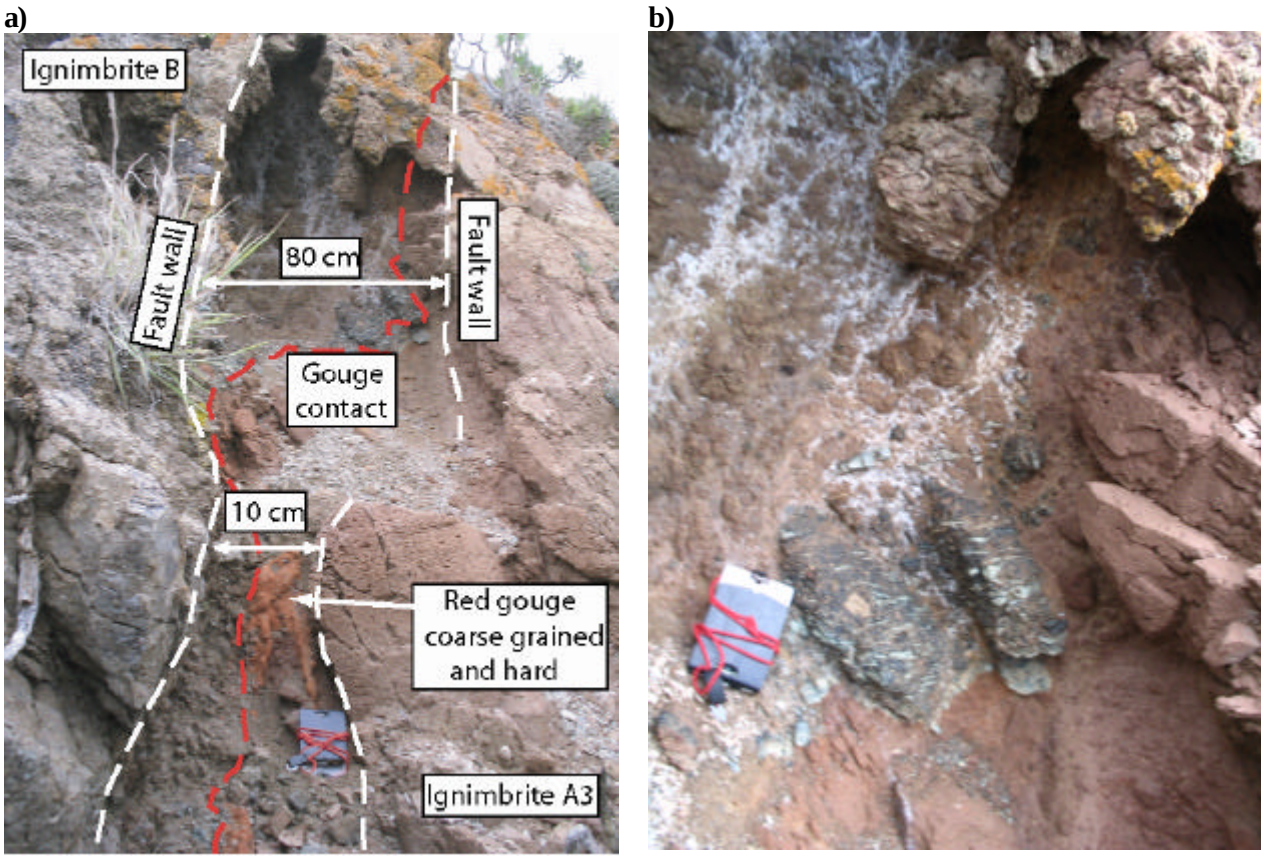

Figure 71: C5 fault core

a) There is no slip plane but an irregular contact between the ignimbrite A and B gouge. Part of the fault wall in A is covered. b) The fault core material in the upper part of the fault. Ignimbrite B clast size ranges from 0.04 to 50 cm^2, in ignimbrite A clasts are 0.02 to 7cm^2.

Damage zone: The damage zone is 5 to 6 m wide and intensely jointed. The joints are planar, parallel and have a mean N-S orientation (Figure 70c). Joint spacing ranges from 0.01 m to 0.35 m, the average joint spacing is 0.1 m and the mean joint density is 9.4 joints per meter.

Cb15:

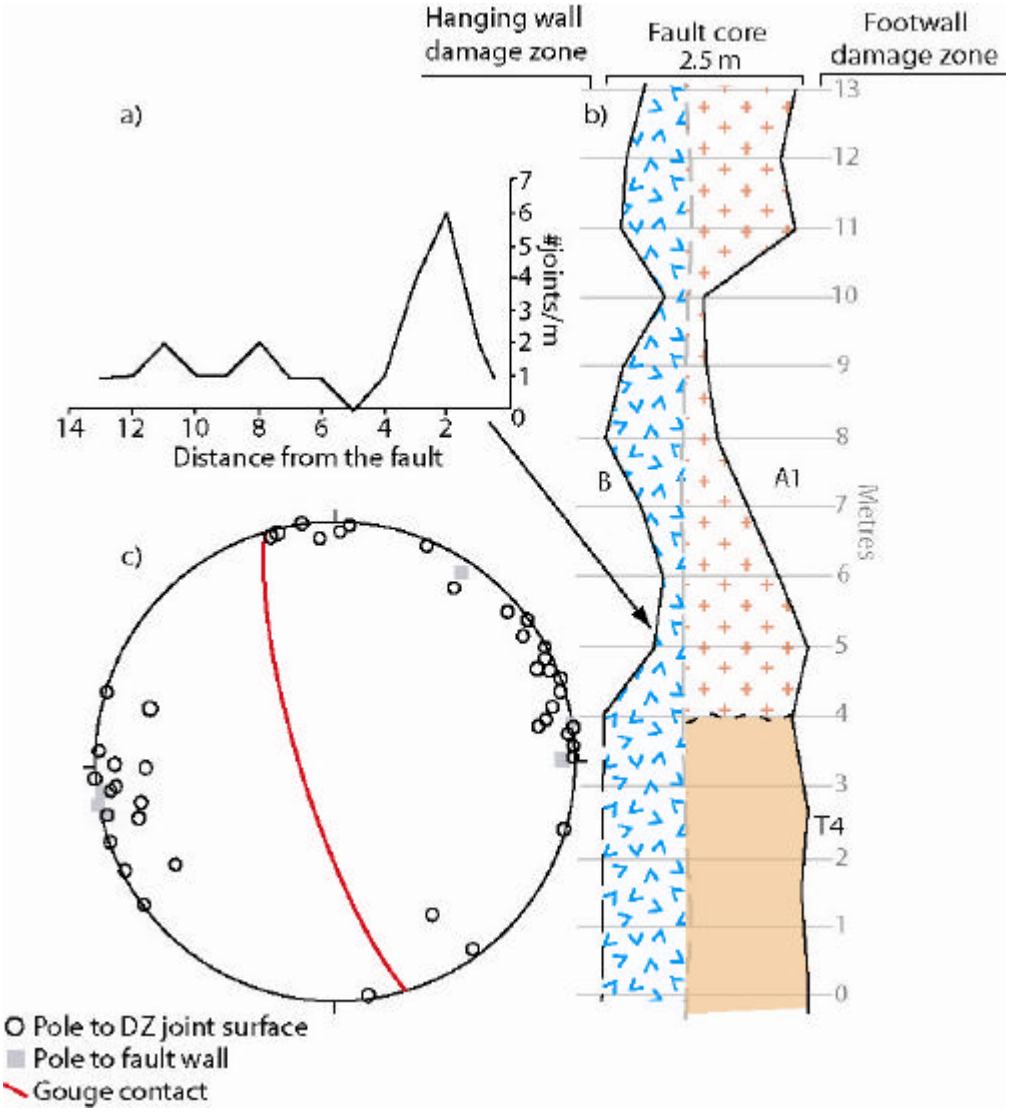

Figure 72: Cb15 fault core log, stereonet and line transect

a) Damage zone joint density line transect (arrow indicates start point of the transect) b) Cb15 fault core log, ignimbrite B fault core width changes dramatically up dip, the contact with the A gouge in the fault core is irregular (Figure 73) c) Poles to damage zone joint surfaces and fault walls in ignimbrite B, orientation of the gouge contact is shown by the great circle.

Fault core: The fault core width ranges from 0.4 m to 1.2 m (Figure 72b). The core is composed of angular, randomly orientated clasts of B and the clast to matrix ratio is 55:45 (Figure 73b & Figure 73c). The fault wall is a smooth planar surface and the core immediately adjacent to it contains meter scale blocks (Figure 73a); the gaps between which are filled with smaller clasts and fine grained gouge.

Damage zone: The CB15 damage zone has a very low level of deformation. Joint spacing is from 0.05m to 1.76 m, with an average spacing of 0.51 m. The average joint density is 1.95 joints per meter and the damage zone width is 3 m. Joints are orientated NNW-SSE with occasional NE-SW joints (Figure 72c).

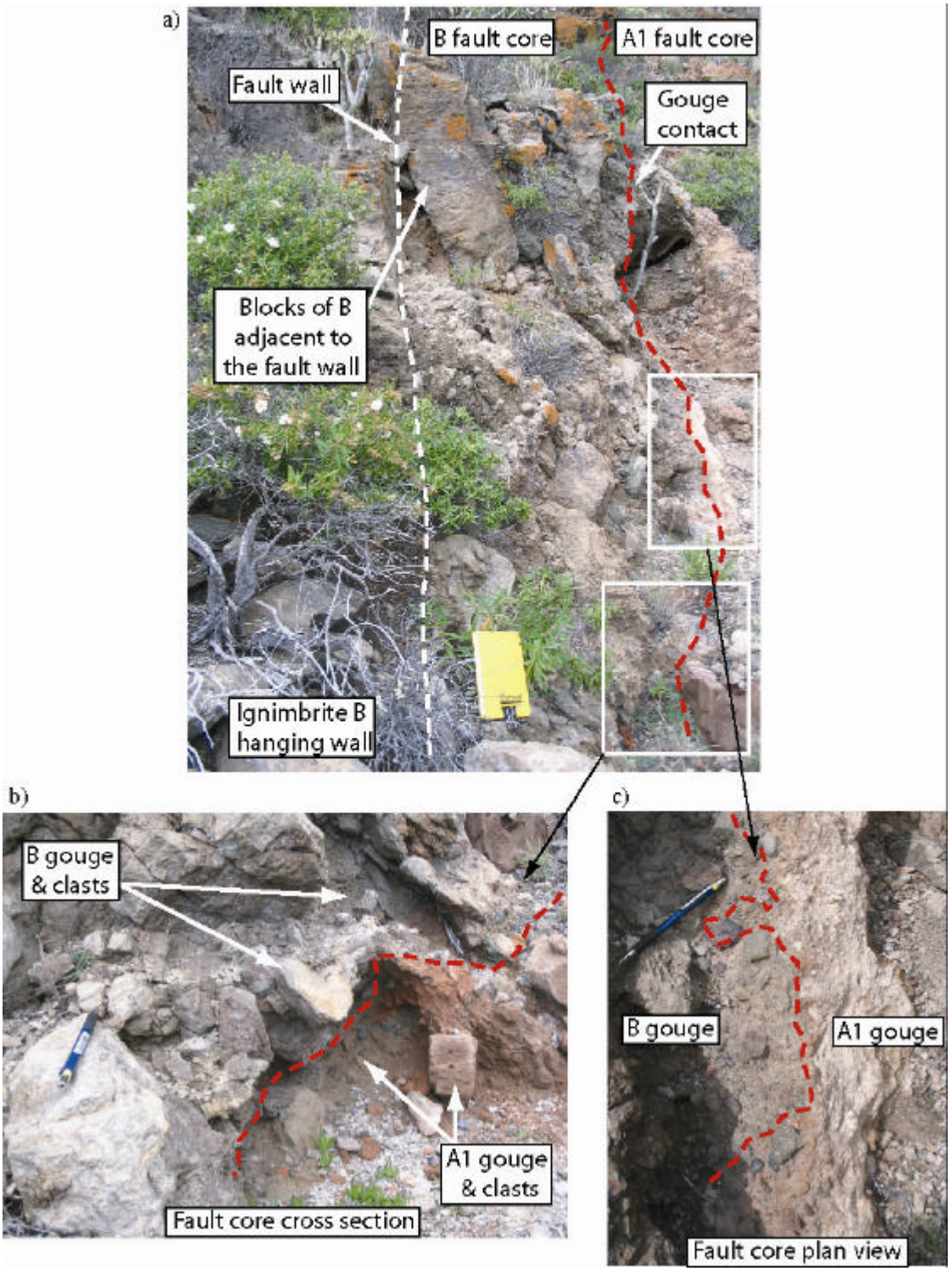

Figure 73: C15 fault core

a) The edge of damage zone and fault core in ignimbrite B b) fault core cross section c) plan view of the fault core, the contact between the A and B gouge is irregular. The core material in B comprises some large blocks of B particularly in the top part of the core (a).

Cb22:

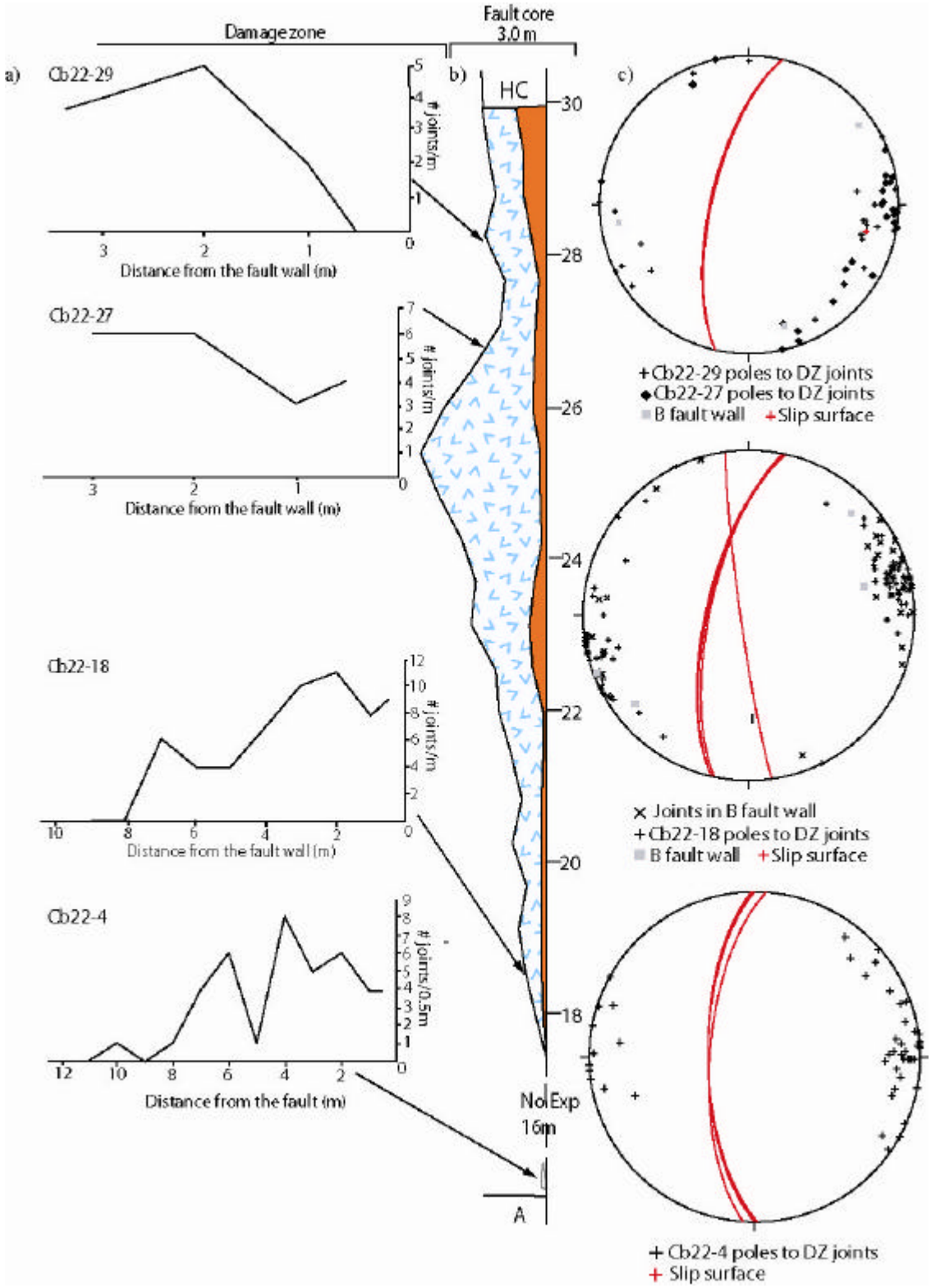

Figure 74: Cb22 fault core log, stereonet and line transect

Cb22 fault core is best exposed from the mid-section of ignimbrite B 18 m above the unit base, to the top of the unit. A small section of fault core is exposed at the base but the slip surface is not. a) Damage zone joint density line transects taken at different heights above the unit base – 4 m, 18 m, 27 m and 29 m b) Cb22 fault core log starting at 18 m above the unit base to the top of the unit. The slip surface in the fault core is composed of ash, scoria and basalt form the T4 lava flow (orange band), the thickness of the layer changes moving up the slip surface c) Poles to damage zone joint surfaces for each of the line transects and the orientation of the slip surface moving up the fault.

Fault core: The fault core width ranges from 0.09 m to 3 m (Figure 74b). The Cb22 fault is the only fault in which a distinct slip surface is present. The slip surface is composed of a red-orange fine-grained gouge containing clasts of blue lava from the underlying T4 lava unit (Figure 75a). The width of this band varies along the fault plane from 1-2 cm up to 30 cm thick (Figure 74b). The contact between this red slip surface material and the ignimbrite B gouge is sharp but irregular; there is no grain scale mixing of material and the two gouges remain distinct from each other (Figure 75b). Very occasionally clasts of blue lava intermingle with the B gouge or clasts of B protrude into the red-orange gouge.

a)

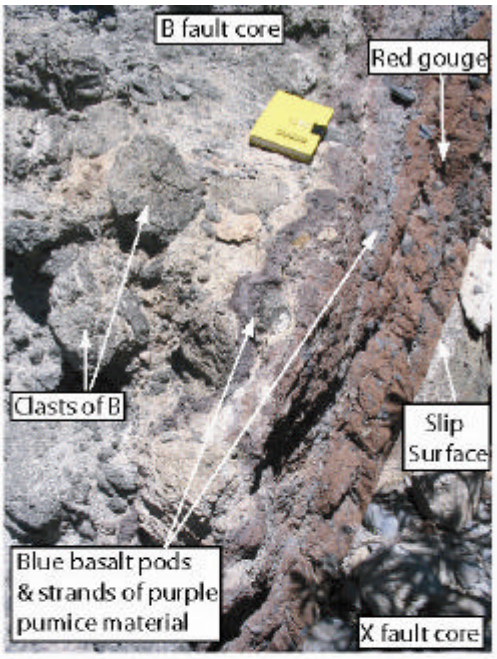

b)

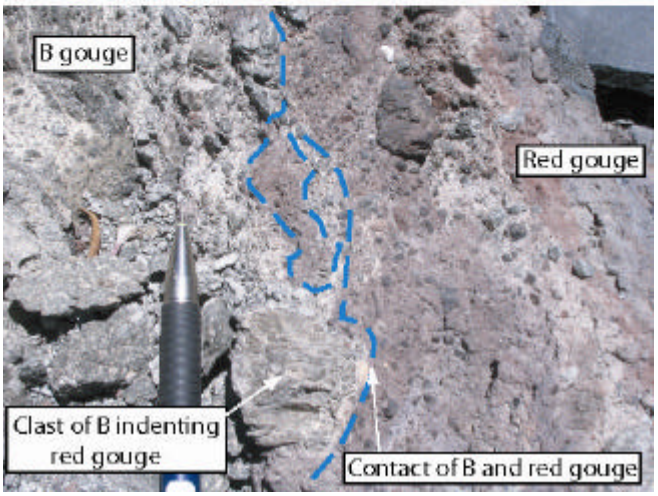

Figure 75: Cb22 fault core

a) Cb22 fault core, the slip surface is composed of a fine ash sized gouge and clasts of pumice and basalt from the T4 unit b) The contact between the red gouge and the slip surface is irregular but sharp (blue dashed line), there is no mixing of the material at the grain scale, the two gouges remain as two distinct units.

The ignimbrite B fault core material is composed of coarse gouge and angular to sub-angular blocks of B that increase in size moving up the fault (Figure 75a) The unit mid-section has a median clast size of 3.16cm^2 and clast size range of 0.06 cm^2 to 890.00 cm^2. At the top of the B unit the median clast sizes are 6.14 cm^2 and 8.69 cm^2, the clast size range is from 0.10 cm^2 to 3810.00 cm^2. The fault core is matrix supported; the clast matrix ratio is 30:70. The fault wall in ignimbrite B is stepped (Figure 76a & b) and the contact with the fault core is sharp.

a) **b)**

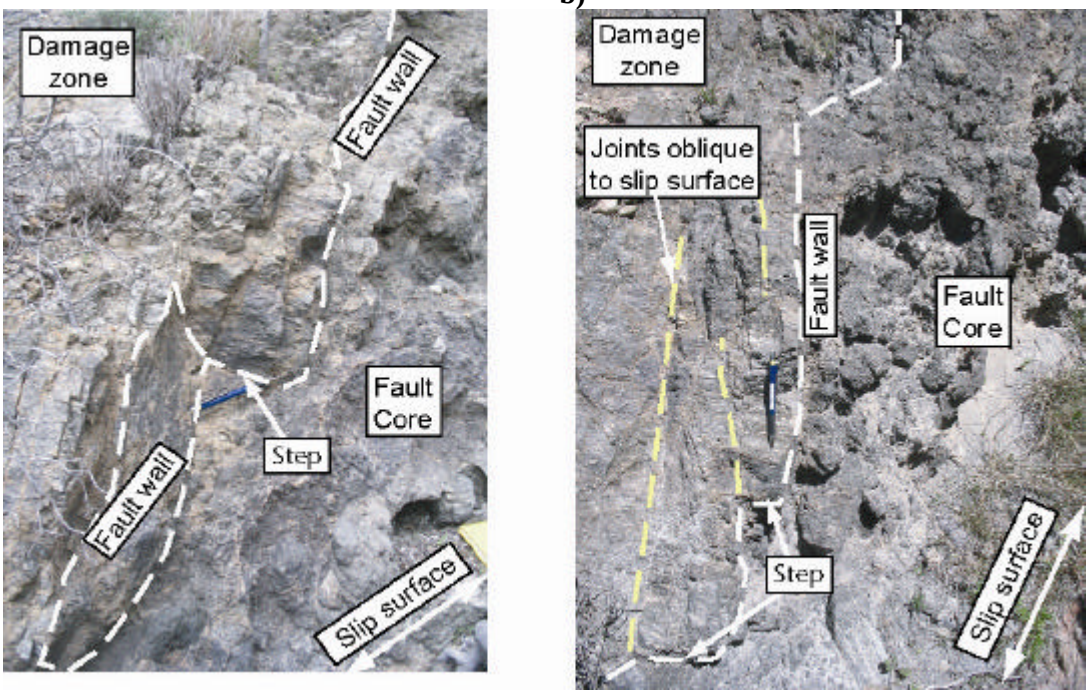

Figure 76: Cb22 fault wall

a) The fault wall in Cb22 has a smooth surface but it is stepped along the length of the fault core b) The joints in the damage zone are oblique to the slip direction which is indicated by the white arrow.

4.3 Comparison of fault zone architecture

4.3.1 Damage zone

Joint frequency adjacent to the fault core is greater than background levels (0.6 to 3.2 joints per metre,), but varies for each of the faults (Figure 77a & b). The narrowest damage zones are the CB15 and CB22-29 damage zones being 3 m and 2 m wide respectively. They also have the lowest joint numbers; the maximum value in either is 5 joints per meter and joint frequency for the most part falls below background level. The widest damage zones occur in CB22 at 4 m and 18 m above the base of the unit. The TB2.5, CB5 and CB22-18 have the highest levels of joint intensity. Overall the intensity of jointing increases moving away from the fault core before decreasing, reaching a maximum level 2-3 metres away from the fault wall. Damage zone joint frequency varies both between faults and within an individual fault (Figure 77).

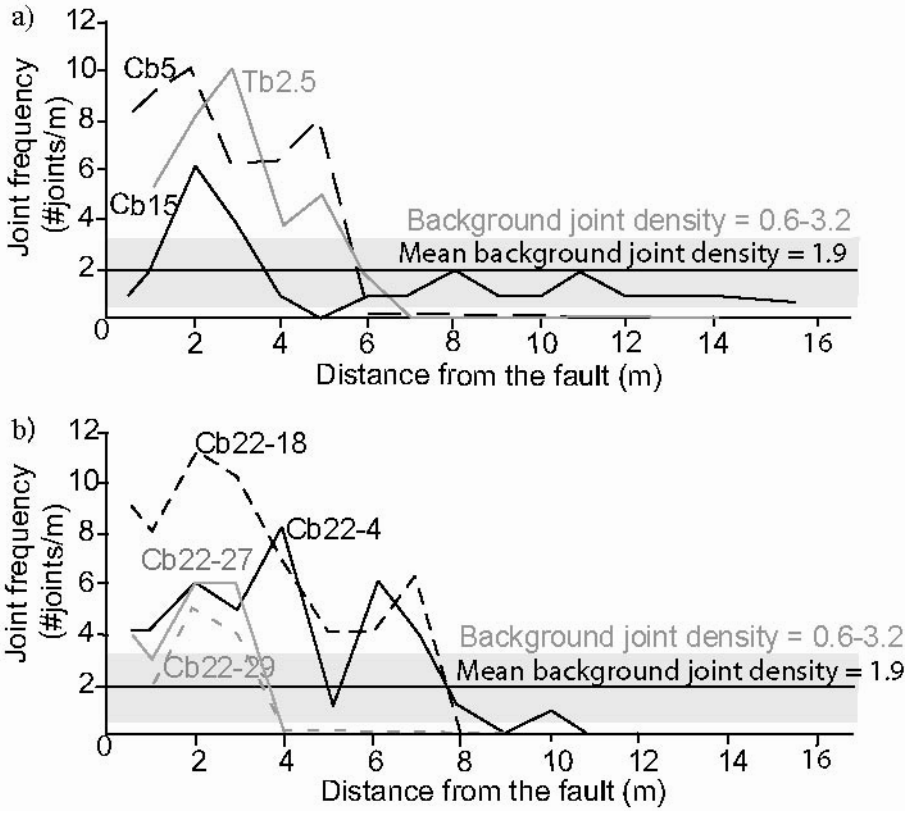

Figure 77: Joint frequency in ignimbrite B damage zone

The plots show joint frequency with increasing distance from the fault for a) Tb.5, Cb5 and Cb15 and b) Cb22 fault at dfferent heights from the unit base. The black lines are the maximum and minimum background joint density values. Background joint density was calculated from unfaulted sections at Los Frailes and Taurito. Joint frequency increases moving away from the fault with a maximum ~2-3 m away from the fault wall. C15 has levels of deformation lower than average background levels.

The box plot shows the median joint spacing and range of joint spacing in each damage zone (Figure 78). The median joint spacing is relatively constant for each of the damage zones and the range of joint spacing increases slightly with increasing displacement. The only exception is in the CB15 damage zone where there is a wide range of joint spacing and the median is much greater than the other faults.

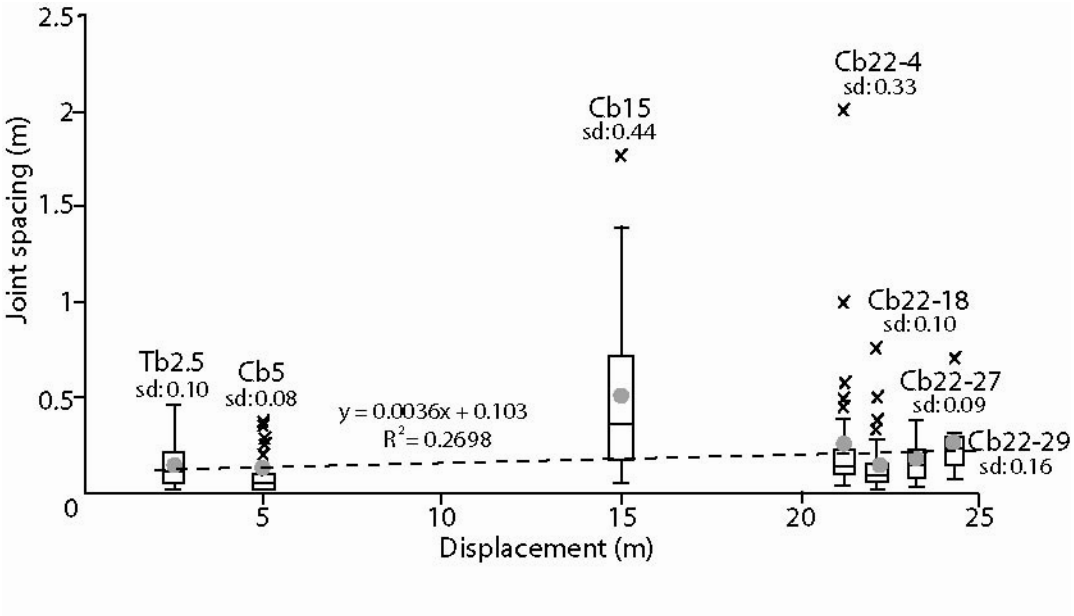

Figure 78: Joint spacing in ignimbrite B damage zones

The plot shows the mean (grey dot), median, upper and lower extremes and the range of damage zone joint spacing for each of the ignimbrite B faults (Tb2.5, Cb5, Cb15). In the case of Cb22 the damage zone joint spacing at different heights above the unit base are shown (4 m, 18 m, 27 m and 29 m above the base of the ignimbrite B unit). The boxes for the Cb22 fault have been plotted at different displacements so that they are clearly visible but each has undergone 22 m of displacement. The median and mean joint spacing and range of joint spacing in each of the damage zones remains relatively constant with increasing displacement, as illustrated by the trend line for the joint spacing mean values. Except for Cb15 which has a larger median and range of joint spacing.

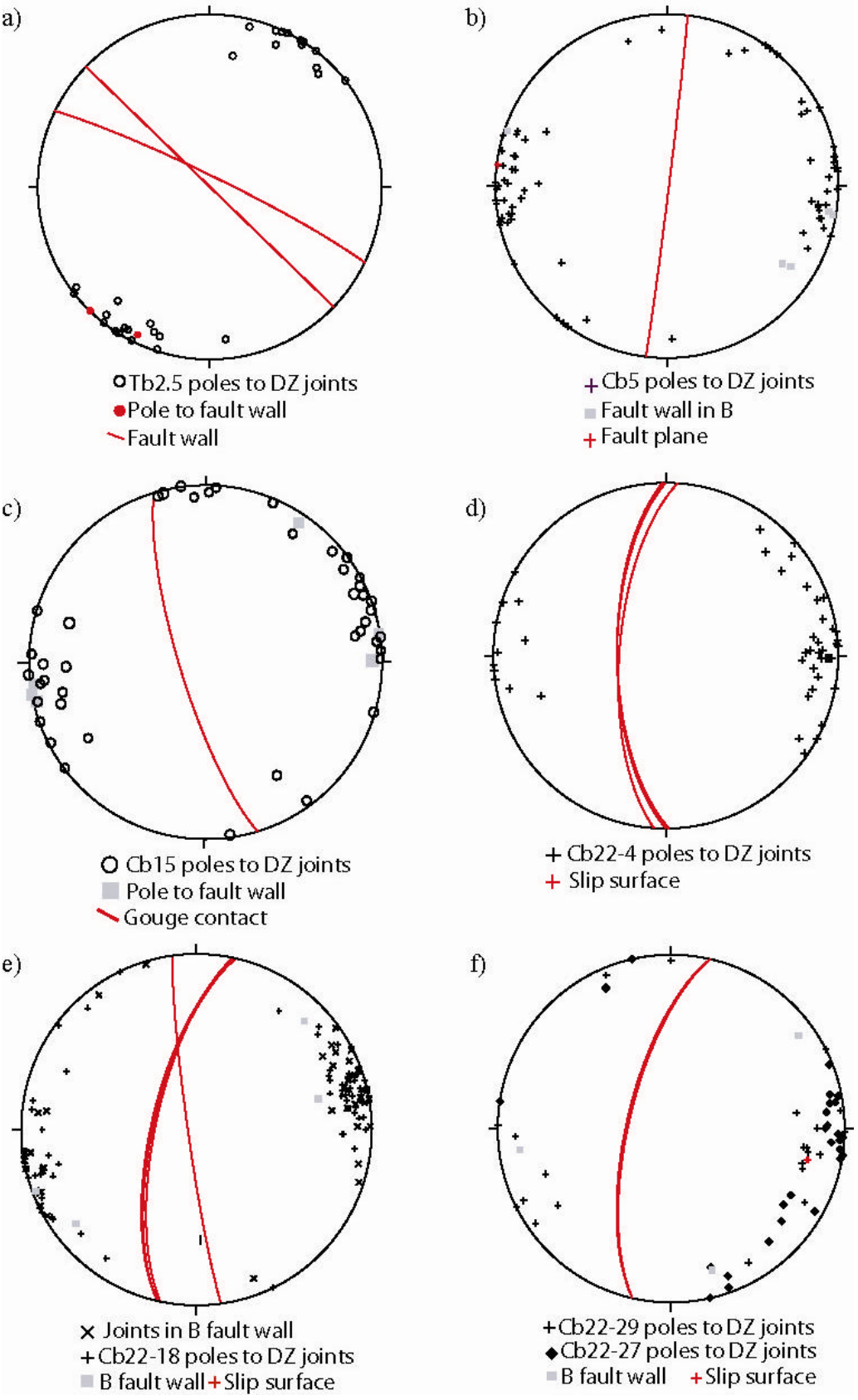

Figure 79: Stereonets for joints in ignimbrite B damage zones

Poles to joints are perpendicular to the slip direction in a) Tb2.5, b) Cb5 and c) Cb15. The Cb5 and Cb15 poles to joint surfaces lie in the same fields as the joints in the Cb22-4 (d) and Cb22-18 (e) fields. The Cb22-27 and Cb22-29 poles have a slightly greater spread of orientations (f)

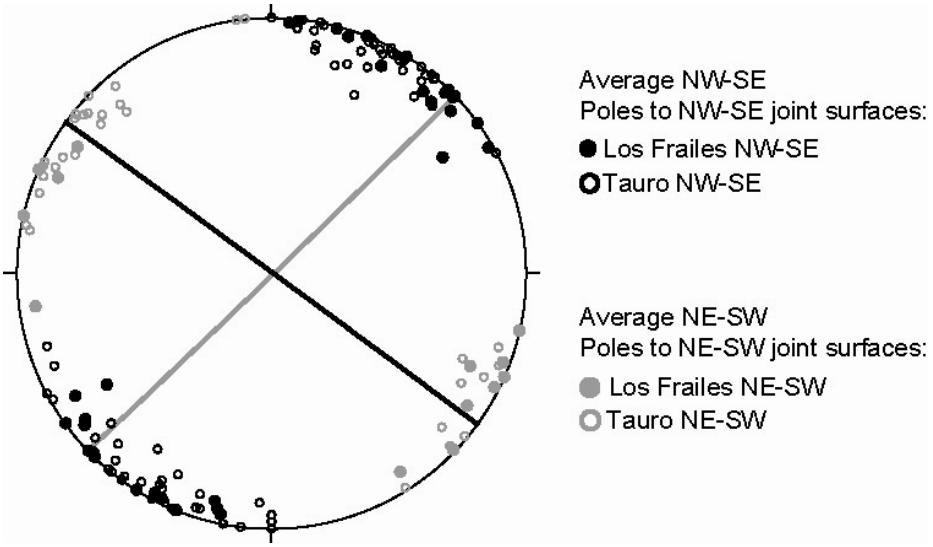

Figure 80: Stereonet of joints in unfaulted ignimbrite B protolith at Tauro and Los Frailes Joints in the Tb2.5 (Figure 79a) damage zone have the same orientation as protolith joints that are concentric to the caldera margin

As is the case with ignimbrite A, the 5 m and 15 m faults in ignimbrite B have no slip surface however a slip surface is well developed in the Cb22 fault core. The damage zone joints and fault walls/slip surface of each fault have a similar orientation to each other and to the other faults (Figure 80). The joints in CB5 and CB15 damage zones are parallel to the fault walls and direction of fault slip (Figure 80b & c). The trend of the Cb22 slip surface changes by a few degrees moving up dip over a vertical distance of 30 meters (Figure 80 d, e & f). Damage zone joints and fault walls in Tb2.5 have the same orientation as the concentric joints in the unfaulted sections of Los Frailes and Tauro (Figure 80 a & g). The joints and fault walls at Cedro are approximately concentric to the caldera margin further to the east.

4.3.2 Fault core width

Median fault core width increases only slightly with displacement, the median fault core width is the same in the Tb2.5 and Cb15 faults and there is only a slight increase in the Cb22 fault (Figure 81). The faults show dramatic variations in fault core width along dip especially Cb22 (Figure 81 and fault core logs section 4.2.2). The extremes in width, illustrated by the whiskers show that the narrowest fault core occurs in the largest displacement fault Cb22.

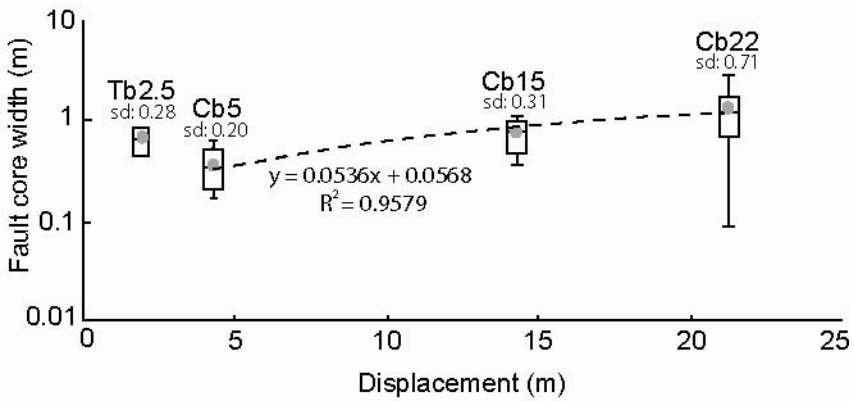

Figure 81: Ignimbrite B fault core width vs. displacement

Box plot of displacement against fault core width. There is a slight increase in fault core width with displacement, the slope of the trend line for the population means (grey dots) is 0.0536. The highest offset fault Cb22 has one of the narrowest fault cores. Note log scale on the Y axis.

The shape of fault core as defined by the bounding fault walls also varies between the faults. There are two types of fault wall morphology in Ignimbrite B, straight planar walls and stepped walls. The planar fault walls are found along Tb2.5, Cb5 and Cb15 where the damage zone joints are smooth, planar and parallel to the fault walls and slip direction. The stepped fault walls occur in the Cb22 fault core, where the joints in the damage zone are smooth and planar but have a slightly oblique orientation to the slip plane (Figure 76).

4.3.3 Fault core elements – Clast morphology

As discussed in Chapter 1, clast size in the fault core is expected to decrease with increasing displacement due to abrasion and attrition of the material within the fault core when displacement occurs. In the faults examined in this study fault core clast size does not decrease with increasing displacement (Figure 82). The median clast size decreases from Tb2 to Cb15 but the median values for locations in the Cb22 fault core increase. The high displacement Cb22 fault has clast size distributions closer to Tb2.5 clasts than Cb5 and Cb15.

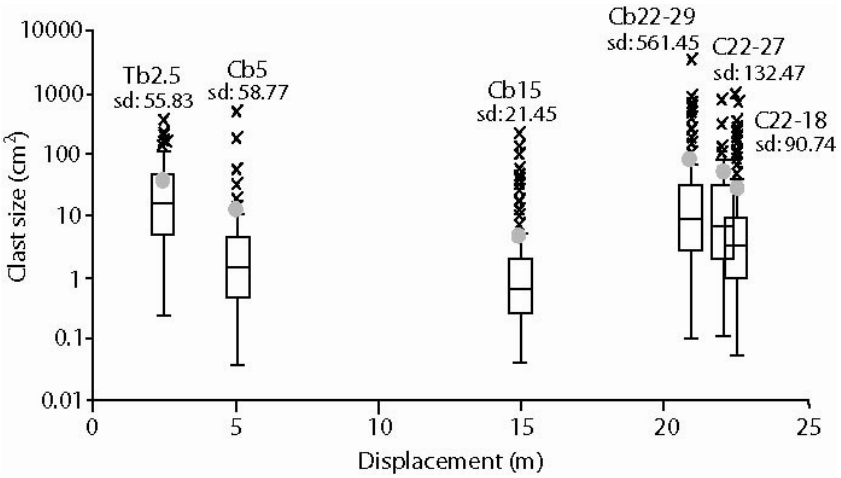

Figure 82: Ignimbrite B fault core clast size vs. displacement

Box plot and means (grey dots) of displacement against clast size (surface area). Clast size decreases from 2.5 m to 15 m of displacement and then increases in the 22 m displacement fault. Note log scale on the Y axis.

Table 9 more clearly demonstrates that as slip increases up to 15 meters of displacement, clast size decreases and the range of clast size and upper extremes also decrease. The clast size and range of clast sizes increases moving up through the Cb22 fault core. The top of the Cb22 fault has some of the largest clasts of any of the faults. The clast size range reflected by the inter-quartile range decreases from Tb2.5 to Cb15 indicating the greater amount of abrasion the material has undergone with increasing displacement, but the Cb22 fault shows an increase in clast size range moving up the fault core despite having undergone the most displacement.

Clast size	**Median (cm^2)**	**IQR**	**Lower extreme (cm^2)**	**Upper extreme (cm^2)**
TB2.5	15	40.68	0.25	106.39
CB5	1.46	4.56	0.04	11.95
CB15	0.63	1.79	0.04	4.72
CB22-18	3.16	16.21	0.06	41.51
CB22-27	6.14	29.27	0.1	76.1
CB22-29	8.69	30.57	0.1	78.24

Table 9: Fault core clast size in each of the Ignimbrite B fault cores

Fault core clast size listed in order of increasing displacement. Median, IQR (inter quartile range) and upper extreme of clast size decreases from 2.5 m slip to 15 m slip. After which the clast size as a whole increases for the CB22 fault and also moving up through the CB22 fault core.

Comparing clast axial ratios with displacement we see that the median clast axial ratio and range of axial ratios in a fault core decreases with increasing displacement. Table 10 shows that as slip increases the median values for clast axial ratio moves towards 1.4. Mean clast axial ratios for Cb15 and Cb22 clasts are around 1.5 and the IQR is approximately 0.5

Clast axial ratio	Median	IQR	Mean	Upper extreme
TB2.5	1.69	0.99	1.92	3.58
CB5	1.38	0.71	1.63	2.88
CB15	1.35	0.52	1.48	2.4
CB22-18	1.37	0.48	1.51	2.33
CB22-27	1.45	0.41	1.46	2
CB22-29	1.34	0.54	1.52	2.5

Table 10: Clast axial ratios for clasts in each of the Ignimbrite B fault cores
Clast axial ratios value decreases from 2.5 m to 15 m of displacement, after this point clast shape remains constant

The normalised clast axial ratio frequency for each of the faults is shown in Figure 83. The graph for clasts in Tb2.5 is uneven, indicating the Tauro fault core contains clasts with a range of axial ratios. After 15 m of displacement the shape of the Cb22 and Cb15 clast axial ratio graphs are very similar. The range of clast shapes has decreased with increasing slip, become more uniform and tended toward an equant shape. Clasts with larger aspect ratios may be new material incorporated from the fault walls at a later stage that has not undergone a large amount of attrition within the core.

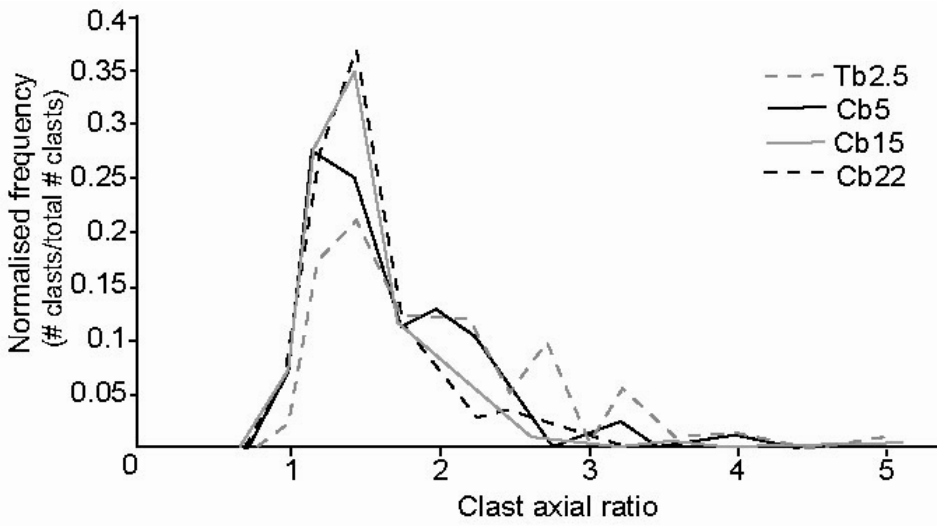

Figure 83: Ignimbrite B fault core clast axial ratios

As displacement increases the ratio of max to min axis decreases, therefore the clasts are becoming more symmetrical. Normalised frequency is the number of clasts in each bin size (0.5 cm^2 0.75 cm^2, 0.1 cm^2……4 cm^2, 4.5 cm^2, 5cm^2) divided by the total number of clasts measured in that fault core.

4.4 Summary

The data presented in this and the previous chapter demonstrate that displacement is not the primary controlling factor on fault growth or resultant fault architecture. Fault core width does not show a linear increase with displacement and fault core width varies along individual faults; suggesting that fault growth is controlled by a mechanism other than displacement related abrasion and attrition.

The frequency of joints in the damage zone does not increase with displacement and the highest joint frequencies occur 2 to 3 metres away from the fault wall and not adjacent to it. Furthermore joints in the host rock at Tauro have a similar orientation to the damage zone joints and both host rock and damage zone joints are parallel to the Tauro faults. At Cedro the joints and faults also share a similar orientation. These observations suggest that joint formation is unrelated to faulting and that the joints may be pre-existing structures on which the faults later formed.

There are also distinct differences in the style of fault architecture both between ignimbrite units and within an individual unit when sub-units occur (Ignimbrite A); indicating that the host rock petrophysical properties exert a strong influence on the deformation processes and subsequent deformation structures formed.

In the following section I present a model of fault formation and evolution based on these observations in which joint frequency and orientation are the main influence on fault architecture. I examine the evidence that the joints are acting as pre-existing weaknesses on which faults form and

that joint spacing controls the evolution of the fault core. Finally I discuss the influence host rock properties has on fault development and discuss the commonalties and differences of fault formation between ignimbrite A and B

5

Mechanism of fault initiation and evolution

From the observations of fault populations in ignimbrite A and B I have developed a new conceptual model of fault initiation in ignimbrites. In this model initial fault development is controlled by the population of joints in the host rock, with subsequent fault core growth being controlled by host rock fabric and petrophysical properties.

The model is based on observations of fault populations cutting two ignimbrite units having very different petrophysical properties. Each population contained faults with varying amounts of displacement, this "space-for-time" substitution allowed me to examine the evolution of the faults, the deformation processes active at certain stages and the change in processes with increasing displacement. As a number of the faults offset the different ignimbrite units against each other I could negate displacement as a factor, as both units had experienced the same amount of movement, and observe the effects different host rock properties had on the developing fault architecture.

The similarities in fault core width and damage zone joint intensity between faults with differing displacements suggested that displacement was not a primary control on fault evolution. The relationship between joint and fault orientation and between joint spacing and fault core width implied fault formation and growth was joint controlled. Fault walls were observed at a range of displacements, from centimetres (Tb0.35) to ten's of metres (Cb22), where slabs of rock were spalling off into the fault core suggesting fault growth via slab incorporation from joint surfaces. Further evidence for this mechanism was the consistently rectangular shape of the fault core clasts in ignimbrite B. The absence of such fault core clasts in ignimbrite A faults and the uniform width of fault cores cutting ash rich units regardless of displacement (Ca5 and Ca30), implied that the petrophysical properties of the host rock exerted a strong control on fault evolution. The rectangular nature of ignimbrite B clasts at a range of scales from mm's to cm's also suggested that the fabric of ignimbrite B controlled the clast shape within the fault core. In this chapter I present the conceptual models for ignimbrite A and ignimbrite B and the evidence supporting the models and controls on fault growth.

However before presenting these models I would like to acknowledge some of the limitations and unknowns of the models. Firstly at each displacement I found only one fault, thus other fault architectures may be possible at the same displacement. Also the smaller displacement faults are found at Tauro which is some distance from Montana Cedro where the larger offset faults are found and therefore may have undergone a slightly different stress history. However given the areal extent of the caldera both locations are most likely to have experienced the same stresses. What may differ between the two localities is the level of vapour phase alteration which affects the porosity and mechanical properties of the host rock and thus the deformation processes.

My model is based on faulting of existing joints when the joints undergo sufficient extension to eliminate frictional resistance between the joint walls and allow gravitational driven slip to occur. There are however jointed areas (Los Frailes) that are not faulted. As discussed in Chapter 2 joint density may be affected by the topography of the deposition surface or levels of secondary vapour phase alteration. High levels of jointing may occur in sections that have been deposited on sloping topography and undergone stretching, or have lower levels of secondary alteration and thus higher porosities and greater mechanical contrasts between matrix and fiamme. There may be a critical level of jointing at which faults form, when excessive jointing weakens the rock layer making it more prone to faulting. All faults observed in this study are located 2-3 metres from an area of high joint density or joint swarm. A similar joint swarm may have existed prior to the fault formation and the un-jointed rock between the two swarms was used as a wall against which slip occurred. No joint swarms or peaks in joint density where observed in unfaulted areas, however as previously discussed the background joint levels observed in this study may not be a true representation of joint density levels in uunfaulted units.

Another obvious possibility for fault formation is the upward propagation of an underlying fault. At Cedro the largest fault Ca30/Cb22 is a growth fault and therefore the structures associated with it are the result of a propagating fault tip. In section 5.2.1.1 I show that joints in the CA30 and CB22 damage zones are at a higher angle to the fault compared to those in the other fault damage zones. Therefore joints formed by a propagating fault and pre-exiting joints are distinguishable by there orientation to the fault. In all faults except Ca30/Cb22 the joints parallel the fault and so could not have been formed ahead of a underlying fault.

Although there are limitations to the models I feel the field data I have gathered in this study strongly supports the proposed fault growth mechanisms and the issues raised here could be resolved through further field work and data acquisition from other areas within the same units.

5.1 Fault growth model

5.1.1 Ignimbrite A

The initial stages of this model are based on the small, centimetre-offset faults at Barranco Tauro. Subsequent fault growth up to tens of metres of displacement is based on the large faults at Montana Cedro.

The host rock is cut by vertical and sub-vertical joints (Figure 84a), formed by caldera activity (section 5.2). Subsequent dilation of these joints during later caldera activity (Figure 92) causes them to slip with limited fracturing or cataclasis of the surrounding rock. For instance the smallest offset fault at Tauro has 17cm of displacement (Figure 84b), the slip surface is irregular, there is no gouge or pockets of breccia and there are no subsidiary joints extending from the slip surface. The block in the hangingwall appears to be slightly rotated from its original position creating gaps between the hangingwall and footwall (Figure 85). After 32 cm of displacement (Figure 84c) minor amounts of gouge have formed on the slip surface. The rock adjacent to the slip surface is becoming fractured; the limit of this fractured zone is a joint parallel to the slip surface. As I discuss in section 5.2.1.1 this bounding joint is most likely an existing joint in the host rock and unrelated to faulting.

The joint surface and initial slip surface are now the fault walls bounding the proto-fault core material. Subsequent slip events fractures and rotates the material within the proto-fault core forming the first clasts and gouge of the fault core (Figure 84d). Irregularities are removed from the creating a fault core composed of clasts and gouge bounded by two planar fault walls.

The slip surface in the initial stages of displacement (Figure 84b & c) is not smooth and planar. According to Power et al. (1988) model of asperity grinding surface irregularities are removed after a finite amount of slip due to mismatch between the surfaces, asperities on opposite surfaces come into contact and are removed or ground down to produce wear material. In this model Power assumes that dilation of the surfaces is minimal. Schopfer (2005) modelled faults at different confining pressures and found that with increasing confining pressure there was a decrease in fault surface irregularities. The irregular slip surface observed here suggests that dilation of the joint was sufficient to allow slip to occur with minimal contact of the joint surfaces and therefore movement on these faulted joints likely occurred under low confining pressure or in a tensile stress regime.

As the fault core is bound by the faulted joint and an existing joint it seems reasonable to assume that the spacing between these pre-existing joints dictates the width of the initial fault core. However although initial slip occurs on joints, it appears that the host rock properties dictate whether the fault core will continue to grow with increasing displacement or maintain its initial

width. Joints adjacent to the Ca5 and Ca30 fault cores are closely spaced and the fault core is narrow despite the differences in accumulated displacement. Joints flanking the Ca15 fault are also closely spaced but the fault core is wider and has a range of widths; these factors are discussed further in section 6.2.

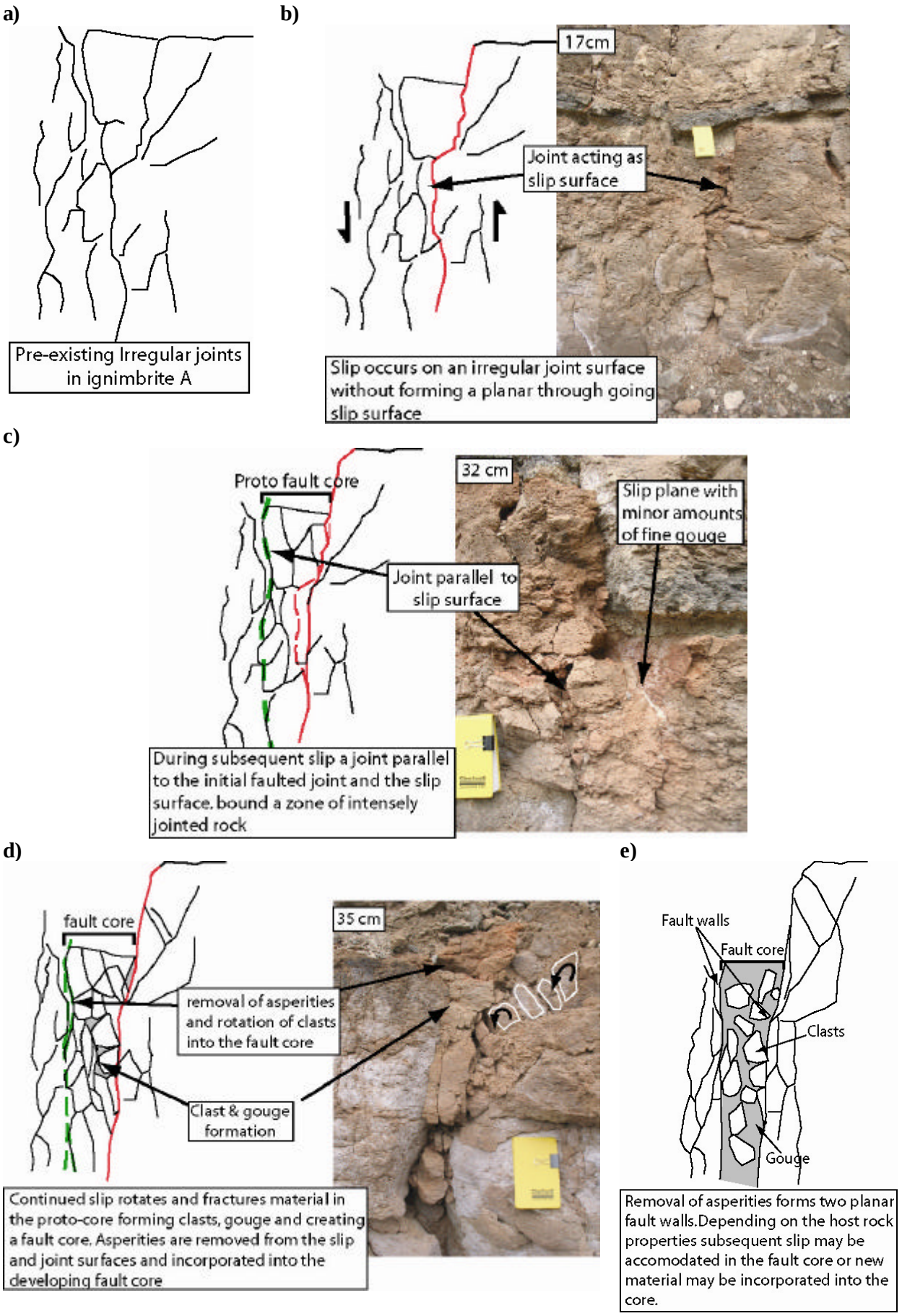

Figure 84: Model of fault initiation and growth in Ignimbrite A, see text for discussion

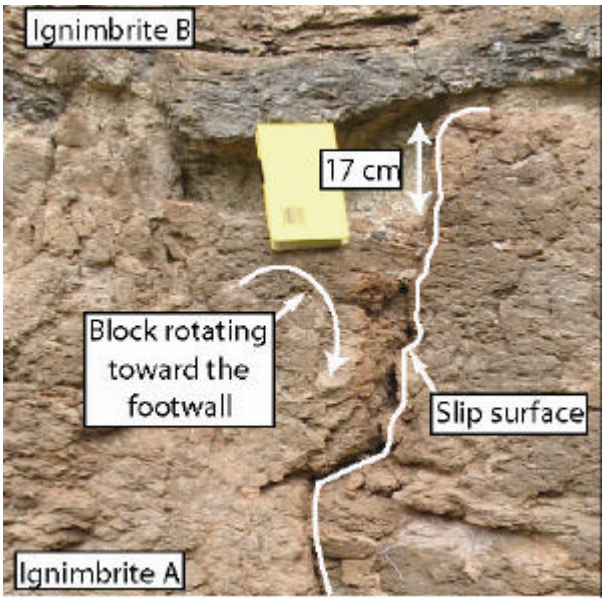

Figure 85: Close up of TA0.17
The slip surface is irregular and the block in the hangingwall appears to be rotated towards the footwall. Note that the fault does not extend up into the overlying ignimbrite B

5.1.2 Ignimbrite B

As in ignimbrite A, initial slip occured on existing joints in the ignimbrite B host rock (Figure 86a) that undergo further dilation during caldera activity (Figure 92). The dilation of the joints allows rock fragments to fall into the joint openings and the joint-bounded rock pillars to shuffle past each other (Figure 86b). Movement of the pillars causes a further increase in the joint opening and more material falls inwards from the joint surfaces. The material is rotated within the joint forming a proto-fault core consisting of two planar joint surfaces or fault walls bounding a zone of rock fragments (Figure 86b). Continued displacement forms minor joints adjacent to the proto-fault core (Figure 86c). The joints grow and intersect the faulted joint surface, delineating slabs of rock that are incorporated into the core during subsequent slip events (Figure 86c). In the fault core these slabs are rotated and fragmented, forming angular clasts and minor amounts of gouge.

After initial offset the amount the fault core expands by is controlled by the width of the slab incorporated into the fault, which is equivalent to joint spacing (Figure 86d). Widely spaced joints form thick slabs that on incorporation cause a large increase in fault core width, and closely spaced joints form thin slabs that allow only small increases in fault core width. The field data shows that areas with widely spaced joints correspond to wide fault cores and large clast sizes and areas with closely spaced joints have narrow fault cores and small clast sizes. It is by this process of slab delineation and incorporation that the fault core widens with increasing displacement. As slabs are removed from joint surfaces the exposed joint surface becomes the new fault wall, as a result joint morphology and orientation controls the morphology of the fault walls and fault core.

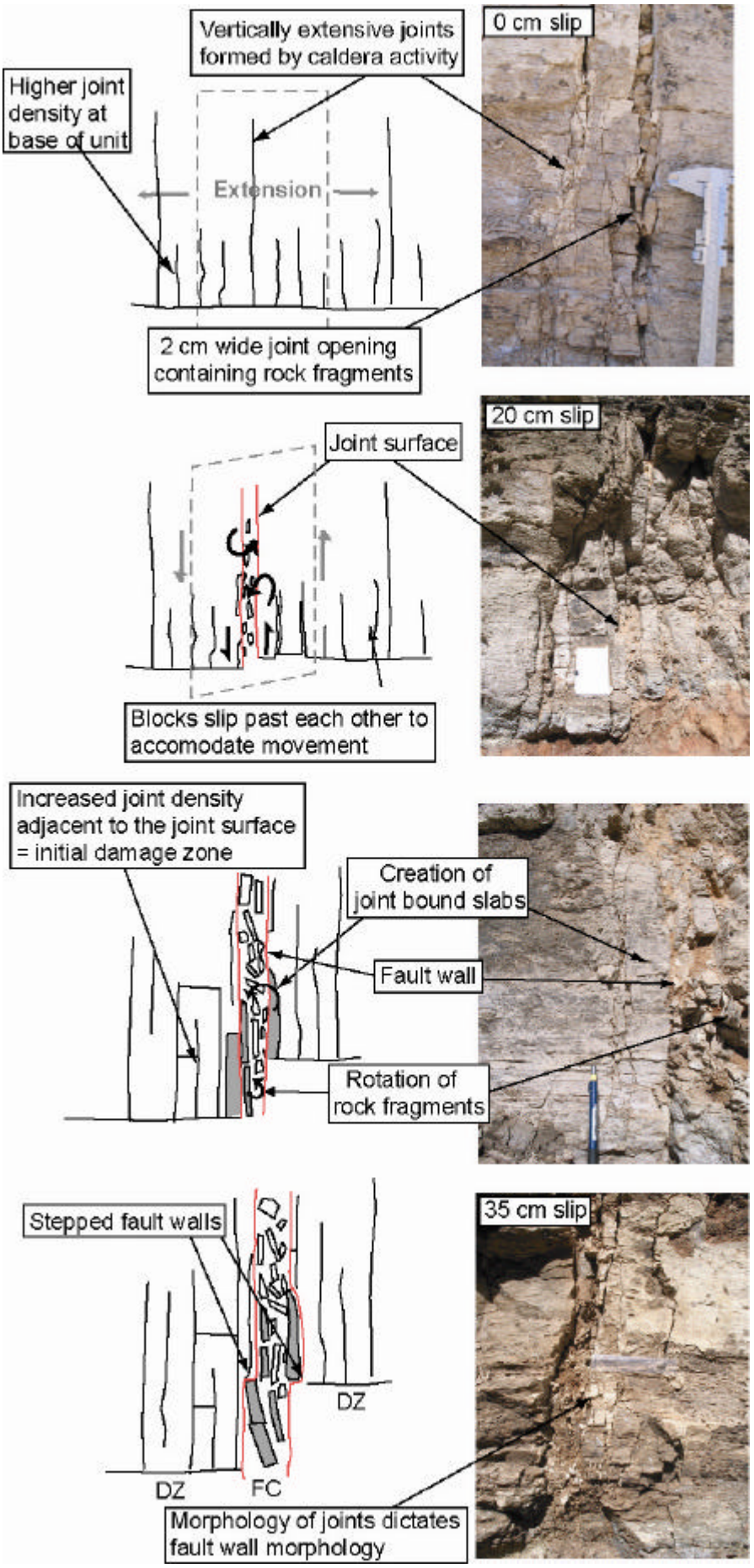

Figure 86: Model of fault initiation and growth in ignimbrite B, see text for dis cussion.

5.2 Discussion

5.2.1 Fault initiation

As discussed in Chapter 1 previous models of fault initiation are based on the linkage of minor pre-existing joints due to a rotation of the stress field or formation of cross-joints and eventual formation of a through going shear plane. The resulting architecture is a slip zone with the pre-existing joints at a high angle to the shear zone. Joints formed subsequent to fault formation as a result of slip are also at a high angle to the shear zone.

I suggest that the faults investigated in this study initiated on pre-existing joints in the host rock. The joints formed in the extensional environment created by caldera collapse and subsequent extension caused hybrid failure of some joints resulting in fault formation parallel to the pre-existing joints.

5.2.1.1 Joint orientation

Calderas are dominantly extensional settings; extension occurs all around the caldera during doming (Gudmundsson, 1998; Walker, 1984) and in the extracaldera region during caldera deflation syn- and post-eruption (Branney, 1995). Doming of the intracaldera floor was recorded at the Sierra Negra volcano, Galapagos prior to eruptions (Chadwick et al., 2006). The inflation was interpreted as magma intruding into a sill beneath the caldera. At Long Valley caldera (Simons et al., 2000) and Campi Flegrei, Italy (Usai et al., 2000) 2-4 cm of doming per year has been recorded. Extracaldera radial faults on Gran Canaria are also interpreted as being the result of inflation prior to eruptive events (Troll et al., 2002; Walter and Troll, 2001).

Caldera collapse causes downsag of the caldera floor and centripetal extension of the extracaldera region forming grabens and faults concentric to the caldera margin (Branney, 1995; McBirney and Williams, 1969; Walter and Troll, 2001). In experimental simulations of caldera collapse the flanks of the caldera tilt inward after which a concentric fault pattern forms (Troll et al., 2002). The extracaldera faults may be several kilometres away from the caldera rim (Walter and Troll, 2001). In the case of a multi-cyclic caldera such as Gran Canaria which has undergone numerous doming and collapse events, resurgence forces the caldera periphery to uplift causing expansion and dilation of the radial and concentric extracaldera faults (Walter and Troll, 2001). Repeated resurgence and deflation is also responsible for the concentric growth faults with both normal and reverse sense of slip such as the largest offset fault at Cedro (Walter and Troll, 2001).

In this study each location examined has a different set of joint and fault orientations due to their positions with respect to the caldera. All faults and damage zone joints examined are concentric to the caldera margin and so their orientation changes from NW-SE in the southwest of the island to

approximately N-S in the west of the island. The unfaulted ignimbrite units at Los Frailes and Barranco Tauro contain two joint sets. In Ignimbrite A both host rock joint sets are sub-parallel to the caldera margin (Figure 87c). In ignimbrite B the host rock joint sets are orthogonal to each other, one is concentric and the other radial to the caldera margin (Figure 87e). These joints are likely to have formed by deflation (concentric joints) and inflation (radial joints) of the caldera.

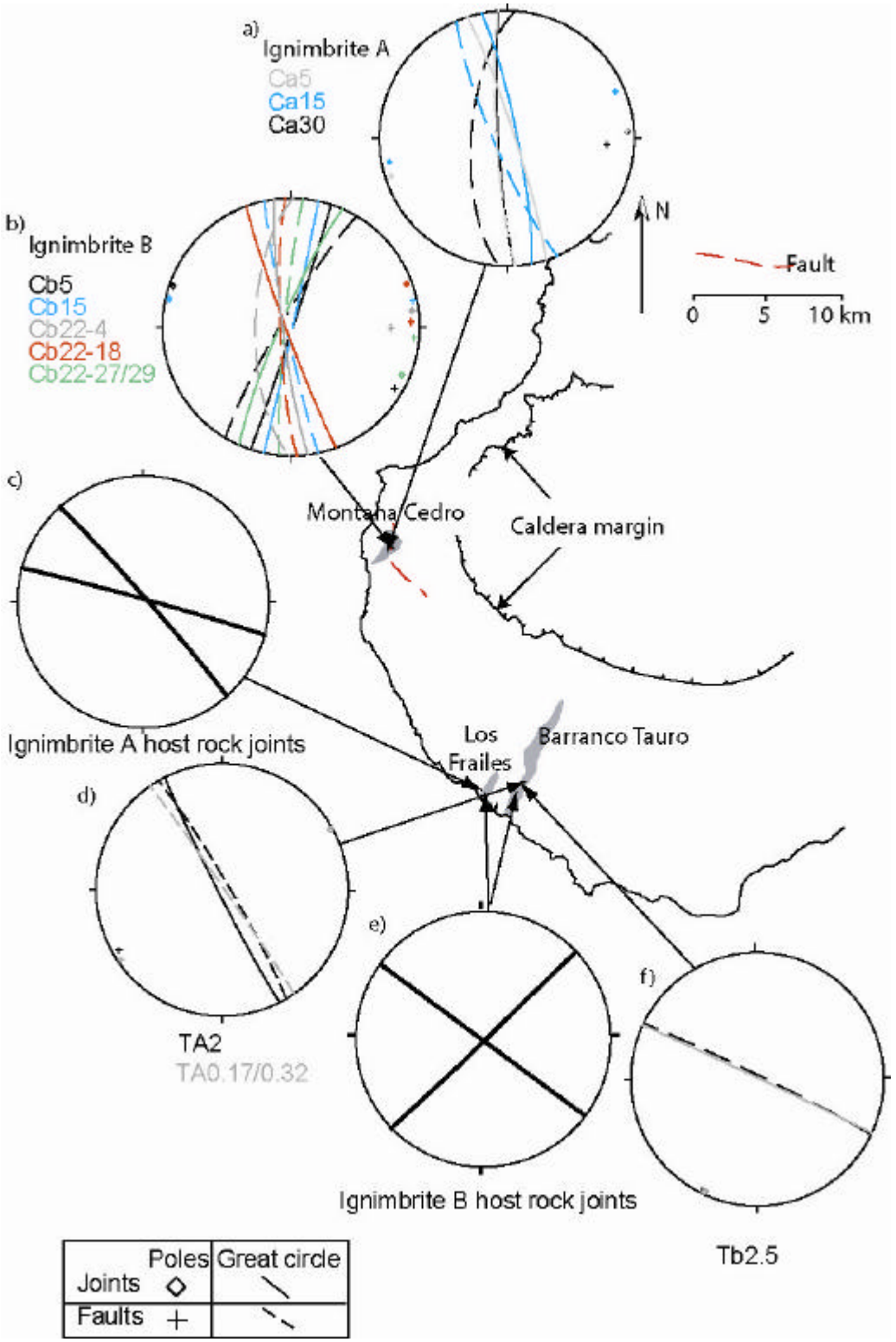

Figure 87: Location map of stereonets showing host rock joints and damage zone joints Stereonets show mean poles and great circles for joints and faults. Arrow indicates the area from which the data was measured.

If the faults are initiating on these pre-exisitng joints through continued dilation as my model suggests, then the faults should have similar orientations and morphologies to the joints. If the joints formed due to the propagation of a shear fault we would expect joint orientation to be linked to the local stress field around the propagating fault tip. The resulting damage zones should contain joints at high angles to the fault and not parallel to it (Hancock, 1985; Kim et al., 2004).

At Tauro and Cedro the damage zone joints in ignimbrite A and B have the same morphology as the host rock joints, both have smooth planar surfaces and are vertically extensive. Furthermore damage zone joints close to the faults exhibit no wing cracks and limited cross joint development. The joints in the TA2 (Figure 87d) and Tb2.5 (Figure 87f) damage zone have the same average orientation as the ignimbrite A (Figure 87c) and B (Figure 87e) host rock joints respectively. The shared morphology and orientations suggest that the damage zone joints are derived from the same joint population as the host rock joints. The morphology and orientation of the TA2 and Tb2.5 fault walls are the same as the adjacent damage zone and host rock joints for that ignimbrite unit. Therefore the faults are initiating on joints that were formed by extension of the ignimbrite unit during post-eruption subsidence of the caldera.

At Cedro there is more variation in the joint and fault wall orientations and I have used Fischer statistics to assess the level of similarity between these damage zone joints and faults. The Fischer method is used to analyse orientation data and calculate the radius of the 95% confidence interval cone ($?_{95}$). The cone has at its centre the mean dip vector of the measured sample data set (n), the boundary of the cone is a distance of $?_{95}$ degrees away (Figure 88). The cone indicates that we are 95% confident that the mean vector for a much larger population of measurements (N) will lie within a circle of radius $?_{95}$ degrees from the mean vector of the smaller sample population. A small radius indicates that the mean vector of the large population (N) is close to the sample mean vector (n) and that the sample data set is a good representation of the larger data set. A cone with a large radius means the data is more variable and that the sample population may not truly represent the larger population.

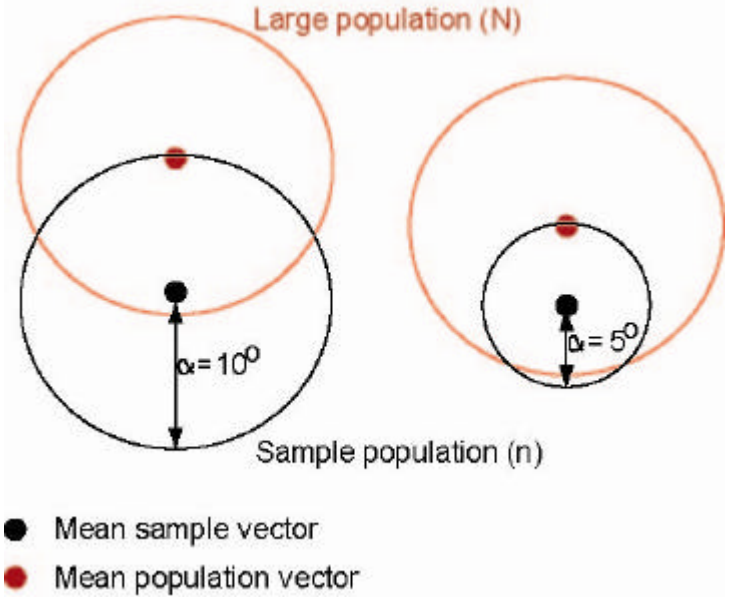

Figure 88: Fischer statistic method

The overlap between the sample and large population is greater when the radius of the 95% confidence interval ($?_{95}$) is small. The sample mean of the population on the right is closer to that of the larger population. We are 95% certain that the sample (n) does represent the larger population (N).

If the joints present in the ignimbrite units at Cedro are indeed pre-existing and a result of caldera deflation then the joints should be from the one joint population; i.e. formed at the same time in the same stress field. The results of this analysis for joints in ignimbrite A are given in Table 11. The mean vector of all the joints measured in ignimbrite A at Cedro has a $?_{95}$ of 2.04 degrees. This suggests that if it were possible to measure all the joints in ignimbrite A at Cedro then the mean of that population (N) would lie within 2.04 degrees of the sample mean. Therefore the sample is a good representation of the larger joint population and the joints in each of the individual damage zones likely belongs to one larger population. The similarity between damage zone joint sets can be seen in the stereonet in Figure 87. The mean joint orientation of the Ca5 and Ca15 damage zones are almost identical, the joints in the Ca30 damage zone have similar strikes but dip in the opposite direction towards the southwest.

	All ignimbrite A damage zone joints	Ca30 DZ joints	Ca15 DZ joints	Ca5 DZ joints
Mean dip azimuth	287.2	266.6	78.6	72
Mean dip angle	88.7	84.6	83.3	84.9
95% CI ($?_{95}$)	2.04	2.49	5.18	3.59

Table 11: Ignimbrite A damage zone joint statistics, Cedro

Mean dip azimuth, mean dip angle and 95% confidence interval (CI) for the damage zone joints in each individual ignimbrite A fault at Cedro and all of the Cedro ignimbrite A damage zone joints taken together.

In ignimbrite B the 95% confidence-interval cone for all the damage zone joints has a radius of 1.1 degrees (Table 12); therefore the mean vector for the entire population is very close to the mean of our sample which again is composed of joint populations from each of the three fault damage zones. This implies that the joints in the three damage zones are not distinct joint populations but were formed in the same stress field. Again the mean damage zone joint orientation for Cb5 and Cb15 is almost identical. The Cb22 damage zone has a greater variation in joint orientation moving up along the fault: Cb22-4 (262.5 84.6), Cb22-18 (249.6 86.6), Cb22-27/29 (293.7 83.4). This may be a result of the greater vertical extent of the Cb22 fault or that this is the actively propagating tip of the growth fault and the joints are forming in response to the fault tip stress (McGrath and Davison, 1995).

	All ignimbrite B damage zone joints	**Cb22 DZ joints**	**Cb15 DZ joints**	**Cb5 DZ joints**
Mean dip azimuth	265.3	268.2	102.2	108.2
Mean dip angle	87.5	85.7	89	88.8
95% CI (?$_{95}$)	1.1	1.34	2.82	2.35

Table 12: Ignimbrite B damage zone joint statistics, Cedro

Mean dip azimuth, mean dip angle and 95% confidence interval (CI) for the damage zone joints in each individual ignimbrite B fault at Cedro and all of the Cedro ignimbrite B damage zone joints taken together.

It would appear that the individual damage zone joint populations are from one larger joint population. Furthermore these joints are orientated parallel to the caldera margin, implying that their formation is the result of caldera flank extension and not fault propagation.

If we compare the mean dip azimuth and mean dip angle of all the damage zone joints in ignimbrite A and ignimbrite B at Cedro we see that the mean dip azimuth differs by 22° and the mean dip angle by only 1°. If the damage zone joints within A and B are from the same population it is reasonable to assume that the joint population in each individual ignimbrite unit is actually part of one large joint population that formed in response to the far-field extensional stress. Combining all the joint orientation data into one sample yields a ?$_{95}$ of 1, a mean azimuth of 269.9 and a mean dip of 88°. Thus we can be 95% certain that all joints in ignimbrite A and B at Cedro are orientated parallel to the caldera margin and so formed during an episode of caldera flank extension.

If ignimbrite A had undergone deflation then resurgence prior to the emplacement of ignimbrite B we would expect the joint system in A to be more complicated and varied than the joint system in ignimbrite B. Whereas in fact the joints in both units are sub-vertical, parallel to each other with limited joint branching or cross-joint formation. Therefore both ignimbrite units were deformed in

the same deflation episode and both had been deposited before extension and faulting of the units began.

Further evidence that both units were emplaced before deformation began can be found in the C5 fault. The fault is a single sharp surface that can be traced up into B. The contact between B and A is planar, there is no bending of the ignimbrite B vitrophyre as seen in Tauro when B was deposited across minor faults in the top of ignimbrite A (section 2.3.2). Indicating that ignimbrite B was emplaced across a flat surface and displacement occurred afterwards.

I have applied the same logic in comparing fault and joint orientations as I did for the joint populations in ignimbrite A and B. If the faults were once joints their mean orientation should be the same or quite similar to the mean orientation of the damage zone joints, as they were originally all part of the same joint population. The results of this analysis for faults and joints in ignimbrite A and B are shown in Table 13 and Table 14 respectively.

	Ca30 DZ joints n = 89	**Ca30 fault n = 9**	Ca15 DZ joints n = 16	**Ca15 fault n = 3**	Ca5 DZ joints n = 40	**Ca5 fault n = 2**
Mean dip azimuth	266.6	**273.7**	78.6	**246.7**	72	**266.2**
Mean strike	176.6	**003.7**	168.6	**156.7**	162	**176.2**
Mean dip angle	84.6 SW	**67.3 NW**	83.3 NE	**81.7 SW**	84.9 NE	**83.5 SW**
95% CI ($?_{95}$)	2.49	**3.46**	5.18	**6.42**	3.59	**33.4**

Table 13: Ignimbrite A fault and damage zone joint statistics
Mean strike and dip values and 95% confidence interval for the damage zone joints and fault orientations for each of the faults in ignimbrite A.

	Cb22 DZ joints n = 185	**Cb22 fault n = 25**	**Cb15 DZ joints n = 38**	**Cb15 fault n = 5**	Cb5 DZ joints n = 61	**Cb5 fault n = 6**
Mean dip azimuth	268.2	**266.7**	102.2	**257.9**	108.2	**300.7**
Mean strike	178.2	**176.7**	12.2	**167.9**	18.2	**30.7**
Mean dip angle	85.7 SW	**82.9 SW**	89 SE	**87 SW**	88.8 SE	**83.6 NW**
95% CI ($?_{95}$)	1.34	**4.93**	2.82	**5.63**	2.35	**7.53**

Table 14: Ignimbrite B fault and damage zone joint statistics
Mean strike, dip values and 95% confidence interval for the damage zone joints and fault orientations for each of the faults in ignimbrite B.

Orientations of faults and adjacent damage zone joints are similar for faults in both ignimbrite units. The radius of the 95% confidence interval cone is larger for smaller sample numbers as is to be expected. Despite this, the results do show that fault walls have similar orientations as the adjacent joints thus supporting the argument that extensive dilation of the joints causes slip to occur and fault formation.

5.2.1.2 Failure angle

The angle of shear failure is measured between the maximum principal compressive stress and the failure plane (Ferrill and Morris, 2003). Failure angles in rocks undergoing shear tend to be 10^0-20^0 in competent rocks (Figure 89a) and 15^0-45^0 for less competent rocks. For tensile failure the angle is 0^0 (Figure 89b) and displacement is perpendicular to the joint surface. In the case of hybrid failure where displacement is oblique to the joint surface (dilatant faults) failure angles are low (Figure 89c) and lie between 0^0 and the angle predicted by Equation 2 (Ferrill and Morris, 2003).

$$? = +/- (45^0 – f/2)$$

Equation 2: Prediction of she ar failure angle from the angle of internal friction, where ? is the angle of shear failure and f is the angle of friction.

As the fault dip is dependent on the failure mechanism by which it formed the angle of dip indicates the failure mechanism and thus stress system at the time of faulting.

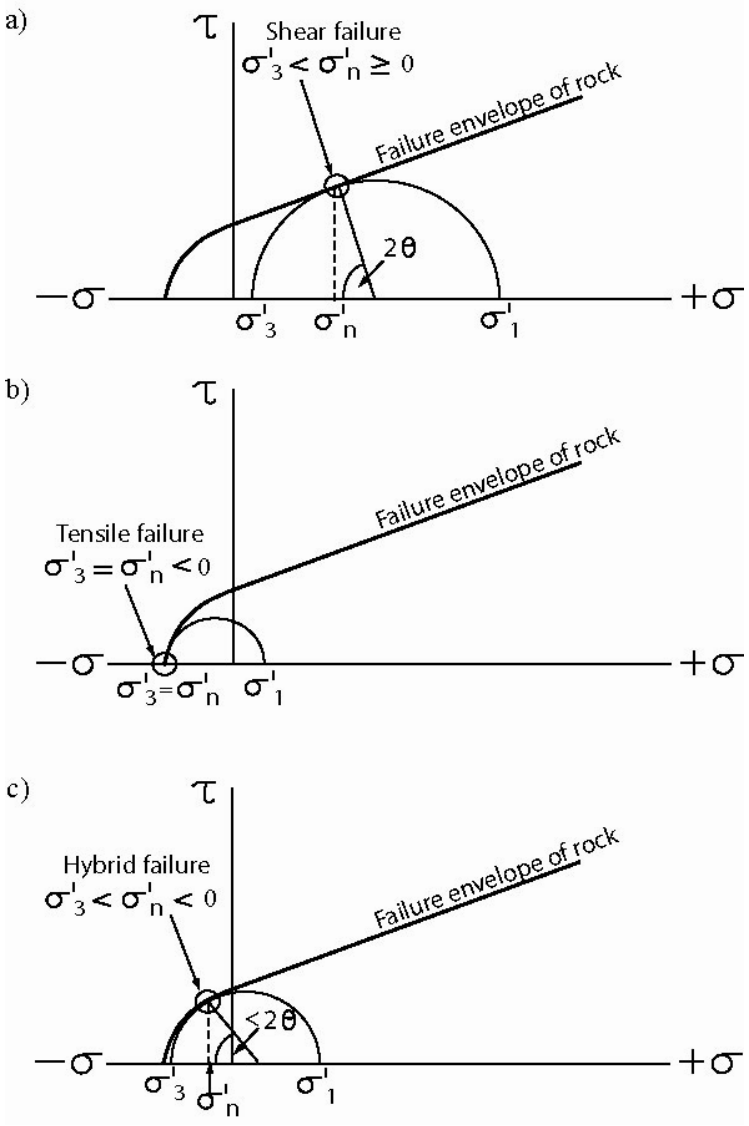

Figure 89: Shear, tensile and hybrid failure modes

Mohr circles with failure envelope illustrating the different failure modes for normal faults a) shear failure , b) tensile failure where s'$_3$ = tensile strength of the rock c) hybrid failure, where s'$_3$ < tensile strength of the rock. Diagram is adapted from Ferril and Morris (2003)

Using the friction angles from section 2.3.1 and the above equation I have calculated the predicted shear failure angle for ignimbrites A and B and compared them with the actual failure angles in each of the faults (Table 15). In order to do this I have inferred a vertical orientation for s_1; the reason for this being that the faults are surface structures and that during caldera deflation as the flank undergoes extension the horizontal stress would be tensile or close to tensile. Therefore the vertical stress (gravity) is much greater than the horizontal stress, hence the assumption of a vertical s_1.

	Range of friction angle (f)	Predicted angle of failure in shear (?)	Actual angle of failure	
			Min	Max
Ignimbrite A	33 - 34	28.5 - 28	**90° - angle of dip assuming vertical s_1**	
TA2			0° *	13° *
Ca5			1°	14° *
Ca15			4° *	12°
Ca30			18°	23°
Ignimbrite B				
Tb2.5	27 - 34	31.5 - 28	0° *	-
Cb5			1°	15° *
Cb15			0° *	12°
Cb22			4°	21°

Table 15: Predicted and actual failure angle for each fault in ignimbrite A and B
As slip surfaces are not present in all the fault cores the failure angle for certain faults was calculated from the fault wall orientation, indicated with an asterisk. The orientation of the fault walls and the slip surfaces changes along dip hence the maximum and minimum values of failure angle are presented here.

All of the actual failure angles are much less than the predicted shear failure angles which implies that all the faults have failed by tensile or hybrid failure mode. The TA2, Tb2.5 and Cb15 faults have minimum failure angles of 0° indicating tensile failure has occurred on these faults. The nature of the fault core material in TA2, being composed of overlying ignimbrite B, supports the idea of a joint undergoing substantial opening perpendicular to the joint surface allowing blocks of B to fall down into the joint prior to slip. The maximum values of failure angle in these three faults may indicate a hybrid component of failure during subsequent fault slip and growth. The tensile-hybrid failure mode indicates that the extension of the layer is the driving force behind slip on these faults.

The Ca30 and Cb22 faults have maximum failure angles much greater than the rest of the faults and closer to the predicted shear failure angles. The Ca30 and Cb22 faults are part of the large growth fault. We know that this fault was active prior to deposition of ignimbrite A and B due to the ignimbrite unit thickness changes across the fault (section 2.1.3). The higher failure angles may be due to the influence of the propagating fault tip. As the ignimbrite units were undergoing extension during caldera deflation the extension would also cause slip on the fault creating a local shear stress. The interaction of the remote tensile and local shear stress fields at the fault tip could account for the larger failure angles in Ca30 and Cb22 faults. The higher angle the Cb22 damage

zone joints have to the fault, compared with other faults, may also be a result of the local shear stress fields. If the influence of a propagating fault tip is to increase the failure angle by promoting a shear component, then it further supports the idea that the other faults initiated on joints undergoing extension and not by shear failure ahead of a fault tip.

The joint orientation together with the tensile to hybrid failure angles strongly argues for caldera control on joint formation. The concentric growth fault is the result of extracaldera extension during caldera collapse; the joints also reflect this extensional setting. Are the joints a result of the far-field stress from flank extension or are they the damage zone joints of the growth fault. The higher failure angles of the growth fault and the oblique orientation of the joints adjacent to it suggest that the fault tip stress is slightly different to the regional stress field and that although it alters the orientation of the immediate joints it is not large enough to affect the remote extensional stress. The similarities between the smaller C5 and C15 faults to the joints imply that the faults formed on the joints at a later stage.

5.2.1.3 Joint frequency and spacing

Previous workers have proposed that as displacement increases there is a corresponding increase in damage zone width (Hull, 1988; Knott et al., 1996) and in the complexity and number of deformation structures (joints, deformation bands, minor slip surfaces) within the damage zone (Caine and Forster, 1999; Fossen and Hesthammer, 2000; Knipe et al., 1998). (Peacock, 2001) suggested a number of features that could be used to determine the relative timing of jointing and faulting. One of these determining factors was increasing joint frequency towards the fault. Joints that formed before or after faulting do not increase in frequency towards the fault. Joints formed synchronously with faults should reflect the same stress state that caused faulting and increase in frequency towards the fault. (Sagy et al., 2001) also noted that joints, identified as having formed as a result of fault movement, increased in frequency towards the fault.

If the joints in this study are pre-existing and where formed not by faulting but by a prior deformation event, then the frequency and spacing of joints for different faults should be similar regardless of displacement accumulated. As joint frequency increases the spacing between joints will decrease. I used joint spacing instead of joint density as it is more relevant to my model of fault growth, as the amount the core grows by depends on the slab width which is controlled by joint spacing.

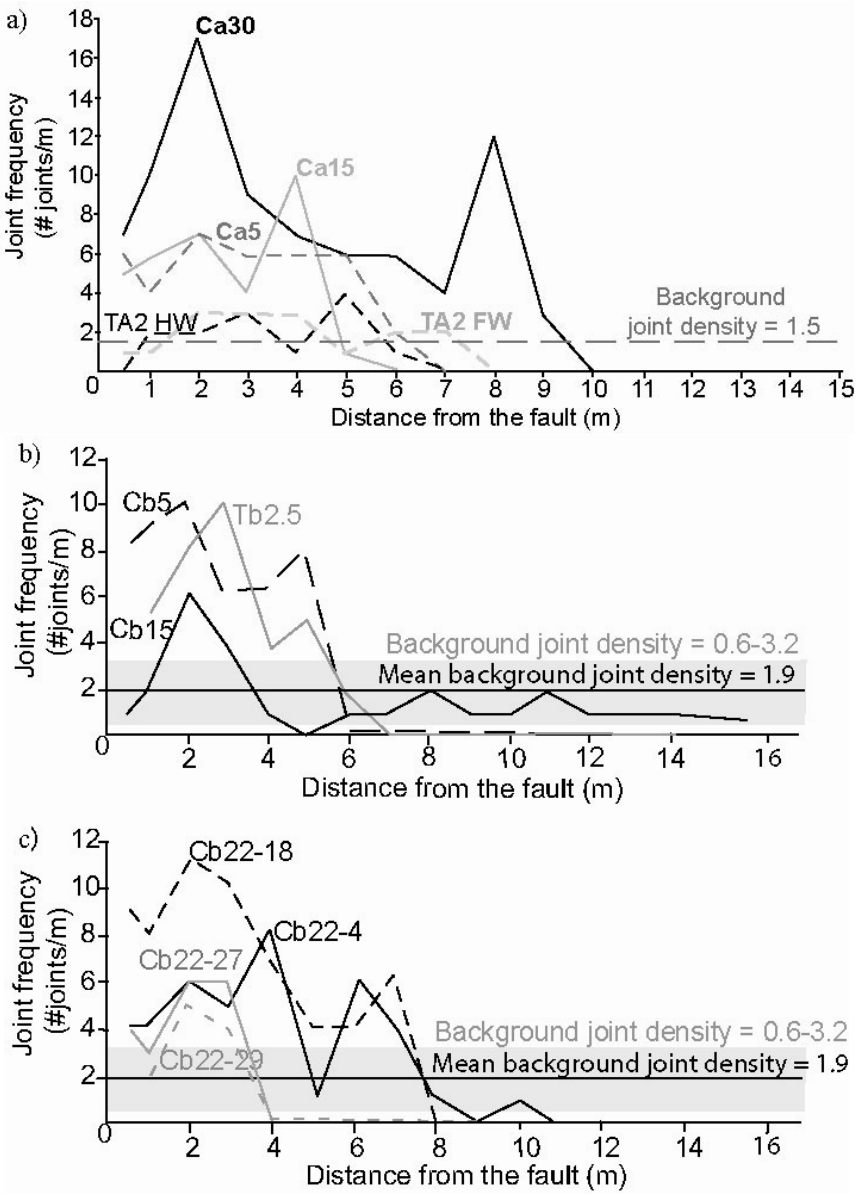

Figure 90: Line graphs of damage zone joint frequency

a) Joint frequency in adjacent to each of the faults in ignimbrite A. The TA2 fault has levels of jointing similar to unfaulted protolith (background joint frequency) b) Joint frequency adjacent to the Tb2.5, Cb5 and Cb15 faults. The Cb15 damage zone has the lowest number of joints; joint frequency is mainly below background levels. The Cb5 and Tb2.5 faults have similar damage zone joint frequencies and are also similar to Cb22-18 (c). The Cb22 fault exhibits a range of joint frequencies at different heights in the ignimbrite B unit despite having undergone the same amount of displacement.

Ca30 is the only fault in ignimbrite A that shows an increase in joint frequency approaching the fault wall (Figure 90a), but its peak is two meters away from the fault and then decreases towards the fault. The maximum number of joints in the ignimbrite B faults is at least 2 meters from the fault wall (Figure 90b & c). The Cb5 and Tb2.5 faults and the mid-section of ignimbrite B Cb22-18 all have a similar number of joints adjacent to the fault, while other faults have joint frequencies barely greater than background level (Figure 90c). If we examine the spacing between these joints (Figure 91) we see that the median damage zone joint spacing and range of spacing values is

relatively constant for the majority of faults in ignimbrite A and B, except TA2 and Cb15.

Faults having undergone different amounts of displacement have similar damage zone joint frequencies and spacing (Figure 90). This suggests that joint formation is not controlled by displacement but that the joints where formed by another deformation event prior to faulting. Furthermore the Cb22 fault shows an increase in median joint spacing from Cb22-18 to the top of the unit at Cb22-27 and Cb22-29 despite having undergone the same amount of displacement. This would indicate that a factor other than displacement is controlling joint spacing.

The occurrence of a fault next to high joint frequencies could imply that fault formation is more likely in areas of intensely jointed rock as the rock is less coherent and more prone to slip. The gap between the joint peak and the fault might suggest that a second peak existed where the fault has now formed. In CB22 the joint orientation is affected by fault tip propagation however it appears that joint formation is not. If joint formation was controlled by tip propagation then the frequency of joints would be the same along the length of the Cb22 fault, which is not the case.

a)

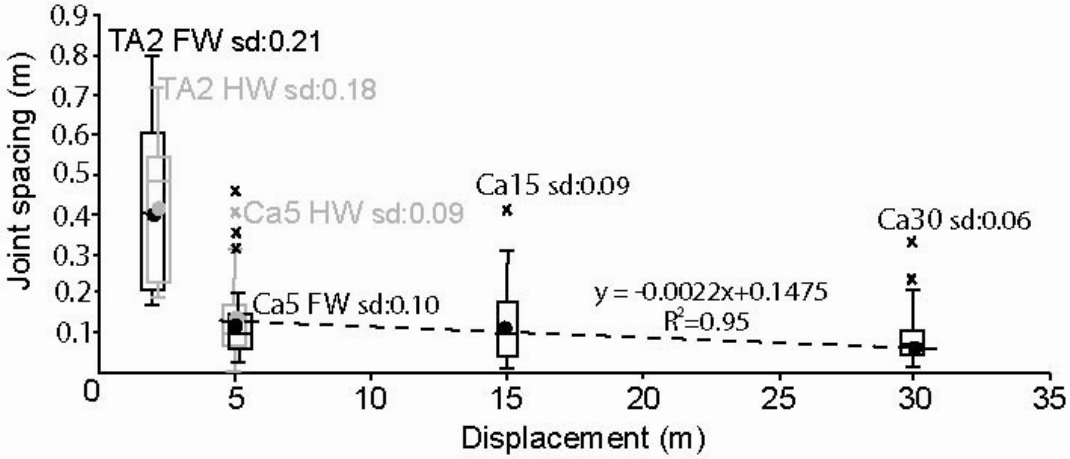

b)

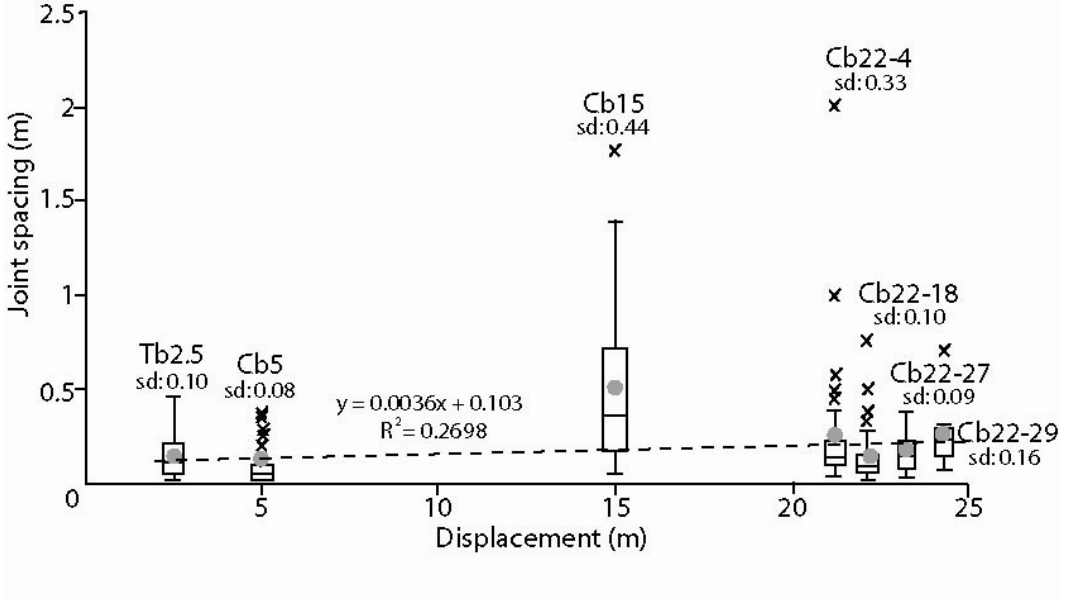

Figure 91: Damage zone joint spacing against displacement for a) ignimbrite A and b) ignimbrite B

Joint spacing remains approximately constant despite increasing displacement for the majority of the faults, as shown by the mean (black dots) and trend line for the Ca5, Ca15 and Ca30 joint data. Exceptions are TA2 and Cb15; TA2 has larger median and mean joint spacing and both have a greater range of joint spacing.

Ferril and Morris (2003) and Schopfer et al. (2006) describe how, as a fault propagates through a sequence of rock layers with different rheologies, the fault dip changes between layers, as the rock strength controls fault dip. The C5 and C15 fault walls have dips of ~90, the C5 and C15 faults don't change orientation passing from one unit to the next implying that either both units have the same strength or that the faults are faulted joints which, having formed in the same stress field would have the same orientation. The Ca30 and Cb22 fault walls have dips of ~70° most likely the result of interaction between remote tensile stress and local shear stress from the underlying propagating fault tip. Therefore the difference in orientation between the growth fault joints and the smaller fault joints indicates that the smaller faults did not propagate upwards and interfere with the remote tensile stress forming the joints. Instead the smaller faults formed later after joint formation in the ignimbrite A and B units.

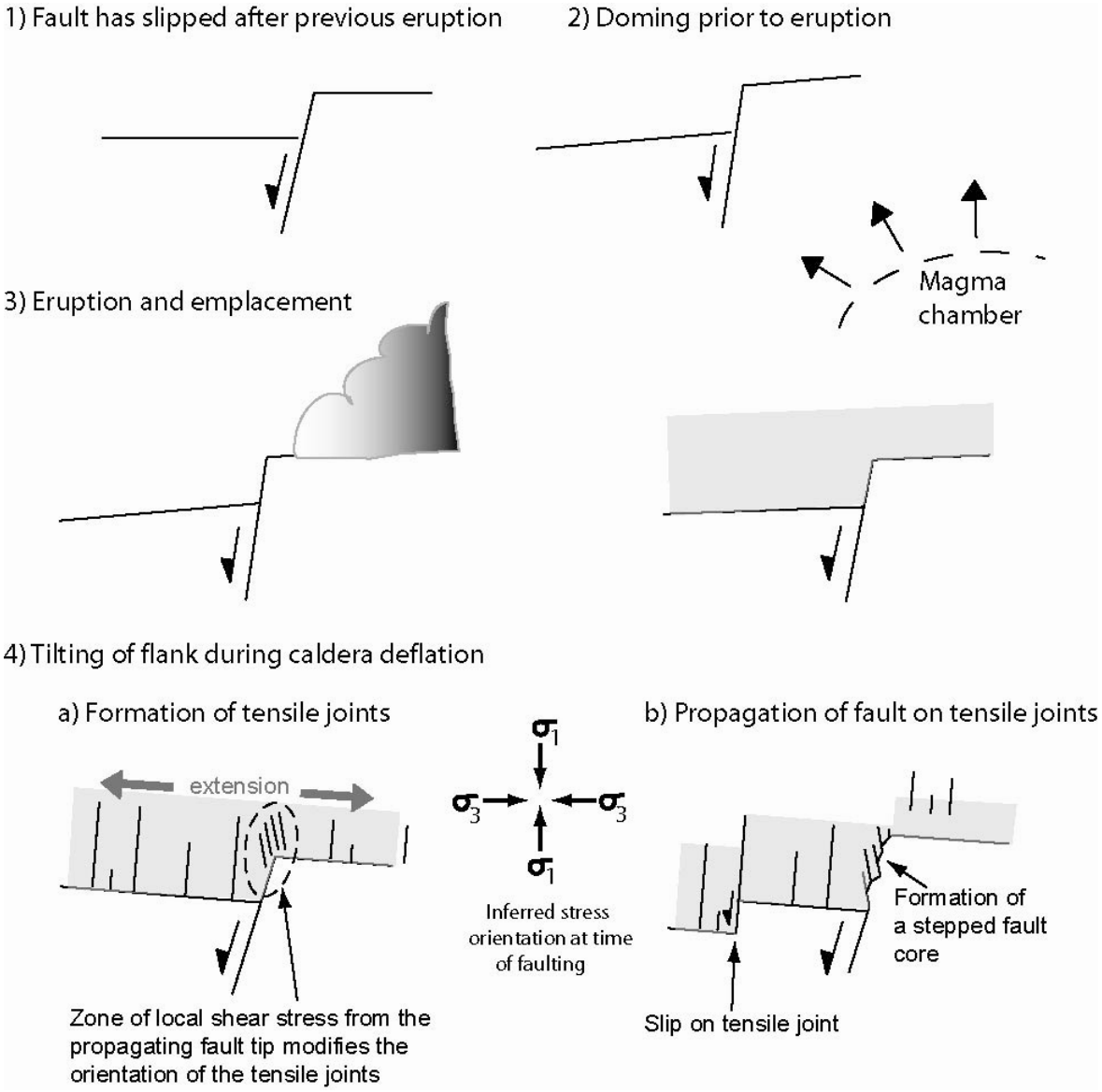

Figure 92: Evolution and growth of faults.

Prior to an eruption (fig. 2) doming causes the flanks of the caldera to be uplifted After ignimbrite eruption (fig. 3) the flanks of the caldera undergo extension (fig 4a). Extension occurs to accommodate the space created by evacuation of the magma chamber. As this process is occurring at the surface the maximum principal stress is inferred to be vertical (gravity) and the horizontal stress is tensile or near tensile due to the downsag of the layer into the evacuated chamber. The extension forms joints in the newly deposited and older underlying ignimbrite units and causes the existing growth fault to slip (fig. 4a). The propagation of the fault into the overlying unit creates an area of shear stress above the fault tip; the local shear stress interacts with the regional extension and alters the orientation of the joints immediately above the fault. The existing fault propagates upwards utilising the oblique joints (fig. 4b) resulting in the formation of a stepped fault wall. Dilation of the newly formed tensile joints causes slip to occur forming a faulted joint (fig. 4b). Displacement is accumulated on the faulted joint during subsequent events.

Fault core evolution

After fault initiation the evolution of the fault core in ignimbrite A and B diverges. In ignimbrite B the fault core expands by incorporation of material from joints. In ignimbrite A the fault core either has a constant fault core width and no expansion or has an erratic increase in width along its length. In both ignimbrites the deformation process causing fault core growth are controlled by the physical (fabric) and compositional characteristics of the host rock.

5.2.1.4 Fault core growth

Having examined fault core expansion in terms of increasing displacement and found a rather weak relationship I examined how fault core growth relates to the adjacent joint spacing.

Looking first at ignimbrite A, the median joint spacing decreases from TA2 to Ca5 (Figure 91), thus decreasing with increasing displacement. From this point on however there is no substantial change in joint spacing with displacement. The median fault core width is constant between TA2 and the Cedro Ca5 and Ca30 faults despite the different median joint spacing (Figure 93a). The fault core widths do not reflect the adjacent joint spacing, wide joint spacing does not correlate with wide fault cores. Instead the median fault core width is constant regardless of the adjacent joint spacing. The exception to this is Ca15; although it has the same joint spacing as Ca5 it has a greater median fault core width and larger spread in values (IQR) of fault core width.

a)

b)

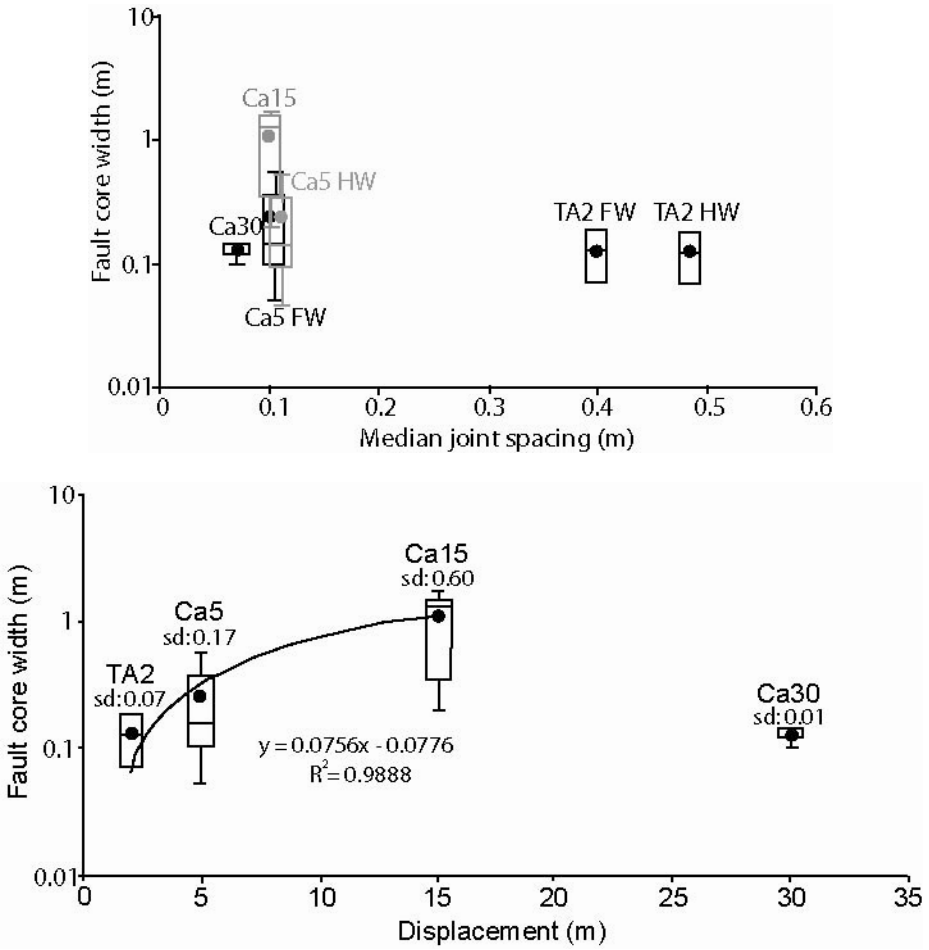

Figure 93: Ignimbrite A fault core width against joint spacing and displacement a) Fault core width against median joint spacing, fault core width does not correlate with joint spacing. Faults in the same rock type (Ca5, Ca30 and TA2) do have a similar range of fault core widths and the same mean fault core width (black dots) b) Fault core width increases with displacement from TA2 to Ca15 but the largest offset fault has one of the narrowest fault cores.

From this we can surmise that although the faults in ignimbrite A initiated on pre-existing joints their subsequent growth is not controlled by the joints. The fault cores in TA2, Ca5 and Ca30 can be considered as having the same constant width along dip, the Ca15 fault core width is greater and varies much more along dip (Figure 93). What differentiates the Ca15 fault from the other faults is that Ca15 cuts the A1 unit but the Ca5 and Ca30 cut the A3 unit. The ignimbrite material which the TA2 offsets is much the same as the A3 unit. The A3 unit is ash rich, has few fiamme and where these occur they are less than 0.5 cm in size (section 2.3.2). The A1 unit is fiamme and lithic rich, fiamme are larger than in A3 and the unit is far more heterogeneous than A3 (Table 16).

Ignimbrite A	Mean % porosity	Mean % pumice clasts (glass shards, fiamme, pumice clasts)	Mean % phenocrysts	Mean % lithics
A1 protolith	18	25.4	14.6	2.2
Ca15 DZ (A1)	N/A	34.1	18	6.5
Ca30 DZ (A3)	15.83	8.4	5.2	0.0

Table 16: Composition of ignimbrite A A1 flow unit

The A1 unit of which the Ca15 DZ is composed have a much larger proportion of fiamme, phenocrysts and lithics than the A3 unit. The A3 unit has a much more homogeneous composition with very few inclusions.

The constant thickness of the TA2, Ca5 and Ca30 fault cores suggests that the ash-rich material is friable and easily broken down by processes of wear and abrasion in the fault core. As a result most of the strain is accommodated within the fault core during slip and is not partitioned into the adjacent rock. With little friction acting on the fault walls there is no new material incorporated into the core and so the width of the fault core reaches a steady state.

The Ca15 fault damage zone has similar joint spacing to Ca5 and Ca30 but a wider fault core and greater range in fault core width. These observations suggest a stronger fault core material that is more resistant to abrasion. The strength of the fault core material partitions strain into the fault wall rock, fragmenting the wall rock and dragging new material into the fault core thus increasing its width.

The consistent fault core width in faults cutting ash-rich, fiamme poor material and the expansion of the fault core in different material indicates a strong petrophysical parameter controlling fault core growth.

		Median (m)	IQR	Lower extreme	Upper extreme
TA2	**FC width m (n=2)**	**0.125**	**0.11**	**0.07**	**0.18**
	FW Joint spacing m (n=16)	0.40	0.39	0.175	0.80
	HW Joint spacing m (n=13)	0.48	0.32	0.19	0.72
Ca5	**FC width m (n=7)**	**0.15**	**0.26**	**0.05**	**0.55**
	HW joint spacing m (n=37)	0.11	0.10	0.01	0.33
	FW joint spacing m (n=25)	0.10	0.08	0.03	0.2
Ca15	**FC width m (n=9)**	**1.3**	**1.15**	**0.2**	**1.7**
	Joint spacing m (n=33)	0.10	0.13	0.01	0.31
Ca30	**FC width m (n=7)**	**0.12**	**0.02**	**0.1**	**0.14**
	Joint spacing m (n=56)	0.07	0.06	0.02	0.2

Table 17: Values for Ignimbrite A fault core widths and damage zone joint spacing

Median fault core width values are approximately constant in all faults except Ca15 and the spread of fault core width values (IQR) is low despite the large differences in displacement. Joint spacing values are approximately constant in all damage zones except TA2. A direct correlation cannot be drawn between fault core width and displacement or fault core width and joint spacing.

Let us now look at the faults in ignimbrite B and their relationship to the adjacent joint spacing. The median joint spacing has a strong correlation with fault core width (Figure 94a). As joint spacing increases the fault core width also increases, neither correlates with increasing displacement (Figure 94b). The variation in fault core width along the Cb22 fault and the clear link with increasing median joint spacing is strong support for fault core growth by incorporation of joint bounded slabs. Areas with widely spaced joints form thick slabs that on incorporation allow greater expansion of the fault core than thin slabs or closely spaced joints. The one exception is Cb15 (Figure 94a); this may suggest that there is a critical joint spacing or upper limit to the width of slab that can be incorporated into the fault core. The dilation of the joint or fault core must be greater than the width of the slabs defined by the joints. Otherwise the slabs are too large to be rotated into the fault core, inhibiting the entrainment of material and further growth of the core.

a)

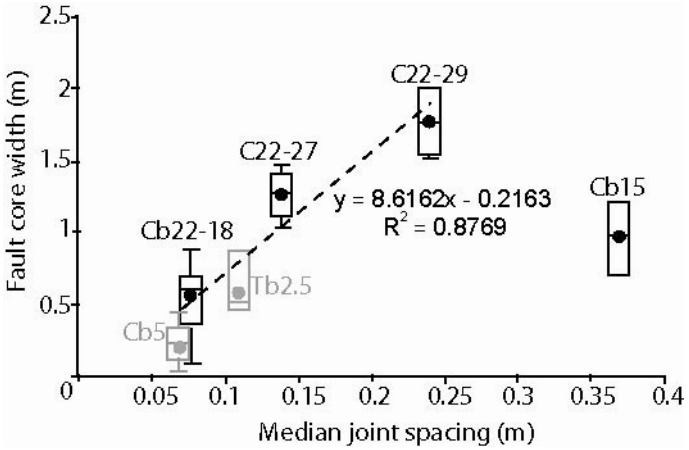

b)

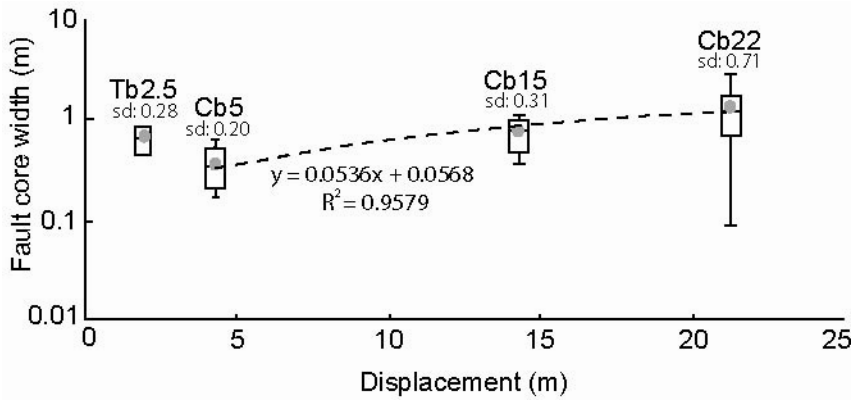

Figure 94: Ignimbrite B fault core width against joint spacing and displacement a) Fault core width against displacement, as median joint spacing increases fault core width increases. The exception is Cb15 which has the widest joint spacing but a fault core width similar to C22-27 and Tb2.5 b) Fault core width against displacement, There is a very weak correlation between increasing displacement and fault core width. Tb2.5 and Cb15 have the same median and mean fault core width despite the difference in displacement. The Cb22 fault core exhibits a range of widths that span those of the other three faults. Note fault core width is on a log scale. The grey and black dots are the mean value for each of the data populations

What then causes this variation in joint spacing if it is not displacement? The areas that have closely spaced joints also have abundant flattened fiamme. The Tb2.5 and Cb5 are located at the base of the ignimbrite B unit. At Tauro a strong foliation has developed and although the surface at Cedro is quite weathered the fiamme appear highly flattened. The mid-section of ignimbrite B at Cedro (Cb22-18) also contains a large proportion of flattened fiamme. The affects that this fabric has will be discussed in detail in chapter 6. But in brief the flattened fiamme overlap and form alternating layers with the ash forming centimetre thick sub-mechanical layers. These layers allow more closely spaced joints to form thereby forming thin slabs and narrow fault cores.

Not only do the joints control fault core growth in ignimbrite B they also influence the fault core morphology. Joints adjacent to all the ignimbrite B faults, except Cb22, parallel the fault walls i.e. the direction of slip. The joints have smooth, planar surfaces as do the faults. In Cb22 the joints in

the damage zone are slightly oblique to the slip surface and the fault walls are stepped not planar. These observations would support fault core growth by slab incorporation from joints. When a slab is incorporated into the core from a joint parallel to slip the joint surface becomes the fault wall, therefore the fault wall has a planar morphology. A slab incorporated from a joint oblique to the slip direction reveals a joint surface that is oblique to slip; therefore the fault wall is also oblique to slip and has a stepped morphology.

The correlation of joint spacing and orientation with fault core width and morphology strongly supports a joint controlled model of fault growth. The fault core is growing by plucking slabs from along joint surfaces and not by the abrasion or attrition of two opposing surfaces (Figure 95). Models of abrasion increasing fault core width with displacement would not result in the Cb22 fault core morphology nor would it account for the relationship between fault core width and joint spacing.

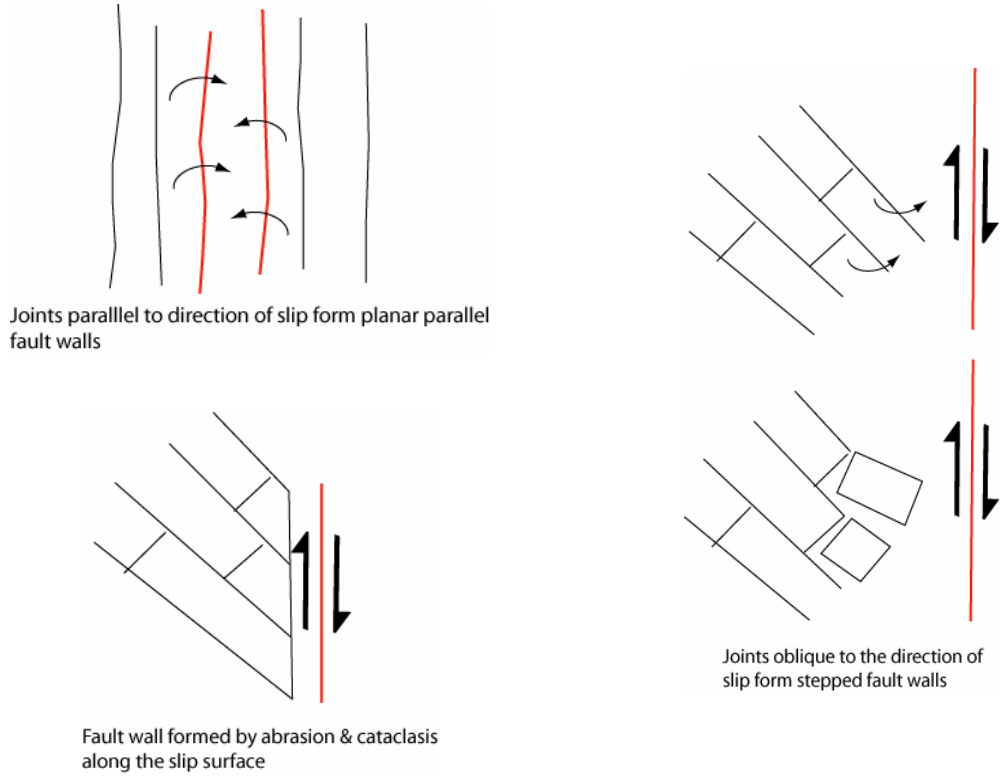

Figure 95:Influence of joint orientation on fault wall morphology
In fault zones that contain joints parallel to the direction of slip the fault walls have the same orientation as the joints, when joints are oblique to the direction of slip the fault walls are stepped. Indicating that the fault is growing by the incorporation of material from along the joints and not simply by the abrasion of material along a slip surface. This is a schematic representation of what happens in the fault core, in ignimbrite B this process has be observed and at the millimetre scale up to 10's of centimetres.

5.3 Summary

The joint linkage models of previous workers are not applicable in this case. The data presented here does not support linkage of joints via secondary wing cracks or pinnate joints and there is no indication of a stress rotation between formation of joints and faulting. The orientation and morphological evidence coupled with the hybrid failure angle of the faults, indicating dilatant faulting, implies that faults formed on pre-existing joints that underwent extensive dilation during caldera deflation causing the joint surfaces to slip past each other. The dilation of the joints is significant enough to allow slip to occur without the formation of cross joints or reorientation of the stress system. Large scale opening of joints is evident at Barranco de Tauro; the TA2 fault appears to be a single joint that underwent exceptional dilation allowing blocks of ignimbrite B to fall in from above and the units to slide past each other. The consistent relationship between joint and fault orientations to the caldera margin indicate the strong influence the regional scale caldera movement had on deformation.

Several criteria as identified by Wilkins et al., (2001) for distinguishing faulted joints from primary faults are found in these fault populations. The faulted joints belong to a larger set of parallel fractures that include pure opening-mode joints implying an opening-mode origin for all fractures. The damage zone joints geometric similarity to non-faulted bed-confined joints at Los Frailes and Barranco Tauro, their lack of conjugate pairs, and subperpendicular alignment with bedding.

In ignimbrite A fault core growth is controlled by the compositional characteristics of the host rock (ash, fiamme and lithic content, degree of welding or compaction of pumice clasts, porosity, vapour phase alteration and products of VPA e.g. cristobalite v tridymite). Units that are ash rich are friable and easily abraded in the fault core, focussing strain and inhibiting incorporation of new material. Those units that are more heterogeneous have a greater resistance in the fault core causing greater friction between the fault core material and fault wall, encouraging fault core growth. The width of the initial fault core is dictated by joint spacing as slip occurs on pre-existing joints but growth of the fault core is dictated by host rock petrology.

In ignimbrite B the fabric of the host rock controls joint spacing that in turn controls the expansion of the fault core. The morphology of the fault core is a result of joint orientation with respect to the direction of slip.

The physical and compositional characteristics of the ignimbrite host rock controls their mechanical behaviour, style of faulting and development of deformation elements in the fault zone. Fault growth is governed by many factors; amount of displacement is not the over-riding factor and in some cases the least important. All physical factors present in the environment at the time of

faulting should be considered in a single interlinked process that modifies fault architecture and fault zone characteristics through time. The physical factors influencing deformation in ignimbrites will be examined in greater detail the following chapter.

6

Influence of ignimbrite petrophysical properties

6.1 Introduction

As shown in the previous chapter the faults in this study initiate on pre-existing joints. Joint density, not displacement, is the controlling factor on fault core growth in ignimbrite B. What then controls joint density? In this chapter I firstly review some of the concepts of joint formation and controls on joint density in layered rock sequences. Followed by an examination of the host rock properties influencing joint formation in the ignimbrite units, such as high degrees of welding and rheomorphic flow producing eutaxitic textures, devitrification and vapour phase alteration forming secondary mineral phases which reduce porosity and strengthen the rock. By understanding how the ignimbrite fabric and composition controls the formation of deformation structures we can make predictions about fault zone architecture based on the petrophysical characteristics of any given ignimbrite.

6.2 Controls on joint density

6.2.1 Mechanical layer thickness

The frequency with which joints occur in any one locality is not constant but depends upon the physical properties of the rock layer and the surrounding layers, and is influenced by the degree of tectonic deformation (Hobbs, 1967). It has been proposed that the spacing between a given joint set is constant and proportional to the thickness of the layer in which the joints occur (Becker and Gross, 1996; Narr and Suppe, 1991; Price, 1966; Wu and Pollard, 1995), this relationship is true for both compressional and extensional regimes (Huang and Angelier, 1989). Previous observations of joint spacing and layer thickness have been based on layered sedimentary rocks.

The process of joint formation in layered rocks has been described as “sequential infilling” (Gross, 1993). A layer subject to a remote extensional strain will form joints when the strain exceeds the tensile strength of the layer. As the strain increases, more joints form between existing joints thus decreasing the joint spacing. This process continues until the joints are so closely spaced that no new joints form, the existing joints will continue to open to accommodate the extensional strain.

The point at which joint formation ceases is called joint saturation; a number of models have been proposed for this phenomenon and are presented below.

The spacing between joints at joint saturation has been defined as the critical segment length Lc, by Ji and Saruwatari (1998) and Jain et al. (2007) using the stress transfer model first proposed by Hobbs (1967). The model is based on a layered composite composed of two incompetent (non-jointing) layers bounding a competent (joint forming) layer, the competent layer has a higher Youngs modulus than the incompetent layer. The interfaces between the layers are assumed to be welded. The competent layer is assumed to already contain natural joints forming competent layer segments. As the segments are bound at either end by a free surface (joint surface) the extensional strain cannot be applied directly to the segment. The tensile stress in a joint bound segment is due to stress transfer from the non-jointed incompetent layers (Ji and Saruwatari, 1998). When the composite is placed under a uniform extensional strain, parallel to the layers, stress is transferred from the incompetent layers to the competent layer. The resultant tensile stress is higher in the competent layer than in the incompetent layers. When the tensile stress in the competent layer reaches the critical tensile strength of the material a new joint forms midway between the existing joints and the tensile stress goes to zero at this point. The joints do not propagate into the bounding incompetent layers because the competent layers fail at lower magnitudes of extensional strain (Ji and Saruwatari, 1998).

For a given strain the length of the competent segment controls the magnitude of maximum tensile stress in the centre of the segment (Jain et al., 2007; Ji and Saruwatari, 1998) Large segments achieve magnitudes of maximum tensile stress greater then the tensile strength of the competent layer material. Thus a large segment will break when placed under an extensional strain. As the segment length decreases the magnitude of maximum tensile stress in the segment decreases. When a segment gets to a certain length its maximum tensile stress is less than the tensile strength of the layer material and the segment will not break (Ji and Saruwatari, 1998). The critical segment length (Lc) is the shortest segment that can fracture; segments shorter than this can not achieve tensile stress in excess of the competent materials' tensile strength. Therefore the shortest possible segment length is Lc/2 (Ji and Saruwatari, 1998; Jain et al. 2007) and so is the closest possible joint spacing or joint saturation. At joint saturation no new joints can form so joint spacing remains constant regardless of increasing levels of extensional strain.

Another explanation for the lower limit of joint spacing is the stress shadow (Gross and Engelder, 1995; Pollard and Segall, 1987). In a layer undergoing extension the joint-normal stress at the joint surface is zero (in the absence of fluid pressure). This stress increases with increasing distance from the joint and eventually reaches the value of the far-field extensional strain. Within the area of reduced stress around the joint, new joints cannot form as the level of tensile stress is less than the

tensile strength of the rock. This stress shadow defines a minimum joint spacing for a given applied strain.

Bai and Pollard (2000) proposed an alternative model for joint saturation, in which there is a critical joint spacing (S) to layer thickness (T_f) ratio of 0.8 to 1.2. If the S/T_f falls below the critical value the normal stress acting perpendicular to the joints changes from tensile to compressive, this stress transition prevents the formation of new infilling joints. Hence for joint formation driven by layer parallel extension this critical joint spacing to layer thickness ratio defines joint saturation. However arguments have been made against the stress transition theory (Li and Yang, 2007). Bai and Pollard (2000) believed that it was from the centre point of the competent layer that a new joint would nucleate and thus the stress transition from tensile to compressive at this central position would prevent further joint formation. Li and Yang (2007) modelled the joint normal tensile stress parallel to the joints and found that the point of maximum normal-tensile stress is located at the interface between the competent and incompetent layers. The minimum tensile stress is found at the centre of the competent layer due to the free surface effect of the open fracture. They concluded that the most likely place for joint initiation is at the layer interface and that a change in stress from tensile to compressive at the centre of the competent layer is insignificant and will not affect joint saturation.

Sagy et al. (2001) observed dolomite layers in the Dead Sea basin area that where highly joint oversaturated. The joints had a 'tree like' or branching structure composed of a main joint with secondary joints branching from it, in a sub-parallel orientation. Using layered composites under an applied extension they investigated the development of these joints. At strain rates of ~$1x10^{-3}$ branching joints formed, at higher strain rates ($2x10^{-3}$ – $7x10^{-3}$) they observed the formation of clustering fractures; groups of branching joints that crosscut each other. From these experimental and field observations they suggested that the branching joint morphology and clustering fractures where a result of dynamic fracturing, and dynamic fracturing could be a mechanism for creating high fracture density. In my study joints are planar and the branching structures found by Sagy et al. (2001) are not observed, hence further discussion shall focus on studies concerning similar planar joints only.

In reporting the level of jointing in layered sedimentary rocks the fracture spacing ratio (FSR) is widely used. The FSR is the ratio of the fractured layer thickness (T_f) to the median fracture spacing of the layer (S). An FSR of 1.3 was observed in sedimentary rocks of the Monterey Formation, California by Narr and Suppe (1991), and was found to be constant in different rock types and in different structural locations over a large part of the Monterey formation area. The inverse of the FSR was used by Bai & Pollard (2000) as the focus of their models was on the relationship between joint spacing rather than joint density. They grouped the S/Tf ratios from many studies in the literature into four ranges shown in **Table 18**

Range	S/T_f	Layer is:
I	>1.2	Joint undersaturated, new joints will continue to form
II	$0.8 < S/T_f < 1.2$	Critical spacing to layer thickness ratio, joint spacing is at or near saturation level.
III	$0.3 < S/T_f < 0.8$	Joint oversaturated i.e. joints are closely spaced.
IV	< 0.3	

Table 18: S/Tf ratios from the literature divided into ranges, presented by (Bai and Pollard, 2000)

It is important to remember that these models are based on homogeneous, intact rock. In reality rocks are inhomogeneous; contain many flaws and inclusions that may act to magnify remote stresses. If the stress intensity of a flaw between the joints reaches the fracture toughness of the rock, the flaw will act as a site of joint initiation (Gross, 1993; Ji and Saruwatari, 1998). Bai and Pollard (2000) suggest that joint spacings in range III and IV are the result of joint initiation from flaws or crack growth driven by internal fluid pressure or overburden pressure. In the next section I briefly discuss how flaws and cavities influence joint initiation and joint spacing.

6.2.2 Flaws

It is generally accepted that joints initiate from flaws (Pollard and Aydin, 1988; Weinberger, 2001). The contrast in elastic properties between the flaw and the surrounding rock perturbs and magnifies the remote stress until the local tensile stress at the flaw exceeds the tensile strength of the rock (Fischer and Polansky, 2006; McConaughy and Engelder, 2001; Pollard and Aydin, 1988) making flaws preferred sites for joint initiation. The remote stress can be a tensile stress or a far-field compressive stress converted to a local tensile stress (Pollard and Aydin, 1988). The flaws can be a variety of features such as fossils, bedforms, trace fossils, concretions, intraclasts, soft-sediment deformation structures and cavities (Pollard and Aydin, 1988; Weinberger, 2001; McConaughy and

Engelder, 2001; Fischer and Polanksy, 2006).

The stress perturbation caused by a flaw depends on the size, shape, orientation and material properties of the flaw. As a result the tensile strength of a rock layer is spatially heterogeneous over scales greater than a few metres (Fischer and Polanksy, 2006). Various workers have produced models that test the dependence of joint initiation, joint spacing, spatial density and joint length on the initial distribution of flaws, flaw size and shape and material properties.

(Renshaw and Pollard, 1994) showed that the initial number of flaws in their model controlled the spatial density, length and average joint spacing. Fischer and Polansky (2006) examined the influence mode flaw size, flaw density, size range and size distribution skewness has on joint spacing and the rate at which joint saturation is reached. They found that low flaw densities led to lower FSRs or more widely spaced joints. Beds with a large range of flaw sizes approach joint saturation more slowly and so have fewer joints prior to saturation than beds with a narrow flaw size range. Skewness of the flaw size distribution also affected the rate at which joint saturation was reached and joint spacing.

Cavity driven joint initiation was investigated by Weinberger (2001). He examined the influence cavity geometry (size, shape and orientation) and distribution (isolation and location within the layer) had on joint nucleation. The preferred cavities for joint initiation were generally isolated, located close to the top of the layer and larger than those cavities not associated with joints. In the absence of cavities joints initiated from bedding interfaces. Joints initiating from bed interfaces were also observed by McConaughy and Engelder (2001) in a shale-siltstone sequence of the Ithaca formation, Appalachian Plateau. In these mechanically coupled beds the joint-tip stress generated by an existing joint in a siltstone bed is transmitted, across the shale bed, into the adjacent unjointed siltstone bed. The stress perturbation in the unjointed bed may increase the stress concentration of an existing flaw and result in joint formation. They also note that joints initiated in this way are offset from each other along strike and that a 1 cm thick shale layer prevents joint propagation between siltstone beds.

For flaws that are inclusions and not cavities the stiffness of the inclusion controls the magnification of the local tensile stress. The stiffness (k) is described by the ratio of the inclusions' elastic shear modulus (μ_1) to the elastic shear modulus (μ_2) of the rock mass. Stiff inclusions amplify the remote stress inside the inclusion by factors up to 1.5, while the stress surrounding the inclusion is diminished. In the case of cavities or pores the stress surrounding the cavity is amplified by a factor of 3.0 (Pollard and Aydin, 1988).

6.3 Influence of ignimbrite petrophysical properties

6.3.1 Mechanical layer thickness

In order to compare the level of jointing between the ignimbrite units with previous studies of joint levels in layered sedimentary rocks I have calculated the FRS and S/T_f for ignimbrite A, B and X. I have used the FSR of the Monterey Formation, California (Narr and Suppe, 1991) and the ranges of Bai and Pollard as a framework to compare the ignimbrite values with.

The results (Table 19 Table 20 Table 21) show that the units are highly oversaturated with respect to joint spacing and fall well below the lower limit for the lowest range, range IV. The model unit thickness is the range of layer thickness required to produce the expected ratios of 1.3 (Narr & Suppe, 1991), 0.8 and 1.2 (range II, Bai & Pollard, 2000) given the observed joint spacings. Quite obviously the actual ignimbrite units are much thicker than expected values, by two to three orders of magnitude, so what is responsible for the extreme joint oversaturation?

Ignimbrite A	S/T_f	FSR (T_f/S)	Median joint spacing cm (S)	Actual ignimbrite unit thickness cm (T_f)	Model unit thickness (cm)
TA2 HW	0.048	20.704	48.3	1000	40-62
TA2 FW	0.04	25	40	1000	33-52
Ca5 HW (A3)	0.037	27.273	11	300	9-14
Ca5 FW (A3)	0.035	28.846	10.4	300	8-13
Ca15 FW (A1)	0.009	110	10	1100	8-13
Ca30 HW (A3)	0.035	28.986	6.9	200	5-9

Table 19: S/T_f and FSR values for damage zone joints in ignimbrite A
S/T_f and FSR calculated using the observed joint spacings and actual ignimbrite unit thickness at Tauro and Cedro. S/Tf was not calculated for Los Frailes as the thickness of ignimbrite A at Los Frailes is not known

Ignimbrite B	S/T_f	FSR (T_f/S)	Median joint spacing cm (S)	Actual ignimbrite unit thickness cm (T_f)	Model unit thickness (cm)
Los Frailes	0.05	20	50	1000	41-65
Tb2.5 HW	0.013	80	37.5	3000	31-48
Tb2.5 FW	0.004	272.7	11	3000	9-14
Cb5 HW	0.003	400	7.5	3000	6-10
Cb15 HW	0.013	80	37.5	3000	31-48
Cb22-4	0.005	217.4	13.8	3000	11-18
Cb22-18	0.003	392.2	7.65	3000	6-10
Cb22-27	0.005	217.4	13.8	3000	11-18
Cb22-29	0.008	125	24	3000	20-31

Table 20: S/T_f and FSR values for damage zone joints in ignimbrite B

S/T_f and FSR for each of the units at Los Frailes, Tauro and Cedro. Model unit thickness is the unit thickness that would be necessary in order to obtain the expected ratios of 0.8 to 1.3 given the observed joint spacings

Ignimbrite X	S/T_f	FSR (T_f/S)	Median joint spacing cm (S)	Actual ignimbrite unit thickness cm (T_f)	Model unit thickness cm
Entire unit	0.011	87.53	45.7	4000	38-59
Flow unit	0.431	2.319	45.7	106	

Table 21: S/T_f and FSR values for damage zone joints in ignimbrite X

S/T_f and FSR calculated using the entire thickness of ignimbrite X and the thickness of the flow unit in which the joint spacings where observed. Model unit thickness is the unit thickness that would be necessary in order to obtain the expected ratios of 0.8 to 1.3 given the observed joint spacings.

Let us consider the ignimbrite B unit at Los Frailes as this is an unfaulted section and so the joints are the result of tensile stress and overburden compaction, not fault displacement. As discussed in section **2.3.3** the base of the unit is extremely foliated and joint density decreases moving up through the unit. Calculating the joint spacing ratios for these sections separately (Table 22) we see that the unit is still highly joint oversaturated but the base section is closer to predicted ratios and now lies in range IV of Bai and Pollards' classification.

Ignimbrite B Los Frailes	S/T_f	FSR (T_f/S)	Median joint spacing cm (S)	Actual ignimbrite unit thickness cm (T_f)	Model unit thickness cm
Meter thick base	0.221	4.525	22.1	100	18-28
Upper 9 m	0.099	10.056	89.5	900	74-116

Table 22: S/Tf for the basal portion of B
The base is joint oversaturated but is similar to values reported by previous workers

In the field it is evident that the decrease in joint density coincides with a change in the fabric of the unit (Figure 96a & b). The basal meter of the unit contains highly stretched fiamme and distinct centimetre thick layers formed by rheomorphic flow. As discussed in chapter 2, rheomorphic flow forms alternating sheets of stretched fiamme and ash and discolation surfaces. The remainder of unit is massive, fiamme are less abundant and less flattened.

a)

b)

c)

d)

Figure 96: Fiamme at the top and bottom of Ignimbrite B Los Frailes
a) Highly flattened and stretched fiamme in the base of ignimbrite B at Los Frailes. b) Fiamme are thicke and less abundant at the top of the unit (8m above the base). White outline is a 25cm2 used to sampl fiamme. c) Closely spaced joints cutting the base of Los Frailes. d) Foliations in the base of B at Tauro short joints cut these centimetre thick layers.

To quantify the change in fabric moving up through the unit I sampled the fiamme population at the base, mid-section and top of the unit using 25 cm^2 drawn on the rock face (Figure 96). Using the image software package 'Image J', I obtained the maximum and minimum axes, aspect ratio, area and perimeter for each of the fiamme within the sample area (Table 23). A linear regression analysis was performed on the data using height in the unit as the independent variable. The results (Table 24) showed that only two of the parameters were significant – minimum fiamme axis and aspect ratio were significant to a level of confidence >99.9%.

Los Frailes Ignimbrite B	Fiamme perimeter	Major axis	Minor axis	Aspect ratio	# fiamme per 25cm^2
Base	4.58	1.83	0.21	9.95	290
1 m	3.96	1.27	0.22	4.79	495
3 m	5.08	1.61	0.26	5.58	487
8 m	6.67	2.19	0.39	4.97	309

Table 23: Mean values of fiamme size, shape and abundance from Fiamme were measured using 25 cm^2 at increasing heights in the unit.

Name	Coeff	StErr	p-value	SS
y (height)	5.346	0.259	0	272.496
ln (min axis)	0.690	0.092	0	78.336
ln (aspect ratio)	-1.914	0.138	0	131.494
df: 304	RSq: 0.501	**s:** 0.829	**RSS:** 208.93	

Table 24: Ignimbrite B fiamme regression analysis

Results of the regression analysis of the fiamme population moving up through the ignimbrite B unit at Los Frailes.

The regression equation is:

$$\ln(y) = 5.346 + 0.69\ln(\text{min axis}) - 1.914\ln(\text{aspect ratio}) + e$$

Moving up through the unit the minimum axis increases and the aspect ratio decreases thus fiamme are getting thicker and are less flattened (Figure 97). At the base of the unit the fiamme are thin and highly stretched forming sub-mechanical layers of alternating fiamme and ash within the larger unit (Figure 98). Fiamme become thicker and less oblate moving upwards in the unit and the sub-mechanical layers are absent. Thus the centimetre thick sub-layers allow closely spaced joints to form thereby increasing joint density at the base of the unit (Figure 96), the absence of sub-mechanical layers in the upper portions of the unit means that the joint spacing reflects the greater thickness of the entire ignimbrite unit.

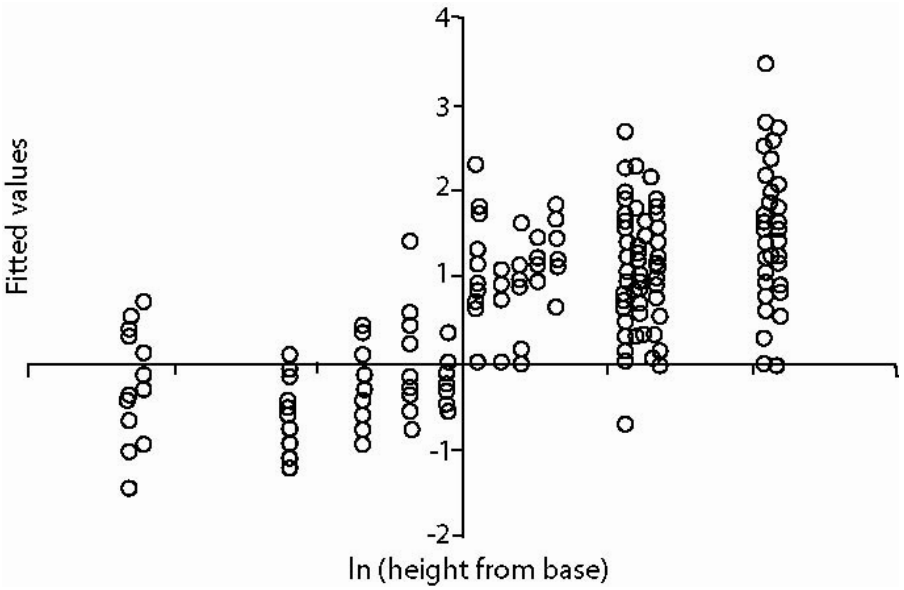

Figure 97: Graph of fiamme minimum axis and aspect ratio using the regression equation for Los Frailes.

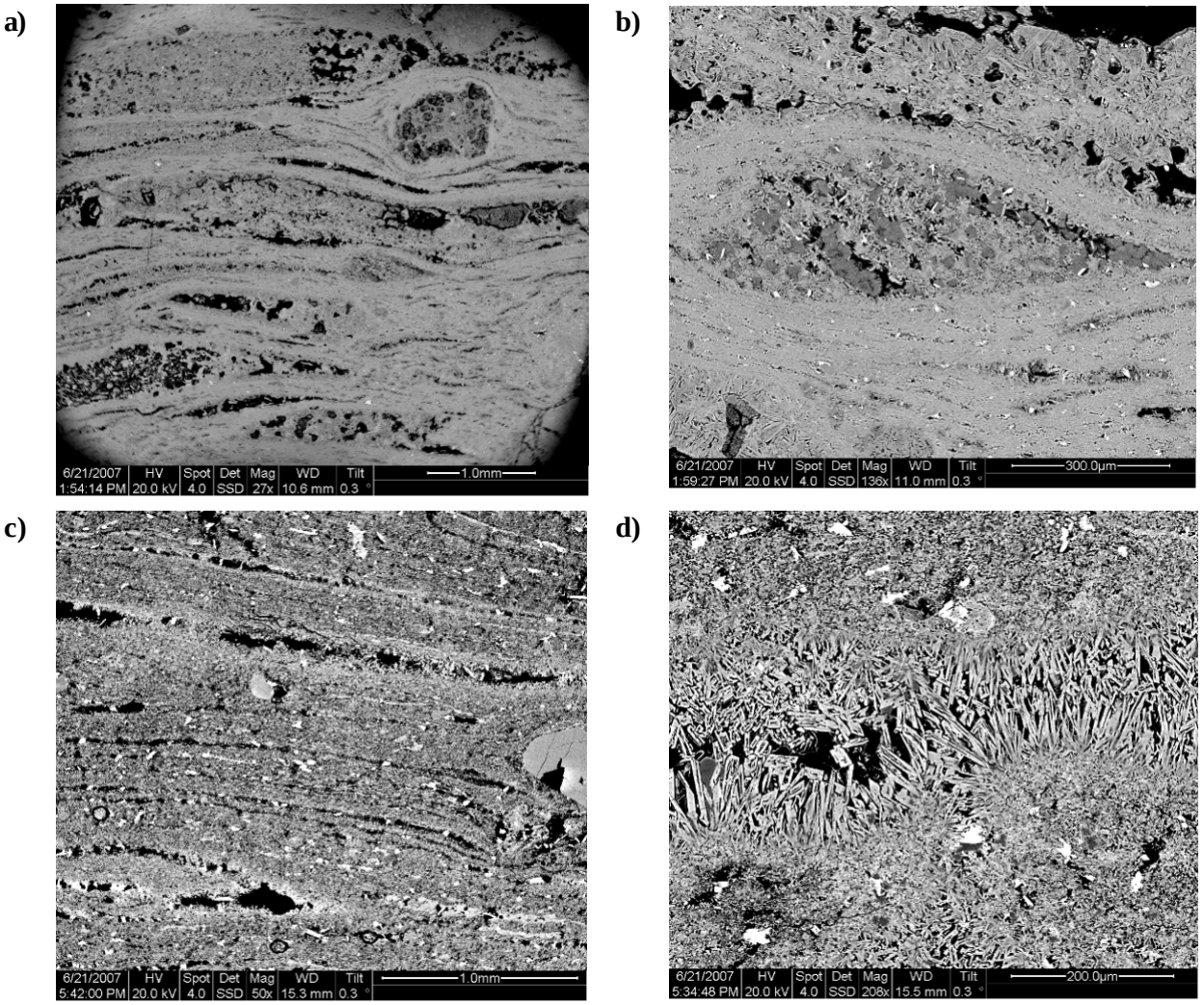

Figure 98: SEM images of ignimbrite B Los Frailes
a & b) Fiamme 6 m above the base of ignimbrite B at Los Frailes. c & d) fiamme from the base of the unit. Fiamme in the base are much more flattened and stretched than those in the top of the unit. The rheology of the fiamme and the ash matrix is very different. At the micron scale the fiamme are composed of coarse acicular crystals and spherulites (c & d), the matrix is composed of a meshwork of short crystals (d).

In the field I measured the thickness of these foliations and the spacing of the joints that cut them (Figure 96d). The S/Tf and FSR for the foliations show that at this scale they are actually joint undersaturated (Table 25). Therefore the flattened fiamme and ash are acting as distinct mechanical layers. The fiamme and ash are emplaced as the one mass and fused together, however the contrast in mechanical properties between them defines a mechanical layer boundary (Figure 98d). The presence of sub-layers in the base of the unit increases the overall joint density and gives the impression that the ignimbrite B unit is highly joint saturated (Figure 99).

Ignimbrite B Tauro foliations	S/T_f	FSR (T_f/S)	Median joint spacing cm (S)	Actual foliation thickness cm (T_f)	Model unit thickness cm
	1.45	0.69	4.05	2.8	3.4 - 5.2
	1.59	0.63	4.05	2.55	3.4 – 5.2
	1.65	0.6	4.05	2.45	3.4 – 5.2
	1.64	0.61	0.9	0.55	0.7 – 1.2
	1.43	0.7	1.5	1.05	1.2 – 2
	1.17	0.86	1.4	1.2	1.2 – 1.8
	2.14	0.47	3.85	1.8	3.2 – 5.0
	0.91	1.1	1.45	1.6	1.2 – 1.9
	1.36	0.74	1.7	1.25	1.4 – 2.2
	1.25	0.8	2	1.6	1.7 – 2.6
	0.3	3.37	4.1	13.8	3.4 – 5.3
Los Frailes base	1.75	0.57	1.4	0.8	1.2 – 1.8
	0.89	1.12	7.85	8.8	6.5 – 10.2

Table 25: Layers are undersaturated, joints are more widely spaced then expected.

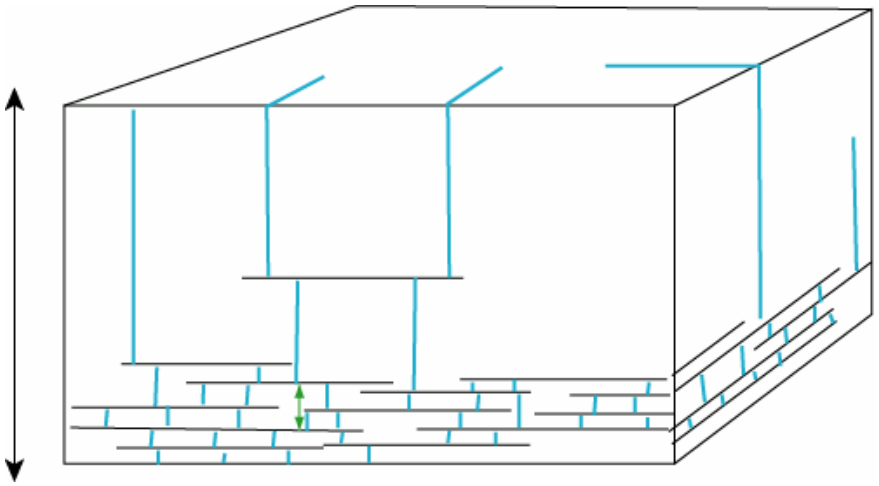

Figure 99: Influence of sub-mechanical layers on joint spacing

Using joint spacing measured from all joints in the unit, the S/Tf ratio is composed of the closely spaced joints formed by the sub-mechanical layers and the widely spaced joints influenced by the entire unit thickness. S/Tf = S(Ti + Ts)/Ti Entire unit thickness (Ti, black arrow), Sub-layer thickness (Ts, green arrow)

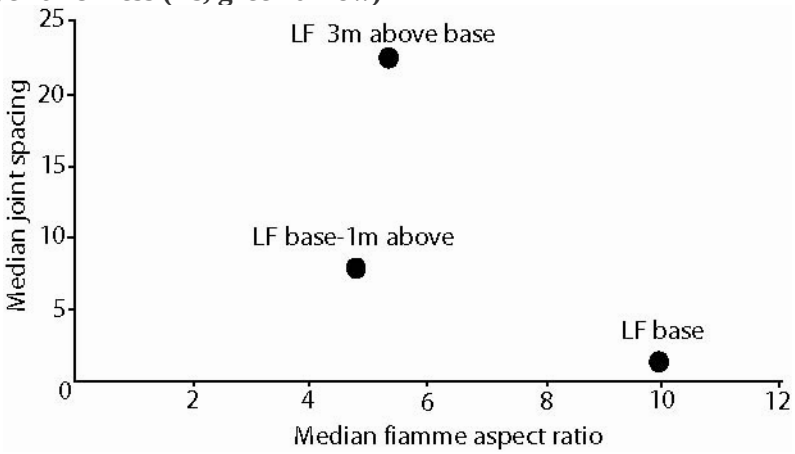

Figure 100: Los Frailes fiamme aspect ratio v joint spacing

The median aspect ratios of fiamme at different heights above the base of the unit are plotted against the median joint spacing at that height. As the fiamme become less flattened moving upwards from the unit base the spacing between joints increases. This suggests that the flattened fiamme are forming sub-mechanical layers within the unit promoting joint formation.

A similar relationship between joint saturation and fiamme shape is seen in ignimbrite B at Cedro. Moving upwards from C22-18 to C22-27 there is a decrease in the major and minor axes and perimeter of the fiamme (Table 26). The mean aspect ratio also decreases, although in the regression analysis this was not found to be to a significant level (Table 27).

Cedro ignimbrite B	Fiamme perimeter	Major axis	Minor axis	Aspect ratio	# fiamme per 25cm^2
18 m	5.02	1.55	0.42	3.25	116
27 m	1.9	0.63	0.2	2.63	173

Table 26: Fiamme dimensions, ignimbrite B Cedro

Fiamme are smaller and more rounded at the top of the unit. Those in the mid-section are much longer and stretched.

Name	Coeff	StErr	p-value	SS
y (height)	2.208	0.229	0	
ln (major axis)	-0.646	0.140	0	0.323
Ln (perimeter)	0.603	0.159	0	1.400
ln (min axis)	-0.209	0.063	0	0.266
df: 124	**RSq:** 0.394	**s:** 0.157	**RSS:** 3.058	

Table 27: Results of the regression analysis of fiamme in ignimbrite B at Cedro.

The regression equation is:

$$\ln(y) = 2.21 - 0.646 \ln(\text{major}) + 0.603 \ln(\text{perimeter}) - 0.210 \ln(\text{minor})$$

The statistical relationship here is weaker as fewer sample squares were obtained due to inaccessible terrain and poor weathered exposure. However, field observation also shows that the fiamme are becoming smaller moving towards the top of the unit (Figure 101b). This is not surprising as during the waning stages of the eruption the eruption energy decreases, thus the size of fragments carried in the pyroclastic flow also decreases.

a) **b)**

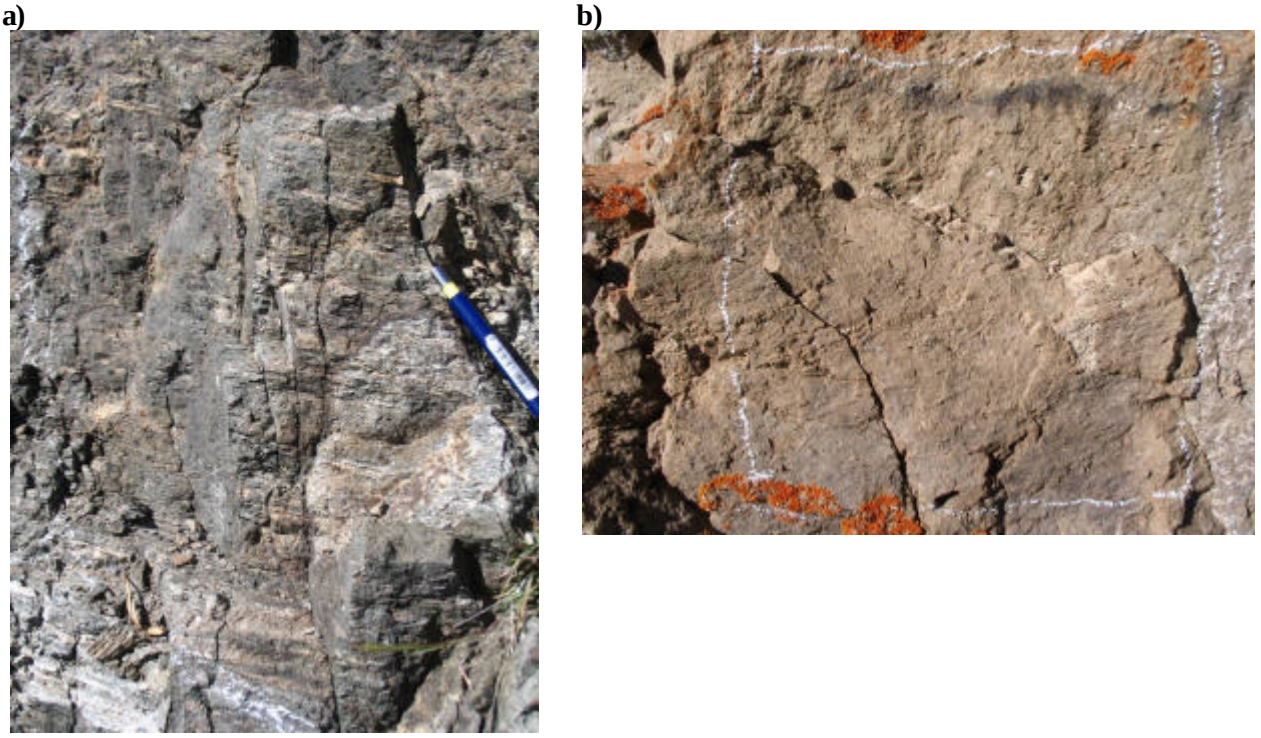

Figure 101: Fiamme in ignimbrite B Cedro

a) Mid-section of ignimbrite B, the stripy appearance of the rock is from the flattened fiamme. b The top of the unit has smaller fiamme that are more rounded and do not overlap, hence do no form layers of fiamme and ash (Chalk square is 25 cm x 25 cm).

The presence of sub-layers is responsible for the changes in joint saturation level in ignimbrite B. However, in the upper portions of unit where the sub-layers are poorly developed the unit is still greatly joint oversaturated, although the fiamme are not as flattened they occur in large numbers. The occurrence of fiamme containing fine fractures that do not extend into the surrounding ash (Figure 102) is evidence that the fiamme are the sites of joint initiation. Either because of their higher Youngs modulus compared to the ash matrix or the presence of cavities at the centre of some devitrified fiamme (Figure 98). Therefore the more fiamme the greater the number of joint initiation sites.

Figure 102: Fractures cutting fiamme,
Some of the fractures exit the fiamme above and below others terminate at the fiamme ash interface suggesting that the fractures initiated in the fiamme.

6.3.2 Influence of flaws

Ignimbrite A is moderately welded, fiamme are slightly oblate but not stretched or flattened to the extent of those in ignimbrite B and consequently ignimbrite A is completely unfoliated. For these reasons I am going to use data from ignimbrite A to talk about the influence of flaws as it factors out sub-mechanical layers. In ignimbrite A a correlation can be made between levels of joint saturation and unit composition. The S/Tf ratios for TA2, Ca5 and Ca30 are ~0.04; the S/Tf for Ca15 is considerably less at 0.009 despite the A1 unit being 1 m and 8 m thicker than Tauro and A3 respectively. As discussed in section 2.3.2 the top of ignimbrite A at Tauro in which TA2 occurs and the A3 unit at Cedro cut by Ca5 and Ca30 have a similar composition. In both locations the material is moderately welded, fine grained with small fiamme. The A1 unit, in which Ca15 occurs, is coarser grained and contains larger fiamme and more phenocrysts. The same process of sampling 25cm2 areas of fiamme was carried out in the A1 and A3 units at Cedro the results are shown in Table **28**.

	Fiamme perimeter	**Major axis**	**Minor axis**	**Aspect ratio**	**# fiamme per 25cm^2**	**S/T$_f$**	**FSR**
A1	2.08	0.68	0.28	2.58	396	0.009	110
A3	1.02	0.37	0.14	2.73	293	0.04	27-29

Table 28: Fiamme dimensions for two sample squares in A1 and one sample square in A3.

Fiamme in the A1 unit have larger major and minor axes and are more abundant than fiamme in the A3 unit. This suggests that the high joint density in A1 is due to the greater number and larger fiamme acting as sites of joint initiation (Figure 103). A1 also contains a greater percentage of lithics which would also increase the number of joint initiation points (Table 29 and Figure 104). This would agree with the modelling done by Fischer & Polansky (2006), where high flaw densities produced large FSRs.

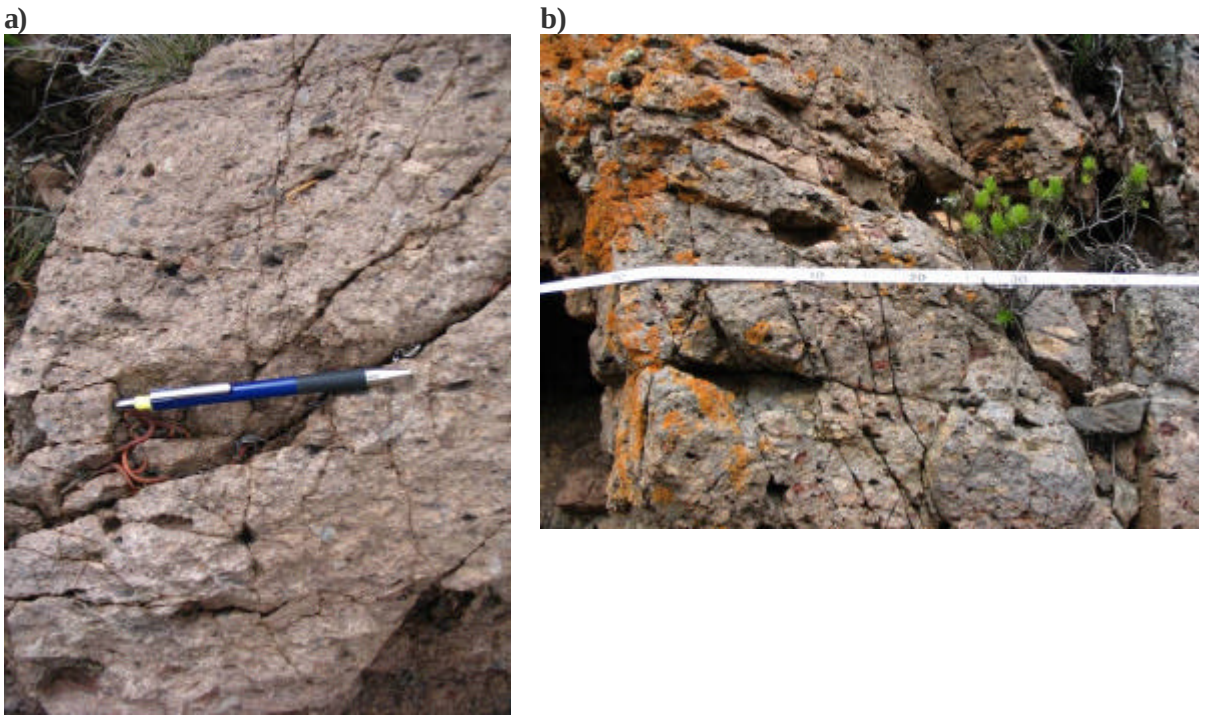

Figure 103: Joints in the A3 sub-unit of ignimbrite A at Cedro.
The fiamme act as sites of joint initiation with many joints radiating out from a single fiamme (a). The abundance of joint initiation sites in the form of fiamme decreases joint spacing levels in the unit (b).

The mechanical property contrast in ignimbrite A, as well as ignimbrite B, is a result of the processes of vapour-phase alteration and devitrification. It seems probable that in an unaltered ignimbrite the contrast between fine ash particle and the extremely fine grained glass that makes up the pumice and fiamme would be quite minor. However, altered fiamme and pumice are composed of large acicular crystals and spherulites (Figure 98b & d), the altered ash matrix is a meshwork of fine micron size crystals (Figure 105a & b). The alteration processes also dissolves portions of the fiamme and pumice creating pore space. As Pollard and Aydin (1998) noted remote stress is amplified by stiff inclusions by a factor of 1.5 and by a factor of 3.0 by pore space.

	Mean % porosity	Mean % pumice clasts (glass shards, fiamme, pumice clasts)	Mean % phenocrysts	Mean % lithics
A1	18	25.4	14.6	2.2
A3	15.83	8.4	5.2	0.0

Table 29:Percentage porosity, pumice, phenocrysts and lithic content was **Percentage was** estimated **using a light microscope**

The A1 unit has a slightly greater porosity but the major difference is in the percentage of fiamme, pumice fragments and phenocrysts. Evidently these are acting as initiation points and are the cause of the higher joint density in A1 compared to A3.

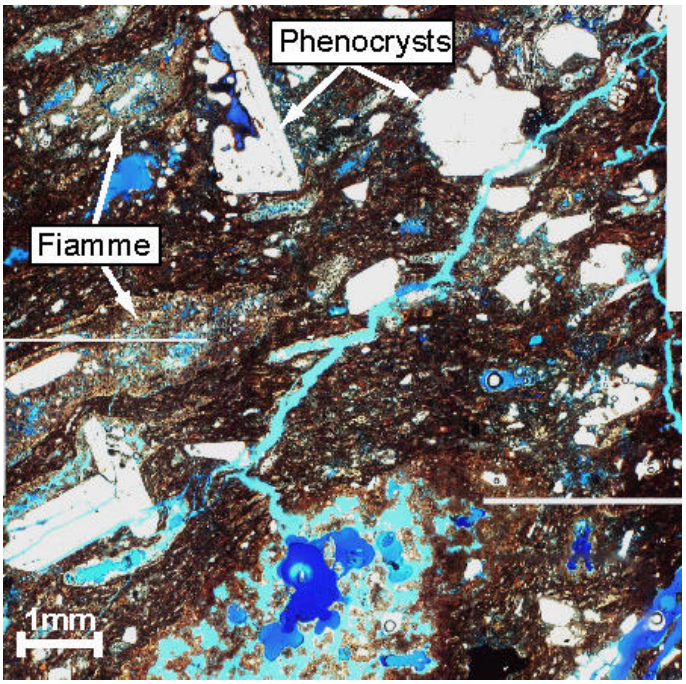

Figure 104: Thin section image of ignimbrite A subunit A1

A1 contains abundant phenocrysts fragments and altered fiamme. The holes in the fiamme will act as joint initiation points (IPs), the mechanical contrast between the phenocrysts and surrounding fine matrix will perturb the stress field and magnify the remote stress thus acting as IPs

a)

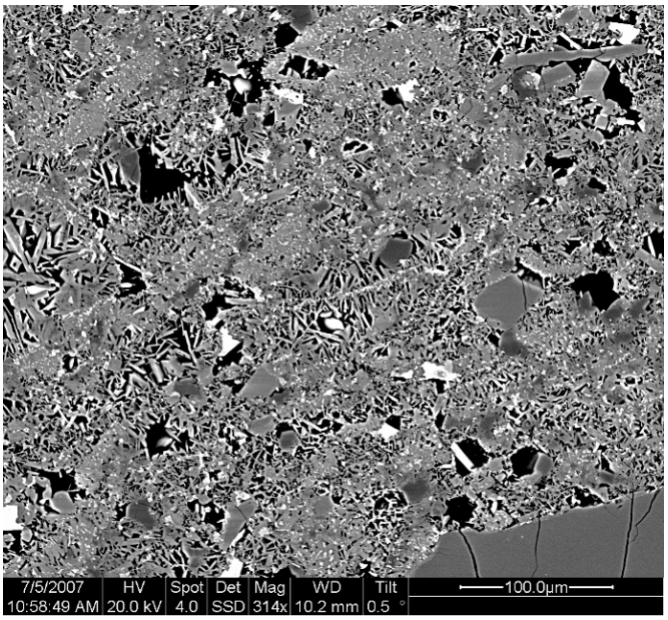

b)

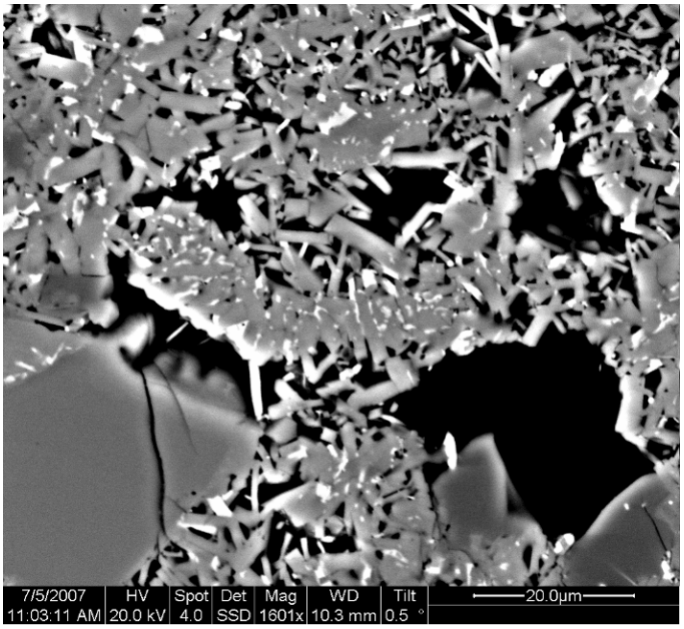

Figure 105: SEM images of ignimbrite A
a) ash matrix of ignimbrite A and b) close up of the matrix. The matrix is composed of micron sized crystals and is quite porous, the pore spaces may act as sites of joint intiation.

The S/Tf ratio for the entire thickness of the ignimbrite X unit is highly oversaturated (0.011), for the individual flow unit this is much lower (0.431) and falls within range III of Bai & Pollards divisions (**Table 18**). The actual flow unit thickness is still greater than that predicted by the model indicating again that a factor other than mechanical layer thickness is controlling joint formation. Ignimbrite X is relatively homogeneous, composed of millimetre size crystals and occasional fiamme that retain a glassy texture. A number of reasons may explain the high joint density in ignimbrite X. The abundant phenocrysts in the ash matrix may be acting to amplify stress and are thus sites of joint initiation (Figure 106a). The matrix is also quite porous being composed of a meshwork of fine acicular crystals (Figure 106b); again this would amplify remote stress. The contrast in mechanical properties between the fiamme and the crystal matrix may be responsible for

the greater levels of joint saturation (Figure 106c). The fabric and components of ignimbrite A, B and X control joint initiation and thus joint density. These elements also have an influence on joint morphology and fault core clast shape.

a)

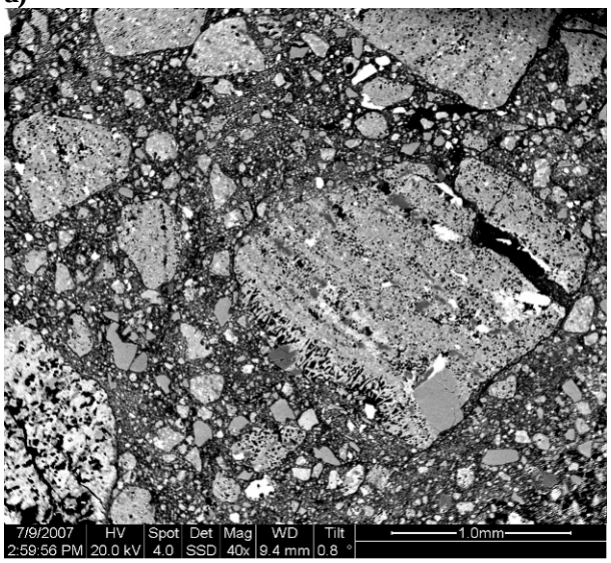

b)

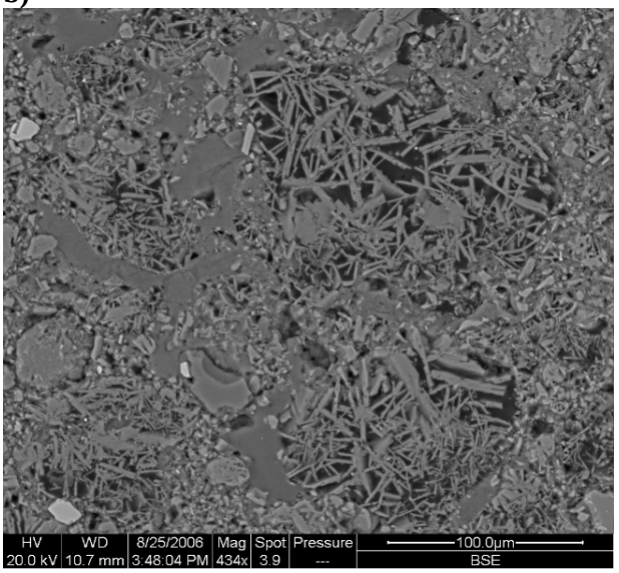

c)

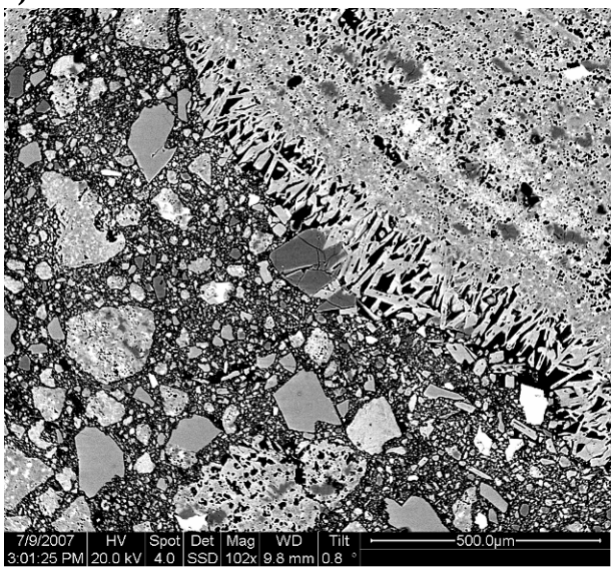

Figure 106:SEM images of ignimbrite X, Cedro a) Ignimbrite X is composed of micron size phenocrysts and millimetre size clasts of ignimbrite b) The matrix itself is a meshwork of acicular crystals with open interstices. c) The contrast in mechanical properties between the clasts/fiamme and the fine matrix may act to concentrate stress at the interface between the clast/fiamme and matrix

6.3.3 Joint morphology

Although the majority of joints seen are relatively planar there are some, particularly in the unfaulted sections, that have a stepped morphology. The joint morphology is altered where joints cut fiamme or meet clasts (Figure 107). As joints pass through fiamme they can be offset along horizontal sections of varying length. The vertical sections of the joint generally intersect the fiamme close to the fiamme endpoints.

a)

b)

c)

Figure 107: Joint morphology, ignimbrite B a) The joint runs along the clast matrix interface and follows the curvature of the clast. Joints also run along flattened fiamme in ignimbrite B (b & c). The fiamme offset the joints creating a stepped morphology.

The degree of flattening of the fiamme influences the extent to which the joint morphology is affected. Figure 108 shows circular to flattened fiamme in ignimbrite A. In highly flattened fiamme vertical joints become offset along horizontal sections (Figure 108a). When fiamme are slightly oblate the joints intersect the ends of the long axis of the fiamme, the area of maximum curvature (Figure 108b). Joints radiate out in all directions from circular fiamme (Figure 108c). Pollard and

Aydin (1988) state that the "local tensile stress is greatest where the radius of curvature is smallest". Therefore when fiamme are flattened or oblate the tensile stress is greatest around the ends of the fiamme. Joints initiate from these sites or preferentially propagate towards this area of greatest tensile stress. The offset of the joint along the fiamme may be due to both ends of the fiamme being in a high tensile stress state and the joint propagating along the path of least resistance. For circular fiamme, as the radius of curvature is the same at any point, the tensile stress would be evenly distributed around the fiamme; thus any point on the fiamme circumference could be a point of joint initiation resulting in a radial joint pattern.

a)

b)

c)

Figure 108: Fiamme-joint interactions a) Flattened fiamme offset joints b) semi-round fiamme and joints link the ends of fiamme (point of greatest curvature) c) Joints radiate outwards from circular fiamme.

As flattened fiamme are most abundant in ignimbrite B the stepped joint morphology is most prevalent in that unit. This fabric also has repercussions for clast shape within the ignimbrite B fault cores.

6.3.4 Clast morphology

As discussed in chapter 5 the fabric in ignimbrite B controls joint spacing, joint spacing also appears to influence clast size in the fault core. Furthermore the consistent dimensions of the clasts in the ignimbrite B fault core indicate that the rock fabric controls clast shape. In chapter 4 I showed that clast size is not related to displacement. So as I have done with the other fault zone components I have compared clast size to joint spacing.

As material entrained into the core is from joint bound slabs it seems likely that the clast size will reflect the thickness of the slabs; particularly in small offset faults where there has been less displacement and thus less abrasion of the fault core material. Figure 109 shows that as the median damage zone joint spacing increases the median clast size in the adjacent fault core increases slightly, except for Cb15. In Cb15 the joints adjacent to the fault core are widely spaced but it has the smallest median clast size and the smallest range of clast size. The Tb2.5 fault has a median joint spacing similar to the other Cedro faults but the largest median clast size and the greatest range in clast size values, possibly due to the fact that the core material has under gone less displacement and abrasion.

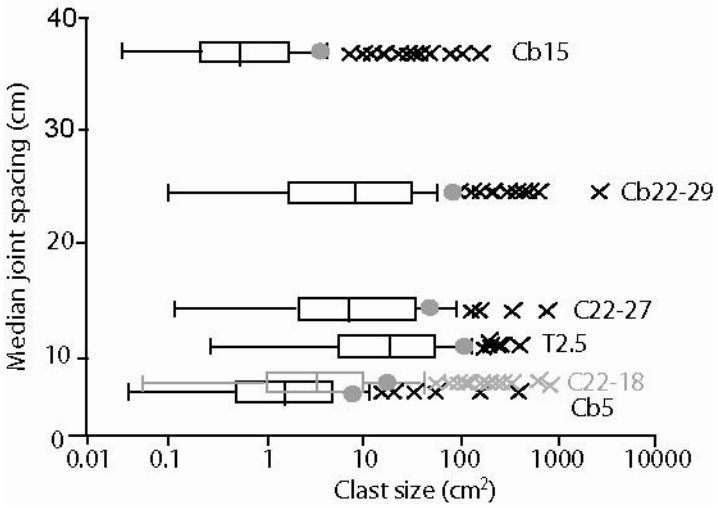

Figure 109: Ignimbrite B fault core clast size vs. median joint spacing
As joint spacing increases there is an increase in median and mean (grey dot) clast size and range of clast sizes, except in Cb15.

		Median	IQR	Lower extreme	Upper extreme
Tb2.5	**Clast size (cm^2) n=96**	**15**	**40.68**	**0.25**	**106.39**
	joint spacing (cm) n=33	11	16.5	2	45
Cb5	**Clast size (cm^2) n=80**	**1.46**	**4.56**	**0.04**	**11.95**
	joint spacing (cm) n=47	7.5	6.2	1	20
Cb15	**Clast size (cm^2) n=278**	**0.63**	**1.79**	**0.04**	**4.72**
	Joint spacing (cm) n=24	37.5	54.35	5.25	140
Cb22-18	**Clast size (cm^2) n=242**	**3.16**	**16.21**	**0.06**	**41.51**
	Joint spacing (cm) n=59	7.65	9.3	1.25	27.3
Cb22-27	**Clast size (cm^2) n=40**	**6.14**	**29.27**	**0.1**	**76.1**
	Joint spacing (cm) n=19	13.8	14.55	3.2	37
Cb22-29	**Clast size (cm^2) n=160**	**8.69**	**30.57**	**0.1**	**78.24**
	Joint spacing (cm) n=11	24	13.4	7.5	31

Table 30: Ignimbrite B joint spacing and fault core clast size
Similar joint spacing gives rise to a variety of clast sizes e.g. Cb5 and Cb22-18, Tb2.5 and Cb22-27.

The clast size was calculated by multiplying the maximum and minimum clast axes to get the 2-dimensional surface area of the clast. However if the mechanism of fault core growth by slab incorporation is correct then only one of the clast axis (slab width) will be controlled by joint spacing. Figure 110 shows that as the mean joint spacing increases the mean clast axes of the clasts increases. The Tb2.5 and Cb22-27 fault have the same mean joint spacing and clast axes.

Fault core material in the lowest offset faults will have undergone less displacement and therefore less abrasion in the fault core. Therefore the clasts in these faults (Tb2.5 and Cb5) will most closely mirror the original slab dimensions from which they formed. This is supported by the joint spacing and clast size IQR values. The Tb2.5 fault has a wide range of joint spacings and an equivalently wide range of clast sizes, the opposite is true for the Cb5 joint spacing and clast size IQR. In Cb22 the range of clast size and the upper extreme increases moving up the fault core. Indicating that abrasion of the material during 22 metres of displacement has reduced clast size increasing the

small clast size fraction; but new material is also being incorporated into the fault core. This new material was incorporated from slabs adjacent to the core and therefore reflects the wide joint spacing.

The exception to this is Cb15; with the widest joint spacing we would expect it to have the largest clast sizes. However, as with fault core width there appears to be a critical joint spacing that inhibits entrainment of material into the core. If the slab width is greater than fault core width the slab will not be rotated into the fault core. If this is the case the clasts in the core were present from initial fault formation. The continual abrasion of these clasts with no new material being entrained would account for the uniformity (small IQR) of clast sizes in the Cb15 fault core.

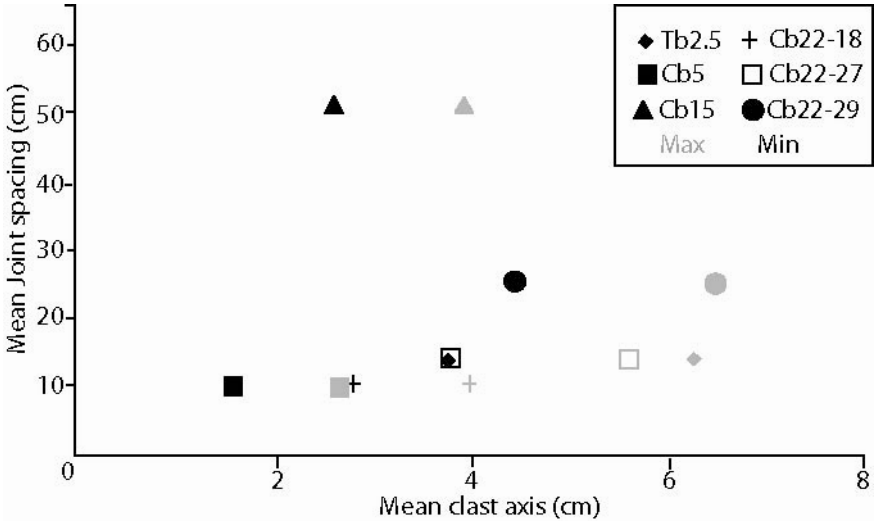

Figure 110: Ignimbrite B fault core clast axis vs. mean joint spacing

There is a correlation between mean minimum (black) and maximum (grey) clast axes and increasing joint spacing. Again the CB15 fault is the outlier to this relationship

If the host rock fabric is controlling joint spacing it will continue to do so when the clasts are fracturing in the fault core. The ratio of maximum to minimum clast axis is quite consistent between the different faults (Figure 110). If the sub-mechanical layers control joint spacing then the ratio of maximum to minimum axis will be constant. Even the poorly developed layering in the upper portions of the unit is enough to control joint spacing and influence clast dimensions. Furthermore as shown in chapter 4 clast aspect ratio becomes more uniform with increasing slip, tending toward a 1.5 aspect ratio (Table 31) suggesting that as clasts are broken down in the fault core they fracture in a regular repeating pattern controlled by the host rock fabric (Figure 111).

	Tb2.5	Cb5	Cb15	Cb22-18	Cb22-27	Cb22-29
Mean Clast aspect ratio	1.67	1.71	1.51	1.42	1.47	1.46

Table 31: Ignimbrite B fault core clast aspect ratio
The clast aspect ratio moves towards 1.5-1.45 with increasing displacement

Figure 111: Fracturing of ignimbrite B fault core clasts, in Cb22 fault
The foliation fabric in the rock controls joint spacing even in fault core clasts. Joint are approximately evenly spaced, thus as the clast breaks down it forms clasts with similar dimensions, white arrows indicate joint spacing. (scale is a 15 cm ruler).

In ignimbrite A median joint spacing values at Cedro range from 6 cm to 11 cm; a similar range to the ignimbrite B damage zones. However, the clast sizes and range of clast sizes is much smaller in the A faults (Table 32). There is a correlation between joint spacing and clast size (Figure 112). The Ca5 and Ca15 faults have similar values for joint spacing and clast size. The Ca15 clast size values are slightly greater, so there is not a linear decrease in clast size with increasing

displacement. More closely spaced joints adjacent to the Ca30 fault core correlate with smaller clast size and a narrower IQR, Ca30 has also accumulated the most displacement.

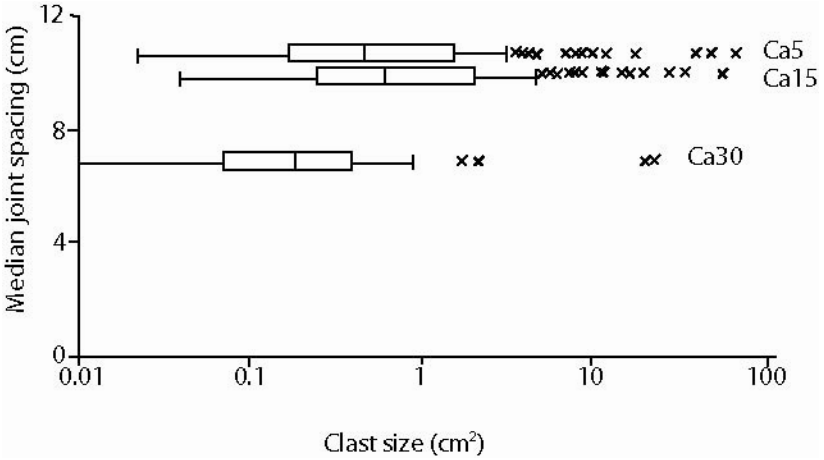

Figure 112: Ignimbrite A fault core clast size vs. median joint spacing
Median clast size decreases with increasing displacement from Ca5 to Ca30, but Ca15 has a slightly higher median and a greater range of clast sizes in its fault core. Note clast size is on a log scale

		Median	IQR	Lower extreme	Upper extreme
Ca5	**Clast size (cm^2) n=80**	**0.46**	**1.322**	**0.02**	**3.24**
	HW joint spacing (cm) n=37	11	10	1.1	33
	FW joint spacing (cm) n=25	10.4	8.37	3.1	20
Ca15	**Clast size (cm^2) n=281**	**0.63**	**1.79**	**0.04**	**4.63**
	Joint spacing (m) n=33	10	13.5	1	31
Ca30	**Clast size (cm^2) n=88**	**0.18**	**0.38**	**0.01**	**0.9**
	Joint spacing (m) n=56	6.92	6.5	1.7	19.9

Table 32: Ignimbrite A fault core clast size and joint spacing
Clast size does not decrease linearly with increasing displacement. The joint spacing in the adjacent damage zones again is constant but the clast size in the fault core varies. Therefore joint spacing is not influencing the clast size

I have shown in section 5 that the fault core width in Ca5 and Ca30 is constant and no new material is being incorporated in to the fault core. The difference in clast sizes and IQR between ignimbrite B and A for the same joint spacings would support this. If clasts where being incorporated from joint bound slabs in A then the fault core should contain larger clasts and there would be a greater variability in clast size range, particularly in Ca5 which has accumulated the least amount of displcaement. The decrease in clast size with increasing slip is as would be expected, as continued abrasion during displacement reduces clast size.

In the Ca15 fault core the clast size median, IQR and upper extreme are the largest of the three faults although joint spacing is similar to Ca5. Suggesting that either new material is being incorporated into the fault core thereby generating a greater range of clast size or the material in the core is not abraded as easily. As established in section 0 the variation in width of the Ca15 fault core suggests new material is being entrained into the core as a result of the strength of the fault core material; the clast size data would support this argument. Again the petrophysical characteristics of the units (A1 and A3) influence the style of deformation and the evolution of the fault core.

Despite similar joint spacing between the ignimbrite B and A damage zones the fault core clasts are not alike. Indicating that the generation of fault core material is quite different in each unit. In ignimbrite B the size and dimensions of the clasts are influenced by joint spacing which in turn is controlled by the host rock fabric. Joint bound slabs are incorporated into the fault core and clast size is a function of joint spacing. Variations in clast size populations are a result of variations in joint spacing.

In ignimbrite A incorporation of material into the fault core is limited. Only Ca15 seems to have entrained new material from the fault walls. The fault core in Ca5 and Ca30 is dominated by abrasion of material present from initial fault formation and the lack of new material being incorporated into the fault. The absence of sub-mechanical layers and the more friable nature of ignimbrite A are responsible for the different deformation processes and evolution of the fault core.

6.4 Summary

Ignimbrites are extremely heterogeneous; they vary in fiamme, lithic and phenocryst content, degree of welding, porosity which can be altered by degree of welding, devitrification and vapour phase crystallisation. Secondary alteration also modifies the mechanical properties of the material and intense welding can form layered fabrics. Ignimbrite units are not uniform in their structure, they can be composed of individual flow units (ignimbrite X and A) or mechanically different sub-units that grade without a distinct break into one another within the overall larger unit (ignimbrite B). Joint spacing and morphology, clast size and shape are controlled by the host rock properties

formed by ignimbrite depositional processes. As a result predictions of joint spacing based on layer thickness should be used with caution and take into account the structural and compositional heterogeneity of ignimbrites.

7

Discussion

Previous investigations of ignimbrite fault architecture have examined faults cutting ignimbrites at Yucca Mountain, Nevada (Gray et al., 2005), the Pajarito Plateau, New Mexico (Wilson et al. 2003) and the Bishop Tuff, California (Evans and Bradbury, 2004). The work carried out by Wilson et al. (2003) and Evans and Bradbury (2004) focussed on the affects of ignimbrite petrophysical properties on fault architecture but did not examine the evolution of fault architecture with increasing displacement. Gray et al. (2005) describe three fault types which they interpret as being part of an evolutionary sequence and another style of fault architecture considered to represent hybrid faulting. In the following sections I present an overview of this work and compare the results to my own study. I then compare my model of fault initiation and fault evolution to models developed for other lithologies e.g. sandstone, granite.

7.1 Comparison of fault growth models and architecture

In the model I have developed for the faults in Gran Canaria the small scale faults initiate on existing joints. The joints were formed during post-eruption caldera deflation. As the chamber beneath the caldera is evacuated the chamber roof sags causing an extension of the caldera flanks and joint formation (Branney, 1995). Continued subsidence and relaxation of the flanks forms faults concentric to the caldera margin (Walter and Troll, 2001). The field data presented in previous chapters shows the consistent correlation between joint and fault orientation, suggesting that the faults formed on the pre-cursory joints. The faulted joints may be a single joint or two joints bounding a pillar of rock which is subsequently broken down to form the fault core material.

After initial displacement the growth of the fault and the evolution of the fault architecture are dependent on the host rock lithology. In ignimbrite B the fault core grows by the incorporation of joint bounded slabs. In the coarse grained, fiamme and lithic rich subunit of ignimbrite A (A1) the fault core grows by incorporating material from the fault walls. The fault core in the more friable ashy subunits (A2 and A3) does not continue to grow after formation but accommodates displacement by the continued abrasion of the fault core material present from initial fault formation.

The damage zone joint frequency observed in ignimbrites A and B does not correlate with displacement; large displacement faults have the same joint frequency as faults with quarter the displacement. These observations suggest that displacement does not result in an increase of deformation adjacent to the faults but that the level of joint intensity observed existed prior to faulting. Displacement may have occurred preferentially in these areas of intense jointing due to the weaker nature of the rock.

Gray et al. (2005) examined faults in the Topopah Spring Tuff (Tpt), Yucca Mountain, Nevada; the host horizon for the proposed high-level nuclear repository. The Topopah Spring Tuff consists of two members; a crystal-rich member and a crystal-poor member. These members are further subdivided into non-welded, moderately welded and densely welded subzones. It is planned to locate the repository in the moderately to densely welded units of the Tuff. In their study Gray et al. (2005) identified four classes of fault zone architecture. Three of these classes they suggested represented a continuum of increasing displacement; the fourth they interpreted as having undergone significant dilation during faulting.

The first of the three linked fault classes consists of discrete slickensided fractures upon which the faults initiated. They have minimal displacement, fault cores not greater than 1 cm wide and little or no damage zone (<2cm wide). Continued displacement (cms to 10s meters) formed well developed brecciated fault cores (10s cm to 1 m thick) that contain poorly cohesive, unfoliated cataclasite. The damage zones are intensely fractured and 1 to 10 m wide. At large displacement magnitudes (10 m to 100s m of displacement) the fault core is composed of cohesive foliated gouge at or near the centre surrounded by poorly cohesive breccia. The damage zones are wide (10s of metres) and well developed. The sequence of deformation processes interpreted by Gray et al. (2005) that link these three fault architectures are initial displacement accommodated by brittle fracturing and cataclasis in the narrow fault core. Further displacement causes strain hardening in the fault core and widening of the fault core. Strain hardening in a fault core is caused by a change in the rheology of the fault rocks (Wojtal and Mitra, 1986); deformation produces fault core material that inhibits further slip in the fault core and so any subsequent displacements causes fracturing of the adjacent host rock and widening of the fault (Wojital and Mitra, 1986). Subsequent displacement of Gray et al. (2005) first class of faults promotes alteration of the volcanic material to smectite and translocation and recrystallisation of clays in part of the fault core, which weaken the fault core and localises the deformation to a narrow zone of foliated gouge at the centre of the core. With increasing displacement the deformation processes intensify the deformation within the fault core and damage zone and increase the width of the fault zone.

The fourth class of fault architecture identified by Gray et al. (2005) consisted of faults that had < 1 m of displacement. The faults have a well developed fault core (2 – 30 cm thick) and either a

poorly developed damage zone a few centimetres wide or no damage zone at all. The boundaries between the core and the damage zone are discrete and slickensided. The fault cores are 2 cm to 30 cm thick and core thickness varies along strike and up and down dip. The core contains rectangular shaped clasts and >65% matrix that is highly mineralised. The clasts are relatively intact and have an undisturbed eutaxitic foliation indicating little progressive cataclasis of the clasts after entrainment into the core. The planar boundaries of the clasts are at right angles to the foliation, which Gray et al. (2005) suggest indicates fault initiation by closely spaced fracturing subparallel to the fault zone boundary. The faults are highly dilational and mineralised and have steep dips (70 – 90°) which the authors suggest may indicate hybrid failure. Hybrid failure is observed at shallow depths and low differential stress, the setting where this fault class has been observed at Yucca Mountain (Gray et al., 2005).

The fault growth sequence and resultant fault architectures described by Gray et al. (2005) have similarities with the fault populations observed in ignimbrite A. At low displacements (17cm) the fault core is narrow and there is no increase in damage adjacent to the fault. With increasing slip the fault core widens and contains unfoliated, non-cohesive breccia and gouge (TA35 and ignimbrite A Cedro faults). At large displacements the fault cores described by Gray et al. (2005) have a foliated central zone and surrounding breccia. This is not the case with the large displacement fault in ignimbrite A. The Ca30 fault core contains small clasts orientated randomly within a fine grained gouge. Similarities between the fault architectures in the two locations may indicate that they share similar modes of growth. In both studies the faults initiate on joints, subsequent brecciation and cataclasis widens the fault cores. At this point the fault evolution in ignimbrite A follows two separate paths, elements of which are observed in the Gray et al. (2005) model. Strain hardening occurs in the ignimbrite A-A1 subunit inhibiting slip in the fault core and promoting the incorporation of material from the fault walls, hence widening the fault core. The Ca30 fault core has not grown which suggests that displacement was accommodated in the fault core material. Whether smectite is present within the fault core has not been investigated in this study. However the Ca30 fault core gouge is not foliated suggesting that deformation was accommodated throughout the fault core material and not localised along bands of material as was the case in the fault set at Yucca Mountain.

The fault architecture of the fourth class of fault described by Gray et al. (2005) is very similar to faults in the densely welded ignimbrite B; the variation in fault core width along dip, the rectangular clasts in a fine gouge matrix and clast boundaries at right angles to the foliation. The similarities suggest that this fault class and those in ignimbrite B grew by the same mechanism, which is one of hybrid failure causing dilation of the fault core and incorporation of material from joints subparallel to the fault core.

The similarities between the fault architectures in both studies suggest that the moderately and densely welded ignimbrites of Yucca Mountain are deforming by the same mechanism as those in Gran Canaria. Therefore my model of fault evolution might provide a more detailed understanding of fault growth at Yucca Mountain and the factors influencing fault growth such as host rock fabric; as well as being useful in predicting fault architectural elements such as fault core width.

As discussed in chapter 1 the most widely accepted model of fault initiation is the joint linkage model based on shear faults (Crider and Peacock, 2004). Faults initiate by shear on existing structures such as en echelon joints or veins. Shearing of joints forms wing cracks and/or cross-joints allowing joint linkage which results in an increase of fault length and displacement (Martel, 1990; Segall and Pollard, 1983) and the formation of a through-going fault zone. Subsequent fault growth is accommodated by attrition and abrasion of the slip surface generating gouge. Asperity grinding or tip line bifurcation removs material from the slip surfaces, forming breccia and smoothing the fault walls (Chapter 1). In my model the faults do not develop via joint linkage but by dilation of the joints that allows joint surfaces to move past each other. The consequences of this failure mechanism for fault architecture are discussed in section 7.3.

A second model of fault initiation and growth has been developed for high porosity material such as sandstones or poorly welded ignimbrites. In this model a single deformation band forms by cataclasis which reduces pore size and fractures sand grains; the shear displacement on the band is a few mm's to cm's (Aydin and Johnson, 1978). The next stage sees the formation of a zone of deformation bands which becomes progressively thicker as the zone accommodates more strain and forms new deformation bands. The displacement is equal to the sum of displacements on each of the deformation bands. Finally, through-going slip surface forms on the margin of a well developed deformation band zone accommodating metre scale displacements (Aydin and Johnson, 1978). In this study deformation bands have been observed in the ash-rich friable units (Ignimbrite A, sub-unit A2 section 3.2), however they are not the main focus of this study but shall be referred to in subsequent sections in relation to their influence on fluid flow.

7.2 Effect of host rock on fault growth and architecture

In the previous chapters I have shown how the host rock fabric and composition of the host rock controls fault growth, fault core morphology, joint frequency and morphology. In this section I summarise the petrophysical host rock properties that control deformation in ignimbrite B and A. Followed by an overview of work carried out by Evans and Bradbury (2004) and Wilson et al (2003) on the affects of ignimbrite properties on deformation processes in moderately and poorly welded ignimbrites and a comparison of my observations with theirs. Finally I compare the influences on ignimbrite deformation with those in other lithologies e.g. sandstone, granite and

limestone.

In ignimbrite B joint spacing is controlled by sub-mechanical layers of flattened fiamme and ash within the larger ignimbrite unit. The mechanism of fault core growth in ignimbrite B is via the incorporation of joint-delineated slabs; the spacing of joints controls the slab width and thus widening of the fault core. Where sub-mechanical layers are present the joints are closely spaced, the delineated slabs are narrow and the fault core is thin. In the absence of sub-mechanical layers the joint spacing is controlled by the greater thickness of the ignimbrite unit. The more widely spaced joints delineate thick slabs that result in wide fault cores. The removal of slabs from the joint surfaces means that the joint surface becomes the fault wall, therefore joint morphology and orientation will control the morphology of the fault wall. When the joints are parallel to the direction of slip, the removal of slabs creates vertical planar fault walls. In the case of the propagating growth fault C22B at Cedro the joints are orientated oblique to the slip direction, due to the interaction of the remote tensile stress and the shear stress at the propagating fault tip. Removal of slabs from these joints creates a stepped fault wall (Chapter 5). The fiamme also influence the joint morphology; vertical joints become horizontal where they intersect a flattened fiamme.

The petrophysical properties of ignimbrite A differ to those of ignimbrite B but the nature of the material still controls deformation. The subunit A1 contains more fiamme, phenocrysts and lithics than the A2 and A3 subunits. The inclusions in A1 act as sites of joint initiation, as a result joint frequency is greater in A1 than A2 or A3. The composition of the ignimbrite A subunits also appears to affect the mechanism of fault growth. As mentioned in the previous section the nature of the fault core material can cause strain hardening or strain softening (in the sense of Wojtal and Mitra, 1986). In strain softening the fault core material is easily deformed and accommodates more of the subsequent deformation within the core without a further increase in the fault core width. This appears to be the case in the A3 subunit which is cut by Ca5 and Ca30. Although there is a 25 metre difference in displacement between the two faults they have similar fault core widths. These observations suggest that the material of the A3 subunit is easily deformed within the fault core and accommodates most of the deformation, as a result fault core growth is inhibited. The Ca15 fault that cuts A1 has a wider fault core that changes width along dip. The greater proportion of inclusions in the material may produce fault core material that results in strain hardening in the fault core, fracturing and entrainment of the adjacent rock and widening of the fault core.

The A2 subunit is an ash-rich friable material, and the only structures observed in this unit were deformation bands. Ignimbrite X is a crystal rich unit, the fault core is a mass of crystal rich gouge with very occasional breccia clasts of either individual lithic inclusions found in the host rock or clasts of the host rock itself. The ignimbrite X fault core is cut by deformation bands and the

damage zone is composed of competent indurated rock cut by joints. These observations suggest that the mechanical behaviour of ignimbrite X changes once it is incorporated into the fault core. Once in the core the material fails by cataclasis forming deformation bands rather than brittle fracture, which may indicate a reduction in strength or increase in porosity of the material.

Evans and Bradbury (2004) examined brittle deformation in non-welded and partially welded ignimbrites of the Bishop Tuff, Eastern California. The units they examined were highly porous with little or no devitrification and composed of alternating layers of finely laminated to massive pumice rich deposits. The Bishop Tuff is undergoing present-day east-west extension. Evans and Bradbury described four areas of deformation cut by faults ranging in displacement from zero to 18 m. The zero displacement area is composed of non to slightly welded, massive ash and pumice material and is located between two faults; the authors suggest it may be the faults damage zone. The area is dominated by closely to widely spaced, planar to sub-planar fractures. A 7 m offset normal fault cuts nonwelded, finely laminated ash deposits interbedded with slightly welded ignimbrite material. The fault is steeply dipping with a narrow fault core (1.5 to 30 cm thick) that contains a discrete fracture surface and multiple layers of fine ash gouge, tectonized clay, and calcite mineralization. The damage zone consists of open, near vertical fractures that are more closely spaced in the more welded ash rich beds. The 9 m offset fault that the authors describe cuts poorly to slightly welded ignimbrites at its base and propagates upwards through densely welded ignimbrite. The basal portion of the fault core is a discrete polished surface 1 to 3 mm thick. Moving up-dip the surface becomes curvilinear and splays into several slip surfaces forming a 1 m wide fault zone. The transition from a single surface to multiple surfaces coincides with a change in porosity from < 15% to 20 %. The final fault examined by Evans and Bradbury (2004) has 18 m of displacement and cuts poorly to non-welded and non-cemented pumice fragments. The fault is a narrow planar contact of fine cataclastically deformed tuff. The fault zone is 50 to 60 cm wide and there is little deformation adjacent to the fault.

Evans and Bradbury summarise that there are two fault types that can be related to the physical properties of the host ignimbrite. Faults in non-welded to poorly welded ignimbrites are composed of very narrow, planar fault cores with little or no damage zone. In moderately to densely welded ignimbrites the fault cores are wide and the damage zones are dominated by fault parallel fractures. They suggest that the degree of welding and/or devitrification that controls porosity also controls the macroscopic deformation mechanism.

Wilson et al. (2003) carried out an investigation of the non-welded ignimbrites of the Pajarito plateau, Los Alamos, New Mexico, that also showed the influence porosity has on deformation processes. Welded units with low porosities contain only fractures; poorly-lithified, non-welded units with high porosities contain only deformation bands. Units that are not welded with

moderately high porosities but have undergone vapour phase crystallisation (VPC) contain both deformation bands and fractures. These structures occur together in the same unit but in spatially distinct zones. Wilson et al. (2003) suggest that the precipitation of vapour phase minerals reduces porosity and increases the strength of the material, thereby allowing fracture formation. They conclude that the degree of welding and secondary crystallisation determine the deformation structures formed in any given ignimbrite

The influences on deformation mechanisms found by Wilson et al. (2003) and Evans and Bradbury (2004) are the same as those observed in this investigation; densely welded ignimbrites undergo brittle fracture and poorly welded, friable ignimbrites undergo cataclasis to form deformation bands. These observations suggest that we may be able to predict deformation processes in ignimbrites and the resultant structures by examining a host rock's petrophysical properties such as fiamme aspect ratio, presence of foliations, abundance of lithics and fiamme, and porosity. The observations made by Evans and Bradbury (2004) of faults in densely welded ignimbrites mirror those made in this study; densely welded ignimbrites are dominated by fault parallel fractures and wide fault cores. In this study I have shown that the spacing of the fault parallel fractures is controlled by the host rock fabric rather than fault displacement.

Previous work has recognised how petrophysical characteristics control the deformation mechanism – brittle fracture or cataclasis. In this study I have shown how the petrophysical characteristics can control the deformation structures themselves (fiamme/ash layers and joint spacing, flattened fiamme and joint morphology, composition and fault core material) and the consequences of this for fault architecture. Combining these studies creates a framework which allows us to make predictions about deformation processes, the structures formed, the frequency of deformation structures and the possible fault architecture.

Deformation structures in other lithologies are also influenced by host rock properties. High porosity sandstones fail by cataclasis and form deformation bands, as discussed in section 7.1 with continued displacement a through-going slip surface forms on the margin of the deformation band zone (Aydin and Johnson, 1978). In impure sandstones with higher clay content clay smear can occur along the fault surface (Cerveny et al., 2004). Low porosity crystalline lithologies such as granite undergo brittle failure forming discrete planar joints. Brittle failure also occurs in carbonate rocks, however when these are interbedded with mudstone beds the deformation structures and fault architecture changes from one bed to the next. Shear failure occurs in the less competent shale beds and the angle of failure is much less than that of brittle joint formation in the competent limestone. As a result the faults develop pull-aparts, oversteps and bends at the bed transitions (Peacock and Zhang, 1994). In poorly lithified sediments ductile deformation structures such as compositional foliations and lineations formed by particulate flow and cataclasis have been

observed (Rawling and Goodwin, 2006). Host rock properties also affect fault evolution. As discussed in Chapter 1 damage zone growth in high porosity carbonates is retarded once the fault gouge thickness reaches a maximum value as strain–softening in the fault core accommodates most of the strain (Micarelli et al. 2006).

7.3 Effect of stress state on fault growth and architecture

A requirement of the shear joint linkage model is a reorientation of the stress field on a regional or local scale. Either the regional stress field rotates relative to the initial joints or the joints rotate relative to the regional stress (Kim et al., 2003; Wilkins et al., 2001). The stress field may also be perturbed locally in the shear zone and reoriented perpendicular to the initial joint set (Mollema and Antonellini, 1999).

The faults in this study have formed by hybrid failure in a tensional stress field. The tensile stress that causes displacement on the joints is the same as the regional stress that formed the joints. As evident from the consistent joint and fault orientations parallel to the caldera margin the regional tensile stress is a result of caldera deflation and controls the formation of deformation structures. Thus there is no re-orientation of the stress field or joints relative to the stress field. The joints are therefore pre-cursory structures in the sense of Crider and Peacock (2004) and the faults are neo-formed faults as described by Angelier (1994).

The hybrid failure mechanism means that the fault architecture evolves with a different geometry than shear faults. In shear faults the damage zone is dominated by abandoned fault splays at high angles to the principal fault surface (de Joussineau et al., 2007). The damage zone may increase in width and complexity as a fault accumulates displacement (Caine and Forster, 1999; de Joussineau and Aydin, 2007; Fossen et al., 2007; Knipe et al., 1998; Shipton and Cowie, 2003). The shear fault core is bounded by two parallel fault walls, and widening of the fault core is accomplished through abrasion of the two opposing surfaces. Conversely a dilational fault forms on pre-cursory joints thus the fault core morphology reflects that of the initial joints and the damage zone joints are parallel to the fault core. In the case of the upward propagating growth fault at Cedro the interaction of the remote tensile stress and the shear stress at the fault tip have led to the joints being orientated obliquely to the slip direction resulting in a stepped fault wall. The hybrid mechanism causes significant opening of the faults as demonstrated by the TA2 fault, into which material from the overlying ignimbrite B has fallen. Therefore wide fault cores are generated with minimal displacement unlike shear faults where fault core growth is a result of fault slip abrasion and attrition. Furthermore in the hybrid faults investigated in this study there is a limited increase in joint density adjacent to the fault core with increasing displacement.

Investigations of truly tensile faults have largely been based on rift systems in which the faults are

hundreds of metres to kilometre scale (Acocella et al., 2003; Grant and Kattenhorn, 2004; Gudmundsson and Backstrom, 1991). The faults examined in this study are on metres scale of both size and displacement, and the joints have much smaller apertures (millimetres and centimetres) compared to the metres wide normal faults examined in Iceland and Ethiopia. However both have similar features; the fault walls and surrounding extension fractures are vertical or near-vertical, the opening between the footwall and hangingwall is filled by debris deposits (Acocella et al. 2003). Small scale hybrid faulting has been identified by Ferril and Morris (2003) in faults cutting mechanically layered sequences at shallow levels. Less competent layers fail by shear while more competent layers have smaller failure angles interpreted to be a result of hybrid failure. Hence faults cutting mechanically layered strata are composed of steep segments in more competent beds and shallower segments in less competent beds. As a result of this fault geometry, displacement is accommodated by shear along the shallow fault segments and dilation of the steeper fault segments. The faults observed in this study show no change in fault dip as faults traverse different ignimbrite units with different petrophysical properties, most likely because the elastic modulus is quite similar between the different units (Table 2,Table 5). The dilation of the ignimbrite faults is a result of layer extension and not shear on shallow fault segments that effectively pulls the fault walls of the steeper segments apart. In this sense the faults in Gran Canaria are more akin to rift style dilational faulting (i.e. truly tensile) on a much smaller scale in a less high strain extensional setting. The study site is more analogous to systems such as Yucca Mountain which is located on the southern margin of a set of nested calderas (Potter et al., 2004).

I suggest that the architecture of faults forming in a truly tensile environment can be predicted from knowledge of the deformation structures present before faulting occurred. As the faults are faulted joints the morphology of the joint dictates the morphology of the fault core. The spalling of material from the joint surfaces into the fault core means joint spacing will influence fault core growth. The spacing of joints themselves may be predicted from host rock properties such as mechanical layer thickness or number of flaws or cavities. Although shear faults grow by different mechanisms I believe that similar principles could be applied to the controls on fault zone evolution in general. In a shear dominated normal fault the maximum compressive stress is vertical and joints open up parallel to it in the damage zone. Therefore the controls on joint formation such as mechanical layer and sub-mechanical layer thickness, the influence of flaws and cavities could be used to predict fault architecture in the same manner as dilational faults in extensional settings. Parameters such a sub-mechanical layer thickness, flaw density and aspect ratio should be measured when analysing faulted lithologies and their influence on joint frequency included in models predicting fault zone architecture. In all deformation environments stress orientation and host rock character plays a vital role in determining deformation processes and controlling the formation of deformation structures respectively.

7.4 Implications for fluid flow

Fault architecture impacts on ore deposition, earthquake nucleation and propagation, hydrocarbon migration and compartmentalization of reservoirs, aquifer recharge, CO_2 sequestration and nuclear waste disposal. Faults can act as either barriers or conduits to fluid flow (Caine et al. 1996); which can inhibit or promote mineral deposition, seal hydrocarbon reservoirs or allow for the transportation of contaminants horizontally and vertically within the subsurface. To predict whether a fault will behave as a conduit or barrier we need to understand the hydraulic architecture of the fault. The hydraulic architecture of a fault depends on the distribution, proportion and permeability structure of the fault components i.e. fault core and damage zone (Caine et al, 1996). The permeability structure depends upon the host rock in which the fault forms, the deformation processes active in the fault and the deformation structures formed as a consequence. As the structure of the fault zone evolves overtime so too does the hydraulic architecture (Evans et al., 1997). I will now examine the different types of hydraulic architecture that occur in faults in general and the factors that control the permeability structure.

The proportion of the fault zone composed of fault core and damage zone are primary controls on the barrier-conduit behaviour of the fault zone. Caine et al. (1996) has proposed four end members of fault architecture and their associated permeability structure. When the fault core is dominant the fault is a localised barrier to flow, a narrow fault core may act as a localised conduit. A well developed damage zone behaves as a distributed conduit when associated with a narrow fault core and as a combined conduit-barrier when associated with a wide fault core. In the damage zone flow pathways will be parallel both vertically and horizontally to the fault. In the fault core across fault flow is prevented except during fault slip when movement of the fault core material can open fractures and increase permeability, allowing the fault core to act as a conduit (Caine et al., 1996)

A major control on deformation processes and fault hydraulic architecture is the petrophysical properties of the host rock. In low porosity, lithified material e.g. granite, densely welded ignimbrites, most volcanic rocks, gneiss, flow is fracture dominated. The damage zone is cut by fractures and minor faults that increase permeability relative to the host rock (Caine et al., 1996; Evans et al., 1997) and the fault core is composed of low permeability gouge or cataclasite. Fractures provide preferential fast flow pathways that can be orders of magnitude faster than flow within the rock matrix (Hinds et al., 2003; Wu and Pollard, 1995). The orientation, length and spacing of fractures affect the connectivity of the fracture network and hence fluid flow in the damage zone. Fractures that share the same orientation have fewer intersections and lower connectivity than a series of antithetic fractures (Figure 113a and b); short fractures terminate in space again lowering fault connectivity whereas longer fractures have a greater probability of intersecting another fracture (Figure 113c and d). The spacing or distribution of fractures also

affects connectivity in the damage zone. Closely spaced fractures can have a high connectivity providing a continuous flow path in a particular direction (Figure 113f); however this is also dependent on fracture orientation. Clustering of fractures may also increase the flow rate through that particular area. Large fracture apertures and high fracture frequencies cause an increase in permeability and a well developed damage zone will enhance fluid flow parallel to the fault plane.

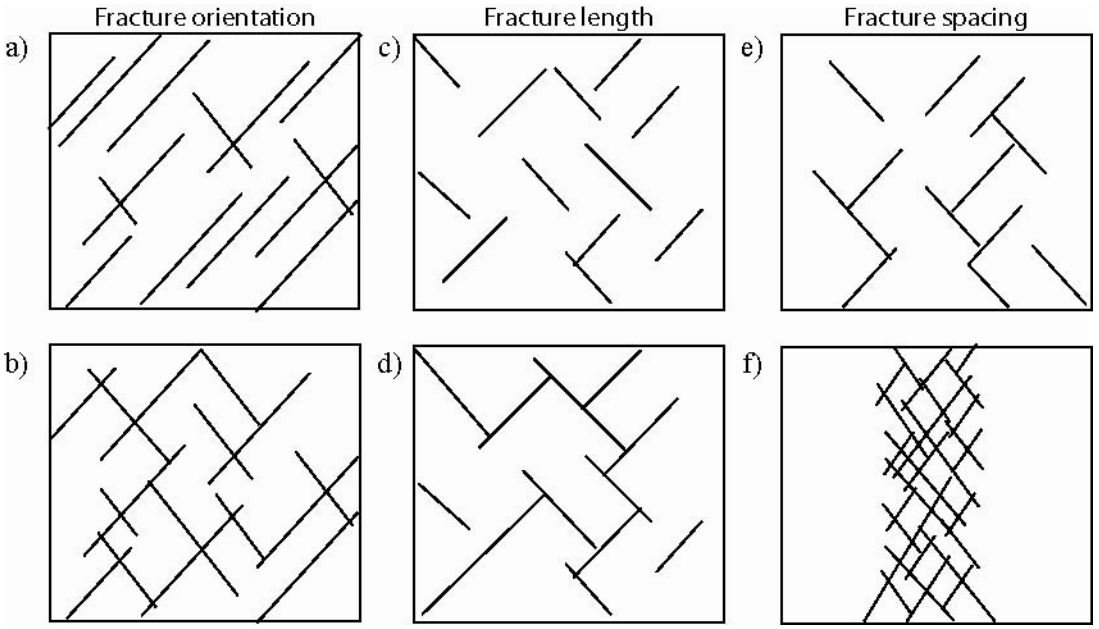

Figure 113: Effect of fracture geometry on fracture connectivity
The affects of fracture orientation on fracture connectivity and flow pathways a) When the majority of joints have the same orientation there is little connectivity between joints and there is no continuous flow pathway b) When joints are dipping in opposite directions there is greater joint connectivity and a continuous flow path across the area. The length of the fractures also influences fracture connectivity and flow paths c) Short fractures that terminate in space result in low fracture connectivity and hence no or short flow paths d) When more joints intersect connectivity is greater promoting flow across the area. Fracture spacing can influence the rate of flow e) Widely spaced connected fractures create a dispersed flow zone that may inhibit flow rate f) Closely spaced fractures create a concentrated flow network that may allow faster flow (figure after (Odling, 1992))

In the fault core deformation processes of abrasion, cataclasis and attrition cause grain size reduction. The creation of smaller sized grains that infill pore spaces between larger grains reduces porosity and generates more tortuous flow paths hence reducing permeability. Mineral precipitation will further restrict across fault flow (Evans et al., 1997). The presence of fractures or deformation bands in the fault core may facilitate across-fault flow depending on the saturation conditions. Through-going open slip-surfaces in the fault core may also increase along fault permeability (Heffner and Fairley, 2006; Shipton et al., 2005)

High porosity rocks e.g. sandstone, poorly welded ignimbrites, deform by the creation of low porosity deformation bands so matrix flow is dominant. Deformation band permeability depends on the saturation conditions. In the saturated zone deformation bands reduce porosity and

permeability (Antonellini and Aydin, 1994; Aydin, 1978; Rawling et al., 2001; Shipton and Cowie, 2003). In the unsaturated zone of arid environments deformation bands increase permeability (Sigda and Wilson, 2003). Therefore deformation bands may act as flow conduits in the unsaturated zone and as barriers to flow in saturated conditions(Evans and Bradbury, 2004; Wilson et al., 2003).The development of a deformation band zone results in the formation of a slip plane at the margin of the zone (Antonellini and Aydin, 1995). Permeability is reduced perpendicular to the slip plane due to the tightly packed deformation bands but a high permeability flow path may form parallel to the slip plane (Shipton et al. 2005; Heffner and Fairley, 2006).

In poorly lithified sediments the fault core is composed of clay and gouge separated from the damage zone by a mixed zone (Heynekamp et al., 1999; Rawling et al., 2001). The mixed zone contains rotated and attenuated beds and mixing of material at the grain scale. The main hydraulic element in the damage zone is the deformation band and jointing is absent. This fault architecture reduces permeability both normal and parallel to the slip plane (Rawling et al., 2001). The occurrence of cementation will increase the lithification of the sediments thus changing the deformation mechanisms to brittle fracturing and altering the hydraulic architecture of the fault zone (Heffner and Fairley, 2006).

Failure mode also controls deformation structures and their permeability structure. In extensional settings, dilation forms open planar joints without cross-joints or wing cracks forming a set of parallel joints with little or no connectivity (Figure 114a). However these joints will likely have wide apertures and if there is no fill or cement they will act as fast flow pathways parallel to the fault core. Shear failure forms a network of primary and connecting secondary fractures with a high connectivity that allows flow parallel and perpendicular to the fault core (Figure 114b). If deformation is not intense and the secondary joints are short they may terminate in open space, hence reducing connectivity and flow through the network. Shear joints may also be closed or very narrow and restrict the rate of flow.

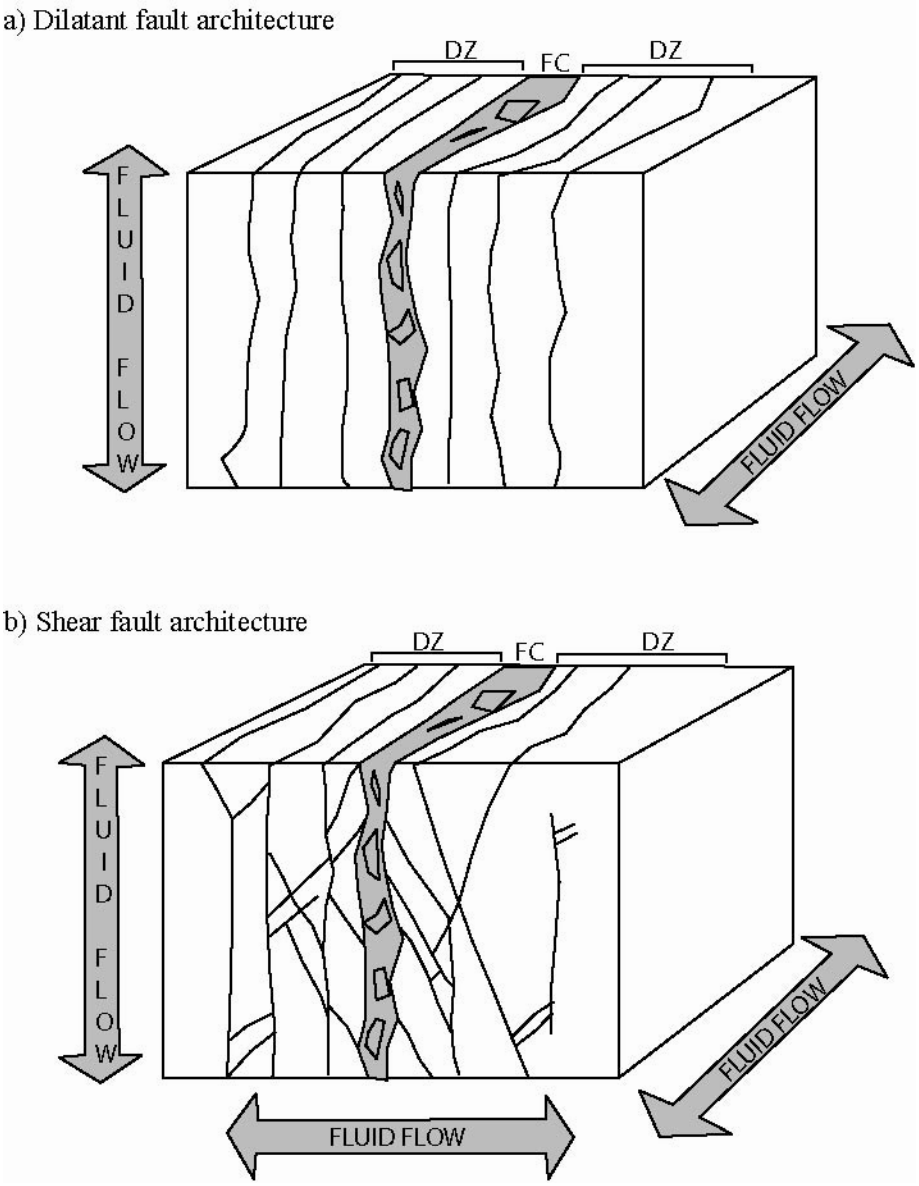

Figure 114: Dilatant and shear fault architecture

The consequences of hybrid/dilatant faulting is that joints are parallel to the faults unlike shear faults where splay fractures and wing cracks link parallel joints forming a network of interconnected joints from the fault core outward. Therefore fluid flow in dilatant faults will be dominantly fault parallel with minimal lateral flow from the fault core out.

The deformation elements formed in ignimbrites depends on the degree of welding and vapour phase alteration the material has undergone. Three different types of fault zone architecture have been observed in ignimbrites in this study each of which has different implications for the fault zone hydraulic architecture.

In the densely welded ignimbrites (Ignimbrite B) the low-offset dilational faults would have very high permeability's as the fault cores are dominated by entrained slabs and large angular blocks that have undergone little abrasion, thus a very minor amount of gouge has formed and spaces between clasts remain open. As displacement increases, attrition of clasts increases the amount of gouge in the fault core and therefore will likely reduce the permeability. Cementation will tend to

decrease the permeability further (Ferrill and Morris, 2003), though little cement was observed at Gran Canaria. In the damage zone the level of joint density remains relatively stable with displacement and therefore permeability is also likely to remain constant. There is little connectivity between the parallel joints which would reduce the cross fault permeability but the extensive vertical nature of the joints may greatly enhance fault parallel flow. A large offset fault in ignimbrite B will act as a combined conduit-barrier to fluid flow.

The hydraulic architecture of ignimbrite A faults will depend on the subunit being faulted. In the ash-rich friable units the fault core material is dominated by fine grained gouge. In the low offset faults observed in the ash-rich unit at Tauro the fault core is composed of a fractured pillar of ignimbrite A, the ash-rich material is easily abraded and forms a very fine grained gouge on the slip surface. The fractures in the brecciated core material may act as flow pathways but overall it is likely that the fault core would have a low permeability. The damage zone joints could act as flow paths parallel to the fault core. As displacement increases, the fault core thickness in the ash-rich units (A2 and A3) remains constant (section 3.2.2), this narrow fault core may act as a localised flow conduit during slip events. In the A1 subunit the fault core is wider and contains fine grained gouge and breccia clasts. The thickness of the fault core and the fine grained nature of the gouge suggests that the fault core may act as a barrier. There is a minimal increase in number of joints in the damage zone with increasing displacement, the joints remain sub-parallel and there is little connectivity between joints. Flow pathways in the damage zone would be fault parallel. The subunit A2 is cut by deformation bands both in the damage zone and fault core of the CA5 fault, these may act as flow pathways in unsaturated conditions.

Ignimbrite X forms joints in the damage zone and deformation bands in the fault core. Implying that induration of the material has strengthened the unit sufficiently to allow joint formation under tensile stress, but when the material is subjected to attrition in the fault core the homogeneous crystal rich material deforms by cataclasis. The ignimbrite X damage zone is dominated by sub-parallel joints therefore flow will likely be enhanced in a fault parallel direction. The joint frequency in the damage zone is low which may reduce the flow rate compared to ignimbrite's A and B that have a greater number of joints. The ignimbrite X fault core contains fine grained gouge which is likely to have a low porosity and permeability and therefore act as a barrier to flow. However like the deformation bands in the friable A2 subunit, the deformation bands that cut the ignimbrite X fault core may act as preferential flow pathways in unsaturated conditions (i.e. if the fault is in the vadose zone) allowing across-fault flow. The presence of deformation bands in two such unalike ignimbrites (ash-rich, crystal poor and crystal-rich, ash poor) suggests that the percentage of ash and crystal in an ignimbrite as well as the competency of the material controls the deformation elements formed.

The observations made in this study suggest that dilational faults may have much higher permeability for a given offset than that predicted for shear faults with a similar offset amount. At small displacements dilational faulting causes further opening of joints, limited gouge formation and the fracturing of rock pillars, all of which generates extensive flow conduits. Furthermore, due to the extension of the layer during faulting there may be more open joints and minor faults adjacent to large dilational faults than estimated from models based on shear-dominated fault growth.

This study has shown that a variety of fault architectures is possible both between ignimbrite units and within a single unit. The variation in hydraulic architecture and permeability structure has important implications for conceptual models used to evaluate fluid movement within faulted ignimbrite units. The flow of fluids in ignimbrites is key to the design of the proposed nuclear waste repository in Yucca Mountain, Nevada. The rate of fluid flux through fractures and matrix, flow pathways and the likelihood of seepage from the storage drifts into the underlying water table are critical factors in the safe storage of the waste material. The proposed repository horizon is the Topopah Spring Tuff (Tpt) part of the Paintbrush Group (Ptn), the unit is in the unsaturated zone ~300m above the water table and the same distance below ground surface (Birkholzer et al., 1999). The Topopah Spring Tuff is densely welded, crystal rich and highly fractured. The majority of faults in the unit have less than 3 metres of displacement and narrow fault zones less than 1 metre wide (Gray et al., 2005). The current design for the repository places over half of the potential waste emplacement drifts in the lower lithophysal zone of the Topopah Spring Tuff with the remaining drifts divided between the middle nonlithophysal zone and the lower nonlithophysal zone (Hinds et al., 2003). The Tpt is overlain by the Pah Canyon and Yucca Mtn tuffs that are non to partially welded and relatively unfractured. Above the Paintbrush Group lies the Tiva Canyon tuff (Tpc) a densely to moderately welded unit that is highly fractured (Potter et al., 2004). Growth strata adjacent to some faults in the Paintbrush Group indicate that faulting initiated before or during ignimbrite deposition (Day et al., 1998).

The current model of fluid flow through the unsaturated zone is one of rapid percolation from the ground-surface through the fractures of the Tiva Canyon tuff. Fracture flow changes to matrix dominated flow in the non-welded units of the Paintbrush Group. Thus the non-welded units are considered to be a natural buffer to water percolation, slowing flow rates and limiting the water available to transport waste material and radionuclides from the unsaturated zone to the saturated zone (Zhang et al., 2006). Uncertainties with this model are the assumption of steady state flow and layer-averaged rock parameters that homogenise the heterogeneous fracture and matrix permeabilites. Wu et al. (2002) suggested that volume averaged parameters may overlook localization of flow along preferential pathways such as well connected large fractures. Pruess et al. (1998) envisage flow in thick unsaturated zones as occurring in a non-volume averaged fashion;

flow in the matrix will be slow while fracture flow is much faster.

My investigation has demonstrated not only how different each ignimbrite unit is to each other but also how the host rock characteristics can vary within each unit. Changes in fabric and composition affect the deformation structures. Sublayers formed by flattened fiamme form closely spaced joints parallel to each other and perpendicular to the foliation fabric. Abundant flaws in the form of fiamme or lithic inclusions act as joint initiation points. Jointing patterns and joint morphology are affected by fiamme shape; joints radiate from round fiamme and oblate fiamme cause a joint offset or step. The joint density, morphology and pattern will all have implications for flow within a unit. Applying average parameters greatly reduces the complexity of this system and may result in an inaccurate hydraulic model for flow pathways, transport and storage. In particular using average parameters may underestimate fast flow along highly localised high fracture density pathways. Therefore it is essential to understand what controls the distribution of high fracture density pathways and the controls on their hydraulic properties.

Large scale joints greater than 10 metres in length have been focussed upon in the analysis of the Topopah Spring Tuff as they were considered to be the most important flow pathways. The unit is intensely fractured and the fractures form a well connected network (Birkholzer et al., 1998). Field observations of seepage velocities on the order of 10m/year indicate fast flow in fractures and that at Yucca Mountain fracture flow may be dominant particularly in the welded fractured units (Pruess et al., 1998). Small-scale (cms up to 3 m's in length) fractures form dense populations in the Tpt (Birkholzer et al., 1998). They may not contribute to large scale flow in the unsaturated zone but may facilitate interflow between large scale fractures and surrounding matrix blocks, or act as a buffer between large fractures and matrix due to their high storage capacity compared to that of large fractures. Therefore they have an important affect on radionuclide transport (Wu and Pollard, 1995). However most of the small scale fractures have not be mapped in any of the repository units, although considerable variation in fracture trace length, spacing, permeability and capillarity is seen between and within units (Hinds et al., 2003). My model relating host rock properties to deformation structures could be used to predict the nature of the small-scale fracture population. Incorporating information on fracture frequency, distribution and morphology, based on an analysis of fiamme shape, fiamme abundance and presence of sublayers in the host repository horizon, will improve the fluid flow model and the accuracy of predictions made from it.

Application of this model may also help in the development of a fluid flow model in the welded ignimbrites at the Sellafield site, Cumbria. The majority of information about the proposed repository horizon has come from boreholes, which gives a rather limited view of large scale fault architecture. The proposed ignimbrite host horizons have very similar characteristics to ignimbrite B and A. The units are densely welded, show evidence of rheomorphic flow (eutaxitic and

parataxitic fabrics) and contain fiamme rich or lithic rich layers (Millward et al., 1994). Outcrop studies of joint spacing, morphology and joint patterns would indicate whether any of the features seen in Gran Canaria are present here and therefore the model could be applied to generating a hydraulic architecture model for faults in the area. A generalised stratigraphic log of the ignimbrite units at Sellafield (the Borrowdale Volcanic Group) and predictions of the fault architecture is shown in the next section.

7.5 Predicting fault architecture and hydraulics

In Chapter 1 I discussed two displacement scaling relationships, the displacement-fault thickness relationship and the relationship between fault core clast size and displacement. The displacement-thickness relationship proposed for shear dominated faults by Scholz (1987) and Hull (1988) suggests that there is a linear increase in fault thickness with displacement. This is based on the assumption that the fault core grows by abrasion of the fault slip surfaces and subsequent production of wear material. The fault core clast size displacement relationship suggests that as displacement increases the number of grain fracturing events also increases causing a reduction in grain size and changing grain shape (Billi and Storti, 2004; Blenkinsop, 1991, Sammis et al., 1987; Engelder, 1974).

As shown in previous chapters the evolution of the dilational faults presented here does not follow either of these relationships. In ignimbrite A the largest offset fault Ca30 has the narrowest fault core and of the four faults examined in ignimbrite A only the Ca30 damage zone shows any increase in joint frequency. In ignimbrite B there is only a slight increase in the mean fault core width from the lowest displacement fault (Tb2.5) to the largest displacement fault (Cb22), however Cb22 has a range of fault core widths the lowest of which is narrower than the Tb2.5 fault core. Damage zones in ignimbrite B have the same joint frequency regardless of displacement magnitude; similar levels of joint frequency are observed in the Tb2.5, Cb5 and Cb22 damage zones.

In the ignimbrite A fault cores the largest clasts are found in the Ca15 fault not the Ca5 fault as would be expected if clast size is decreasing with increasing displacement. The range of clast sizes in the Ca30 fault core is slightly smaller than those in the Ca5 fault core. In ignimbrite B the largest clasts are found in the lowest offset fault (Tb2.5) and the largest offset fault (Cb22). From these observations I suggest that displacement is not the controlling factor in the evolution of these faults but, as discussed in section 7.2, the host rock petrophysical properties that controls the deformation processes and deformation structures is the primary control on fault growth and evolution.

Fault core expansion is controlled by joint spacing in ignimbrite B and host rock composition in ignimbrite A. As was reported by Grant and Kattenhorn (2004) for dilational faults in Iceland, the

faults in Gran Canaria show no evidence of abrasion of surfaces and only one fault contains a slip surface. Asperity removal is from existing joint surfaces and not due to fault tip-line bifurcation (Childs, 1996). The joint density adjacent to faults does not reflect the amount of displacement on the fault; instead joint density is a function of the host rock fabric.

In ignimbrite B the overall fault gouge and clast size population does not decrease with increasing displacement due to the way material is entrained into the ignimbrite B fault cores from joint bound slabs rather than abraded from opposing surfaces. This mechanism results in an increase in the large size fraction of the fault core material by the addition of blocks from joint bound slabs, the size of which are controlled by joint spacing. In Ignimbrite A the friable ash rich material produces a strain softening response in the fault core; the fault rocks become progressively easier to deform and strain is localised within the fault core. Subsequent displacement is accommodated in the fault core inhibiting fracturing of the fault walls and incorporation of new material. The rock volume originally bounded by the faulted joints is broken down to form gouge and centimetre size clasts, as a consequence the fault core width is defined by the original spacing of the faulted joints.

This study demonstrates that accurate predictions of fault architecture in ignimbrites can not be solely based on displacement scaling relationships. Furthermore the use of the displacement-thickness relationship based on relationships from other lithologies might also result in inaccurate models of fault architecture in ignimbrites. The uncertainties of this global scaling relationship for all lithologies have been discussed by Shipton et al. (2006). We found that although there was a positive increase in fault thickness with displacement there was three orders of magnitude scatter at any value of displacement. Furthermore predictions based on site-specific fault thickness data could vary by at least two orders of magnitude. Such wide variation has ramifications for models of earthquake rupture which are based on centimetre thick fault cores that vary only by 10's of centimetres between different models. Shipton et al. (2006) suggest that separate scaling relationships for each fault component and separate scaling relationships for faults in different lithologies would be more useful.

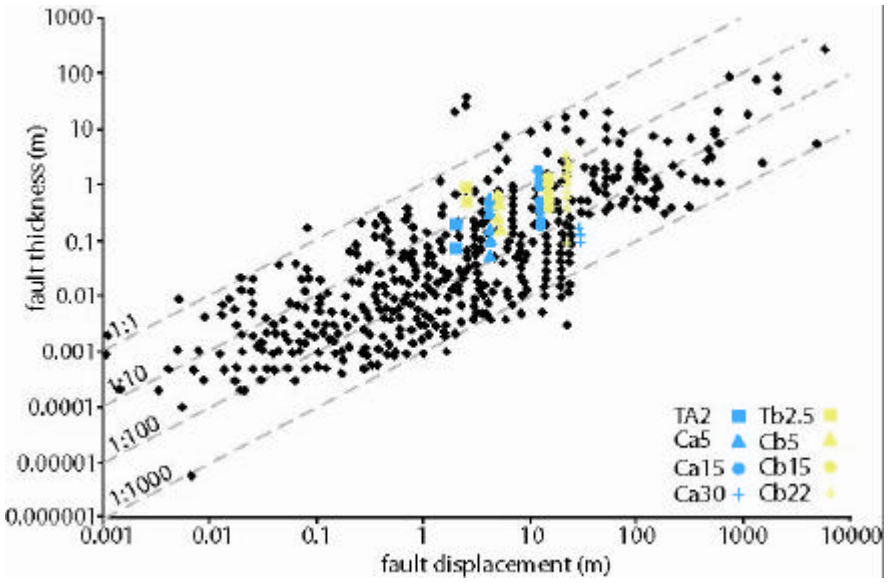

Figure 115: Log-log plot of a compilation of FC thickness-Displacement datasets The plot from Shipton et al. (2007) shows 16 fault thickness datasets reported in the literature (black dots) including the data used by Hull (1988). Overlaid are the fault core thickness data for the faults in this study. For an individual value of fault displacement fault core thickness can vary over three orders of magnitude. The fault core thickness for the ignimbrite faults varies by up to an order of magnitude within any one fault; therefore knowledge of the displacement on the fault would not give a correct value for fault core width.

Considering the dependence of fault architecture on host rock properties and stress state at the time of faulting, characterisation of faults within the same lithology and under different conditions (extensional or shear) may produce more valuable relationships on which to base fluid flow and earthquake models. In Figure 116 I have compiled data on ignimbrite deformation structures and the factors that appear to be the most important to their formation, from this and other studies (Evans and Bradbury, 2004; Wilson et al., 2003). This figure is by no means complete and further work is required to fill in the blanks e.g. in densely welded but lithic-poor units.

Using this figure we can make some general predictions of deformation structures and fault architecture in ignimbrites. Densely welded units with a high percentage of flattened fiamme and eutaxitic texture will have high joint frequencies. Moderately to poorly welded units with a large proportion of lithics may also have high joint frequencies as the lithics and fiamme act as joint initiation points. Poorly welded ignimbrites with few lithics and/or fiamme form deformation bands. However if the precipitation of secondary crystals from vapour phase crystallisation is high the material is more competent and jointing can occur. If faults are initiating on joints the growth of the fault may be controlled by joint spacing and so in areas of high joint frequencies joints will be closely spaced and the fault core will be narrow. My model of fault growth has been based on dilational faults, and the ignimbrites examined by Wilson et al. (2003) and Evans and Bradbury (2004) were also in an extensional rift-related settings; observations of shear faults in ignimbrites, and/or faults developed in compressional conditions would further enhance the usefulness of this framework.

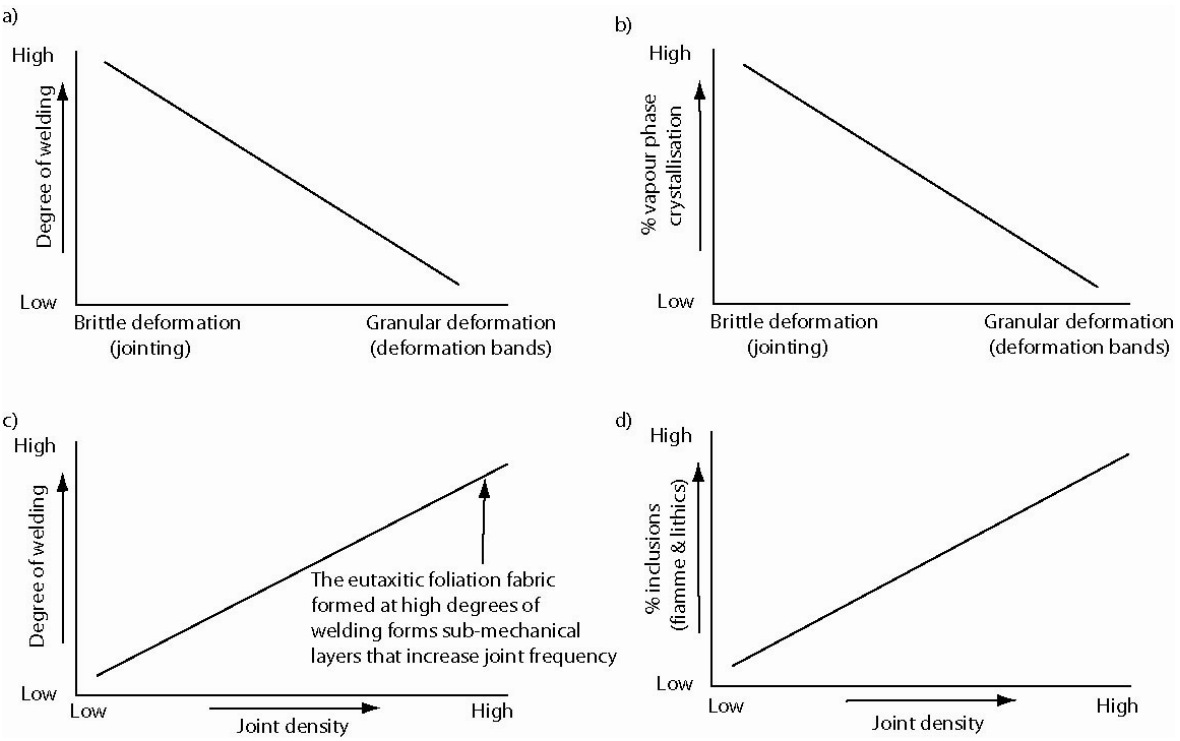

Figure 116: Controls on ignimbrite fault architecture

Fault architecture in ignimbrites is controlled by three main factors. In this figure I have summarised the affect each variable has on deformation processes and the resultant deformation structures. a) When the unit is densely welded the material undergoes deforms by brittle failure and forms joints; low levels of welding allow the material to deform by granular flow and form deformation bands. b) Secondary crystallisation and vapour phase alteration infill pore spaces creating a more massive unit which deforms in a brittle manner; at higher porosities i.e. low levels of vapour phase alteration the material forms deformation bands as cataclasis is the main deformation process rather than fracturing. The joint density within a unit is also affected by these parameters c) Densely welded units form a eutaxitic fabric of alternating fiamme and ash matrix. These sub-layers allow more closely spaced joints to form thereby increasing joint density. d) Fiamme and lithics act as sites of joint initiation within the material thus the greater the percentage of inclusions the greater the number of joints formed. More data on deformation structures in ignimbrites with varying degrees of welding, % inclusions and % vapour phase crystallisation may identify threshold values for degree of welding and vapour phase alteration at which the deformation process changes from brittle failure to cataclastic flow.

Similar diagrams have been complied for reservoir rocks (Cerveny et al. 2004) in which varations in lithification state, clay content and fragmentation are used to classify fault rocks in sandstones and shale. It may be valuable to take this approach in characterising fault architecture in all lithologies (crystalline, sedimentary, lithified, non-lithified.); identifying key deformation structures and the host rock characteristics that produce them in each lithology. Such a database would highlight the most important controls on deformation processes, increase the accuracy of fault architecture models and the predictions based upon them.

In the following sections I use my model to predict the deformation structures and fault architectures in two different settings – Yucca Mountain, Nevada and Sellafield, Cumbria. The

stratigraphic logs include the proposed nuclear waste host repository horizon in Yucca Mtn. and the previously proposed repository horizon in Sellafield.

The host horizon in Yucca Mtn is the Topopah Spring Tuff (Tpt) the upper units are non-welded moving down into moderately and densely welded units. The Tpt is overlain by the minor non-welded Pah Canyon and Yucca Mtn tuffs and the thicker welded Tiva Canyon Tuff (Tpc). Both the Tpt and Tpc are composed of two subunits, one crystal-rich member and one crystal-poor member. These members are further divided into units containing lithophysae and units without, densely welded units and moderately welded units. Given this degree of heterogeneity we would expect a fault cutting these units to have a complex architecture.

I have used the observations made in this study to predict the intensity of jointing in each of the sub units and the possible fault architecture. The lithophysal zones of the Tiva Canyon Tuff and Topopah Tuff may have high joint frequencies as these cavities act as joint initiation points. Lower joint frequencies would be expected in the non-lithophysal zones where there are fewer flaws to promote joint formation. Joints may radiate outwards from circular lithophysae; the type of joint distribution and frequency has important implications for the flow network. A radiating joint network will have greater vertical and lateral connectivity compared to a joint set formed parallel to the maximum compressive stress

The densely welded and moderately welded zones will form joints and the non-welded zones will form deformation bands. The joint spacing in the densely welded unit will depend on whether the degree of welding and the proportion of fiamme were great enough to develop a foliation. If like the upper portion of the ignimbrite B unit there are few fiamme then the joint spacing will be controlled by the overall thickness of the Tuff unit. If fiamme are abundant, highly flattened and stretched they will form layers with the ash and thus joints will be closely spaced.

If faults in the Tpt and Tpc are forming by the same mechanism as those in ignimbrite B then the spacing of the joints will control the fault core growth. Gray et al. (2005) have observed fault architectures that they interpreted to be a result of hybrid failure therefore there are faults in Yucca Mtn similar to those in ignimbrite B. If we want to predict the width of the fault core in these faults we need to know whether a foliation is present in the densely welded unit; Gray et al. (2005) did not indicate if this was the case.

The joints in the Tpt have been defined as either cooling joints or tectonic joints (Throckmorton and Verbeek, 1995). Cooling joints are long, planar and have exceptionally smooth surfaces. In some places the cooling joint surfaces are cut by tubular structures or channels that form a braided pattern in the plane of the joint surface. Tectonic joints have planar to gently curving traces and their surfaces are as smooth as or slightly rougher than cooling joints (Throckmorton and Verbeek,

1995). Thus faults forming on these joints will have planar to slightly undulating fault walls. In ignimbrite B the centimetre scale and Tb2.5 offset faults were dominated by angular blocks with minimal amounts of gouge, after 5 metres of displacement the fault core clasts were surrounded by fine grained gouge. If this is also true of small scale faults with 1-2 metres of displacement in the Tpt the faults would act as significant conduits to fluid flow. Evans and Bradbury (2004) suggested that smooth surfaces, such as the fault walls, could promote fast water flow as sheets or rivulets along the surface.

In my study the crystal-rich unit (ignimbrite X) formed joints in the fault damage zone and deformation bands in the fault core. The crystal-poor unit (ignimbrite A) formed joints in the damage zone and the material in the fault core was strain softening inhibiting fault core growth. Therefore faults cutting the crystal-poor members of the Tpc and Tpt may be quite narrow regardless of displacement accumulated and faults in the crystal-rich units may contain deformation bands in the fault core which will have implications for across-fault fluid flow. A limitation of my model is that only one fault in ignimbrite X was studied; this fault had a total of 140 m displacement and so little can be said about the evolution of the fault core with increased displacement in a crystal rich ignimbrite.

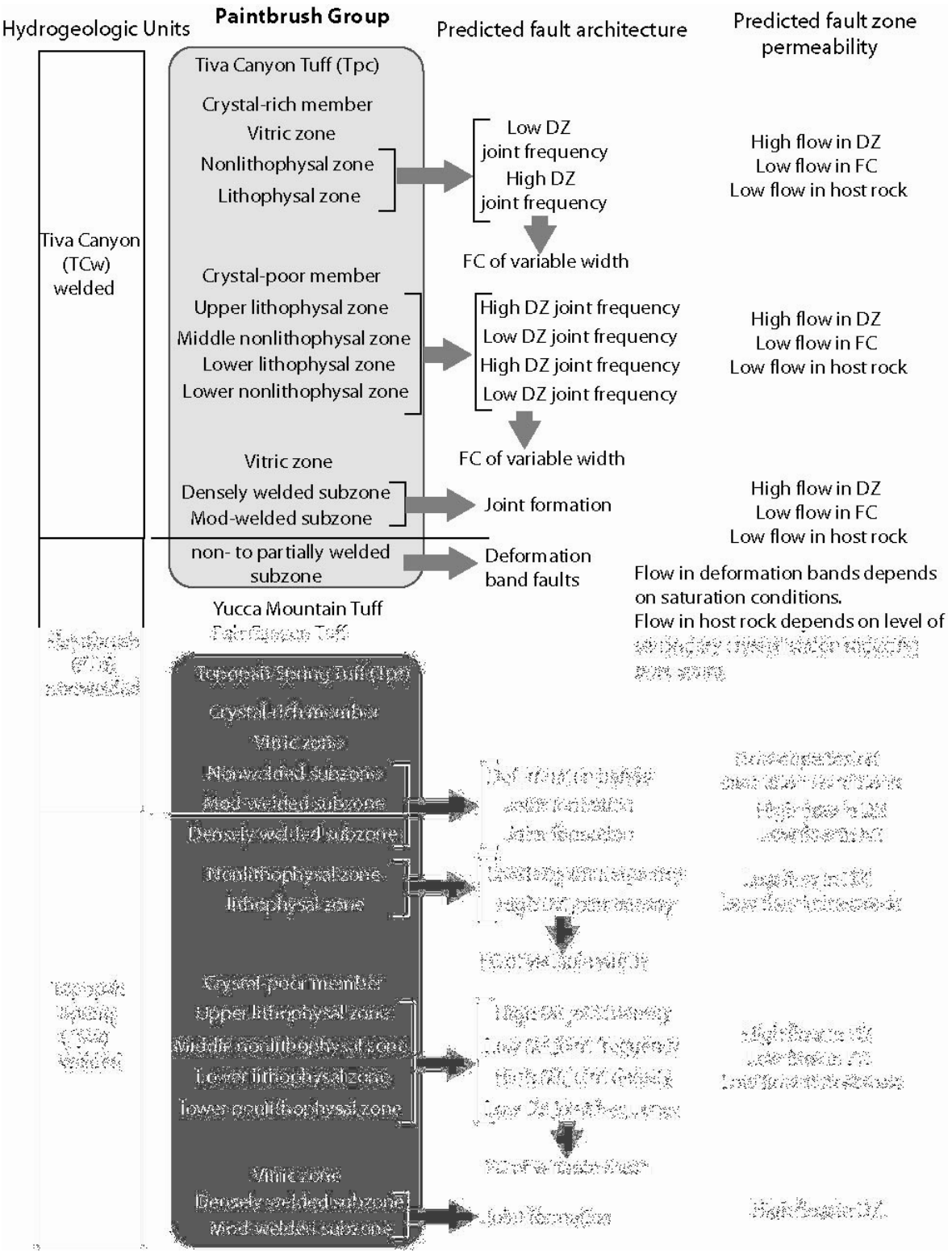

Figure 117: Stratigraphic log of proposed host repository horizons at Yucca Mtn Lithological and hydrogeologic descriptions of host horizons at Yucca Mtn. (Flint, 1998). Predicted fault architecture is based on the observations made in this study. Lithophysae are open cavities and will concentrate stress thus acting as joint initiation points, therefore lithophysal units will have high joint frequencies and non-lithophysal zones will have low joint frequencies. If the fault core is growing by slab incorporation then areas with high joint frequencies will have closely spaced joints and thus narrow fault core and vice versa for non-lithophysal unit. As was the case with the ash-rich A3 subunit in ignimbrite A the crystal-poor member may undergo strain softening and thus the fault core will be narrow regardless of displacement accumulated.

At Sellafield, Cumbria it has been proposed to locate a nuclear waste-repository in the rocks of the Borrowdale Volcanic group. The group is composed of volcaniclastic sedimentary rocks, tuffs, and breccias. The stratigraphic log shown in Figure 118 is from one borehole drilled in the area and does not shown the full range of formations in the area.

In this log the fabric of the host rock is shown, three of the units are densely welded as indicated by the eutaxitic and parataxitic fabrics. These highly stretched fiamme may form sub-mechanical layers that control joint formation and joint spacing. If the faults are forming by hybrid failure and growing by slab incorporation the fault cores will be narrow in the areas with a eutaxitic fabric as joints will be closely spaced. The fault core width will be wider in the massive, glassy part of the unit where the joint spacing is controlled by the thickness of the entire ignimbrite unit. Further investigations of joint frequency in densely welded units with foliation fabrics grading into massive material would help to firmly establish if flattened fiamme are acting as sub-mechanical layers and controlling joint spacing.

The heterogeneous tuff may behave in a similar manner to ignimbrite A sub-unit A1. The lithics may act as sites of joint initiation thus generating a high joint frequency in fault damage zones. In the fault core the material may cause strain hardening and promote fault growth therefore fault cores in these units could be wider then displacement scaling would predict.

The predicted hydraulic fault architectures in the densely welded parataxitic tuffs would be dominated by fracture flow. Vertical fractures forming between sub-mechanical layers would accommodate fault parallel flow and inhibit flow normal to the fault. The fault core itself may act as a localized conduit at low displacements when the core is dominated by clasts and higher offset amounts gouge will infill the interstices and the core would be a barrier to flow. In the heterogeneous units the majority of joints will be vertical but circular lithics may form radial joints which will increase the lateral connectivity in the unit. Again the fault core may act as a conduit at low displacements and become a barrier with increasing gouge formation.

The ignimbrites examined at Sellafield are much older than any previously discussed. The Gran Canaria ignimbrites examined in this study are 13 Myr old, the Yucca Mountain tuffs were erupted between 11 and 15 Myr old, the tuffs examined by Wilson et al. (2003) are 1.6 Myr and 1.2 Myr old and the Bishop tuff was erupted ~750 ka (Evans and Bradbury, 2004). These ignimbrites occur close to the surface and have undergone few deformation events other than the extension that formed the joints and faults. The Borrowdale Volcanic Group at Sellafield is around 460 Ma and the top of the volcanic rocks is at a depth of 400 to 600 metres (Nirex, report No. 525). The group is overlain by a Permian breccia and Triassic sandstones. The volcanic rocks have been subjected to faulting and folding throughout their history and the faults that cut the volcanics also cut the overlying formations therefore the faults are likely to have formed much later and unlike the faults

in Gran Canaria are not contemporaneous with ignimbrite deposition. As a result of the many deformation events that the Borrowdale volcanics have undergone fault formation could have occurred in either a compressive or extensional stress regime and so the observations made in this study and my model of fault formation may not be as applicable. However examination of the fault zone structures and how they relate to the host rock fabric (e.g. is there a higher joint frequency where a eutaxitic and parataxitic fabric is present compared to the massive parts of the tuff) would indicate if my observations hold for any stress regime or fault failure mode.

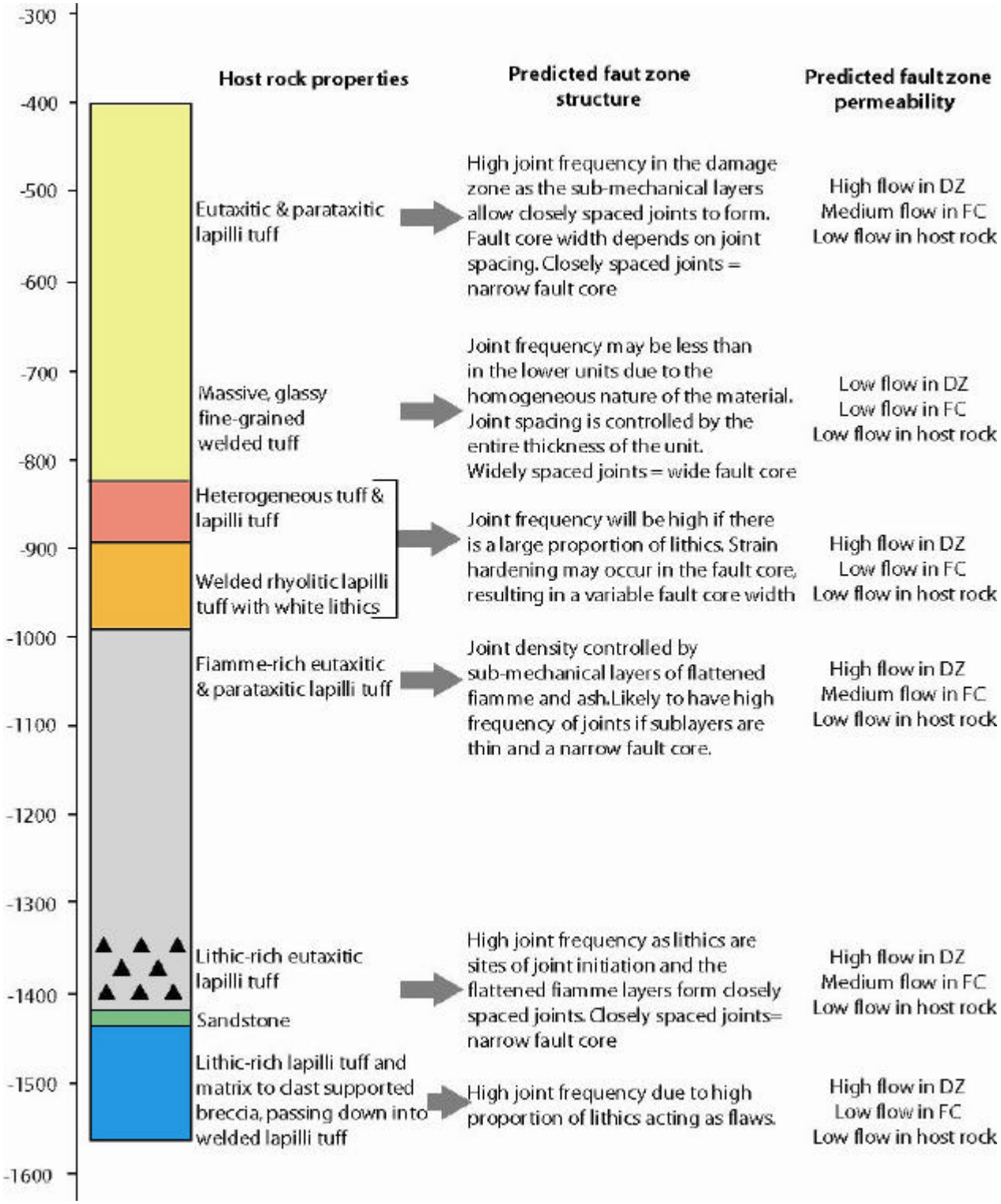

Figure 118: Stratigraphic log and host rock properties of Borrowdale Volcanic Group, Sellafield from the Nirex Report no 525

Predicted fault architectures are based on observations from this study. The eutaxitic and parataxitic fabrics will form sub-mechanical layers that control joint spacing as happens in ignimbrite B. The heterogeneous tuffs are similar to the A1 subunit in ignimbrite A. The inclusions will act as sites of joint initiation and thus joint frequency will be high in these units. High flow in the DZ is accommodated by high joint frequencies, flow in the FC depends on the amount of displacement on the fault, low offset faults in densely welded units with eutaxitic fabrics may be dominated by slabs with little gouge therefore acting as flow conduits.

7.6 Summary

Fault growth mechanisms, deformation processes and the resultant fault architecture depend on host rock lithology. Deformation processes differ both between lithologies and within the same lithology as a function of porosity, composition and competency. In this study I have demonstrated how differences in host rock petrophysical properties can affect the nature of the deformation structures and the resultant fault architecture. I have also shown how the host rock properties are of greater influence than displacement and that by examining the host rock composition and fabric we can make predictions about deformation structures and fault architecture.

The structural setting at the time of faulting also has important implications for the style of fault formed. In shear faults the linkage of primary joints via wing-cracks and cross-joints increase the connectivity of the fracture network in the fault damage zone. In dilational faults the damage zone is dominated by fault parallel joints with minimal linkage that accommodate fault parallel flow only. The hybrid failure mechanism also means the wide fault cores can be generated after minimal amounts of displacement. These small-offset faults are dominated by clasts with minimal amounts of gouge filling the spaces between clasts; therefore the fault will act as a flow pathway.

The variable nature of fault zone processes and architecture has implications for scaling relationships and the models based upon them. A conceptual fluid flow model based on crystalline rock will not be applicable to high porosity sandstones or poorly welded ignimbrite. Indeed ignimbrites show a range of deformation structures and fault types that mirror those in crystalline rock, sedimentary rock and unconsolidated sediments. The complexity possible in a single lithology indicates that scaling relationships encompassing all lithologies are over-simplified. Instead scaling relationships focussing on individual lithologies and encompassing all the possible variables within that lithology would be more useful in predicting fault architecture. This is what I have attempted to do in Figure 116; however this framework is far from complete. Observations of shear and compressional ignimbrite faults would establish if the same petrophysical properties control deformation structures in these settings as in extensional. Also if mechanical layer thickness controls joint spacing then densely welded, fiamme and lithic poor units without sub-mechanical layers should have joint spacing that correlates to the thickness of the whole unit. Data such as this would make the framework more accurate and also a sounder base from which to model fault architecture. A similar database for controls on fault deformation in granites, sandstones, mudstones etc would be more useful than the generalised scaling laws currently in use.

8

Conclusions and future work

8.1 Conclusions

Understanding fault zone architecture at shallow crustal levels is important to the development of fluid flow models in both the saturated and unsaturated zone. Previous models used to predict fault architecture have often been based on generalised scaling laws such as the fault thickness-displacement scaling relationship (Hull, 1988; Scholz, 1987). This relationship proposes that as displacement increases so too does fault core thickness. The linear increase in fault core thickness with displacement has been suggested to be due to wear and abrasion of the slip surfaces producing amounts of wear material proportional to the displacement amount of each slip event (Scholz, 1987). However this wear model does not take into account fault roughness or the cushioning affect of gouge. Fault wall asperities may be sheared off during displacement adding more to the wear material than predicted from the displacement amount (Childs et al., 1996; Power et al., 1988). As gouge forms the contact between the fault walls is reduced and, along with the gouge layer, lessens the abrasion of the two surfaces hence reducing the amount of wear material produced with increasing displacement. In this study I have developed two new models of fault initiation and growth based on moderately and densely ignimbrites in Gran Canaria, Spain. The faults examined range in displacement from centimetres to tens of metres and cut two different ignimbrite types. The fault populations allowed an examination of the evolution of the fault core with displacement and the affects host rock characteristics had on fault architecture. In these models host rock fabric, host rock composition and structural setting are the most important controlling factors and displacement is secondary.

Structural setting – Hybrid faulting

In my model faults initiate on pre-cursory joints formed by post-eruption caldera deflation. Deflation causes downsag in the centre of the caldera and extension of the caldera flanks thus forming joints. With continued extension the joints undergo vertical as well as horizontal displacement leading to the formation of hybrid faults. Slip can occur on a single joint into which material from the joint surfaces fall; generating a proto-fault core bounded by the joint surfaces

which are now the fault walls. Slip can also occur on two parallel joints; the parallel joints bound a pillar of rock that is fractured and brecciated in subsequent slip events and becomes the fault core material.

My model of fault initiation differs to previous models proposed for the formation of shear faults. In the shear fault model fault formation is achieved through the linkage of primary joints by secondary wing cracks and splay fractures. The formation of the secondary structures requires a rotation of the stress field that formed the primary joints or a rotation of the rock relevant to the stress field. In this study it has been observed that the joints and faults have similar orientations and both are orientated parallel to the caldera margin, suggesting the joints and faults formed synchronously in the same stress field. The faults formed by dilation of the joints followed by displacement along the joints. This hybrid failure mode, where there is both horizontal and vertical displacement as a result of the tensile environment caused by caldera deflation, has consequences for the resultant fault architecture. Firstly the fault and damage zone joints are parallel and there are no cross-joints or splay fractures formed as is the case in shear faults. Secondly, wide fault cores can form from small amounts of displacement (e.g. 85 cm wide fault core after 2.5 m of displacement) due to the dilational component of fault slip. In densely welded ignimbrites where slabs are incorporated into the core during fault growth small offset fault cores are dominated by large clasts. In shear faults small amounts of displacement produce minor amounts of gouge through abrasion of the slip surfaces.

Host rock petrophysical properties

In the faults examined neither fault core thickness nor damage zone joint frequency increase linearly with displacement. Within any one fault the fault core can have a range of thicknesses and sections with the highest offset fault often contain the narrowest fault core. Faults with more than twenty metres difference in accumulated offset have similar damage zone joint frequencies. These observations indicate that the evolution of the fault core is not controlled by displacement; instead the field data suggest that fault growth and architecture depends primarily on the petrophysical properties of the host rock.

In densely welded ignimbrites the fault core grows by the incorporation of slabs from joints adjacent to the faulted joint; thus the thickness of the slab dictates the amount the fault core grows by. The slab thickness is controlled by the joint spacing (closely spaced joints delineate thin slabs and widely spaced joints delineate thick slabs) therefore joint spacing controls fault core growth. Furthermore as slabs are incorporated from the joint surfaces the exposed surface becomes the new fault wall. The joint spacing is controlled by the ignimbrite fabric. Densely welded ignimbrites develop a foliation when fiamme are highly flattened, the flattened fiamme form layers that alternate with layers of ash. These layers act as sub-mechanical layers within the larger ignimbrite

unit and allow closely spaced joints to form that delineate thin slabs; hence a fault forming in such an area will have a narrow fault core. In areas without a foliation the joint spacing is controlled by the thickness of the ignimbrite unit and so joints are more widely spaced and fault core thickness would be greater.

In moderately welded ignimbrites fault core evolution is controlled by the composition of the unit. Faults cutting the friable ash-rich units with a homogeneous composition have narrow fault cores despite having large displacements; this suggests the material in the fault core is friable and easily deformed. This strain softening accommodates most of the subsequent displacement within the fault core thus inhibiting incorporation of new material and fault core growth. In this case the width of the fault core is dictated by the initial spacing of the faulted joints. Lower offset faults in competent ignimbrite units that contain a large proportion of fiamme and lithics have wider fault cores, suggesting that the material causes strain hardening in the fault core. The strain hardening inhibits displacement in the fault core and any further displacement causes fracturing of the adjacent host rock, thus incorporating material and widening the fault core.

The host rock petrophysical properties also affect deformation structures in the fault damage zone and the unfaulted host rock. I have mentioned how flattened layers of fiamme and ash in densely welded ignimbrites control joint frequency, however in moderately welded ignimbrites less flattened and circular fiamme also affect joint frequency. In moderately welded ignimbrites with larger proportions of inclusions such as fiamme and lithics joint frequency is greater than in more compositionally uniform ash-rich units. In the lithic rich material the contrast in mechanical properties between the inclusions and surrounding ash matrix concentrates stress at the inclusion-matrix interface. This area of high stress is a site of joint initiation and thus units with high proportions of fiamme and lithics have many joint initiation points and large numbers of joints. The proportion of ash and crystals also appears to affect how the material deforms. The A2 subunit in ignimbrite A is ash-rich and very friable; deformation bands are observed in both the host rock and in the core of the fault which cuts the unit. Ignimbrite X is crystal rich and indurated; joints form in the damage zone but deformation bands cut the ignimbrite X fault core material. These observations suggest that once the crystal-rich material is incorporated into the fault core it loses its competency and becomes a friable material similar to A2; deforming by cataclastic flow rather than brittle fracture as it did in the damage zone.

Fiamme affect the joint morphology both in fault damage zones and in unfaulted areas; joint morphology has consequences for fracture connectivity and flow pathways within the units, the morphology of the joints can also be used to predict the morphology of the fault walls. Vertical joints have been observed intersecting one end of a flattened fiamme becoming horizontal for the length of the fiamme, and returning to vertical upon exiting the opposite end of the fiamme. Other

vertical joints become sub-vertical as they pass upwards through a number of fiamme as each fiamme refracts the joint slightly. When fiamme are less flattened and more circular joints radiate outward from the fiamme boundary.

The affect the host rock petrophysical properties have on deformation structures also has implications in engineering terms. Ignimbrite A and B have similar elastic modulus (range from 8-13.8 Gpa) however fail in very different fashions. The joints in B are vertical forming regular blocks, the irregular joint pattern in ignimbrite A forms irregular shapes. As a building material ignimbrite B is more useful, it is easily quarried in large blocks along the natural joints and readily broken along the planes created by the flattened fiamme. The importance of ignimbrite B as a building material on the island of Gran Canaria is demonstrated by its common use in walls etc. In other areas globally where densely welded ignimbrites occur they may also be an important source of easily worked building material.

Fault hydraulic structure

The host rock petrophysical properties and stress regime under which faulting occurs has important implications for the fault hydraulic architecture. In the faults in this study the dilational faulting means that the damage zone is dominated by fault parallel joints. There is little connectivity between joints and therefore flow is likely to be dominantly fault parallel. In moderately welded units with circular fiamme that can form radial joint patterns there may be greater joint connectivity. Thus there is an increased likelihood of flow normal to the fault core. In the densely welded ignimbrites fault core growth via slab incorporation means that low offset faults are clast dominated with minor amounts of gouge in the clast interstices. These faults are highly permeable and could act as flow pathways. In the moderately welded units the fault core may be composed of a pillar of fractured rock, the permeability of the rock may be low and act as a flow barrier but the fractures could act as flow pathways. As displacement increases in the ash-rich units the width of the narrow fault core does not increase. This narrow core may act as a localised conduit. In the heterogeneous units the fault core is wider and composed of gouge and breccia suggesting it will be a barrier to fluid flow. In the crystal rich ignimbrites fault parallel joints form in the damage zone but the fault core is composed of fine material cut by deformation bands. In unsaturated conditions the deformation bands will behave as flow pathways facilitating across-fault flow.

In this study I have shown how host rock petrophysical properties and stress state at time of faulting influence fault initiation and evolution of the fault architecture. For the faults in Gran Canaria these parameters are the primary controls on fault evolution and not displacement. Scaling relationships such as fault thickness-displacement are not a reliable method on which to base predictions about fault architecture. A better approach would be to examine the composition and fabric of the host rock and consider how these will affect deformation structures and hence fault

zone architecture. The primary influences will differ between lithologies and in different structural environments; therefore scaling relationships based on individual lithologies and their behaviour in different stress regimes may be more useful in predicting fault architecture than a global scaling relationship. My model based on densely and moderately welded ignimbrites together with previous investigations of deformation in non-welded ignimbrites provides such a framework for predicting fault zone architecture in ignimbrites. Further data collection from faults in ignimbrites would help to establish if the controls on fault architecture I have suggested and the predictions based upon them are accurate and useful, and would also fill in the blanks of this framework.

8.2 Future work

Structural setting

My model and the factors influencing fault evolution is based on dilational faults. To ascertain if my method of predicting fault architecture is applicable to ignimbrites in all structural settings (shear, compressive) further field data on ignimbrite faults in different tectonic regimes and stress states is required. A more comprehensive data base would help to determine if the same factors control the deformation processes and deformation structures, and if the host rock properties such as foliation fabric and flaws have the same influence on fault zone evolution. Such a database may also help to identify the limits of my model; are there stress states at which the host rock properties no longer have an influence?

Comparing my model to dilational faults in lithologies with similar petrophysical properties such as poorly sorted sedimentary rocks may indicate if the host rock fabric has the same control on deformation structures. Would the lithics and layering in sedimentary rocks have the same influence on joint frequency, would a dilational fault core grow by the same mechanism of slab incorporation?

Host rock petrophysical properties

I have assumed that strain softening occurs in the fault core of ignimbrite A's ash-rich sub-units and that deformation is distributed across the fault core. A detailed petrographic investigation of the fault core gouge may identify shear fabrics, lineations or banding that would indicate localised deformation and preferential accommodation of strain in the core material. An analysis of the gouge would also indicate the presence of any clays such as smectite that were found by Gray et al. (2005). They suggested that smectite weakened the fault core and facilitated strain softening.

I have not examined the affect porosity or secondary crystallisation has on joint formation. Detailed SEM analysis of porosity in the different host rock ignimbrites may indicate what impact if any, the host rock porosity has on joint formation. Do the pores act as flaws and thus joint initiation points and at what level of porosity do deformation bands start to form? Secondary crystallisation reduces porosity and thus affects the strength of the material and the failure mechanism (brittle or cataclastic). However Wilson et al. (2003) suggested that the type of crystallisation phase affected the deformation structures. They suggested that when cristobalite rather than tridymite was the dominant secondary mineral precipitated in the pore spaces, joints formed in preference to deformation bands. Carrying out an XRD analysis of the host rock would identify what secondary vapour phases are present and what affect they have on joint formation.

Rather than using equivalent strength data from other authors I would carry out strength tests on the ignimbrite units in this study to obtain accurate mechanical data. Contrasts in strength between and within units may also act to influence deformation processes and fault evolution.

In order to determine if the flattened fiamme and ash layers are truly acting as individual mechanical layers it would be necessary to carry out a strength test (Point load test) on the fiamme and the ash material to see if there have different mechanical properties and behave as individual mechanical layers.

I have shown how the fiamme act as sites of joint initiation in ignimbrite A, how great does the mechanical contrast between the ash matrix and fiamme have to be in order to affect the stress concentration? If the fiamme are fully vapour phase altered and contain coarse crystals is there a greater contrast and thus greater stress concentration at the fiamme ash interface then if the fiamme were still glassy? Again strength testing of the fiamme and ash matrix would determine the mechanical properties of each and the level of contrast between them.

Preliminary computer simulations have been carried out examining the affect flattened fiamme have on joint propagation, two aspects have been examined – fiamme orientation and mechanical contrast between the fiamme and ash matrix (Soden and Moir, 2007). Initial results show that fiamme do affect the propagation path of joints. When flattened fiamme are slightly inclined a propagating vertical joint will cut straight through the fiamme and then propagate along the fiamme boundary. The joint resumes its vertical path on reaching the opposite fiamme tip but is displaced. Similar behaviour is observed when the mechanical contrast is increased between the fiamme and matrix. Further investigations on fiamme aspect ratio, number of fiamme and distribution of fiamme may display similar joint patterns to those observed in the field.

Fault hydraulic structure

I have suggested that the fault hydraulic architecture of these faults will be dominated by fault parallel fracture flow in the damage zone and that there will be limited fault normal flow. I have also suggested that the large offset well developed faults will act as barriers to flow within and across the fault. A detailed geochemical survey of the fault zone area is required to identify any chemical gradients that may be a result of fluid flow. If the fault core is acting as a barrier there could be differences in the chemistry on either side of the fault. If fault parallel flow is dominant in the damage zone the upper or lower part of the unit may be depleted or enriched depending on the direction of flow. Variations in chemistry along the fault core may be a result of the core acting as a flow conduit perhaps during slip events. Pump tests at subsurface sites could also be used to determine if there is either across-fault or along-fault flow.

Appendix A: Figure and sample locations

Barranco de Tauro

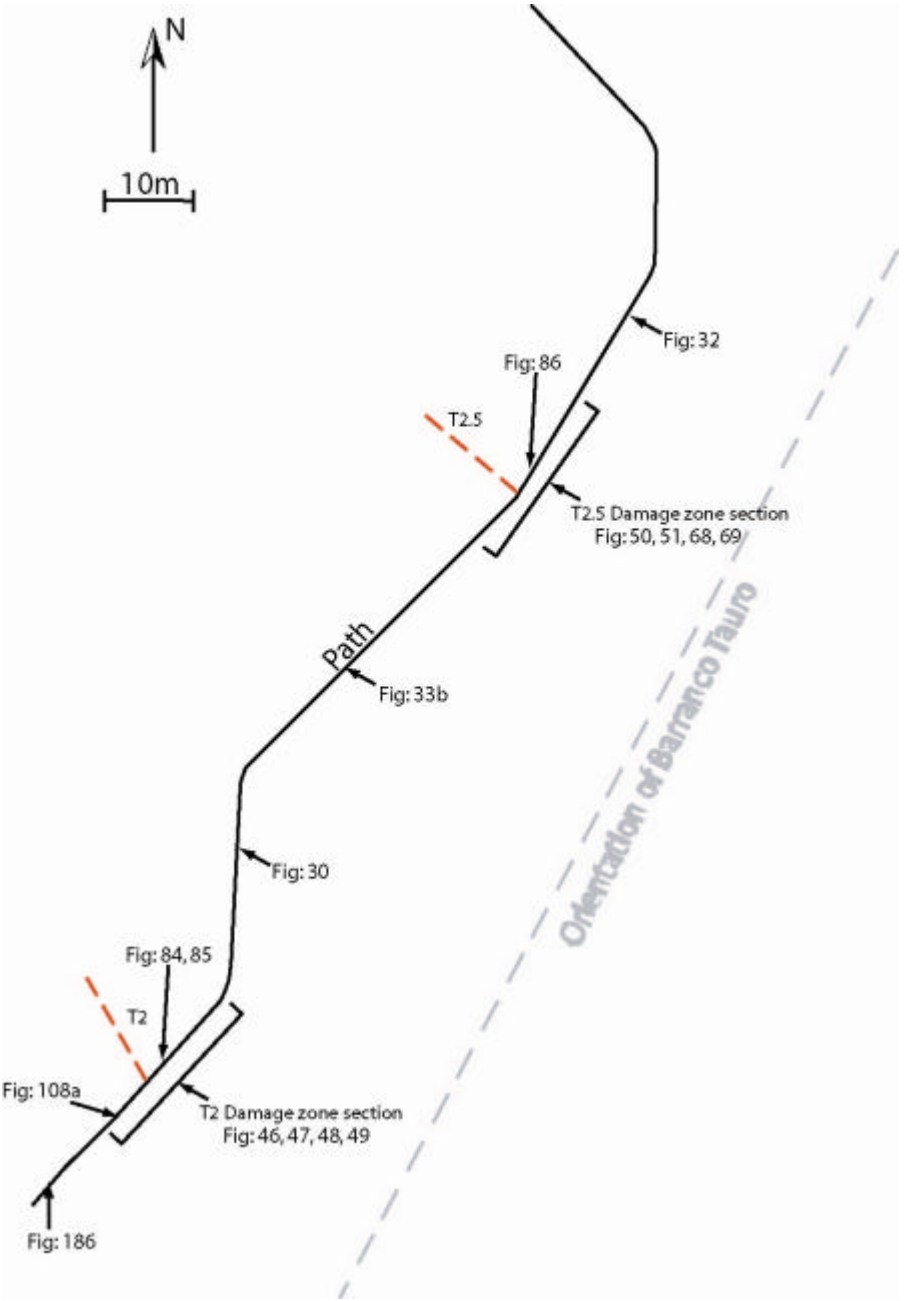

Plan view map of Barranco Tauro showing the location for each of the images taken at Tauro

Montana Cedro

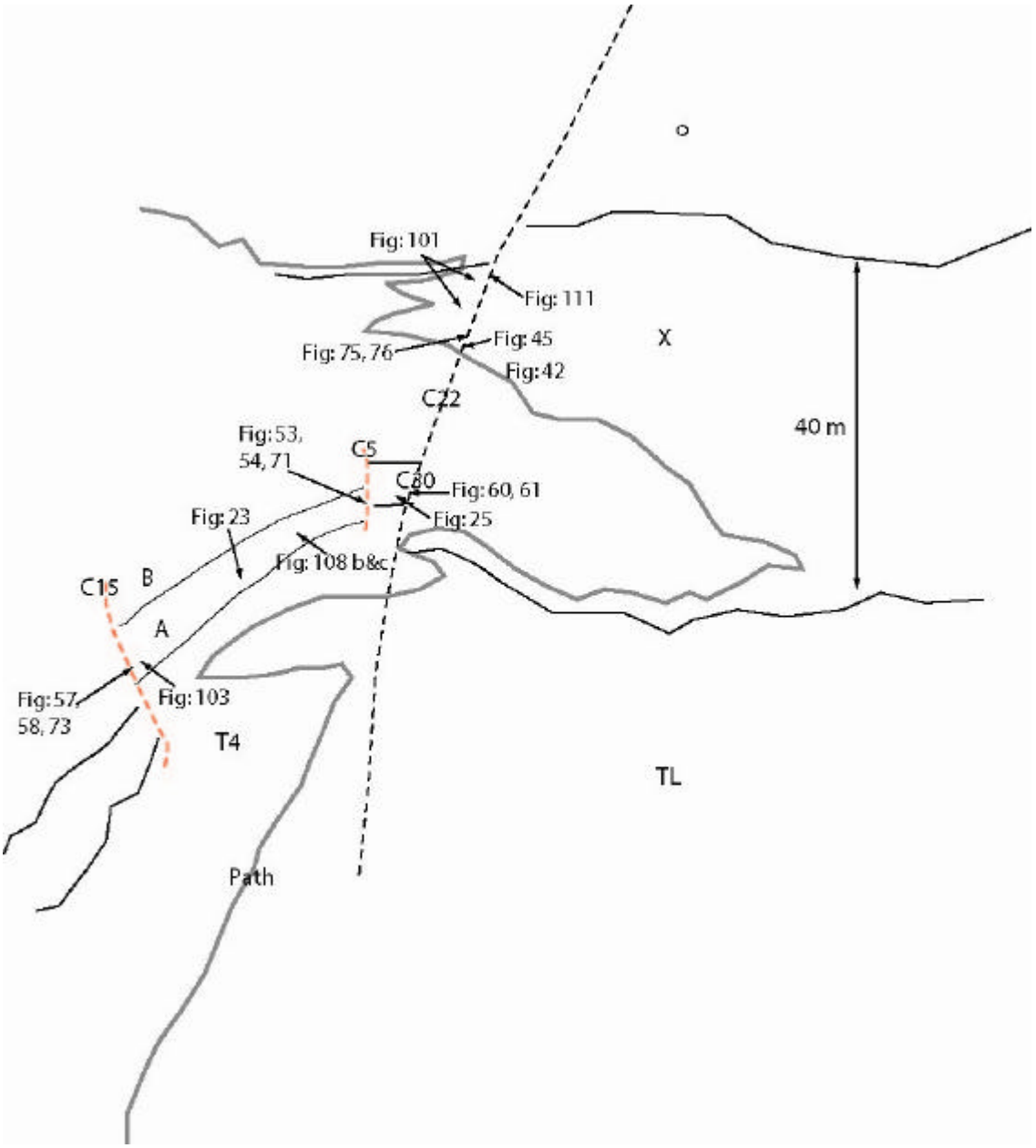

Line drawing of figure 19 showing the location for each of the images taken at Cedro

Los Frailes

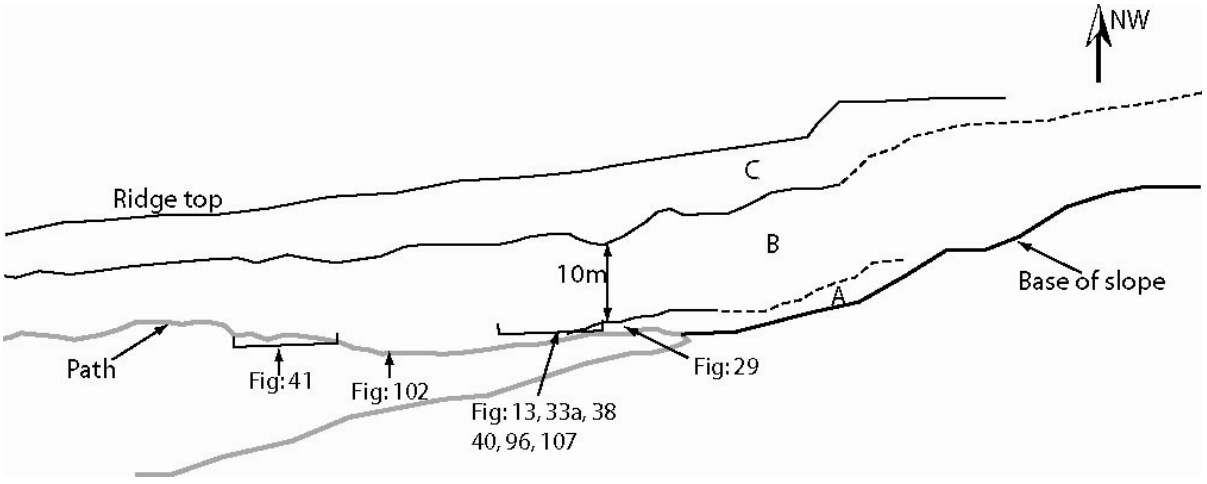

Line drawing of figure 17 showing the location for each of the images taken at Los Frailes

Thin section and SEM samples

Figure No:	Sample No:	Location:
15	ET-02-04	Tb2.5 footwall, 1 m above base of B, 15 cm from fault wall
15, 26	LF-07-06	Sample of A 230cm below contact with overlying B
24	MC-81-05	A1 protolith,2ms above base of unit along path
27	MC-03-04	A2 material adjacent to Ca30 fault wall
34	MC-127-05	B at path 5 m from Cb22 fault.
35, 98	LF-06-06	B from base in foliated area, have striations on the bottom surface
36	ET-01-04	Tauro base of B in footwall 3 m from Tb2.5
43	MC-150-05	X long stretch of path between C22 fault & far corner of path
55	MC-12-06	A2 adjacent to Ca30 fault core
98	LF-03-06	B 6m above base of B
104,105	MC-04-04	A1 3m from C15 fault wall
106	MC-121-05	Sample of X 3 m from fault wall.

Appendix B

How Thick is a Fault? Fault Displacement-Thickness Scaling Revisited

Zoe K. Shipton, Aisling M. Soden, James D. Kirkpatrick
Department of Geographical and Earth Sciences, University of Glasgow, Glasgow Scotland
Aileen M. Bright
Department of Geology, Trinity College, Dublin, Ireland
Rebecca J. Lunn
Department of Civil Engineering, University of Strathclyde, Glasgow, Scotland

Fault zone thickness is an important parameter for many seismological models. We present three new fault thickness datasets from different tectonic settings and host rock types. Individual fault zone components (i.e., principal slip zones, fault core, damage zone) display distinct displacement-thickness scaling relationships. Fault component thickness is dependent on the type of deformation elements (e.g., open fractures, gouge, and breccia) that accommodate strain, the host lithology, and the geometry of pre-existing structures. A compilation of published fault displacement-thickness data shows a positive trend over seven orders of magnitude, but with three orders of magnitude scatter at a single displacement value. Rather than applying a single power-law scaling relationship to all fault thickness data, it is more appropriate and useful to seek separate scaling relationships for each fault zone component and to understand the controls on such scaling.

INTRODUCTION

Faults are generally composed of three components: one or more principal slip zones (PSZ, also referred to as principal displacement zones or principal slip surfaces) sitting within a fault core (FC) where most of the displacement is accommodated, surrounded by an associated zone of fractures known as the damage zone (DZ) [*Caine et al.*, 1996; *Schulz and Evans*, 1998; *Chester et al.*, 2004]. Although some co-seismic slip may occur within the DZ it is likely that the majority of earthquake slip occurs within the FC and PSZ. Many processes that may explain the dynamic reduction of shear resistance during earthquakes require that the zone that slips during an earthquake has a specific thickness. Elastohydrodynamic fault lubrication could occur between surfaces less than 1 to 5 mm apart [*Brodsky and Kanamori*, 2001]. Frictional melting and transient thermal pressurization of fluids requires that the PSZ is less than centimeters in thickness [*Bizzarri and Cocco*, 2006; *Wibberley and Shimamoto*, 2005]. Conversely the acoustic fluidization model of *Melosh* [1996] requires fluidization of a zone 1 to 20 m thick. Damage zone thickness will constrain the magnitude of potential energy sinks due to creation of new fractures or slip along existing fractures around a dynamically slipping fault [*Poliakov et al.*, 2002; *Dalguer et al.*, 2003; *Andrews*, 2005]. Geophysical data also image different parts of the PSZ/FC/DZ system. Anomalous low resistivity zones up to 1 km thick across the San Andreas fault are attributed to fluid-filled fractures in the DZ [*Unsworth et al.*, 1999]. Conversely, co-location of aftershocks [*McGuire and Ben-Zion*, 2005] and microearthquake distribution [*Nadeau and McEvilly*, 1997] shows that the region that slips during an earthquake (the PSZ) may be as narrow as 1–5 m.

In this paper we present three new displacement-thickness datasets, from fault populations in three different lithologies. Fault core and DZ thickness have been measured at points where true displacement can be calculated from slip vector orientations and the separation of markers across the fault.

We distinguish here between *displacement* measured on an exhumed fault and the *slip* that occurs in an earthquake that ruptures along a fault. Fault zone components are distinguished on the basis of the type of deformation elements that they contain (structures within the fault such as gouge, fractures, breccia, deformation bands) and the spatial distribution and density of those deformation elements. We compare our data to a compilation of fault "thickness" data from previous studies of faults in a wide range of host rock types and tectonic settings. Although a correlation apparently exists between thickness and displacement, we

argue that a single power law relationship is not appropriate, and is not useful for describing or predicting fault zone thicknesses. Distinct thickness-displacement relationships can arise depending on the deformation elements dominant in different lithologies, at different times in the development of a single fault, and under different deformation conditions.

SHALLOW NORMAL FAULTS IN SANDSTONE

Faults in sandstone with porosity greater than 10% are dominated by deformation elements called deformation bands [see review in *Schultz and Siddharthan*, 2005]. Deformation bands are mm-thick tabular zones of grain crushing with mm of displacement. Increased displacement is accommodated by the addition of more bands to a zone until a slip-surface nucleates. Once nucleated, slip-surfaces propagate, often along the edges of zones of bands, to forma through-going slip-surface (PSZ) which can accommodate meters to kilometers of total displacement. The Big Hole normal fault in central Utah developed in the 20-24% porosity Navajo Sandstone at overburden depths of 1.5 to 3.0 km [*Shipton and Cowie*, 2001]. The fault core consists of amalgamated deformation bands and occasional breccias. At any point on the fault the FC thickness varies by an order of magnitude (Figure 1), but it tends to be thicker at areas of fault linkage [*Shipton and Cowie*, 2001].The DZ surrounding the FC consists of deformation bands with occasional short segments of slip-surfaces [*Shipton and Cowie*, 2001]. There is a positive correlation between DZ thickness and displacement, but there is no change in the mean thickness of the fault core as fault displacement increases (Figure 1).

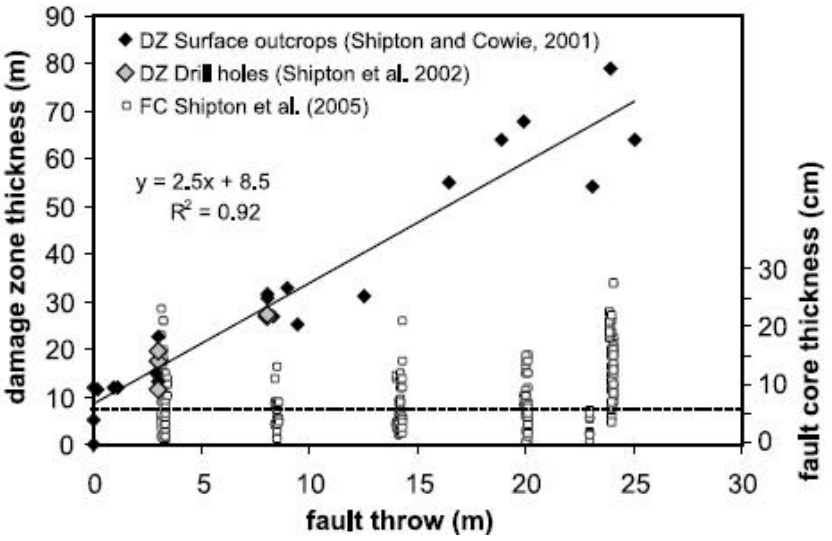

Figure 1. Damage zone and fault core thickness for the Big Hole normal fault, Utah, plotted against the vertical displacement (fault throw) of the top of the Navajo Sandstone. The horizontal damage zone thickness is measured from an envelope that surrounds all the damage zone deformation elements. The solid line shows a linear regression through the damage zone thickness data. Fault core thickness measurements were taken every 30 cm along six 10to 25 m-long transects along the PSZ. Note that there is an order of magnitude scatter in thickness at each of the six locations. The dotted line shows the mean fault core thickness (6 cm) for all the locations.

REACTIVATED NORMAL FAULTS IN IGNIMBRITES

Cycles of eruption on the volcanic island of Gran Canaria deposited numerous ignimbrite flows across active normal fault scarps [*Troll et al.*, 2002]. Ignimbrites are deposited from flows of hot ash, crystals and pumice fragments and are classified by the degree of welding (intensity of compaction and fusion that occurs during deposition). More welded ignimbrites are denser and have lower porosity. Data in Figure 2 are from normal growth faults that cut several ignimbrites with different mineralogies and degrees of welding.

Only one of the studied faults contains a recognizable PSZ. In the remaining faults, deformation is distributed within the FC. The deformation elements in the FC are gouge and/or breccia. In high- to moderately-welded ignimbrites, the DZ is defined by intense jointing, with joint density decreasing away from the FC. In poorly welded ignimbrites the damage zone contains deformation bands. The FC thickness is dependent on joint

spacing in the DZ: wide fault cores coincide with widely spaced joints regardless of displacement. Damage zone joint density is controlled by two main factors. Thin ignimbrites have closer spaced joints than thicker ignimbrites so each ignimbrite may be acting as a mechanical layer that controls joint spacing [see *Baiand Pollard* 2000]. Ignimbrites with a lower proportion of pumice clasts and pores tend to have DZs containing fewer joints. *Moon* [1993] and *Wilson et al.* [2003] suggest that the size, proportion and elastic moduli of heterogeneities such as pumice clasts and pore spaces influence stress concentrations and therefore joint density.

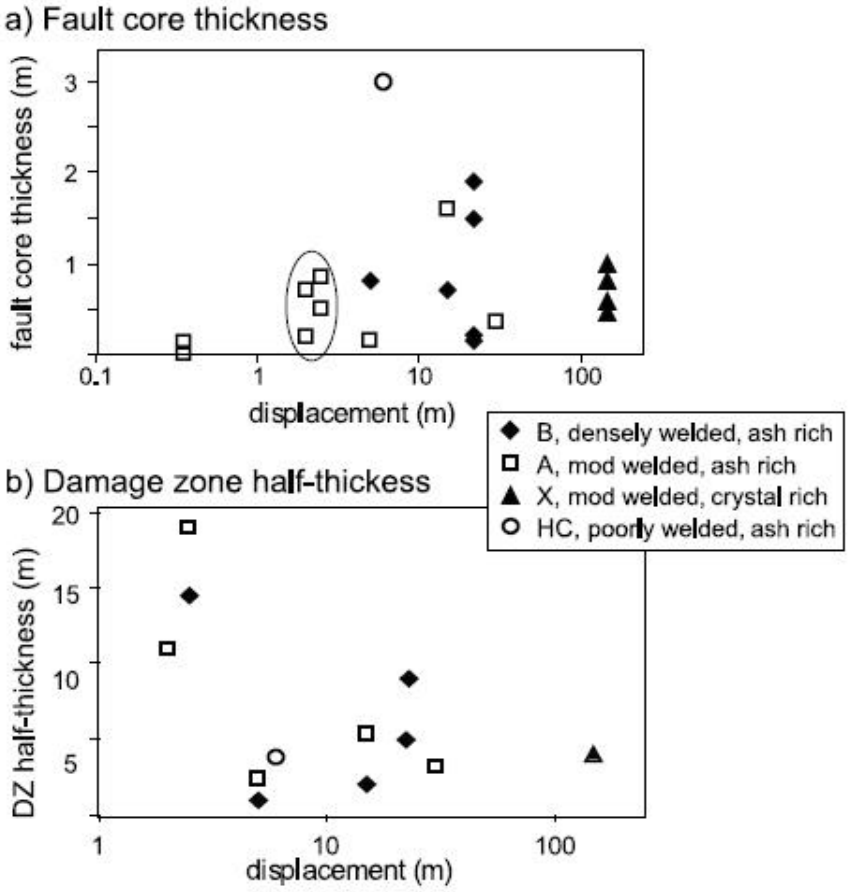

Figure 2. Log-normal plots of a) fault core thickness and b) damage zone half-width against displacement for normal faults cutting ignimbrite units of varying composition from Gran Canaria, Spain. Fault core and damage zone thickness were measured from cross sections through a number of normal fault zones with displacement values defined by the separation of ignimbrite packages. At many sites the faults juxtapose different ignimbrite units so only half of the DZ thickness can be measured (from the FC to one edge of the DZ). However, the full thickness of the FC is measured at each location. The measurements circled in a) are taken from locations1.5m apart along the same fault, which shows that the FC thickness changes significantly down-dip over short distances.

STRIKE-SLIP FAULTS IN GRANITES FROM SEISMOGENIC DEPTHS

Strike-slip faults cut granodiorite at many localities in the central Sierra Nevada, California. Isotopic dating of micas formed in fault gouge coupled with amphibole geobarometry suggests that some of the faults in the area were active near the base of the seismogenic zone [*Pachell and Evans*, 2002]. Faults in the Mount Abbot area nucleated on preexisting cooling joints [*Segall and Pollard*, 1983]. Single reactivated joints linked, through dilational splay fractures developed at their tips, into mature 'compound fault zones' [*Martel*, 1990]. Compound fault zones are defined by two parallel fault cores bounding a zone of highly fractured host rock. In the Granite Pass area (*Evans et al.* 2000) some of the faults developed according to *Martel's* [1990] model, but others have a FC defined by a single zone of cataclasite and ultracataclasite. The damage zone of both fault styles consists of open mode fractures and minor faults, especially around points where large faults linked (see Figures 4 and 5in *Evans et al.*, 2000).For reactivated joints not linked to other small faults, the FC is defined by a narrow, mineral-filled sheared joint. The thickness of these sheared joints does not change with displacements up to 1m (Figure 3). For larger faults with single cataclasite FCs, the thickness increases

with displacement. For compound fault zones, both the total thickness of the two bounding faults, and the distance between the bounding faults, increases with displacement.

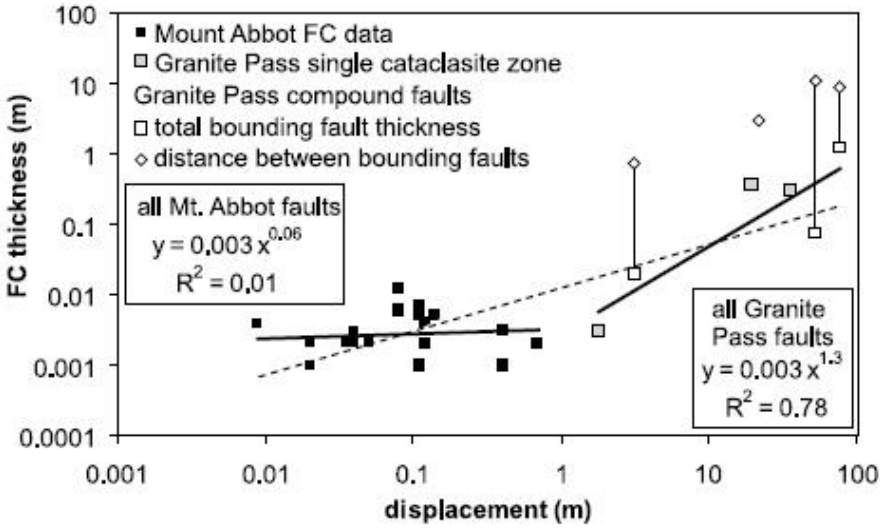

Figure 3. Log-log plot of fault core thickness against displacement from the Sierra Nevada, California showing two distinct trends. Strike-slip displacement was defined by the separation of dykes. Faults with displacement <1m from the Mount Abbot area show that thickness does not increase with displacement. Thickness increases with displacement for longer faults in the Granite Pass area where some of the faults are compound fault zones in the sense of *Martel* [1990] (open symbols) and some of the faults have a single cataclasite and ultracataclasite FC (grey squares). For compound fault zones, diamonds show the distance between the bounding faults and squares show the total thickness of the two bounding faults. Vertical lines connect data collected from the same fault. Note that a single power-law for this dataset (dashed line) would underestimate thickness for faults with displacement
<10 cm and >10 m.

DISCUSSION AND CONCLUSIONS

The existence of a scaling relationship between thickness and displacement would allow predictions to be made of the thickness of fault zones at seismogenic depths. *Robertson* [1983], *Scholz* [1987] and *Hull* [1988] suggested that a linear scaling relationship exists between fault thickness and displacement. However *Blenkinsop* [1989] and *Evans* [1990] argued that this relationship was spurious as it included fault thickness data from many fault populations in a wide range of rock types. These authors also stress that the data presented by *Scholz* [1987] and *Hull* [1988] often did not explicitly state how the net displacement was determined and in what direction thickness was measured relative to the slip vector.

thickness of fault zones at seismogenic depths. *Robertson* [1983], *Scholz* [1987] and *Hull* [1988] suggested that a linear scaling relationship exists between fault thickness and displacement. However *Blenkinsop* [1989] and *Evans* [1990] argued that this relationship was spurious as it included fault thickness data from many fault populations in a wide range of rock types. These authors also stress that the data presented by *Scholz* [1987] and *Hull* [1988] often did not explicitly state how the net displacement was determined and in what direction thickness was measured relative to the slip vector. The type of deformation elements present in a fault zone is highly dependent on the lithology being deformed and the pressure, temperature and strain rate during deformation. There are no standard criteria to define fault components across all fault zones, because the definition of FC and DZ depends on the deformation elements that occur within the fault zone. This leads to a degree of subjectivity in the definition of the boundaries of the fault core and damage zone. In fact, *Schultz and Evans* [1998, their figure16] showed that the width of a single fault's DZ can vary by an order of magnitude depending on which deformation elements are used to define the DZ. Furthermore, the DZ is often asymmetric around the FC and PSZ [e.g., *Shipton and Cowie*, 2001; *Heermance et al.*, 2003; *Dor et al.*, 2005]. The dominant deformation elements within each part of the fault zone may also change over time, for instance due to varying stress conditions [*Knipe and Lloyd*, 1994] or rock rheology [*Johansen et al*., 2005]. *Power et al.* [1988] suggested that smoothing of rough surfaces as displacement accumulated could lead to a steady state FC thickness. However a fault with self-similar roughness samples asperities with larger amplitudes as displacement increases, so real faults may not reach a steady-state thickness [*Power et al*., 1988].Often the FC contains distinct deformation elements from the DZ. For instance, the DZ of faults in

high porosity sandstones typically contain deformation bands with subsidiary slip surfaces, whereas the FC is characterized by a through going slip surface surrounded by amalgamated deformation bands, gouge and breccia. *Shipton and Cowie* [2003] suggest that bulk strain hardening results in an increase of DZ thickness as the number of displacement events at a point on the fault increases. Conversely, the FC is dominated by linkage of DZ faults with the main FC resulting in a highly heterogeneous FC thickness along strike, which has no simple relationship with displacement. Different lithologies may deform with different deformation elements under the same stress state, strain rate etc. In the dataset presented in Figure 2, ignimbrite lithology and fabric exert a strong control on DZ thickness. In heterogeneous moderately-welded (unit A) to highly-welded (unit B) ignimbrites the FC is formed when slabs between joints are rotated and broken down to form breccia and gouge. Joint spacing will therefore control the width of the slabs and ultimately the amount of wear material formed in the FC. In these heterogeneous units, the thickness of the joint-dominated DZ decreases with displacement. However these units have only a weak increase of FC thickness with displacement. The more homogeneous unit (unit X) permits more bulk deformation at the grain scale, limiting joint formation and therefore the extent of the FC and Zither geometry of pre-existing structures also exerts a strong control on fault geometry. The Sierra Nevada faults nucleated on pre-existing joints, and FC thickness for the small faults (<1m displacement) is controlled by the width of the pre-existing opening mode fractures. Once the faults start to link up to form larger fault zones, more material is progressively included into the FC, resulting in a positive scaling of thickness and displacement. The change in deformation process from joint reactivation in the small faults, to linkage of reactivated joints and cataclasis in the large faults, produces a corresponding change in the scaling of FC thickness and displacement.

Given the dependence of fault thickness on so many interrelated factors, we suggest that a single displacement-thickness correlation is not appropriate for making predictions about fault zone properties. Figure 4 shows a compilation of fault displacement-thickness data from sixteen fault populations, including data from *Scholz* [1987] and *Hull* [1988]. The thickness-displacement dataset in Figure 4 is available in the CD-ROM attached to this volume. Although an overall positive trend can be observed over seven orders of magnitude, there is more than three orders of magnitude scatter at any value of displacement. The relationships for individual datasets are often not well described by the best fit line to the overall trend. Towards the top of Figure 4, two DZ datasets from sandstone are clearly not well predicted by the best fit line, which would predict DZ thicknesses in sandstone at small displacements (10cm or less) at least four orders of magnitude too small. Three relationships for granite are also shown on Figure 4. Whilst the individual datasets are not too far from the overall trend line, their gradients vary significantly. Consequently, predictions based on the site-specific fault thickness data for a displacement of ~10m would vary by at least two orders of magnitude, with only the pseudotachylyte prediction being close to the overall trend line. Although many of the fault datasets in Figure 4 are not from unequivocally seismogenic faults [i.e., do not host pseudotachylytes, see *Cowan* 1999], this compilation is still useful to show that *global* fault zone thickness correlations should not be used to understand earthquake processes. Different fault zone components will host different active processes during an earthquake event.

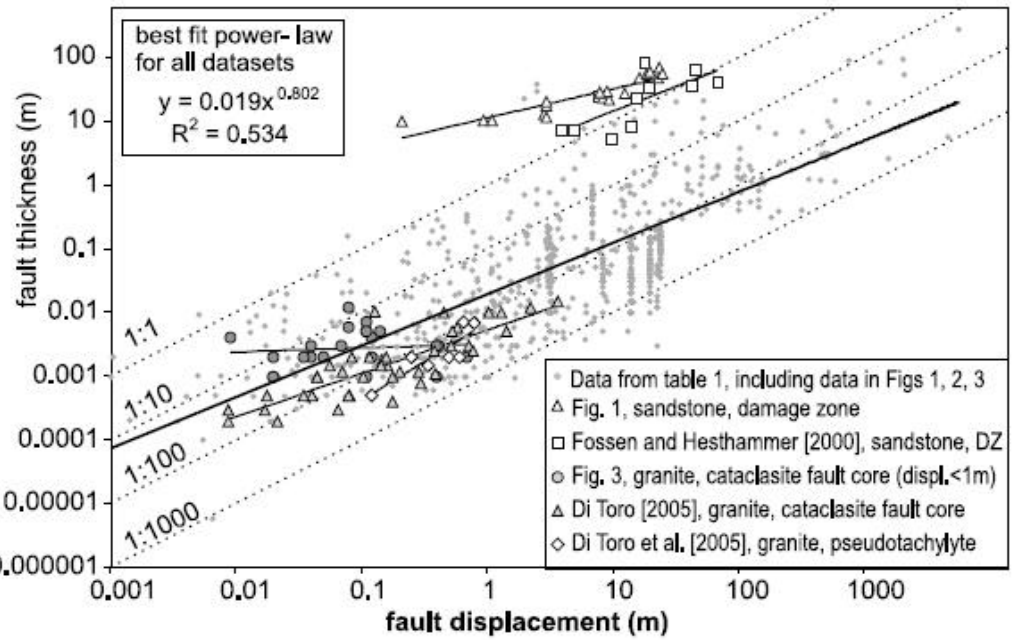

Figure 4. Log-log plot of a compilation of 16 fault thickness datasets reported in the literature including the data used by *Hull* [1988], and the three datasets in this paper. In many reported datasets no distinction is made between FC and DZ thickness. Five individual datasets are highlighted with their best-fit power laws to emphasize that the trend for the global dataset rarely describes that for individual datasets. Table 1 is available in the CD-ROM attached to this volume.

The thickness of zone of active slip during an earthquake (the PSZ and perhaps the FC) will have important controls on slip-weakening mechanisms and energy loss on the slip plane. The thickness of the damage zone may affect the magnitude of the energy sink that the damage zone provides and control the rupture propagation along the fault surface. Future field studies should explicitly state which deformation elements are used to define the principal slip zone, fault core and damage zone, and to measure the thickness of each of these independently. It would be highly valuable to undertake studies of the controls on fault thickness within seismogenic faults that have developed by specific faulting processes, and under different deformation conditions. Fault structures from exhumed outcrops will contain deformation elements created during seismic slip but also during the interseismic period [*Cowan*, 1999], both of which will contribute to the final displacement on an exhumed fault. Further studies are needed to recognize features which might allow us, in the absence of pseudotachylytes, to distinguish which parts of a fault zone were formed during seismic ruptures and which were produced a seismically.

Acknowledgments. Fabrizio Storti, Rick Sibson and Giulio DiToro gave constructive reviews of this paper. AMS and JDK are supported by University of Glasgow graduate scholarships; AMB was supported by Enterprise Ireland grant SC/02/261 Thanks to the US National Park Service and the USDA Forest Service for permission to work in the Sierra Nevada, to Valentin Troll for guidance on Gran Canaria, and Jim Evans, Tom Blenkinsop, Emily Brodsky and Rachel Abercrombie for valuable discussions.

REFERENCES

Andrews D. J. (2005), Rupture dynamics with energy loss outside the slip zone, *J. Geophys. Res., 110,* B01307, doi:10.1029/2004JB003191.

Bai, T. and D. D. Pollard (2000), Closely spaced fractures in layered rocks: initiation mechanism and propagation kinematics, *J. Struct. Geol., 22,* 1409–1425.

Blenkinsop, T. B. (1989), Thickness-displacement relationships for deformation zones: Discussion, *J. Struct. Geol., 11,* 1051–1054.

Bizzarri, A., and M. Cocco (2006), A thermal pressurization model for the spontaneous dynamic rupture propagation on a three-dimensional fault: 1. Methodological approach, *J. Geophys. Res., 111,* B05303,doi:10.1029/2005JB003862.

Caine, J. S., J. P. Evans, and C. B. Forster (1996), Fault zone architecture and permeability structure, *Geology, 24*, 1025–1028.

Chester, F. M., J. S. Chester, D. L. Kirschner, S. E. Schulz, and J. P. Evans(2004), Structure of large-displacement strike-slip fault zones in the brittle continental crust. In: *Rheology and Deformation in the Lithosphereat Continental Margins*, edited by Karner, G. D., B. Taylor, N. W. Driscoll, and D. L. Kohlstedt, Columbia University Press, New York.

Dalguer L. A., K. Irikura, and J. D. Riera (2003), Simulation of tensile crack generation by three-dimensional dynamic shear rupture propagation during an earthquake, *J. Geophys. Res., 108*(B3), 2144, doi:10.1029/2001JB001738.

Dor O., T. K. Rockwell and Y. Ben-Zion, (2006), Geologic observations of damage asymmetry in the structure of the San Jacinto, San Andreas and Punchbowl faults in southern California: A possible indicator for preferred rupture propagation direction, *Pure Appl. Geophys., 163*,301–349, DOI 10.1007/s00024-005-0023-9.

Evans, J. P. (1990), Thickness-displacement relationships for fault zones,*J. Struct. Geol., 12*, 1061–1065.

Evans, J. P., Z. K. Shipton, M. A. Pachell, S. J. Lim and K. Robeson (2000),The structure and composition of exhumed faults, and their implications for seismic processes. In: *Proc. 3rd Conf. on Tectonic Problems of the San Andreas Fault System.* Bokelmann, G. and Kovach, R.L. (eds.) Stanford University Publications, Geological Sciences 21, 67–81.

Heermance, R., Z. K. Shipton, and J. P. Evans (2003), Fault structure control on fault slip and ground motion during the 1999 rupture of the Chelungpu fault, Taiwan, *Bull. Seis.l Soc. Am., 93*, 1034–1050.

Hull, J. (1988), Thickness-displacement relationships for deformation zones, *J. Struct. Geol., 10*, 431–435.

Johansen, T. E. S., H. Fossen, and R. Kluge (2005), The impact of synfaulting porosity reduction on damage zone architecture in porous sandstone: an outcrop example from the Moab Fault, Utah, *J. Struct.Geol., 27*, 1469–1485.

Knipe, R. J., and G. E. Lloyd (1994), Microstructural analysis of faulting in quartzite, Assynt, NW Scotland: Implications for fault zone evolution, *Pure Appl. Geophys., 143*, 229–254.

Martel, S. J. (1990), Formation of Compound Strike-Slip-Fault Zones, Mount Abbot Quadrangle, California, *J. Struct. Geol., 12*, 869.

Melosh H. J. (1996), Dynamical weakening of faults by acoustic fluidization,*Nature, 379*, 601–606.

McGuire, J., and Y. Ben-Zion (2005), High-resolution imaging of theBear Valley section of the San Andreas fault at seismogenic depths with fault-zone head waves and relocated seismicity, *Geophys. J. Int., 163*, 152–164.

Moon, V. G. (1993), Geotechnical characteristics of ignimbrite: A soft pyroclastic rock type, *Eng. Geol., 35*, 33–45.

Nadeau, R. M., and T. V. McEvilly (1997), Seismic studies at Parkfield; V, Characteristic microearthquake sequences as fault-zone drilling targets, *Bull. Seis Soc Am., 87*, 1463–1472

Pachell, M. A., and J. P. Evans (2002), Growth, linkage, and termination processes of a 10-km-long strike-slip fault in jointed granite: the Gemini fault zone, Sierra Nevada, California, *J. Struct. Geol., 24*, 1903–1924.

Poliakov, A. N. B., R. Dmowska, and J. R. Rice (2002), Dynamic shear rupture interactions with fault bends and off-axis secondary faulting, *J. Geophys. Res., 107* (B11), 2295, doi:10.1029/2001JB000572.

Power, W. L., T. E. Tullis, and J. D. Weeks (1988), Roughness and wear during brittle faulting, *J. Geophys. Res., 98* (B12), 15268–15278.

Robertson, E. C. (1983), Relationship of fault displacement to gouge and breccia thickness, *American Institute of Mining Engineers Transactions, 274*, 1426–1432.

Scholz, C. H. (1987), Wear and gouge formation in brittle faulting, *Geology, 15*, 493–495.
Schulz, S. E., and J. P. Evans (1998), Spatial variability in microscopic deformation and composition of the Punchbowl fault, southern California: implications for mechanisms, fluid-rock interaction, and fault

morphology, *Tectonophys., 295*, 223–244.

Schultz, R. A. and R. Siddharthan (2005), A general framework for the occurrence and faulting of deformation bands in porous granular rocks. *Tectonophys. 411*, 1–18.

Segall, P., and D. D. Pollard (1983), Nucleation and Growth of Strike Slip Faults in Granite, *J. Geophys. Res., 88*, 555–568.

Shipton Z. K. and P. A. Cowie (2001), Damage zone and slip-surface evolution over ⌈m to km scales in high-porosity Navajo sandstone, Utah, *J. Struct. Geol., 23*, 1825–1844.

Shipton, Z. K., and P. A. Cowie (2003), A conceptual model for the origin of fault damage zone structures in high-porosity sandstone, *J. Struct. Geol., 25*, 333–345.

Sibson, R. H. (2003), Thickness of the seismic slip zone, *Bull. Seis. Soc. Am, 93*, 11 69–11 78.

Troll, V. R., T. R. Walter, and H.-U. Schmincke (2002), Cyclic caldera collapse: Piston or piecemeal subsidence? Field and experimental evidence, *Geology, 30*, 135–138.

Unsworth, M, G. Egbert, and J. Booker (1999), High-resolution electromagnetic imaging of the San Andreas fault in central California, *J. Geophys. Res., 104* (B1), 11 31–11 50, 10.1029/98JB01755.

Wibberley, C. A. J. and T. Shimamoto (2005) Earthquake slip weakening and asperities explained by thermal pressurization, *Nature 436* doi:10.1038/nature03901

Wilson, J. E., L. B. Goodwin, and C. J. Lewis (2003), Deformation bands in non-welded ignimbrites: Petrophysical controls on fault zone deformation and evidence of preferential f luid f low, *Geology, 31*, 837–840.

Aileen M. Bright, Department of Geology, Trinity College, Dublin 2, Ireland
James D. Kirkpatrick, Zoe K. Shipton*, Aisling M. Soden, Department of Geographical and Earth Sciences, University of Glasgow, Glasgow G12 8QQ, Scotland * zoe.shipton@ges.gla.ac.uk
Rebecca J. Lunn, Department of Civil Engineering, University of Strathclyde, Glasgow, G4 ONG, Scotland

References

Acocella, V., Cifelli, F., and Funiciello, R., 2000, Analogue models of collapse calderas and resurgent domes: Journal of Volcanology and Geothermal Research, v. 104, p. 81-96.

Acocella, V., Korme, T., and Salvini, F., 2003, Formation of normal faults along the axial zone of the Ethiopian Rift: Journal of Structural Geology, v. 25, p. 503-513.

Angelier, J., 1994, Fault slip analysis and paleostress reconstruction, Pergamom Press, Oxford, 53-100 p.

Antonellini, M., and Aydin, A., 1994, Effect Of Faulting On Fluid-Flow In Porous Sandstones - Petrophysical Properties: AAPG Bulletin-American Association Of Petroleum Geologists, v. 78, p. 355-377.

—, 1995, Effect of faulting on fluid flow in porous sandstone: Geometry and spatial distribution: AAPG Bulletin, v. 79, p. 642-671.

Aydin, A., 1978, Small faults formed as deformation bands in sandstone Pure and Applied Geophysics, v. 116, p. 913-930.

Aydin, A., and Johnson, A.M., 1978, Development of faults as zones of deformation bands and as slip surfaces in sandstone Pure and Applied Geophysics v. 116, p. 931-942

Bai, T., Maerten, L., Gross, M.R., and Aydin, A., 2002, Orthogonal cross joints: do they imply a regional stress rotation?: Journal of Structural Geology, v. 24, p. 77-88.

Bai, T., and Pollard, D.D., 2000, Fracture spacing in layered rocks: a new explanation based on the stress transition: Journal of Structural Geology, v. 22, p. 43-57.

Becker, A., and Gross, M.R., 1996, Mechanism for joint saturation in mechanically layered rocks: an example from southern Israel: Tectonophysics, v. 257, p. 223-237.

Billi, A., and Storti, F., 2004, Fractal distribution of particle size in carbonate cataclastic rocks from the core of a regional strike-slip fault zone: Tectonophysics, v. 384, p. 115-128.

Birkholzer, J., Guomin, L., Tsang, C.-F., and Tsang, Y., 1999, Modeling studies and analysis of seepage into drifts at Yucca Mountain: Journal of Contaminant Hydrology, v. 38, p. 349-384.

Blenkinsop, T.G., 1989, Thickness-displacement relationships for defromation zones: Discussion: Journal of Structural Geology, v. 11, p. 1051-1054.

—, 1991, Cataclasis and processes of particle size reduction: Pure and Applied Geophysics, v. 136, p. 59-86.

Bogaard, P., Schmincke, H.-U., Freundt, A., Hall, C.M., and York, D., 1988, Eruption ages and magma supply rates during the miocene evolution of Gran Canaria: Naturwissenschaften, v. 75, p. 616-617.

Branney, M.J., 1995, Downsag and extension at calderas: new perspectives on collapse geometries from ice-melt, mining, and volcanic subsidence: Bulletin of Volcanology, v. 57, p. 303-318.

Bruhn, R.L., Parry, W.T., Yonkee, W.A., and Thompson, T., 1994, Fracturing And Hydrothermal Alteration In Normal-Fault Zones: Pure And Applied Geophysics, v. 142, p. 609-644.

Caine, J.S., Evans, J.P., and Forster, C.B., 1996, Fault zone architecture and permeability structure: Geology, v. 24, p. 1025-1028.

Caine, J.S., and Forster, C.B., 1999, Fault zone architecture and fluid flow: Insights from field data and numerical modeling in Faults and Subsurface Fluid Flow in the Shallow Crust Geophysical Monograph, v. 113, p. 101-127.

Cerveny, K., Davies, R., Dudley, G., Fox, R., Kaufman, P., Knipe, R.J., and Krantz, B., 2004, Reducing Uncertainity with fault-seal analysis: Oilfield Review, v. 16, p. 38-51.

Chadwick, W.W., Geist, D.J., Jónsson, S., Poland, M., Johnson, D.J., and Meertens, C.M., 2006, A volcano bursting at the seams: Inflation, faulting, and eruption at Sierra Negra volcano, Galápagos: Geology v. 34, p. 1025-1028.

Chester, F.M., Evans, J.P., and Biegel, R.L., 1993, Internal Structure And Weakening Mechanisms Of The San-Andreas Fault: Journal Of Geophysical Research-Solid Earth, v. 98, p. 771-786.

Childs, C., Watterson, J., and Walsh, J.J., 1996, A model for the structure and development of fault zones: Journal of the Geological Society, London, v. 153, p. 337-340.

Crider, J.G., and Peacock, D.C.P., 2004, Initiation of brittle faults in the upper crust: a review of field observations: Journal of Structural Geology, v. 26, p. 691-707.

d'Alessio, M., and Martel, S.J., 2005, Development of strike-slip faults from dikes, Sequoia National Park, California: Journal of Structural Geology, v. 27, p. 35-49.

Davatzes, N.C., Eichhubl, P., and Aydin, A., 2005, Structural evolution of fault zones in sandstone by multiple deformation mechanisms: Moab fault, southeast Utah: GSA Bulletin, v. 117, p. 135-148.

Day, W.C., Dickerson, R.P., Potter, C.J., Sweetkind, D.S., San Juan, C.A., Drake, R.M., and Fridrich, C.J., 1998, Bedrock geologic map of the Yucca Mountain area, Nye County, Nevada: U.S. Geological Survey Geologic Investigations Series Map I-2627, scale 1:24,000, 21 p. pamphlet.

de Joussineau, G., and Aydin, A., 2007, The evolution of the damage zone with fault growth in sandstone and its multiscale characteristics: Journal of Geophysical Research, v. 112.

de Joussineau, G., Mutlu, O., Aydin, A., and Pollard, D.D., 2007, Characterisation of strike-slip fault-splay relationships in sandstone: Journal of Structural Geology, v. 29, p. 1831-1842.

Engelder, J.T., 1974, Cataclasis and generation of fault gouge: Geological Society of America Bulletin, v. 85, p. 1515-1522.

Evans, J.P., 1990, Thickness-displacement relationships for fault zones: Journal of Structural Geology, v. 12, p. 1061-1065.

Evans, J.P., and Bradbury, K.K., 2004, Faulting and Fracturing of Nonwelded Bishop Tuff, Eastern California: Deformation Mechanisms in Very Porous Materials in the Vadose Zone: Vadose Zone Journal, v. 3, p. 602-623.

Evans, J.P., Forster, C.B., and Goddard, J.V., 1997, Permeability of fault-related rocks, and implications for hydraulic structure of fault zones: Journal of Structural Geology, v. 19, p. 1393-1404.

Faulkner, D.R., Lewis, A.C., and Rutter, E.H., 2003, On the internal structure and mechanics of large strike-slip fault zones: field observations of the Carboneras fault in southeastern Spain: Tectonophysics, v. 367, p. 235-251.

Ferrill, D.A., and Morris, A.P., 2003, Dilational normal faults: Journal of Structural Geology, v. 25, p. 183-196.

Fischer, M.P., and Polansky, A., 2006, Influence of flaws on joint spacing and saturation: Results of one-dimensional mechanical modeling: Journal of Geophysical Research, v. 111. B07403, doi: 10.1029/2005JB004115

Fisher, R.V., and Schmincke, H.-U., 1984, Pyroclastic rocks, Berlin: Springer. 472 pp

Flint, L.E., 1998, Characterisation of hydrogeologic units using matrix properties, Yucca Mountain, Nevada: U.S Geological Survey, Water-resources Investigations Report 97-4243.

Fossen, H., and Hesthammer, J., 2000, Possible absence of small faults in the Gullfaks Field, northern North Sea: implications for downscaling of faults in some porous sandstones: Journal Of Structural Geology, v. 22, p. 851-863.

Fossen, H., Schultz, R.A., Shipton, Z.K., and Mair K., 2007, Deformation bands in sandstone - a review: Journal of the Geological Society, London. v. 164, p. 755-770

Giordano, D., Nichols, A.R.L., and Dingwell, D.B., 2005, Glass transition temperatures of natural hydrous melts: a relationship with shear viscosity and implications for the welding process: Journal of Volcanology and Geothermal Research, v. 142, p. 105-118.

Grant, J.V., and Kattenhorn, S.A., 2004, Evolution of vertical faults at an extensional plate boundary, southwest Iceland: Journal of Structural Geology, v. 26, p. 537-557.

Gray, M.B., Stamatakos, J.A., Ferrill, D.A., and Evans, M.A., 2005, Fault-zone deformation in welded tuffs at Yucca Mountain, Nevada, USA: Journal of Structural Geology, v. 27, p. 1873-1891.

Gross, M.R., 1993, The origin and spacing of cross joints: examples from the Monterey Formation, Santa Barbara Coastline, California: Journal of Structural Geology, v. 15, p. 737-751.

Gross, M.R., and Engelder, T., 1995, Strain accommodated by brittle failure in adjacent units of the Monterey Formation, U.S.A.: scale effects and evidence for uniform displacement boundary conditions: Journal of Structural Geology, v. 17, p. 1303-1318.

Grunder, A., and Russell, J.K., 2005, Welding processes in volcanology: insights from field, experimental, and modeling studies: Journal of Volcanology and Geothermal Research, Welding Processes in Volcanology, v. 142, p. 1-9.

Gudmundsson, A., 1992, Formation and growth of normal faults at the divergent plate boundary in Iceland: Terra Nova, v. 4, p. 464-471.

—, 1998, Formation and development of normal fault calderas and the initiation of large explosive eruptions: Bulletin of Volcanology, v. 60, p. 160-170.

Gudmundsson, A., and Backstrom, K., 1991, Structure and development of the Sveingja graben, Northeast Iceland: Tectonophysics, v. 200, p. 111-125.

Hancock, P.L., 1985, Brittle microtectonics: principles and practice: Journal of Structural Geology, v. 7, p. 437-457.

Heffner, J., and Fairley, J., 2006, Using surface characteristics to infer the permeability structure of an active fault zone: Sedimentary Geology, v. 184, p. 255-265.

Henry, C.D., and Wolff, J.A., 1992, Distinguishing strongly rheomorphic tuffs from extensive silicic lavas: Bulletin of Volcanology, v. 54, p. 171-186.

Heynekamp, M.R., Goodwin, L.B., Mozely, P.S., and Haneberg, W.C., 1999, Controls on fault zone architecture in poorly lithified sediments, Rio Grande rift, New Mexico: Implications for fault-zone permeability and fluid flow in Haneberg, W. C., et al., eds., Faults and subsurface fluid flow in the shallow crust: American Geophysical Union Monograph, v. 113, p. 27-51.

Hinds, J.J., Bodvarsson, G.S., and Nieder-Westermann, G.H., 2003, Conceptual evaluation of the potential role of fractures in unsaturated processes at Yucca Mountain: Journal of Contaminant Hydrology, v. 62-63, p. 111-132.

Hobbs, D.W., 1967, The formation of tension joints in sedimentary rocks: an explanation: Geological Magazine, v. 104, p. 550-556.

Holland, M., Urai, J.L., and Martel, S., 2006, The internal structure of fault zones in basaltic sequences: Earth and Planetary Science Letters, v. 248, p. 301-315.

Holohan, E.P., Troll, V.R., Walter, T.R., Munn, S., McDonnell, S., and Shipton, Z.K., 2005, Elliptical calderas in active tectonic settings: an experimental approach: Journal of Volcanology and Geothermal Research, v. 144, p. 119-136.

Huang, Q., and Angelier, J., 1989, Fracture spacing and its relation to bed thickness: Geological Magazine, v. 104, p. 355-362.

Hull, J., 1988, Thickness-displacement relationships for deformation zones: Journal of Structural Geology, v. 10, p. 431-435.

Jain, A., Guzina, B.B., and Voller, V.R., 2007, Effects of overburden on joint spacing in layered rocks: Journal of Structural Geology, v. 29, p. 288-297.

Ji, S., and Saruwatari, K., 1998, A revised model for the relationship between joint spacingand layer thickness: Journal of Structural Geology, v. 20, p. 1495-1508.

Kim, Y.S., Peacock, D.C.P., and Sanderson, D.J., 2003, Strike-slip faults and damage zones at Marsalforn, Gozo Island, Malta: Journal of Structural Geology, v. 25, p. 793-812.

—, 2004, Fault damage zones: Journal of Structural Geology, v. 26, p. 503-517.

Knipe, R.J., Jones, G., and Fischer, Q.J., 1998, Faulting, fault sealing and fluid flow in hydrocarbon reservoirs: an introduction, in Faulting, Fault Sealing, and Fluid Flow Geol. Soc., Lond., Spec. Pub.147. p. 7-21.

Knott, S.D., Beach, A., Brockbank, P.J., Lawson Brown, J., McCallum, J.E., and Welbon, A.I., 1996, Spatial and mechanical controls on normal fault populations: Journal of Structural Geology, v. 18, p. 359-372.

Kobberger, G., and Schmincke, H.-U., 1999, Deposition of rheomorphic ignimbrite D (Mogan Formation), Gran Canaria, Canary Islands, Spain: Bulletin of Volcanology, v. 60, p. 465-485.

Leat, P.T., and Schmincke, H.-U., 1993, Large-scale rheomorphic shear deformation in Miocene peralkaline ignimbrite E, Gran Canaria: Bulletin of Volcanology, v. 55, p. 155-165.

Li, Y., and Yang, C., 2007, On fracture spacing in layered rocks: International Journal of Rock Mechanics and Mining Sciences, v. 44, p. 936-941.

Martel, S.J., 1990, Formation Of Compound Strike-Slip-Fault Zones, Mount Abbot Quadrangle, California: Journal Of Structural Geology, v. 12, p. 869-&.

McArthur, A.N., Cas, R.A.F., and Orton, G.J., 1998, Distribution and significance of crystalline, perlitic and vesicular textures in the Ordovician Garth Tuff (Wales): Bulletin of Volcanology, v. 60, p. 260-285.

McBirney, A.R., and Williams, H., 1969, Geology and petrology of the Galapagos Islands: Geological Society of America Memoir, v. 118, p. 1-197.

McConaughy, D.T., and Engelder, T., 2001, Joint initiation in bedded clastic rocks: Journal of Structural Geology, v. 23, p. 203-221.

McGrath, A.G., and Davison, I., 1995, Damage zone geometry around fault tips: journal of Structural Geology, v. 17, p. 1011-1024.

Melosh, H.J., 1996, Dynamical weakening of faults by acoustic fluidization: Nature, v. 379, p. 601-606.

Micarelli, L., Benedicto, A., and Wibberley, C.A.J., 2006, Structural evolution and permeability of normal fault zones in highly porous carbonate rocks: Journal of Structural Geology, v. 28, p. 1214-1227.

Millward, J., Beddoe-Stephens, B., Williamson, I.T., Young, S.R., and Peterson, M.G., 1994, Lithostratigraphy of a concealed caldera - related ignimbrite sequence within the Borrowdale Volcanic Group of West Cumbria: Proceedings of the Yorkshire Geological Society, v. 50, p. 25-36.

Mollema, P.N., and Antonellini, M., 1999, Development of strike-slip faults in the dolomites

of the Sella Group, Northern Italy: Journal of Structural Geology, v. 21, p. 273-292.

Moon, V.G., 1993, Geotechnical characteristics of ignimbrite: A soft pyroclastic rock type: Engineering Geology, v. 35, p. 33-48.

Myers, R., and Aydin, A., 2004, The evolution of faults formed by shearing across joint zones in sandstone: Journal of Structural Geology, v. 26, p. 947-966.

Narr, W., and Suppe, J., 1991, Joint spacing in sedimentary rocks: Journal of Structural Geology, v. 13, p. 1037-1048.

Nirex, report No. 525, Scientific Update 1993: Nirex deep waste repository project.

Odling, N.E., 1992, Network properties of a 2-dimensional natural fracture pattern: Pure and Applied Geophysics, v. 138, p. 95-114.

Patton, T.L., Logan, J.M., and Friedman, M., 1998, Experimentally generated normal faults in single-layer and multilayer limestone specimens at confining pressure: Tectonophysics, v. 295, p. 53-77.

Peacock, D.C.P., 2001, The temporal relationship between joints and faults: Journal of Structural Geology, v. 23, p. 329-341.

Peacock, D.C.P., and Zhang, X., 1994, Field examples and numerical modeling of oversteps and bends along normal faults in cross-section: Tectonophysics, v. 234, p. 147-167.

Pioli, L., and Rosi, M., 2005, Rheomorphic structures in a high-grade ignimbrite: the Nuraxi tuff, Sulcis volcanic district (SW Sardinia, Italy): Journal of Volcanology and Geothermal Research, v. 142, p. 11-28.

Pollard, D.D., and Aydin, A., 1988, Progress in understanding jointing over the past century: Geological Society of America Bulletin, v. 100, p. 1181-1204.

Pollard, D.D., and Segall, P., 1987, Theoretical displacements and stresses near fractures in rock, with applications of faults, joints, veins, dikes, and solution surfaces, In Fracture Mechanics of Rock (ed: Barry Kean Atkinson), Academic Press. London, 277-349 p.

Potter, C.J., Day, W.C., Sweetkind, D.S., and Dickerson, R.P., 2004, Structural geology of the proposed site area for a high-level radioactive waste repository, Yucca Mountain, Nevada: GSA Bulletin, v. 116, p. 858-879.

Power, W.L., Tullis, T.E., and Weeks, J.D., 1988, Roughness and wear during brittle faulting: Journal of Geophysical Research, v. 93, p. 15,568-15,278.

Price, N.J., 1966, Fault and joint development in brittle and semi-brittle rocks, Pergamon Press, Oxford, 176 p

Pruess, K., Faybishenko, B., and Bodvarsson, G.S., 1998, Alternative concepts and approaches for modeling flow and transport in thick unsaturated zones of fractures rocks: Journal of Contaminant Hydrology, v. 38, p. 281-322.

Quane, S.L., and Russell, J.K., 2003, Ranking welding intensity in pyroclastic deposits: Bulletin Of Volcanology, v. 67, p. 129-143.

Ramsey, J.M., and Chester, F.M., 2004, Hybrid fracture and the transition from extension fracture to shear fracture: Nature, v. 428, p. 63-66.

Rawling, G.C., and Goodwin, L.B., 2006, Structural record of the mechanical evolution of mixed zones in faulted poorly lithified sediments, Rio Grande rift, New Mexico, USA: Journal of Structural Geology, v. 28, p. 1623-1639.

Rawling, G.C., Goodwin, L.B., and Wilson, J.L., 2001, Internal architecture, permeability structure, and hydrologic significance of contrasting fault-zone types: Geology, v. 29, p. 43-46.

Renshaw, C.E., and Pollard, D.D., 1994, Numerical simulation of fracture set formation: A fracture mechanics model consistent with experimental observations: Journal of Geophysical Research, v. 99, p. 9359-9372.

Roche, O., Druitt, T., and Merle, O., 2000, Experimental study of caldera formation: Journal of Geophysical Research, v. 105, p. 395-416.

Ross, C.S., and Smith, R.L., 1961, Ash-flow tuffs: their origin, geologic relations and identification: U.S. Geol. Survey Prof. Paper 366, p. 1-77.

Sagy, A., Reches, Z.e., and Roman, I., 2001, Dynamic fracturing: field and experimental observations: Journal of Structural Geology, v. 23, p. 1223-1239.

Sammis, C., King, G., and Biegel, R., 1987, The kinematics of gouge deformation: Pure and Applied Geophysics, v. 125, p. 777-812.

Schmincke, H.-U., 1974, Volcanological aspects of peralkaline welded ash-flow tuffs: Bulletin Volcanologique, v. 38, p. 594-636.

—, 1998, Geological field guide of Gran Canaria, Pluto Press, Kiel, 179 p.

Scholz, C.H., 1987, Wear and gouge formation in brittle faulting: Geology, v. 15, p. 493-495.

Schopfer, M.P.J., Childs, C., and Walsh, J.J., 2006, Localisation of normal faults in multilayer sequences: Journal of Structural Geology, v. 28, p. 816-833.

Schultz, R.A., and Li, Q., 1995, Uniaxial strength testing of non-welded Calico Hills tuff, Yucca Mountain, Nevada: Engineering Geology, v. 40, p. 287-299.

Segall, P., and Pollard, D.D., 1983, Nucleation and growth of strike slip faults in granite: Journal of Geophysical Research, v. 88, p. 555-568.

Sheridan, M.F., and Wang, Y., 2005, Cooling and welding history of the Bishop Tuff in Adobe Valley and Chidago Canyon, California: Journal of Volcanology and Geothermal Research, v. 142, p. 119-144.

Shipton, Z.K., and Cowie, P.A., 2003, A conceptual model for the origin of fault damage zone structures in high-porosity sandstone: Journal of Structural Geology, v. 25, p. 333-

344.

Shipton, Z.K., Evans, J.P., Dockrill, B., Heath, J., Williams, A., Kircher, D., and Kolesar, P.T., 2005, Natural leaking CO2 - charged systems as analogs for failed geologic sequestration reservoirs: In: Thomas D. and Benson S. M. (Eds). Carbon Dioxide capture for storage in deep geologic formations - results from the CO2 capture project, vol 2, Elservier Science. 699-712.

Shipton, Z.K., Soden, A.M., Kirkpatrick, J.D., Bright, A.M., and Lunn, R.J., 2006, How thick is a fault? Fault displacement-thickness scaling revisited: In: Geophysical Monograph Series, Volume 170, Earthquakes: Radiated Energy and the Physics of Faulting. Editors: R. Abercrombie, A. McGarr, G. Di Toro and H. Kanamori, p. 193-198.

Sigda, J.M., and Wilson, J.L., 2003, Are faults preferential flow paths through semiarid and arid vadose zones?: Water Resources Research, v. 39, p. 1225.

Simons, M., Fialko, Y., Rivera, L., Chapin, E., Hensley, S., Rosen, P.A., Shaffer, S., Webb, F.H., and Langbein, J., 2000, Analysis of geodetic measurements of crustal deformation at Long Valley Caldera: EOS Trans Am Geophys Union, v. 81, p. 1322.

Smith, J.V., Yamauchi, S., and Miyake, Y., 1994, Coaxial progressive deformation textures in extrusive and shallow intrusive rocks, southwest Japan: Journal of Structural Geology, v. 16, p. 315-322.

Soden, A.M., and Moir, H., 2007, The influence of host rock fabric on joint morphology: MOPEDZ modelling: Geological Society Bicentenary Conference.

Sparks, R.S.J., 1976, Grain size variations in ignimbrites and implications for the transport of pyroclastic flows: Sedimentology, v. 23, p. 147-188.

Throckmorton, C.K., and Verbeek, E.R., 1995, Joint networks in the Tiva Canyon and Topopah Spring Tuffs of the Paintbrush group, southwestern Nevada: U.S. Geological Survey, Open-file report 95-2.

Troll, V., Walter, T., and Schmincke, H.U., 2002, Cyclic caldera collapse: Piston or piecemeal subsidence? Field and experimental evidence: Geology, v. 30, p. 135-138.

Usai, S., Sansosti, E., Lanari, R., Tesauro, M., Fornaro, G., Berardino, P., and Lundgren, P., 2000, Deformation time series analysis and modeling surface deformation observed with SAR interferometry at Campi Flegreicaldera: EOS Trans Am Geophys Union, v. 81.

Walker, G.P.L., 1984, Downsag calderas, ring faults, and caldera sizes: Journal of Geophysical Research, v. 89 B10, p. 8407-8416.

Walter, T.R., and Troll, V.R., 2001, Formation of caldera periphery faults: an experimental study: Bulletin of Volcanology, v. 63, p. 191-203.

Watterson, J., Childs, C., and Walsh, J.J., 1998, Widening of fault zones by erosion of asperities formed by bed-parallel slip: Geology, v. 26, p. 71-74.

Weinberger, R., 2001, Joint nucleation in layered rocks with non-uniform distribution of cavities: Journal of Structural Geology, v. 23, p. 1241-1254.

Wentworth, C.K., and Williams, 1932, The classification and terminology of the pyroclastic rocks: National Research Council Bulletin, v. 89, p. 19-53.

Wibberley, C.A.J., and Shimamoto, T., 2005, Earthquake slip weakening and asperities explained by thermal pressurization: Nature, v. 436, p. 689-692.

Wilkins, S.J., Gross, M.R., Wacker, M., Eyal, Y., and Engelder, T., 2001, Faulted joints: kinematics, displacement-length scaling relations and criteria for their identification: Journal of Structural Geology, v. 23, p. 315-327.

Willemse, E.J.M., Peacock, D.C.P., and Aydin, A., 1997, Nucleation and growth of strike-slip faults in limestones from Somerset, U.K: Journal of Structural Geology, v. 19, p. 1461-1477.

Wilson, E.J., Goodwin L. B., and Lewis, C.J., 2003, Deformation bands in nonwelded ignimbrites: Petrophysical controls on fault-zone deformation and evidence of preferential fluid flow: Geology, v. 31, p. 837-840.

Wojtal, S.F., and Mitra, G., 1986, Strain hardening and strain softening in fault zones from foreland thrusts: Geological Society of America Bulletin, v. 97, p. 674-687.

Wu, H., and Pollard, D., 1995, An experimental study of the relationship between joint spacing and layer thickness: Journal of Structural Geology, v. 17, p. 887-905.

Zhang, K., Wu, Y.-S., and Pan, L., 2006, Temporal damping effect of the Yucca Mountain fractured unsaturated rock on transient infiltration pulses: Journal of Hydrology, v. 327, p. 235-248.